THE UPLIFT BEHAVIOUR OF SHALLOW FOUNDATIONS

By

Michael James Rattley

UNIVERSITY OF SOUTHAMPTON
SCHOOL OF CIVIL ENGINEERING AND THE ENVIRONMENT

June 2007

A dissertation submitted for the
degree of Doctor of Philosophy at the University of Southampton

UNIVERSITY OF SOUTHAMPTON

ABSTRACT

FACULTY OF ENGINEERING, SCIENCE AND MATHEMATICS

SCHOOL OF CIVIL ENGINEERING AND THE ENVIRONMENT

Doctor of Philosophy

THE UPLIFT BEHAVIOUR OF SHALLOW FOUNDATIONS

Michael James Rattley

An investigation into the uplift capacity of shallow foundations has been undertaken. The main focus of the research contained in this thesis is experimental, with a large quantity of model tests undertaken in a geotechnical centrifuge in three main areas:

A series of uplift tests have been undertaken in a geotechnical centrifuge to investigate the behaviour of shallow plate anchors embedded in sand and clay. Uplift response and capacity has been studied at a range of displacement rates and particular attention has been paid to the role of negative pore pressures developed at the anchor base during uplift. The investigation has also considered the effects of anchor width and anchor inclination. The results of the centrifuge study have been examined in relation to the limits of fully drained and fully undrained behaviour and the failure mechanisms developed at uplift velocities leading to partially drained response are discussed. In addition numerical solutions for anchor uplift capacity over the range of velocities are compared to the experimental results obtained.

The contribution to uplift stiffness and capacity provided by the clay at the base of transmission tower footings has also been investigated in the centrifuge. Negative pore pressures developed at the base of such foundations are measured directly across a range of uplift velocities and are used to provide insight into the influence of uplift rate on the failure mechanism at the footing base. Data from a series of triaxial extension tests, conducted at high axial strain rates, highlight the rate dependence of the stiffness and undrained strength of the underlying clay. These results are combined with finite element back analyses of the centrifuge tests to predict the uplift capacity and load displacement response of footings on clay subject to high rate of uplift such as those which may be experienced by transmission tower foundations in service.

Finally, the effect of modifying a loose granular backfill using cement on the uplift performance of shallow anchors is examined. These centrifuge model tests involved a range of cement contents and are supported using a series of laboratory element tests and Finite Element analyses. Conclusions are drawn in relation to peak foundation capacity and load displacement response.

Keywords: shallow foundations; uplift capacity; suction; centrifuge test; rate effects; transmission towers; clay

ACKNOWLEDGEMENTS

First and foremost I would like to gratefully acknowledge the supervision provided by Dr David Richards who has been a fantastic source of sound advice and encouragement throughout my studies. He has presented me with many great opportunities during my time at the University of Southampton, not least the chance to spend a hugely enjoyable year at the University of Western Australia (UWA).

I am also particularly thankful to Professor Barry Lehane who, despite his busy schedule, always found time to share his knowledge and provide me with invaluable guidance and support during my stay at UWA.

The geotechnical centrifuge facility at UWA is renowned for producing high quality research and such a reputation would not be possible without the help of an excellent technical support staff. In particular I would like to mention Bart Thompson who never faltered when there was testing to be done, even on the weekend when he could have been out sailing on the Swan River. Many thanks go to Dr Christophe Gaudin for his technical advice and support and to Don Herley, Tuarn Brown and John Breen for all their assistance when things didn't quite go as planned. The support provided by all the members of the workshop in assembling various test apparatus is gratefully acknowledged.

I am extremely thankful to Hardev Sidhu at Surrey Geotechnical Consultants without whose generosity and expertise I would not have completed the laboratory testing. Many thanks also to Nilo Consoli for his assistance in conducting the laboratory testing of cemented sand.

Thanks to all members of the geotechnical research groups, both staff and students at the Universities of Southampton and Western Australia for all the help and discussion during my studies.

The financial backing provided by National Grid Plc. is gratefully acknowledged and many thanks must also go to the EPSRC for funding this research. I would also like to take this opportunity to acknowledge the financial assistance provided by the F.C. Lunoe Trust and to thank them for their continued support.

Finally, to all my friends and family who have provided support and reminded me that there is a life outside of research I offer my sincere appreciation. In particular I would like to thank my beautiful fiancée Jen for her love and enthusiasm and for putting up with me over the past few years. I remain, as always, indebted to my parents for all their love, support and encouragement for which I will be forever grateful.

Michael

TABLE OF CONTENTS

LIST OF FIGURES

LIST OF TABLES

SYMBOLS

Roman

A	Area of anchor/footing base
B	Width of anchor/footing
c'	Cohesion intercept
c_v	Coefficient of consolidation
C_c	Compression index
D	Diameter of anchor/footing
e	Void ratio
E	Young's modulus
E_u	Undrained modulus
F_{su}	Uplift force generated at the base of a foundation
F_u	Total uplift force
$F_{\phi'}$	Shear force generated along the uplift failure surface
g	Gravitational acceleration
G_s	Relative density
G_0	Small strain shear modulus
H	Embedment depth
k_h	Horizontal coefficient of permeability
k_v	Vertical coefficient of permeability
K_0	Pressure coefficient
L	Length of anchor
n	Centrifuge scale factor
N	SPT blowcount
N_c	Bearing capacity factor
N_u	Total uplift capacity factor
N_{ub}	Breakout uplift capacity factor
N_{uc}	Reverse bearing capacity factor
N_{us}	Sand breakout capacity factor
p'	Mean principle effective stress
q	Deviator stress

q_c Corrected CPT tip resistance

q_{ct} T-bar bearing pressure

q_{fu} Normalised anchor capacity

q_{uc} Unconfined compressive strength

s Anchor shape factor

s_u Undrained shear strength

s_{uss} Undrained shear strength in simple shear

s_{utc} Undrained shear strength in triaxial compression

s_{ute} Undrained shear strength in triaxial extension

$s_{uT\text{-}bar}$ Undrained shear strength derived from T-bar

t Time

t_f Time to failure

u Pore water pressure

v_f Uplift velocity (displacement rate)

w Anchor/footing displacement

W_b Self weight of backfill material

W_f Self weight of foundation

z Depth in centrifuge sample

Greek

γ Unit weight

γ_w Unit weight of water

ε_a Axial strain

ε_f Axial strain at failure

ρ_s Saturated density

θ Anchor inclination

θ Slip surface angle

σ_h Horizontal total stress

σ_v Vertical total stress

σ'_h Horizontal effective stress

σ'_v Vertical effective stress

τ Shear stress

ϕ' Effective angle of friction

$(\phi')_{peakq}$	Friction angle at peak deviator stress
ψ	Dilatancy angle

SUBSCRIPTS

cr	Critical value
f	Value at failure
max	Maximum value
min	Minimum value
nc	Normally consolidated
oc	Over consolidated
p	Peak value
ref	Reference value
sand	Relating to an anchor/footing founded on sand

ABREVIATIONS

DSS	Direct simple shear
OCR	Overconsolidation ratio
PACB	Plate anchor with clay backfill
PAIB	Plate anchor with improved backfill
PASB	Plate anchor with sand backfill
PIV	Particle image velocimetry
TC	Triaxial compression
TE	Triaxial extension
TTFS	Transmission tower footing with sand backfill
UWA	University of Western Australia

Chapter 1

INTRODUCTION

1.1 Introduction

National Grid Plc owns, maintains and operates the high-voltage electricity transmission system in England and Wales. There are currently around 22,000 transmission towers (Figure 1.1) in operation, each typically utilising four individual under-reamed shallow footings for tension and compression foundation support. These footings are generally unlike the majority of other foundation systems as they may be subjected to large uplift loads (from wind induced loading and broken cable conditions) in excess of their working compression loading, such that the uplift capacity is often the controlling load case in design.

Transmission tower failures in the United Kingdom are extremely rare indicating that current design methods offer a satisfactory margin of safety for the conventional loading conditions applied in the past. Failures that have occurred however, such as during high intensity storm winds recorded in 1986, have indicated that tower collapse has been related to structural damage. Evidently the resistance to uplift of the tower footings under high magnitude transient loading was such that shear failure of the tower leg above the footing or tensile failure of the concrete stub, as shown in Figure 1.2, occurred before ultimate failure of the foundation. Such evidence points towards the generation of uplift capacities, under rapid loading, which are well in excess of the design loads and indicates that the ability of such foundations to resist short term, high intensity loading should be an important aspect not currently recognised during conventional design. Previous modifications made to the design methods used for

transmission tower foundations have generally led to a reduction in the calculated uplift capacities of the foundations. There is also a requirement in the UK to increase the size of transmission towers and in particular their conductors in response to a greater demand for power. These trends have led to a growing interest from National Grid in establishing a more reliable method of assessing the uplift capacity and general uplift behaviour of both new and existing tower foundations. More recently field testing undertaken in the UK by the University of Southampton, in conjunction with National Grid, has investigated transmission tower response to controlled broken wire events (Clark *et al.* 2006). Data retrieved from strain gauges located on transmission tower legs was used to deduce loading rates transmitted to the tower foundations due to a broken wire/conductor event (a particular design loading condition for transmission towers in the UK). These transmitted load rates have been shown to be of a very high magnitude however no visible signs of foundation distress were recorded during testing.

A review undertaken by the University of Surrey into the uplift capacity of transmission tower footings (Clayton *et al*, 1994) concluded that the current National Grid design methods would over-predict foundation capacity relative to other more established methods. It has also been established that foundation design capacity is rarely seen to correlate with the results of field testing and although simple in their application, the design methods do not account for many factors known to influence foundation uplift capacity. It was proposed by Clayton *et al.* (1994) that factors such as enhanced backfill properties and suctions/adhesions developing at the base of the footing could account for higher foundation capacity under rapid loading conditions. While a number of aspects regarding the strain-rate dependent behaviour of soil have been researched extensively in the past, the application of this knowledge to foundation design is very limited. In general, transmission tower foundations are designed to resist static loads and there is much uncertainty with regard to the prediction of uplift capacity under rapid loading. Given this the primary aim of the research presented in this thesis is to provide an understanding of the dynamic uplift behaviour of shallow foundations and to suggest how this knowledge may be applied directly in the design of transmission tower foundations.

While a large number of the existing design methods, including those employed by National Grid, are based on equilibrium formulations and the results of laboratory investigations, together with empirical corrections, these methods do not necessarily lend themselves to a study of dynamic behaviour. In contrast the technique of centrifuge modelling can recreate stress fields which are similar to those in prototype applications and has the potential to provide a more adequate model in which to investigate the rate dependent uplift behaviour of shallow foundations. Investigation into the dynamic resistance of transmission tower footings to uplift using centrifuge techniques has been previously undertaken (Richards, 2002) and has illustrated that such techniques can allow valuable insight into foundation performance under fast rates of loading.

1.2 Objectives

The primary objective of the research described in this thesis is to investigate the performance of shallow foundations under rapid uplift loading conditions. This broad objective can be divided into the following specific aims:

1. To provide an overview of the current state of the art in the design of shallow foundations subject to uplift loads.
2. To evaluate the uplift behaviour and ultimate capacity of shallow foundations at various uplift rates.
3. To assess factors such as suctions/adhesions developing at the base of the footing and enhanced soil properties under rapid uplift loading and determine their relative contribution to uplift performance.
4. To assess the potential of current transmission tower foundations to resist short term uplift loading.
5. To provide a relationship between the rate dependent behaviour of soils and the rate dependent uplift behaviour of shallow foundations which can be used to develop a modified design method for transmission tower foundations.

1.3 Thesis Structure

This thesis is presented in 10 chapters:

Chapter 2 provides a review of the current state of the art with regard to the uplift capacity of shallow foundations and the rate dependent behaviour of soils. An overview of current design methods for transmission tower foundations in the UK is also presented along with a brief review of selected foundation field testing.

Chapter 3 presents the results of some preliminary finite element modelling undertaken to assess the impact of using a scaled representative model to predict shallow foundation capacity. Results from a large number of the studies reviewed in *Chapter 2* are also presented and compared.

The results of laboratory testing undertaken to determine the general properties of the respective soils selected for use in the centrifuge testing programme are provided in *Chapter 4*. A brief review of the current knowledge regarding the behaviour of kaolin clay is also presented.

Chapter 5 outlines the centrifuge test program. Details of the entire centrifuge testing programme undertaken in this research are provided and include descriptions of the centrifuge facility and the general apparatus used throughout the centrifuge tests. Specific details of the centrifuge soil sample preparation procedures and sample characterisation are also presented.

The results of centrifuge tests related to the uplift behaviour of shallow plate anchors are discussed in *Chapter 6*. Results for plate anchors with sand and clay backfills are presented.

Chapter 7 presents the results of a series of effective stress finite element analyses undertaken to directly model the centrifuge tests described in *Chapter 5*. Comparison is provided from the results of the centrifuge testing provided in *Chapter 6* and

recommendations made for the implementation of numerical analyses as a design tool in the prediction of foundation behaviour under rapid loading.

The results of centrifuge tests related to the uplift performance of transmission tower foundations embedded in clay are discussed in *Chapter 8*.

Chapter 9 presents the results of a series of centrifuge tests undertaken to investigate the uplift behaviour of shallow plate anchors with cement stabilised backfill. The application of such backfill improvement methods to transmission tower foundations is also discussed.

Chapter 10 brings together the major conclusions arising from all aspects of the research programme and provides recommendations for related future research.

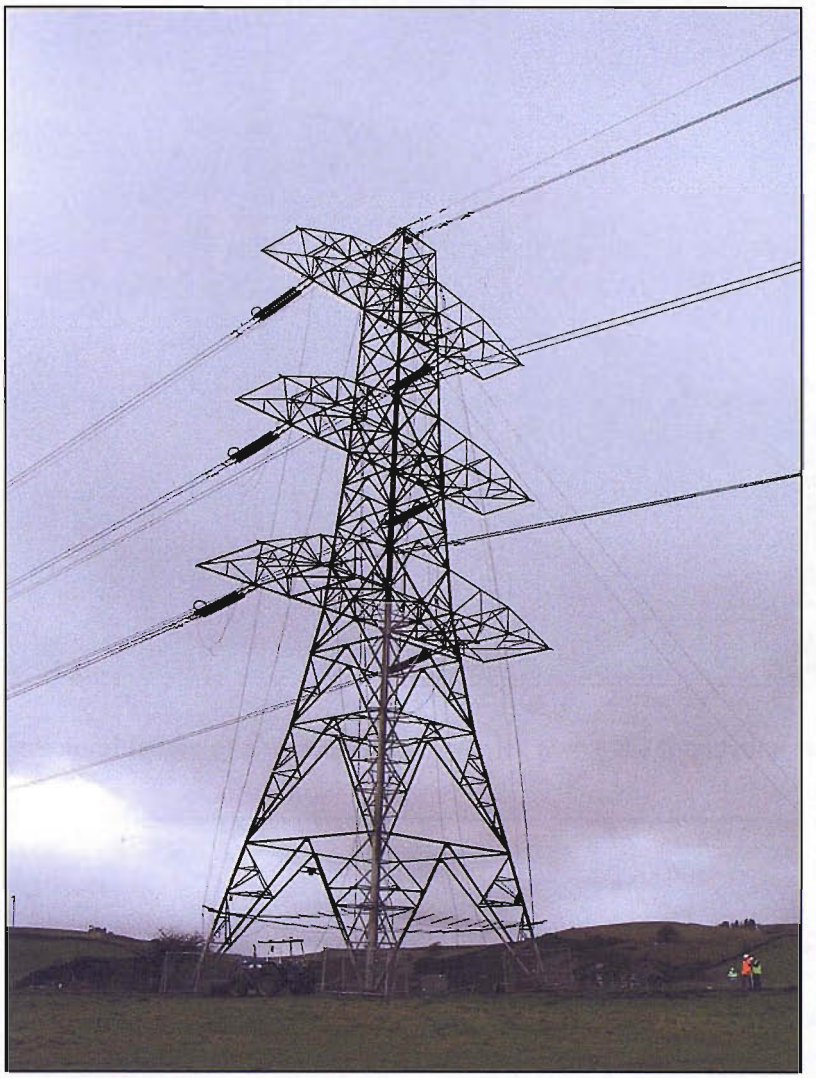

Figure 1.1 A tension tower in the UK

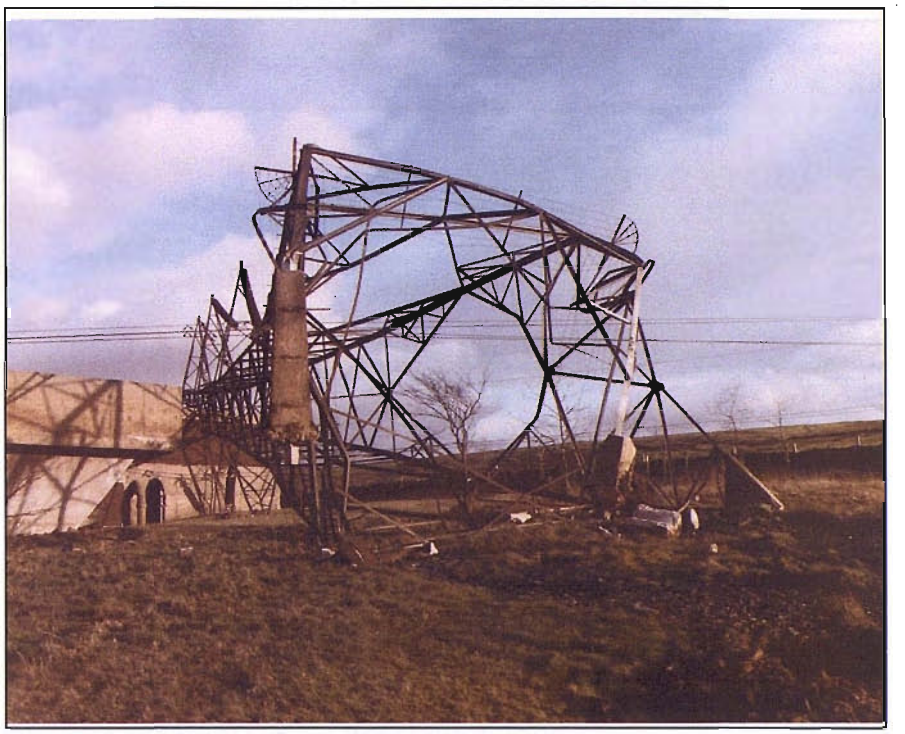

(a) Structural failure of a transmission tower leg above the foundation stub

(b) Tensile failure of an un-cleated footing stub

Figure 1.2 Transmission tower failures in the UK (1986)

Chapter 2

BACKGROUND & LITERATURE REVIEW

2.1 Introduction

2.1.1 Regarding the uplift of shallow foundations

There are many applications where foundation systems are required to resist uplift loads. The phrase "subjected to pullout loading", however, is often considered as a prohibitive factor when considering shallow foundations as a design solution. This uncertainty arises as knowledge, particularly that associated in current design methods, of the exact behaviour of shallow foundations subject to uplift loading is limited or in many cases oversimplified. Although ground anchors have been used for many centuries to support structures experiencing uplift forces the majority of published research on the subject has only been undertaken during the last thirty years or so, and is largely related to plate anchor behaviour in granular soil. Shallow foundations are already widely used as a means to support electricity transmission towers and are currently considered as to be an economical anchorage system for offshore oil platforms. Given the range of applications where shallow foundations might provide useful foundation support as an alternative to current solutions, an understanding of the mechanisms governing their behaviour, particularly in fine-grained soils, should be sought. This Chapter provides an overview of previous investigations into the uplift behaviour of shallow foundations. Empirical derivations for anchor uplift capacity will be compared with the results of experimental investigations and more recent numerical studies.

2.1.2 Regarding current design methods

The research described in Chapters 5, 6 and 7 has been supported by National Grid Plc and is focused toward shallow anchors typically used to support electricity transmission towers in the UK. That is not to say that the research contained herein is overly narrow, indeed particular effort has been made to ensure that parametric studies of anchor behaviour described here are valid for a range of applications. Recommendations made later are however aimed at developing new design guidelines for transmission tower foundations and so an appreciation of the current methods is required. Given the deficiency of knowledge surrounding uplift behaviour it is unsurprising that design methods such as those employed by National Grid have previously been concluded to be overly simplified (Clayton *et al.* 1994). These design methods rely heavily on empiricism and limit equilibrium concepts and involve the use of arbitrary assumptions concerning the geometry of the failure surface and influence of the soil above the footing. Despite such limitations, attempts to refine these design methods are often met with disapproval on the basis that transmission tower foundation failures in the UK are very rare.

2.1.3 Regarding rate effects

The rate at which uplift loads are transmitted to shallow anchors in service may be either reasonably slow or rapid such as when foundations are required to resist high intensity, short duration wind or wave events. The former is of particular importance for transmission tower foundations where design loadings allow for high wind loads. This in turn may lead to broken wire conditions generating further substantially increased rapid loadings on the foundation system. The foundations must therefore be designed to withstand such events and the mechanisms by which foundations are able to resist these rapidly applied uplift loads is an important behavioural aspect which is not generally well understood. Given this and the fact that a large number of transmission tower foundations in the UK are embedded in clay, the contribution to uplift resistance provided at the base of the foundation is of considerable interest. This contribution may be significantly enhanced during rapid loading due to the strength-strain rate dependence of the underlying clay and an understanding of these rate effects is therefore required.

The available literature concerning strain rate effects and time dependent behaviour for clay is extensive and it is well documented that clay soil may exhibit increased strength under transient loading conditions. This knowledge has important implications in the dynamic uplift behaviour of shallow anchors as time dependency can be a key factor in increased capacity of foundations in clay.

This Chapter provides a comparison of the results of previous field investigation into the uplift resistance of transmission tower foundations with capacities obtained from current design methods. Also provided is a brief review of the current state of the art for the modelling of the rate dependant behaviour of soil.

2.2 Transmission Tower Foundations

Foundations for transmission towers are required to resist significant uplift loads and in many cases the uplift capacity of the foundation is the dominant component in design. The design of foundations for transmission towers varies between countries depending on the particular ground conditions and the nature and magnitude of the live loads considered during design. The foundations most commonly used to support high voltage transmission line support structures may be classified into several basic types:

i. *Spread foundations*, Figure 2.1(a)
   Spread foundations are the most extensively used foundation type for the more conventional lattice towers and consist of a horizontal structural member embedded in the soil and connected under each leg of a tower. These types of foundation may consist of pre-fabricated grillages (either steel or reinforced concrete), cast in-situ reinforced concrete slabs (or pyramids) or pressed plates, which may be placed via excavation or augered. Each of these foundation types have the advantage of being relatively simple to construct although their uplift capacity may be limited.
ii. *Piled foundations*, Figure 2.1(b)

Where loose or unstable soils exist near the ground surface, piled foundations may be adopted to support each tower leg. Such foundations are not uncommon in practice and a variety of bored, cast in-situ and straight driven piles have been adopted for a range of transmission tower structures. Piled foundations are generally raked and arranged in a tripod fashion below each pile cap in order to provide axial load capacity in addition to shear and moment resistance. Piled foundations are often comparatively costly to construct due to the plant required for installation.

iii. *Helical foundations*, Figure 2.1(c)

A less common foundation solution are helical anchors, primarily a steel shaft to which one or more helices are attached in order to provide increased uplift resistance. The foundations are installed using an auger to rotate the shaft whilst simultaneously applying an axial load. Such a procedure may provide problems with installation in stiffer soils or those containing large rocks or boulders as helices may be damaged and post-installation testing is required to assess their functionality.

iv. *Grouted (rock) foundations*, Figure 2.1(d)

Where solid rock is present at the foundation level grouted foundations may be constructed or used in combination with spread anchors to provide enhanced uplift capacity. The foundation is formed by drilling a hole into the rock into which a steel section or tendon is inserted and then concreted into position below each tower leg. Although these foundations are most effective in providing tensile resistance they tend to provide only very small resistance to shear and bending moments.

This research focuses on transmission tower foundations commonly used by National Grid in the UK. These foundations are of the shallow spread anchor type and consist of a cast in-situ reinforced concrete pyramid (or slab) and chimney, Figure 2.2.

2.2.1 The National Grid design method

National Grid have specific procedures relating to the design and construction of pyramid foundations for lattice transmission towers in the UK. These procedures are defined in specifications which, despite being updated fairly recently (TS 203.04.15, Sept 2004), appear to have remained largely unchanged since their introduction many

years ago. An overview of these foundation geometries and the design assumptions used in calculating their capacity is given in the specification:

"This foundation takes the form of a truncated pyramid surmounted by a chimney. Alternatively the truncated pyramid may be replaced and/or used in conjunction with a reinforced concrete pad. The included angle between the horizontal and the sides of the pyramid shall not exceed 70°.

Uplift resistance is assumed to be provided by the weight of the foundation, the weight of soil contained within the assumed failure surface (an inverted frustum of a pyramid constructed from the lower edge of the base) *and the shear strength mobilised along the failure or slip surface. Due consideration shall be taken of buoyancy effects and reduced backfill densities."*

The frustum (or dead weight of cone method e.g. Kulhawy, 1987) design geometry is illustrated graphically in Figure 2.3. Design parameters from which the assumed frustum angle is selected are based on either undrained shear strength (for cohesive soil) or SPT N values (for non-cohesive soil) and these parameters are summarised in Table 2.1. The National Grid design procedures for pyramidal foundations are presented in full in Appendix A.

Table 2.1 Design parameters for frustum angles

	Design parameter for soil. Undrained shear strength (kPa) or SPT N value (blows/300mm)	
cohesive	$35<s_u<49$	$s_u \geq 50$
non-cohesive	$10<N<20$	$N>20$
frustum angle (degrees)	15	25

Clayton *et al.* (1994) compared foundation uplift capacities predicted by the National Grid design method with those predicted from the German VDE and American EPRI design methods. A range of foundation geometries, representative of those used by National Grid in the UK, and soil parameters were assessed for comparison. It should be noted that all capacities are calculated assuming that the groundwater level is

below the base of the foundation and that no partial material factors have been applied.

It is evident that for cohesive soil and non-cohesive soil at high angles of friction (ϕ'>30°) the National Grid method predicts higher capacities than both the VDE and EPRI methods for all foundation geometries assessed. In some cases (predominantly for the most shallow embedment case reviewed) predicted capacities are around 150% higher than those assessed from the other two methods. Furthermore, these predictions are based on an older National Grid design specification (502/18/GS, May 1993) which has more recently been updated to include consideration of the contribution to resistance of shear strength mobilised along the failure surface (TS 203.04.15, Sept 2004). It is likely therefore, that predictions based on the revised method will be higher than those inferred by Clayton *et al.* (1994) and thus even more in excess of those calculated from the other two methods.

There are significant variations between all the design methods reviewed inferring that none of the three are particularly reliable. In terms of which is the most suitable, the EPRI method may be considered the more robust from a modern soil mechanics perspective as it is based on the principles of effective stress while the advantages of the other two methods lie with their simplicity of application.

2.2.2 Full scale foundation tests

Field testing of transmission tower foundations has been undertaken in the UK since the 1950s and a number of uplift test reports on spread foundations were published by the Electrical Research Association (ERA) during the early 1960s. After 1967 notable results from full sized foundation tests were published through the Foundation Working Group of the Overhead Line Study Committee formed by Conseil International des Grandes Reseaux Electriques (CIGRE). Review of a number of these reports confirms the unreliability of past and present design specifications utilising the frustum (National Grid) method. Whilst some of the available uplift test data from the reports indicates that actual foundation resistance is in excess of the predicted capacity, the overwhelming trend is for foundations failing at loads well below those predicted in design.

In the large majority of the cases examined the disparity between measured and predicted foundation capacity may be attributed to variations in the quality of the backfill soil. For foundations cast into an existing excavation, failure planes inferred from the surface heave profile indicate that the volume of soil uplifted with the footing is often much less than the volume assessed from the 15-30 degree frustum dictated during design. In the case of foundations which have been undercut into the in-situ (virgin) soil the measured capacities are in much greater agreement with, and often exceed, the predicted values. This suggests that the backfill soil is generally much weaker than the in-situ soil. Vanner (1964) drew a similar conclusion during a study of the strength and densities of in-situ and backfill soils around foundations of increasing age. It was found that the strength of granular backfill only approached 70-100% of the in-situ strength after approximately 30 years and could be as little as 30% after just 3-4 years. For clays the difference was even more pronounced, with backfill strengths reaching a maximum of 50% of the in-situ value after 30 years and only 14% after 3-4 years. Various reasons can be suggested for this difference in strength; improper placement/reinstatement and insufficient compaction of the backfill soil, weather conditions during backfill placement and seasonal changes in ground conditions could all contribute to these observed variations (Vanner, 1982). Where foundations are formed in excavations, rather than undercut in the existing soil, design parameters assessed from the in-situ soil do not appear give a reasonable estimation of foundation capacity.

The irregularities between measured and predicted foundation capacity infer deficiencies in the design methods for transmission tower footings which have arisen, mainly due to a lack of understanding in the uplift behaviour of shallow foundations. In order to conceive a more robust design method an increased appreciation of existing analytical approaches is required along with further experimental and numerical investigation.

2.3 The Uplift Capacity of Shallow Anchors

A large number of the existing design methods for shallow plate anchors and under-reamed foundations, such as the truncated pyramid and pad and chimney foundations used by National Grid in the UK (described in section 2.2), are principally formulated from the results of small scale model tests and simple analytical methods. Physical modelling techniques using a geotechnical centrifuge has increased the validity of reduced scale modelling studies since the early 1980's, however the assumed failure mechanism for such anchors remains a source of contention between investigations.

Shallow anchors provide uplift resistance through their self weight and by transferring imposed uplift loads to the surrounding soil. In this way the theoretical solution for the uplift capacity of shallow spread anchors is based largely on the equilibrium conditions shown in Figure 2.4. The overall uplift force, F_u, is generally governed by the following equation:

$$F_u = W_b + W_f + F_{\phi'} + F_{su} \qquad (2.1)$$

where, W_b is the weight of backfill soil displaced above the footing, W_f is the foundation self weight, $F_{\phi'}$ is the shearing resistance mobilised along the displaced soil failure plane and F_{su} is the contribution to resistance at the footing base.

Theoretical approaches for the determination of foundation uplift capacity suggested in existing literature will, in general, consider each of these components in one way or another. The principle source of disparity between most existing methods lies in the size and shape of the failure surface mobilised in the soil above the anchor during uplift. This will obviously affect the resistance provided by the soil above the anchor both in the weight of the soil displaced and by the contribution of shear along the failure surface. The failure mechanism is considered to be influenced by soil type, density and the embedment depth of the foundation. Due to a lack of reliability in most field applications and the absence of a related design criterion, the base uplift resistance is usually assumed to be negligible. While this is thought to be the case for anchors founded on granular soils, under certain circumstances adhesion (at the soil-

footing interface) due to negative pore pressure (suction) developed below foundations founded on clay can provide a significant contribution to the uplift resistance.

Currently, most investigations into the uplift resistance of shallow foundations has been principally concerned with the behaviour of plate anchors in sand. Uplift behaviour for foundations in cohesive soils is markedly different but has, in contrast, received limited attention in published research. The following sections provide an overview of previously published experimental and analytical studies into the uplift behaviour of shallow foundations in sand and clay soils.

2.3.1 Anchor behaviour in sand

The ultimate uplift capacity of a foundation in granular soil is assessed through consideration of the self weight of the foundation, the mass of soil displaced above it and the shearing resistance of the displaced soil during uplift. Where the backfill soil is sufficiently compacted, interaction with the surrounding soil during uplift may create frictional forces leading to the displacement of a greater volume of soil than is directly above the footing.

For a plate anchor, as shown in Figure 2.4, of width B buried at a depth H in free draining sand the total uplift force, $F_{u(t)}$, is given by:

$$F_{u(t)} = F_u + W_f \tag{2.2}$$

where F_u is the ultimate capacity conventionally expressed as:

$$F_u = q_{fu} A \text{ , with } q_{fu} = N_{us} \gamma H \tag{2.3}$$

where A is the anchor base area, q_{fu} is the ultimate footing capacity normalised by the anchor area, γ is the sand's unit weight and N_{us} is a non-dimensional uplift capacity factor for an anchor in sand. The uplift capacity factor is a function of the embedment ratio, H/B, of the anchor and of the sand's peak friction angle (ϕ'_p). The value of N_{us} will theoretically increase with H/B until a maximum value at which point it remains constant, Figure 2.5. The value for H/B at which N_{us} becomes constant is termed the

critical embedment ratio $(H/B)_{cr}$. For embedment ratios less than $(H/B)_{cr}$ the failure zone extends to the soil surface and the mechanism is referred to as shallow anchor behaviour. For embedment ratios greater than $(H/B)_{cr}$ the failure mechanism is localised around the footing base and is denoted as deep anchor behaviour. This review focuses on embedment ratios such that shallow anchor behaviour is the mechanism of failure at ultimate load.

2.3.2 Failure surface models

Design methods suggested in existing literature have previously been roughly categorised based on the proposed geometry of the failure surface in the soil above the footing (e.g. Frydman and Shaham, 1989; Dickin and Leung, 1990; Das and Singh, 1995). The three principle categories include: the vertical failure surface, the curved failure surface and an inverted truncated cone (or pyramid) failure surface model. These failure mechanisms have been proposed for a variety of shallow foundations including horizontal plate anchors, belled piers, screw anchors and piles with enlarged bases.

Vertical Failure Surface Model

Majer (1955) was the first to propose that the soil above the footing would fail corresponding to a vertical failure surface as shown in Figure 2.6(a). Anchor capacity was assessed according to Equation 2.2, consisting of the weight of soil vertically above the anchor and the shearing resistance mobilised along the failure surface. A similar model was later used during examination of full-scale field tests to comprise a design procedure for shallow spread foundations (Trautmann and Kulhawy, 1988).

The vertical failure surface model (or friction cylinder method) is based on simple equilibrium formulations and has been concluded to be conservative for the majority of circumstances.

Curved Failure Surface Model

Since Mors (1959) first considered the soil cone method in determining the uplift capacity of an embedded anchor, the idea of a curved failure surface model became popular in many early studies. Balla (1961) described the failure surface as a tangential curve and employed Kotter's differential equation to relate the distribution

of soil reaction pressure and hence shear resistance along the arc of the failure surface. A vertical failure surface extended from the foundation base was given to intercept with the soil surface at an angle of (45°-ϕ/2) to form an arc curve, Figure 2.6(b). Kotter's equation was also implemented by Matsuo (1968), to determine shearing stresses along a failure surface approximated by a logarithmic spiral.

Khadilkar *et al.* (1971) used a combination of the methods proposed by Balla (1961) and Matsuo (1968) in adopting a logarithmic spiral failure surface to model the behaviour of shallow anchors. Although results produced in the study were in good agreement with experimental data from model tests, it was later concluded by Murray and Geddes (1987) that the method fails to produce an accurate estimate of frictional resistance along the failure surface.

A pyramidal shaped, curved failure plane was proposed by Meyerhof and Adams (1968) after a series of experimental uplift tests on strip, rectangular and circular model anchors. Though the proposed failure plane was curved it differed from that originally proposed by Balla (1961) in that the failure surface extended from the base of the footing at an angle, θ, to the vertical, Figure 2.6(b). It was observed from model tests that θ varied between ϕ/2 and ϕ/4 with an average value of ϕ/3 being adopted for subsequent analysis. For shallow anchors the failure surface was assumed to extend to the soil surface and the uplift capacity was obtained by considering equilibrium of the soil above the anchor.

Ilamparuthi and Muthukrishnaiah (1999) observed that the failure surface for shallow anchors is a gentle curve towards the soil surface, similar to that proposed by Meyerhof and Adams (1968), but conclude that it could be approximated as a plane surface for the estimation of anchor uplift capacity. Citing observations from model tests on half-cut circular anchors in a transparent rectangular tank Ilamparuthi and Muthukrishnaiah (1999) suggest that this plane surface makes an angle of approximately ϕ/2 to the vertical irrespective of sand density and submergence.

Inverted Truncated Cone (or pyramid) Failure Model

Design methods based upon an inverted truncated cone or pyramid failure model involve the assumption that a fan shaped wedge of soil is displaced with the foundation during uplift, Figure 2.6(c). Based on the work of Mors (1959), who investigated uplift capacity predictions based upon a truncated cone failure surface extended from the base of the anchor, Downs and Chieurzzi (1966) concluded that predicted capacities compared favourably with the results of field uplift tests on belled piers in sand. An additional factor was added to Mors' original model by Downs and Chieurzzi to include frictional resistance along the failure surface which had previously been ignored by Mors. In this case it was suggested that the angle made by the failure surface with the vertical, θ in Figure 2.6(c), should be taken as equal to ϕ. This value is higher than the majority of other studies i.e. Meyerhof and Adams (1968), Clemence and Veesaert (1977), Sutherland et al. (1982), Ilamparuthi and Muthukrishnaiah (1999), where an angle θ of $\phi/2$ is generally recommended, and should be considered as an upper bound solution only. Vermeer and Sutjiadi (1985) appear to be the only authors to have proposed an inverted cone failure surface model based upon the dilatancy of the soil. In this case with θ equal to twice the dilatancy angle (ψ).

Murray and Geddes (1987) investigated both a curved failure surface and a straight line truncated pyramid surface using equilibrium and limit analysis approaches respectively. In the former case θ was taken as $\phi/2$ to provide a practical equilibrium formulation. In the latter case, a value for θ equal to ϕ is shown to provide an upper bound solution.

It has been observed in several of the reviewed investigations that the failure surface was generally curved but was subsequently approximated to a plane surface for analytical purposes. It is considered here that while a curvilinear surface may be more representative of observed soil behaviour at failure load, the truncated cone has been shown to be an adequate model and one that is more suited to the development of a design method.

2.3.3 Ultimate uplift capacity in sand

Conventionally anchor capacity in sand is expressed according to Equation 2.3 and design methods are often presented in terms of the uplift capacity factor N_{us}. Comprehensive reviews of anchor capacity in sand have been undertaken previously, (e.g. Das and Singh, 1995 and Merifield *et al.* 2006) and indicate that the majority of published design methods are experimentally based. These empirical methods are usually compared with capacities predicted from equilibrium and limit analyses formulations. More recently the trend has moved towards the development of scaled model studies in a centrifuge as a more reliable method of assessment (e.g. Dickin, 1988) and the use of finite element analysis as a design tool.

2.3.4 Empirical and simple analytical solutions for capacity in sand

Balla (1961) was among the first to develop a rational method based upon the results of laboratory tests on model anchors (*mushroom* foundations) embedded in dense sand. According to Balla's slip surface model the ultimate uplift capacity of a circular anchor is given by:

$$F_u = H^3 \gamma [F_1 + F_3] \tag{2.4}$$

where F_1 and F_3 are dependant on H/B and ϕ' and vary according to Figure 2.7. No distinction is made by Balla between shallow and deep anchor behaviour and the method will over-predict foundation capacity in loose soil where local failure of the soil around the footing may occur at greater embedment.

Vesic (1971), (1972) took a different approach to the problem of anchor capacity in developing a cavity expansion model for a semi-infinite, homogenous and isotropic soil. The concept behind the model proposed by Vesic (1972) is outlined in Figure 2.8 where, by equilibrium, the pressure in the circular cavity is equal to the sum of the component forces in the vertical direction. Uplift capacity factors derived from Vesic's method for shallow circular anchors are presented by Das and Singh (1995).

Meyerhof and Adams (1968) suggest that the uplift capacity factor (for a strip anchor) can be expressed as a function of the soil friction angle, ϕ:

$$N_{us} = \frac{F_u}{\gamma HB} = 1 + \left(\frac{H}{B}\right) K_u \tan\phi \qquad (2.5)$$

A semi-empirical design approach, leading to a fairly consistent value for the coefficient of lateral stress in the soil, K_u, of approximately 0.95 (when ϕ' is assumed to be in the region 30-45°) was examined by Meyerhof and Adams. The analysis was extended to include circular and rectangular anchors through the application of a shape factor, s:

$$s = 1 + m\left(\frac{H}{B}\right) \qquad (2.6)$$

where m is a function of ϕ', as shown in Figure 2.9. The ultimate uplift capacity of a rectangular plate anchor, of length L, was given as:

$$F_u = W_s + \gamma H^2 (2sB + L - B) K_u \tan\phi \qquad (2.7)$$

where W_s is the weight of soil vertically above the anchor. Assuming the same shape factor for square and rectangular anchors and combining Equations 2.3, 2.6 and 2.7, the uplift capacity factor for square anchors in sand may be derived from Meyerhof and Adams' work:

$$N_{us} = 1 + \left[1 + m\left(\frac{H}{B}\right)\right]\left(\frac{H}{B}\right) 2K_u \tan\phi \qquad (2.8)$$

Vermeer and Sutjiadi (1985) considered the work of Meyerhof and Adams (1968) and the effect of soil dilatancy to suggest that a more realistic solution for N_{us} would be given by:

$$N_{us} = 1 + 2\left(\frac{H}{B}\right) \tan\phi \cos\phi_{cv} \qquad (2.9)$$

where, ϕ_{cv} is the critical state friction angle in plane strain. Murray and Geddes (1987) developed equilibrium and limit analysis methods of predicting the ultimate uplift resistance. They found that an equilibrium approach, using a curved failure surface model with $\theta = \phi/2$ would give the capacity of a circular anchor, with diameter D, as:

$$N_{us} = 1 + 2\left(\frac{H}{D}\right)\left(\sin\phi + \sin\frac{\phi}{2}\right)\left[1 + \frac{2}{3}\left(\frac{H}{D}\right)\tan\frac{\phi}{2}(2 - \sin\phi)\right] \qquad (2.10)$$

whereas a limit equilibrium approach, using a pyramidal failure surface model, will yield an upper bound solution of:

$$N_{us} = 1 + 2\left(\frac{H}{D}\right)\tan\phi\left[1 + \frac{2}{3}\left(\frac{H}{D}\right)\tan\phi\right] \qquad (2.11)$$

In each case the lower bound solution is given by the weight of the soil vertically above the anchor (= γAH) only and is thought to be invalid for practical use in design.

2.3.5 Centrifuge modelling of anchors in sand

Theories proposed in the majority of studies reviewed so far have been based on or validated by laboratory model tests conducted for small scale models at normal gravity. From the late seventies, more attention was given to centrifuge modelling applications in determining the uplift behaviour of anchors in sand. Concerns regarding scale errors associated with conventional small scale modelling were shown to be avoided in tests by Ovesen (1979), (1981) and Dickin and Leung (1983) through a modelling of models approach. This method comprises testing different sized scale model footings at varying accelerations in order to confirm that coincident prototype models give consistent results. Dickin (1988) presented results of a series of centrifuge model tests for anchors of varying aspect ratio and embedment ratio which were compared with existing theoretical methods. Centrifuge modelling was subsequently undertaken by Dickin and Leung (1990) to investigate the uplift performance of belled piers. In accordance with previous tests (Dickin, 1988) it was concluded that design methods proposed by Meyerhof and Adams (1968), Vermeer and Sutjiadi (1985), and Rowe and Davis (1982) provided the most accurate agreement with the observed results, as shown in Figure 2.10.

2.3.6 Finite element modelling of anchors in sand

Investigations reviewed up to this point have been principally concerned with experimental results of small scale laboratory tests and semi-empirical analytical models. Where it is increasingly difficult to extend the results of such studies to field

applications Finite Element Analysis (FEA) provides a useful comparison and allows consideration of many different factors which might be excluded from other analyses due to the imposed time constraints. Such investigations have been increasingly popular since the early work of Rowe and Davis (1982) which remains to the current day one of the most extensive standalone FEA studies.

Rowe and Davis (1982) considered an elasto-plastic FEA including plastic and shear failure at a frictional soil interface. Dilatancy will theoretically cause sand above the anchor to lock up during uplift and a substantial plastic region will develop before collapse can occur. This theory is explored by Rowe and Davis through the use of an associated flow rule, whereby $\psi = \phi'$, and comparison with analysis where soil deforms at constant volume. Results show the development of a large plastic region of soil above the anchor which is displaced rigidly with the anchor during uplift. It was observed that dilation was most significant for medium to dense soil where H/B is greater than about 3. The effect of dilation was also investigated by Koutsabeloulis and Griffiths (1989) who concluded that considerable increases in capacity would be observed for circular anchors in associated soil when compared to those in soil where no dilation occurred. Correction factors for the increase in anchor capacity due to dilation and roughness are presented in the study of Rowe and Davis for design purposes.

Tagaya *et al.* (1983), (1988) compared a plasticity theory solution for the uplift resistance of an anchor in sand with experimental and numerical analyses. Reasonable agreement between the results of centrifuge tests and a limited number of FE analyses reported in the study is observed. It has been shown (e.g. Dickin, 1988 and Merifield *et al.* 2006) that shape factors for circular and square anchors may be strongly influenced by soil density, yet no account is made for this in the study of Tagaya *et al.* (1988).

Most recently the advantages of using three-dimensional FEA were described by Merifield *et al.* (2006) in estimating the lower bound of N_{us} for square and circular anchors; previously best approximated as equal only to the weight of soil vertically above the anchor (Murray and Geddes 1987). In each case the lower bound is

observed to be less than 10-15% below the upper bound value predicted from companion displacement FEA for shallow embedment ratios.

2.3.7 Anchor behaviour in clay

The uplift behaviour of anchors in clay has received only limited investigation in previously published literature. As a result the number of available design methods is significantly lower than seen previously for anchors in sand and of those available, most are related to soft saturated clays for offshore applications.

Generally speaking, anchor behaviour in clay can be divided into four categories as shown in Figure 2.11; (a) a shallow anchor with no tension allowed on the underside of the anchor, (b) a shallow anchor with tension allowed on the underside of the anchor, (c) a deep anchor with no tension allowed on the underside of the anchor, (d) a deep anchor with tension allowed on the underside of the anchor. It is evident that anchor behaviour in each of these cases may vary significantly. As seen for anchors in sand the transition point between shallow and deep anchor behaviour is defined as the critical embedment ratio $(H/B)_{cr}$. For anchors in clay however behaviour is also dependant on the overburden pressure ($\gamma H/s_u$) as shown by Merifield *et al.* (2001).

This review will focus on cases (a) and (b) for shallow anchors only, thus behaviour can be categorised by either a 'breakaway' or 'fully bonded' condition. The breakaway condition will occur where the interface between the clay and the base of the anchor is incapable of sustaining tension due to pore pressure dissipation. For the breakaway condition the overall uplift capacity is in the form of Equation 2.3 (given for anchors in sand and equivalent to the drained capacity) and is determined from the mass of soil above the anchor and the shearing resistance along the failure plane (plus the weight of the anchor). The fully bonded condition may occur under rapid loading where the soil beneath the anchor is undrained and the interface is able to maintain tension due to the negative pore pressures developed. In this sense, the suction force developed is likely to be controlled by the consolidation characteristics of the clay and dependent on, among other things, loading rate. In the fully bonded case the uplift capacity is given by those components of the drained case in addition to shearing of the soil below the anchor in the form of an inverted bearing capacity mechanism,

Figure 2.11(b). In this case the capacity is of the form recommended for an anchor in uniform clay under undrained conditions, i.e. Meyerhof and Adams (1968), Vesic (1971), Sutherland (1988), given by:

$$F_u = q_{fu} A \text{, with } q_{fu} = s_u N_{uc} + \gamma H \tag{2.12}$$

where s_u is the undrained shear strength of the clay and N_{uc} is a non-dimensional uplift capacity factor for an anchor embedded in clay.

2.3.8 Ultimate uplift capacity in clay

Generally anchor capacity in clay is expressed according to Equation 2.12, presented in terms of the uplift capacity factor, N_{uc}, and the soil density. In some cases the effect of soil self weight above the anchor is superimposed after calculation of the undrained capacity and uplift resistance is given in terms of N_{uc} only. A review of anchor capacity in clay undertaken previously by Das and Singh (1994) indicated that the majority of previous investigations were experimentally based and focused predominantly on soft, saturated marine clay. In these cases a suction force, F_{su}, is sometimes assessed through comparison of uplift capacities measured where the breakaway condition is enforced and those for the fully bonded (undrained) case, thus:

$$F_{su} = F_{u(breakaway)} - F_{u(bonded)} \tag{2.13}$$

Recent investigation has conventionally taken the form of numerical finite element analysis studies where improved modelling techniques has led to a more accurate assessment of the upper and lower bounds of anchor capacity.

2.3.9 Empirical and simple analytical solutions for anchor capacity in clay

Initial investigation into the uplift capacity of anchors in clay has often been carried out as an aside from principle research into anchor capacity in sand. Theories proposed by Balla (1961), Mariupol'skii (1965), Matsuo (1967) and Meyerhof and Adams (1968) may all be broadly expressed using Equation 2.12 with corrections applied based on the results of laboratory model tests. These theories are based on shear failure conditions arising at the ultimate load state only and thus neglect the effects of the tensile properties of the soil under elastic load conditions.

It is shown in Figure 2.12 that, with the exception of Balla's model, predictions from early research are in relatively good agreement. Davie and Sutherland (1977) later suggested that the aforementioned theories would overestimate the actual uplift capacity given that large anchor displacements required for peak load and tensile stresses within the overlying soil may reduce the actual uplift capacity.

Finn and Byrne (1972) evaluated conventional bearing capacity and reverse bearing capacity for uplift and concluded that the failure surfaces developed below the footing, as shown in Figure 2.13, were comparable. This theory may be extended to shallow anchors where a full reverse bearing capacity failure may occur. Due to the effect of the overburden pressure on the failure mechanism developed at the base of the anchor the uplift capacity may be assessed simply as:

$$q_{fu} = s_u N_{uc} \tag{2.14}$$

In design, consideration should be given to the reverse bearing mechanism and how it develops during uplift of embedded shallow foundations. If the force required to achieve breakout of the foundation is greater than that required to overcome the suction developed below the foundation base then the failure mechanism may not have time to mobilise completely. Dynamic rate effects may assume an important role in increasing the initial suction at the base of the footing to a level whereby the reverse bearing mechanism is allowed to fully develop.

2.3.10 Finite element modelling of anchors in clay

As observed for anchors behaviour in sand, finite element analysis can provide useful comparison to analytical models and results from small-scale and centrifuge model tests. One of the first studies to present finite element results alongside experimental data was that of Davie and Sutherland (1977). Limitations within the program however meant that only very few results were reported and those that were are observed to be accurate only at very small strain.

One of the most rigorous finite element studies into the behaviour of anchors in clay was presented by Rowe and Davis (1982) in a companion paper to a study for anchor plates in sand. Significant differences in the limiting cases of breakaway and fully

bonded anchor behaviour are highlighted by Rowe and Davis (1982), not only in the calculated uplift capacity factors but also in comparison of the plastic regions developed at failure, Figure 2.14. Although the effect of the immediate breakaway and fully bonded conditions have been investigated as limiting cases in the undrained behaviour of anchor plates, (Rowe and Davis, 1982), (Thorne *et al*, 2004) little consideration has been given to the loading rates at which anchor behaviour moves from one failure mechanism to the other. This is considered to be of importance as anchor response in some cases, particularly for wind loading of transmission tower foundations, will lie in this intermediate loading range.

Rowe and Davis (1982) introduced a concept, termed the k_4 failure concept, to overcome the under-prediction of collapse load which was observed to be a consequence of excessive deformation due to contained plastic flow. The concept requires that the failure load is only considered to have been reached when the displacement is four times that required for an entirely elastic response. In reality this failure concept is quite arbitrary and is thought to be unnecessary for anchors that exhibit shallow failure.

It is important to note that the FEA used by Rowe and Davis (1982) and later by Merifield *et al.* (2001), (2003) are based on weightless soil models where the effect of soil density is superimposed after the initial analysis. While this method can lead to errors in predicted anchor response at shallow embedment these are not regarded by either author to be particularly significant for analyses undertaken at very small strains.

Merifield *et al.* (2001) present the results of FE limit analysis for the uplift capacity of strip anchors in clay. Only the immediate breakaway case is considered and hence results produced for uplift resistance are thought to be conservative compared to those produced in previous experimental and analytical studies. An interesting observation of the results from this study is how the overburden pressure is seen to effect the transition from shallow to deep anchor behaviour. It is concluded by Merifield *et al.* (2001) that at a given value of H/B anchor behaviour may be either shallow or deep dependant on the overburden pressure, with an increased tendency for deep anchor behaviour at high values. The presented linear relation between N_{uc} and overburden,

Figure 2.15, would also appear to support the assumption that the effect of the soils unit weight may be superimposed and hence that the use of a weightless soil model is valid. The study undertaken by Merifield *et al.* (2001) is extended to a 3-dimensionl FEA for square and circular anchors by Merifield *et al.* (2003).

Thorne *et al.* (2004) provide numerical analysis for a number of different models which may be applicable to a variety of field situations. In the case of this review it is thought that there are two such models which would be of most interest. A single phase soil model with no total stress tension allowed anywhere in the soil is suggested for field applications involving unsaturated soils where soil at the surface might be expected to fail in tension when total stress becomes negative. Perhaps a more realistic model is presented for saturated soils, a two-phase model with tensile failure allowable if the effective stress reduces to zero. Above the anchor there is no reduction in pore pressure below initial value, below the anchor reduction is permitted and there is no cavitation limit. For the first model, distributions of shear and tensile failure in the soil show that for low overburden pressure failure is caused via tensile failure of the soil above the footing and the anchor separates from the base. For high overburden ratio, separation does not occur and failure is generally controlled by shear above and below the anchor.

2.3.11 Suction force below anchors in clay

For an anchor in saturated clay the uplift capacity assessed according to Equation 2.1 will be affected by the resistance to uplift provided at the anchor base, F_{su}. During uplift the soil above the anchor is subject to compression and an increase in pore water pressure will occur in this zone. Concurrently some degree of stress relaxation will take place in the soil below the anchor resulting in a decrease in pore water pressure or the development of suction. The suction force developed below the anchor can form a significant contribution to the uplift capacity of the anchor dependant on the drainage conditions present below the anchor.

The occurrence of suction force below anchors in clay has been examined in earlier studies by Vesic (1971), Nhiem (1975) and Bemben and Kupferman (1975) but limited investigation had been undertaken to account for the factors controlling its development. Generally the magnitude of F_{su} is assessed as the difference between the

drained and undrained anchor capacity (Equation 2.13) and is given in terms of N_{uc} where:

$$N_{uc} = \frac{F_{su}}{As_u} \tag{2.15}$$

where A is the area of the anchor base, with values of N_{uc} tending to lie within the range 5-7. Baba *et al.* (1989) were among the first to investigate the effect of displacement rate on the development of suction below circular anchors during uplift. Although the results presented are fairly limited they do illustrate the increase in suction generated with increasing uplift velocity. The suction force is seen to contribute approximately 50% of the ultimate resistance at the highest uplift velocity, although the observed trend suggests that further increases in suction would be obtained at even higher rates of uplift (i.e. the soil is not behaving in a fully undrained manner), Figure 2.16.

The existence of a 'mud suction force' developing below anchors during uplift was highlighted by Das *et al.* (1994) and Shin *et al.* (1994). Suction force was assessed by comparison of the uplift capacity of circular anchors embedded in kaolin clay with those where the anchor was placed over a plastic pipe to eliminate suction. Das *et al.* (1994) observe that the magnitude of N_{uc} decreases with increasing embedment ratio although no explanation of this is offered in their paper. It is thought that the observed reduction may come as a result of the transition from shallow to deep anchor behaviour whereby some of the available suction may be relieved by local failure of the clay around the anchor. In this instance a comparison with an anchor placed on a plastic pipe may not be a valid one given the potential interference of the pipe with the developing failure mechanism. This potential limitation is negated by Rao and Datta (2001) who use a fully vented model anchor to enforce the immediate breakaway condition. As seen in the results of their study, far less reduction in N_{uc} is observed with increasing embedment ratio (although the effect is evident). From the study a value of N_{uc} of approximately 6, assessed for anchors at shallow embedment is higher than that reported by Das *et al.* (1994). The reasonably low values observed by Das *et al.* could be attributed to the experimental method used in their study; the tests being

stress rather than strain controlled may have led to the partial dissipation of some rapidly generated negative pore pressure.

In 2002 a study into the determination of dynamic resistance of transmission tower footings to uplift using centrifuge modelling techniques was undertaken (Richards, 2002). The report assessed uplift capacity under conditions of fast pull out and involved, in part, the direct measurement of negative pore water pressure at the base of the footing. Although some problems were encountered with the measurement of base suctions, the results highlight the contribution of a significant suction force corresponding to peak uplift resistance, as seen in Figure 2.17. Results for rapid tests normalised by capacities measured for tests at slow uplift rates yield factors ranging from 1.4-3.9 times the observed capacity.

The only available published data for direct measurement of suction developed below field scale shallow foundations is presented by Yazdanbod *et al.* (1987). Data from this study clearly shows that suction is a significant component of the short term uplift capacity however the suction force does not reach its maximum value until the displacement of the footing is roughly 150mm (approximately 10% of the footing width). Tension effects arising from volumetric expansion of the soil may well dissipate at large displacements and hence it could be inferred that the degree of volumetric expansion is a limiting factor in the generation of suction force at large displacement.

2.4 Rate Effects in Soil

In tests to determine values of shear strength, a timescale ranging from several minutes to a few hours can be required for the stress differential leading to failure to be reached. This may extend to several days for drained tests. In field applications for transmission tower footings rapid load conditions may arise whereby the rate at which shear stress increases can be very much faster and the influence of the rate of loading on the shear strength of soil is of practical concern.

2.4.1 Rate effects in clay

Laboratory and field tests for clay soils are generally carried out under undrained conditions where no volume change takes place and pore water pressures can vary, but not dissipate. Under long term static loading conditions, drainage of pore water occurs during consolidation and loading and no build up of pore water pressure occurs. Long term stability is assessed in terms of effective stress and is governed by the drained strength of the soil.

Short term variable loading which can be encountered by transmission tower structures is usually opposed by the un-drained shear strength of the soil surrounding the foundation and rate effects become apparent in circumstances when soil is loaded very rapidly.

2.4.2 Rate dependency in triaxial compression

The triaxial compression test was developed by Casagrande in 1930 in order to overcome the disadvantages of the direct shear test and is arguably the most widely used test to determine shear strength of soils. The key advantages of the test are that the drainage conditions can be controlled reasonably well and there is no rotation of the principle stresses during shear. Also, the failure plane may occur anywhere within the sample. It has already been seen that many design methods relating to the uplift of shallow foundations assume failure planes which are inclined by some function of ϕ' to the vertical. Such failure surfaces are broadly similar to those developed in a triaxial test sample and as such the influence of increasing strain rate on the development of these failure surfaces (and the related increases in undrained strength) are particularly relevant to these design methods. In the conventional test, a cylindrical soil sample encased in a rubber membrane is situated in the triaxial chamber, subjected to a confining pressure then axially loaded to failure. The time to failure (t_f) of the test may be reduced by applying increased rates of axial loading and it is such tests, undertaken to investigate soil behaviour under rapid loading, which will be considered in the following review. A special case of the triaxial test is the unconfined compression test during which axial load is applied to the sample, with no rubber membrane, under zero confining (atmospheric) pressure. Results from investigations involving such tests (e.g. Casagrande and Shannon, 1949) are discussed later.

The rate dependent stress-strain behaviour of saturated clays has been studied extensively since preliminary research into the compression strength characteristics of soil (Taylor, 1943). Taylor tested samples of remoulded Boston Clay to failure at timescales ranging from 4 minutes to 8 days and found that the strength of a sample was 25% greater for rapid loading than for a sample loaded slowly. Further examination undertaken by Casagrande and Shannon (1949) involved unconfined compression tests on Cambridge Clay and are shown in Figure 2.18 to have resulted in shear strengths for dynamic tests (t_f =0.02 s) of roughly twice the strength for the static test (t_f =465 s). Stress-strain curves produced in the study also show that Cucaracha Shale exhibited a 60% increase in strength as time to failure was decreased from 1000 to 0.05 seconds. The investigation also assessed the impact of the axial strain rate ($\dot{\varepsilon}_a$) on the stiffness of the soils. Consolidated-undrained triaxial tests, where the specimen is allowed to consolidate under hydrostatic pressure but no drainage of pore water occurs during axial loading, on Cambridge Clay showed that the stiffness recorded under dynamic loading was about twice the value for static loading. This relationship has important implications for design criteria involving rigorous serviceability limits and is discussed in more detail later with regard to further undrained triaxial testing (Chapter 4).

Casagrande and Wilson (1951) brought together experimental findings from earlier studies of the strength characteristics of clays and shales under rapid loading with investigations into the effect of slow rates of load application (Casagrande and Wilson, 1949). The latter had shown that some types of undisturbed clay and shale would creep under a sustained load, and ultimately fail at a load appreciably less than the strength indicated by conventional compression tests. Two types of test were investigated; creep strength tests, where the load is built up rapidly and maintained until failure and long-time compression tests, where the specimen is subjected to incremental axial loading. The results obtained from creep strength tests for samples of Cucaracha Clay during the study were correlated with results produced from dynamic testing (Casagrande and Shannon, 1949). The strength ratio for the clay is shown in Figure 2.19 and is observed to vary between approximately 0.25 for the slowest loads and up to 2 for rapid loading conditions. It was concluded in the paper, that at constant water content, sustained loading reduces the strength of fully saturated

brittle clays and clay-shales. However, it is also stated that the strength of compacted and undisturbed soils which are not fully saturated can be seen to increase with time, even when the water content is kept constant. It should be noted however that even at unchanged water content, there is a redistribution of water content within the sample itself, which may change its strength characteristics in a way not representative of effects in a large mass.

For the interpretation of strain-rate studies involving triaxial tests using restrained ends, stress-strain non-uniformity throughout the sample is a potential source of disparity between studies. When the sample is deformed axially, radial strains are created which, due to restraint, become larger at each end of the sample and lead to significant changes in shear stresses in these regions (e.g. the "dead zones" described by Rowe and Barden, 1964). This non-uniformity may have a significant effect on the measured variation in pore pressure, particularly for overconsolidated clay where a large pore pressure difference may be observed between the middle and the ends of the sample. This difference will in turn lead to pore water migration within the sample and a true indication of the undrained shear behaviour will not be obtained. A large proportion of earlier studies (e.g. Bjerrum *et al.* 1958) had proposed that increases in strength at high strain rates may be caused by a change in the excess pore pressure generated during shear. It should be noted that for these early investigations, measurements of pore pressure during undrained shearing were taken from the base of the sample and while the magnitude of undrained shear strength is valid the measurement of pore pressure and thus the observed effective stress-strain behaviour may not be entirely accurate.

Richardson and Whitman (1963) investigated the internal migration of pore water by observing the change in water content distribution during shear using probes inserted into the middle third of the sample. Results from the investigation show that at low strains ($\varepsilon_a < 0.5\%$), the shear strength could be doubled for a reduction in time to failure from 500 minutes to 1 minute. Pore pressure measurements for these low strain rate tests indicate that the pore pressure response tends to slight increases, although remaining unchanged in some cases. For that reason, the increased resistance observed is concluded to have resulted from a higher principle effective stress ratio

(σ'_1/σ'_3). At larger axial strains ($\varepsilon_a < 5\%$) the stress ratio was found to be essentially independent of strain-rate and the increase in undrained shear strength recorded at higher strains was much less significant. Results showed that once the strain rate increases, the water content of the specimen remains constant. The resulting (post dynamic increase) development of negative pore water pressure would appear to reflect the effect of strain rate upon pore pressure at constant volume. On the basis of these observations it is clear that the changing pore pressure response is of equal concern to strain-rate effects leading to increased shear strength in clay.

During the decade 1965–1975 research into strain-rate effects for cohesive soil was largely directed towards creep during drained and undrained loading and the literature concerning creep effects is extensive. While the study of creep effects is not a direct focus of this research, and as such will not be considered in any significant detail beyond the attention already paid to the work of Casagrande and Wilson (1951), results have been shown (Vaid and Campanella, 1977) to support a correspondence between undrained creep and constant strain rate data. This relationship has important implications in unified stress-strain-time constitutive models and the principles of visco-plasticity as a means for modelling strain rate effects and is discussed later.

Perhaps the most prolific study concerning the influence of strain-rate on stress-strain behaviour was undertaken by Graham *et al.* (1983) who tested a variety of lightly overconsolidated natural soft clays in triaxial compression at increasing strain-rates. Results presented by Graham *et al.* are shown in Figure 2.20 and demonstrate increases in the undrained shear strength ratio between 9% and 20% for a 10 fold increase in strain-rate. A strain-rate parameter ($\rho_{0.1}$) defined as the percentage increase in shear strength caused by a log-cycle increase in strain rate above 0.1 %/hour was presented by Graham *et al.* (1983) based on the results of their study. In general this type of relationship, where a reference undrained shear strength at a certain strain rate is specified has proved popular in subsequent investigations and is a useful means by which to relate the strain-rate dependence of a given soil. Cross analysis of results from Richardson and Whitman (1963) indicates that strain rate effects should become more pronounced with increasing overconsolidation ratio for remoulded clays. It is observed by Graham *et al.* (1983), as shown in Figure 2.21, however that for natural

clays the overconsoildation ratio appears to have no appreciable influence on the value of $\rho_{0.1}$ observed in triaxial compression tests.

Up until the late 80's the majority of studies involving strain rate effects in triaxial tests had focused on strain rates in the region 0.001–100 %/hour. Investigation into strain rate effects in the cyclic loading of a range of sensitive soils (Lefebvre and LeBoeuf, 1987) included stress-controlled triaxial compression tests with strain rates of up to around 6000 %/hr. Strain rates varying from 0.05–132 %/hr were also used in strain-controlled compression tests with the results comparing favourably to results from previous studies (an average increase of approximately 10-15 % per log cycle increase in strain rate). This is also true of later cyclic loading tests using direct simple shear apparatus undertaken by Lefebvre and Pfendler, (1996) where equivalent increases of approximately 12% per log cycle were observed at high strain rates associated with cyclic testing.

Sheahan *et al.* (1996) tested samples of re-sedimented Boston Blue clay with overconsolidation ratio (OCR) between 1 and 8 at axial strain rates in the range of 0.005 to 50 %/h. It was observed that for the slowest rates of loading the increase in OCR causes a consistent decrease in the rate sensitivity of the undrained strength. This is not true for the highest strain rates where, as evidenced by Graham *et al.* (1983) no change occurs in rate sensitivity with increasing OCR. It is also observed that the strain rate at which the clay becomes rate insensitive appears to increase with increasing OCR. Between the highest strain rates, the increase in undrained strength across one log cycle increase in strain rate is shown in Figure 2.22 and was observed to be equal to approximately 9.5% ± 2. It is also apparent from the investigation that the increase in shear strength at OCR = 4 and 8 is due to a decrease in the excess pore pressure measured during shear as the effective stress envelope at the peak strength is rate independent for these values. This would appear to be in agreement with the observations of Richardson and Whitman (1963). In order to reduce the effect of non-uniformity within the sample, as discussed earlier, Sheahan *et al.* (1996) used enlarged, lubricated end platens and mid-plane pore pressures were measured during testing. For each value of OCR used in the study the undrained shear strength of the clay (s_u) was well represented by the equation (Ladd and Foott, 1974):

$$\frac{s_u}{\sigma_v'} = S.OCR^m \qquad (2.16)$$

where S is the normally consolidated undrained strength ratio $(s_u/\sigma'_v)_{nc}$ and m is an exponent which represents the increase in strength.

2.4.3 Elastic viscoplastic modelling of rate dependent behaviour

Conventional plasticity models are independent of time and require adaptation in order to allow for rate dependent effects. In-viscid plasticity models modified to accommodate a plastic response as a function of time are referred to as viscoplastic soil models. Japanese researchers were among the first to realise the importance and applications of modelling principles such as viscoplasticity. Yong and Japp, (1969), and Akai *et al.* (1975) proposed unified constitutive methods incorporating both undrained creep and constant strain rate effects which had previously only been considered separately. It was a further five years before stress-strain-time constitutive models became increasingly popular as a method for modelling strain rate effects and the majority of earlier models (e.g. Adachi and Oka, 1982; Borja and Kavazanjian, 1985; and Kutta and Sathialingham, 1992), were based largely on the elastic-viscoplastic framework of Perzyna (1963), (1966). The majority of these studies had focused primarily on modelling one-dimensional straining in oedometer tests. Yin and Graham (1989, 1994) defined concepts, including equivalent time, in developing a constitutive model for one-dimensional applications. These concepts were later expanded to focus on time dependent stress-strain behaviour under triaxial stress states (Yin and Graham, 1999) using a framework based on the Modified Cam-Clay model. Yin and Graham verified their model using data from triaxial tests on samples of a bentonite clay mixture subjected to strain rates of between 0.036 and 9.4 %/hr. Predictions for the model are shown in Figure 2.23 and are seen to be in reasonable agreement with measured results indicating that the effects of shearing rate, relaxation and excess pore water pressure may all be adequately predicted through use of an appropriate EVP model.

2.4.4 Rate effects in granular Soil

Field tests for granular soils are generally carried out under drained conditions as the increased permeability of such soils denotes that pore water can drain very quickly during loading. The undrained behaviour of granular soils can be investigated in laboratory tests where the rate of loading is increased to speeds which exceed those at which water is able to drain, or by prohibiting drainage from the sample. The shear strength of sand is commonly given as:

$$\tau = \sigma' \tan \phi' \qquad (2.17)$$

Granular material is generally considered to be non-viscous but has been shown to display a degree of time dependent behaviour under certain circumstance. Enhanced shearing resistance of sand at increased rates of loading could be accounted by either a significant increase in the effective angle of friction or a decrease in the pore water pressure and hence an increase in the effective stress of the soil (assuming a constant normal stress). It is well documented that water is much more viscous than soil and doubling the shearing rate of water will lead to double the water shear strength and saturated sands can generate negative pore pressures under dynamic loading, just as with clays. These pressures arise from dilation during shear being resisted by the pore water, where small changes in volume are seen to result in large changes in pressure.

A substantial body of literature relating to the time dependent behaviour of granular soil exists, relating mainly to creep phenomena, in both one dimensional compression (Yamamuro *et al.* 1996), and triaxial conditions (e.g. Lade, 1994 and Lade and Liu, 1998). As stated previously for cohesive soil, the creep behaviour of soil, though related to constitutive modelling for time dependent soil behaviour, is not in direct relation to the focus of this research and such, for brevity, is not reviewed herein.

Among the first studies of the dynamic loading of sand formed part of an investigation into the strength of soils under rapid loading (Casagrande and Shannon, 1949). Results from triaxial compression tests undertaken on Manchester sand showed only slight increases (approx. 10%) in the strength of the sand when the time to failure was reduced from 10 minutes to 0.02 seconds. The modulus of deformation (stiffness) of the sand, found to be significantly higher for clay at fast rates, was observed to be

independent of time of loading. The dynamic loading of saturated sands was further investigated by Seed and Lundgren (1954) for a variety of coarse and fine sands with differing relative densities. The strength of dense sands during dynamic loading (t_f =0.02 s) was observed to be roughly 20% greater than that measured strengths for static tests (t_f =10-15 min). A large proportion of this increase was concluded to be due to dilation induced negative pore pressures generated during dynamic loading.

2.4.5 Dilation effects in saturated sands

It is noted earlier in this review that small changes in pore water volume can result in large changes (decreases) in pressure. If this relationship were to occur directly in saturated dense sands, the pore water pressure decreases could become extremely large indeed. Such large decrease in pore pressure is not however recorded to occur during reported investigation where strain rates are large enough for this to be theoretically possible (Seed and Lundgren, 1954). The reason for this is that as pore pressure drops to the vapour pressure of water cavitation occurs and the sample is free to expand. Cavitation generally occurs during undrained shear of most dense saturated sands and the pore pressure developed is dependent on the vapour pressure of the pore water. Results produced for shear tests on dense saturated sand (Whitman and Healy, 1962) displayed only very small variation in friction angle ($< 1^{o}$) as time to failure for the tests was decreased. It was observed during these tests that cavitation occurred regardless of the strain rate and hence pore pressure was dependant only upon the vapour pressure and remained unaffected when reducing time to failure. The strength of saturated loose sands however, was found to be dependent upon the time to failure and for the samples of Ottawa Sand tested, the compressive strength shown in Figure 2.24 increased by roughly 40% for a reduction in time to failure from 5 to 0.025 seconds. This increase is attributed to rate dependency of excess pore water pressures in helping to suppress the volumetric expansion of the sands during shear. Later investigation undertaken by Whitman and Healy (1963) showed that, on the basis of effective stress, the strength of saturated sand increased by approximately 10% for dynamic tests. This increase was attributed to an increased propensity to dilation with increasing strain rate, a theory which was supported by data from torsion shear tests.

The tendency for saturated sand to dilate under dynamic loading conditions is clearly a key factor in the increased resistance at high strain rates in drained and undrained

conditions. Lee *et al.* (1969) considered the effects of confining pressure on loose and dense, dry and saturated soils. At low pressures, such as those used in other studies reported thus far (e.g. Casagrande and Shannon, 1949; Seed and Lundgren, 1954; and Whitman and Healy, 1962 & 1963), dilation in loose sand will usually be minimal. For dense sand however, considerable dilation will typically be observed during shear (e.g. Seed and Lundgren, 1954). Results from static shear testing have shown that the propensity for dilation will reduce with increasing confining pressure. Lee *et al.* (1969) presented an overview of the components of shear strength with increasing confining pressure, shown in Figure 2.25, which was based on drained triaxial compression tests at slow rates of strain. At lower confining pressure the dilatancy component of strength is significant during shear reducing however as the confining pressure is increased and the soil particles begin to crush and rearrange themselves. In tests to investigate the effect of strain rate and confining pressure on loose and dense sand, Lee *et al.* (1969) report up to 20% increase in strength for dense sand at high confining pressure compared to less than half this value at low confining pressure. The larger increase is concluded to be mainly a consequence of increased energy for particle crushing at high strain rate. Increases in strength at low pressure are in accordance with those observed by Whitman and Healy (1963) and as such are thought to be entirely due to increased dilation at high rates of strain. Minimal increase in the strength of loose sand was reported for test at all confining pressures.

Yamamuro and Lade (1993) reported results from drained and undrained triaxial compression tests at high confining pressure on dense Cambria sand. Results from undrained tests indicate an approximate 7% increase in strength with increasing strain rate. In accordance with the assertions of Lee *et al.* (1969) it is thought that at higher strain rates, more energy is required for particle crushing and rearranging, corresponding to an increase in the strength of the sand. This theory is potentially validated by results from Yamamuro and Lade (1993) where higher pore pressures were observed at lower strain rate, these being a consequence of the tendency for increased volumetric compression (where particle rearranging is less restricted) resulting in increased pore pressure in the undrained case.

It would appear from the above that the magnitude of strain rate is of great importance in the time dependent behaviour of granular soil. Whereas for cohesive soil, it is

generally evident that increases in strain rate, even at low orders of magnitude, result in increased strength, for sand it would appear that a failure mechanism resulting in increased strength is only mobilised at very high rates of strain. This assessment is obviously slightly different for saturated sand where viscous resistance and dilatancy are apparent.

2.5 Summary

2.5.1 Uplift of shallow foundations

A number of proposed design methods published from previous investigation have been reviewed and general comparisons drawn between the studies. The large majority of reported investigations are principally concerned with design methods for modelling the behaviour of anchors in sand. These methods are largely based on empiricism and supported by theoretical analysis involving limit equilibrium concepts (e.g. Balla, 1961; Meyerhof and Adams, 1968; Murray and Geddes, 1987 and Dickin, 1988). In general, the methods proposed from a large proportion of studies involve the use of arbitrary assumptions regarding the failure surface mobilised above the anchor during uplift. In general these assumptions regarding the shape of the failure surface have been seen to be split into three categories; the vertical failure surface, curved failure surface and inverted truncated cone surface, with the latter being the most prolifically used in previously published studies.

Commonly applied models for the uplift capacity of anchors in sand are presented in terms of an uplift capacity factor, N_{us} given in equation 2.3. As discussed previously N_{us} is dependent upon the embedment ratio (H/B) and the point of transition between shallow and deep anchor behaviour is termed the critical embedment ratio $(H/B)_{cr}$. Uplift capacity factors given in previous studies for square and circular anchors are compared well by (pre 1989) Frydman and Shaham (1989) as shown in Figure 2.26 and Ilamparuthi et al. (2002) as seen in Figure 2.27.

In contrast, the uplift behaviour of anchors in clay has received less attention in previous research. A significant number of phenomena involving the failure

mechanism for such anchors including the failure surface, tensile and shear failure zones and breakaway condition have, for the most part, yet to be rigorously modelled and as such are open to further research. A comparison of experimental factors for anchor capacity in clay is presented by Rao and Datta (2001) and shown in Figure 2.28. More recently research into foundation behaviour has involved finite element modelling methods (e.g. Rowe and Davis, 1982; Merifield et al. 1999 and 2003 and Thorne et al. 2004). Results from these studies appear to show an increased uniformity of trends and that supplementary experimental investigation could be usefully undertaken to quantify these theoretical results and their implications with regard to transmission tower foundations.

A comparison between the uplift capacity factors calculated from existing published design methods and those predicted from preliminary total stress finite element analysis is presented in Chapter 3.

2.5.2 Rate effects in soil

Rate effects have been shown to be of significant importance to the shear strength of a range of soils. These effects are particularly important for applications involving fine-grained soils and clays have been seen to exhibit increases in strength of up to 100% for large reductions in strain rate. The literature concerning such phenomena is extensive and much investigation has been done on a wide variety of clay and granular material during the last 60 years. The primary means of such research has been that of drained and undrained triaxial compression tests utilising a range of loading methods including constant rate of strain, relaxation and stepwise strain change. Interpretation of triaxial test results has been discussed with regard to sample uniformity and distribution of pore pressures during undrained shear. The overconsolidation ratio of fine-grained soil has been observed to be of considerable importance to the strain dependent behaviour and heavily overconsolidated clays are thought to be far more sensitive to increased rates of loading. The critical state line of the strength envelope for cohesive soils would appear to be independent of rate effects. In general the undrained strength increase for increasing strain rate due to viscous effects observed in a number of studies is accepted to be in the order of 10-15% per log cycle strain rate. The strain-rate influence on the undrained shear strength of fine-grained soils

(pre 1990) was comprehensively reviewed by Kulhawy and Mayne (1990) and is well illustrated in Figure 2.29.

Rate effects have been seen to be far less significant for granular soils although it has been observed in a variety of studies that the effect is not negligible, especially in the case of fully saturated sands. Differences in strength between dry and saturated sand have been observed to be as much as 60% at high strain rates, an increase which is attributed in the available literature to viscous effects in pore water, increased energy demand for particle crushing and rearranging and a higher tendency for dilation, especially in dense sands at lower confining pressure. The strain rate behaviour of sand is principally influenced by density, saturation and confining pressure.

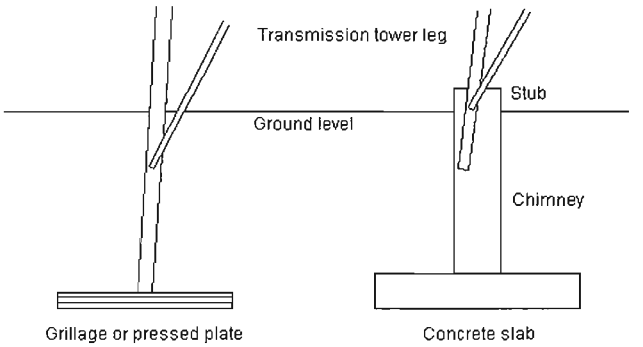

(a) Spread foundation

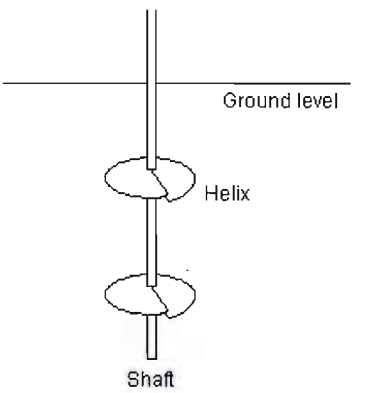

(c) Helical foundation

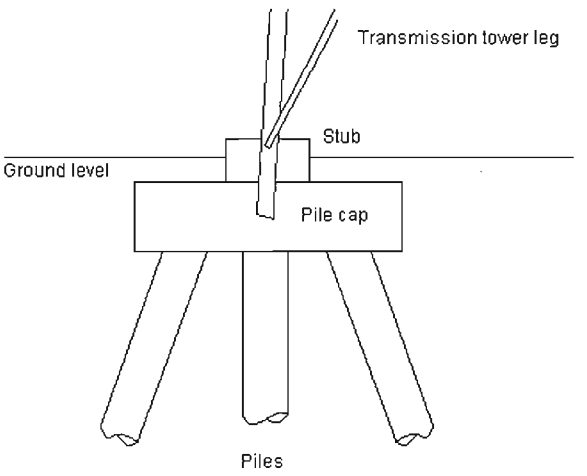

(b) Piled foundation

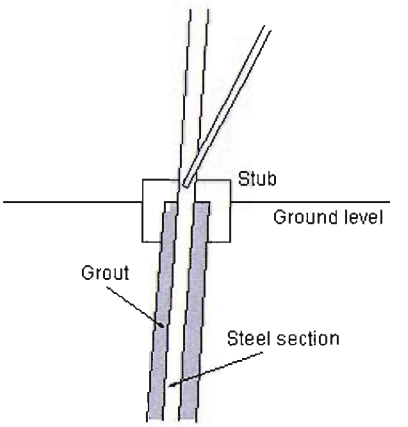

(d) Grouted foundation

Figure 2.1 Transmission tower foundation types

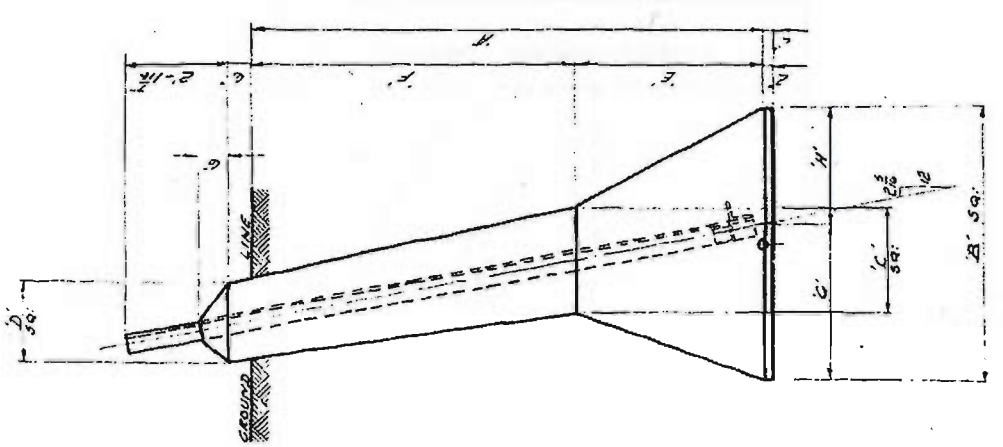

Figure 2.2 Pyramid and chimney type transmission tower footing

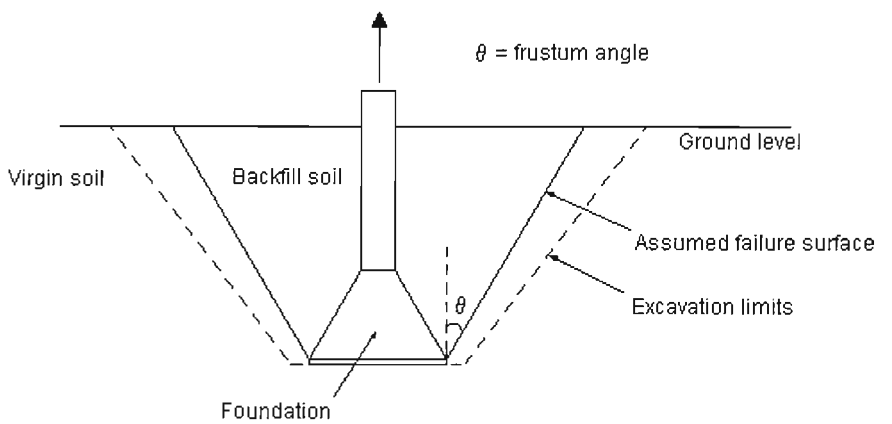

Figure 2.3 Frustum design method geometry

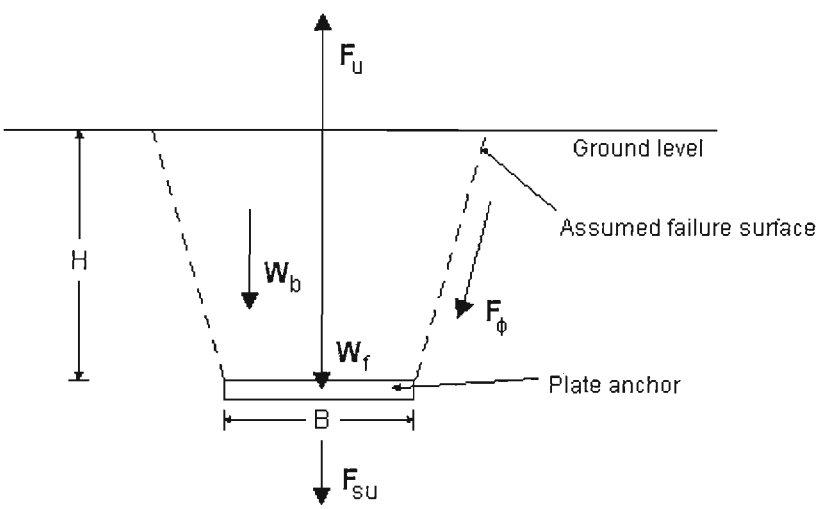

Figure 2.4 Plate anchor equilibrium conditions for uplift

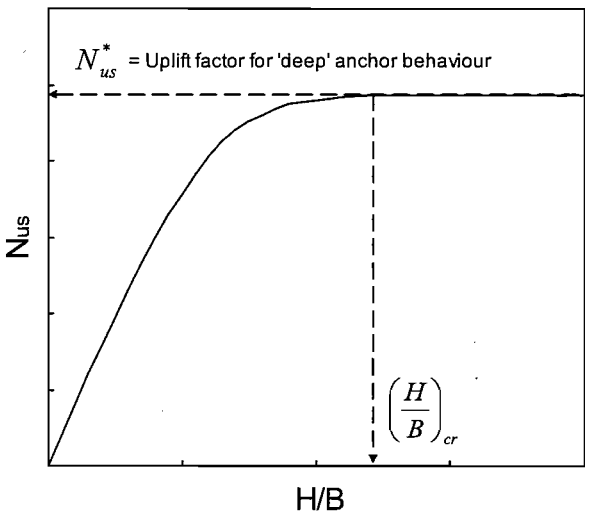

Figure 2.5 Theoretical variation of N_{us} with H/B

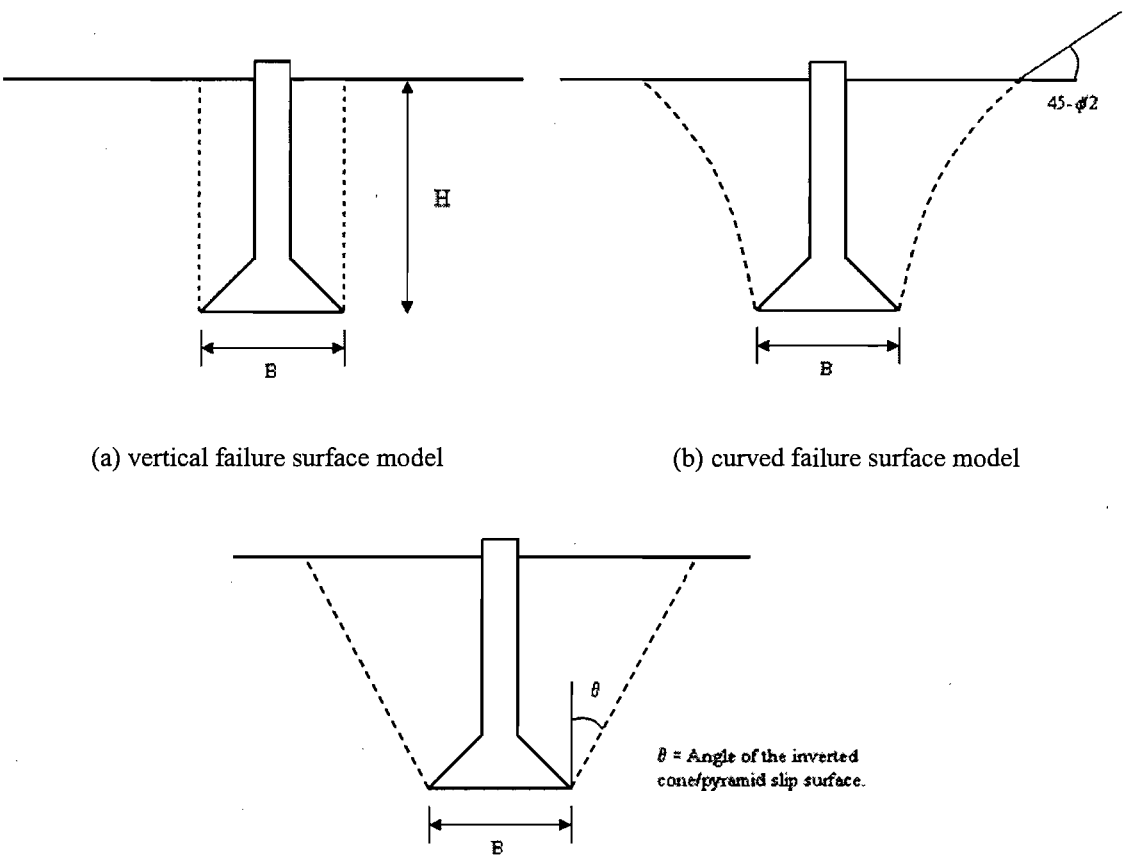

(a) vertical failure surface model

(b) curved failure surface model

(c) inverted truncated pyramid failure surface model

Figure 2.6 Assumed failure surface models for shallow foundations in uplift

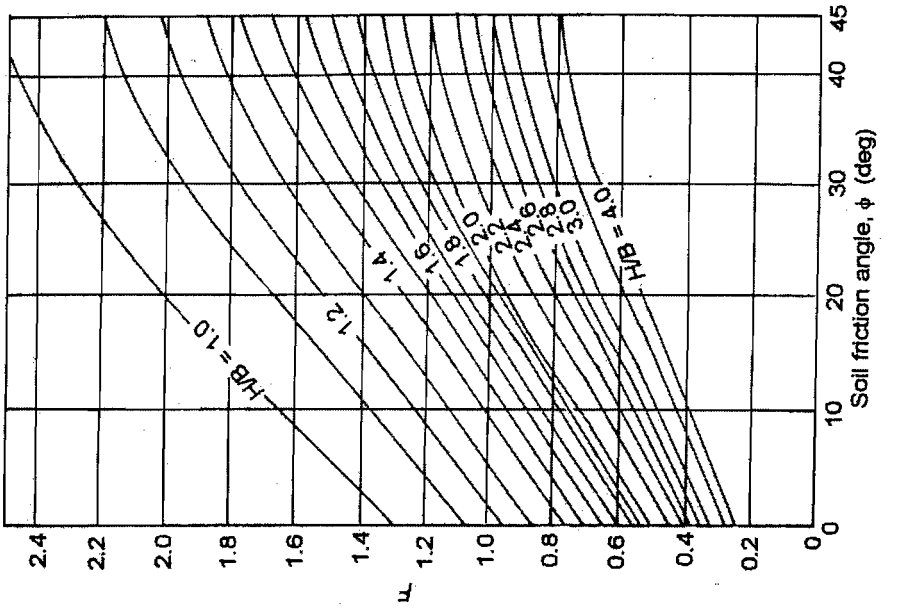

Figure 2.7 Variation of F with H/B and ϕ for shallow foundations in sand (Balla, 1961)

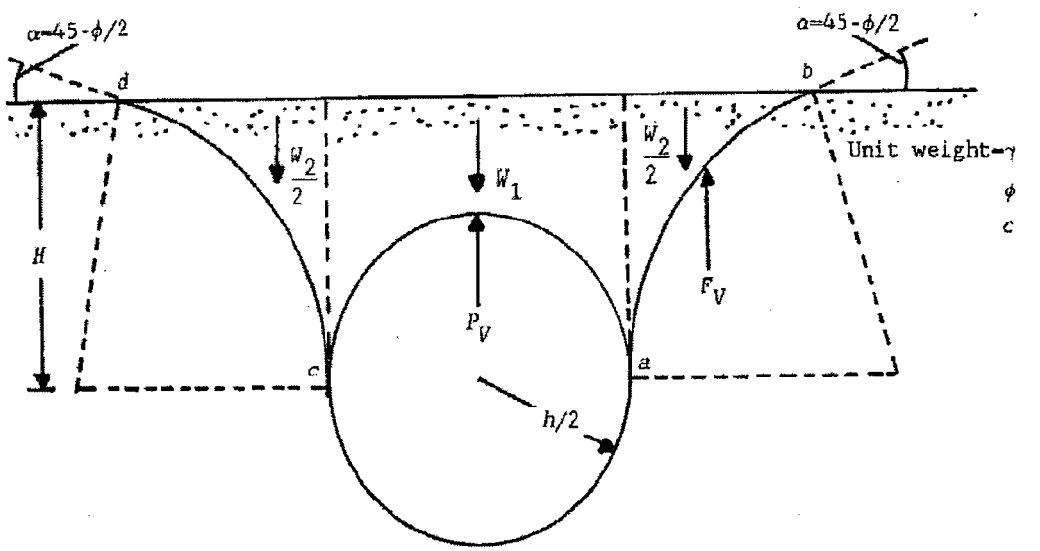

Figure 2.8 Equilibrium conditions for Vesic's (1971) cavity expansion method

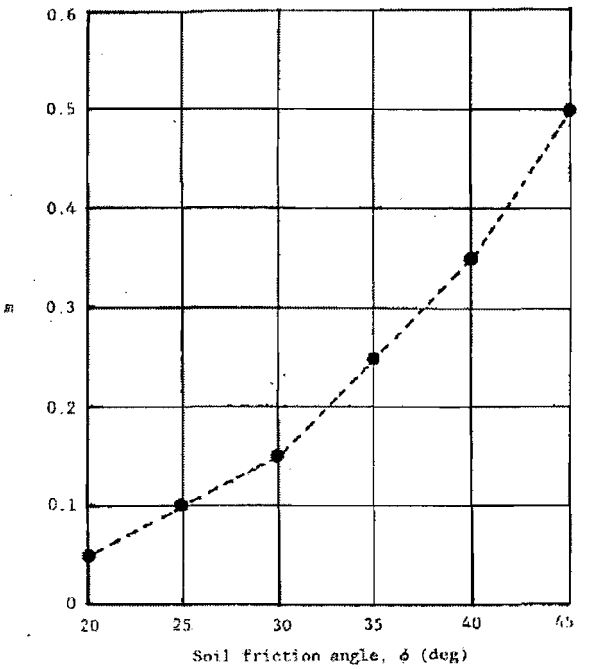

Figure 2.9 Variation of the anchor shape parameter m with ϕ (Meyerhof and Adams, 1968)

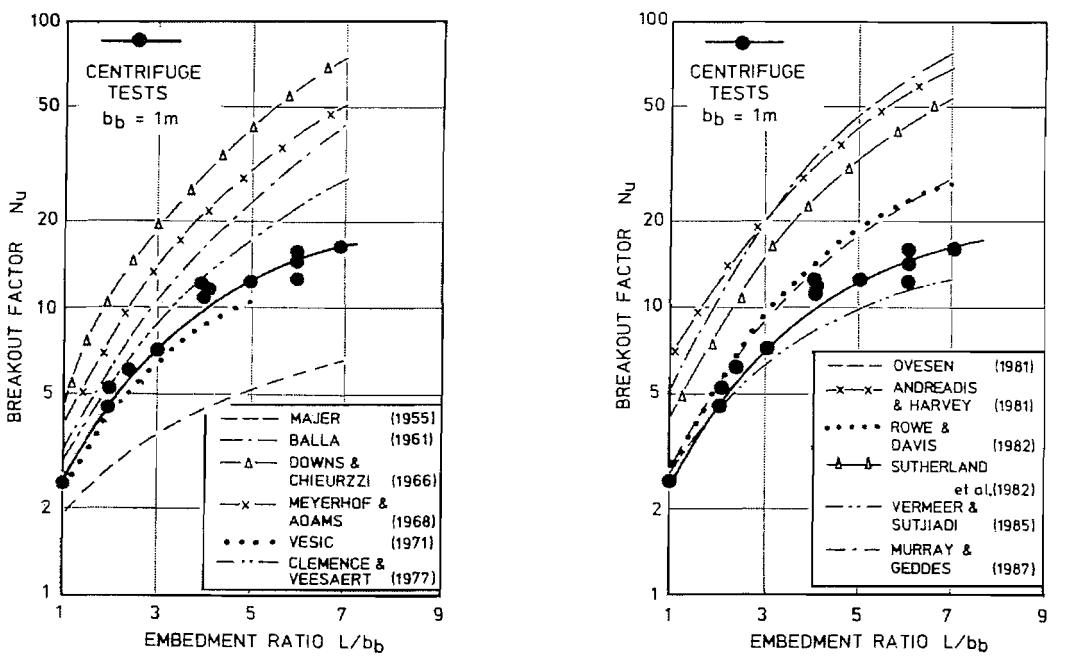

Figure 2.10 Comparison of the results of centrifuge tests on belled piers with other theoretical methods (Dickin and Leung, 1990)

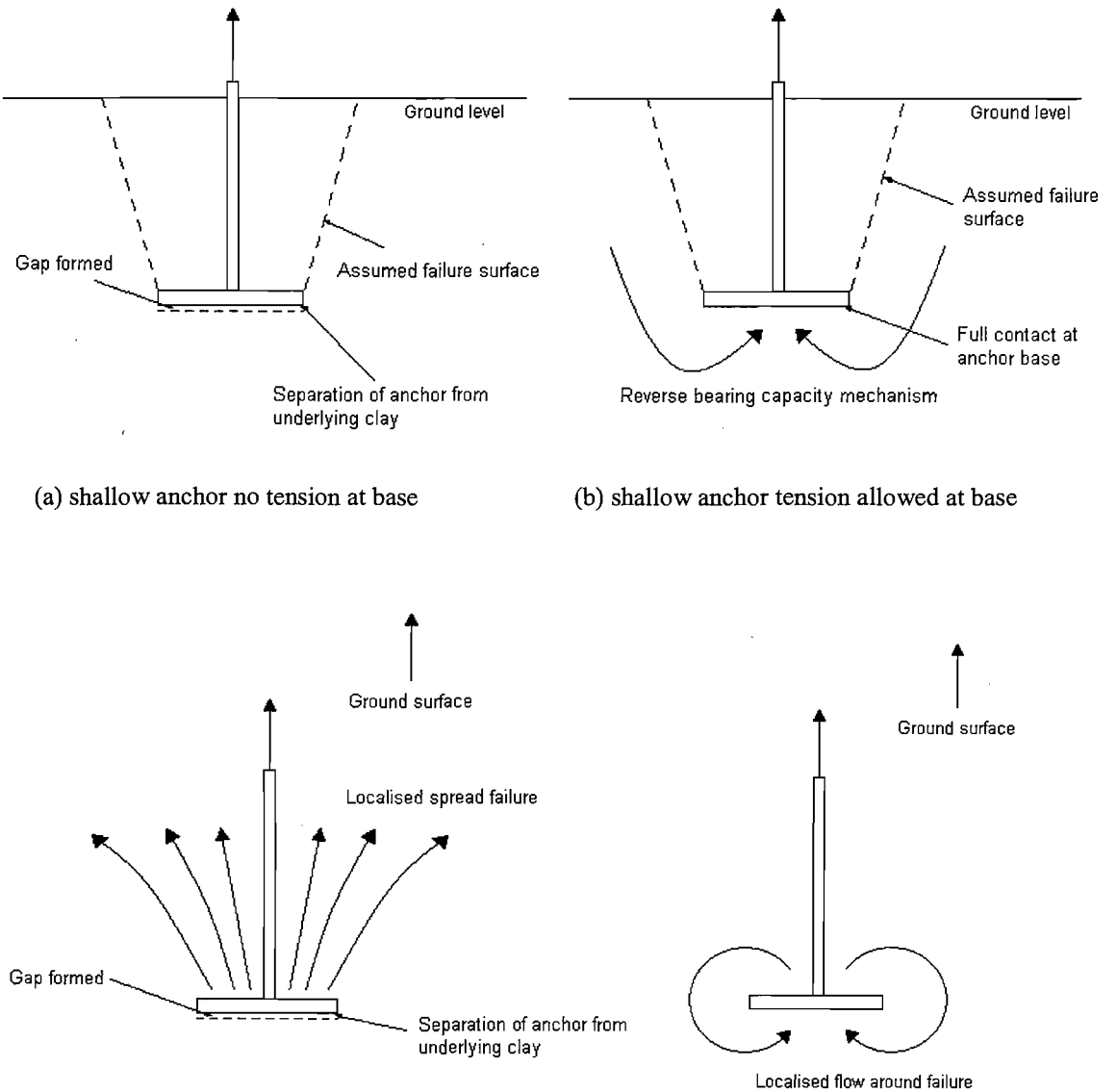

(a) shallow anchor no tension at base

(b) shallow anchor tension allowed at base

(c) deep anchor no tension at base

(d) deep anchor tension allowed at base

Figure 2.11 Uplift failure mechanisms for anchors embedded in clay

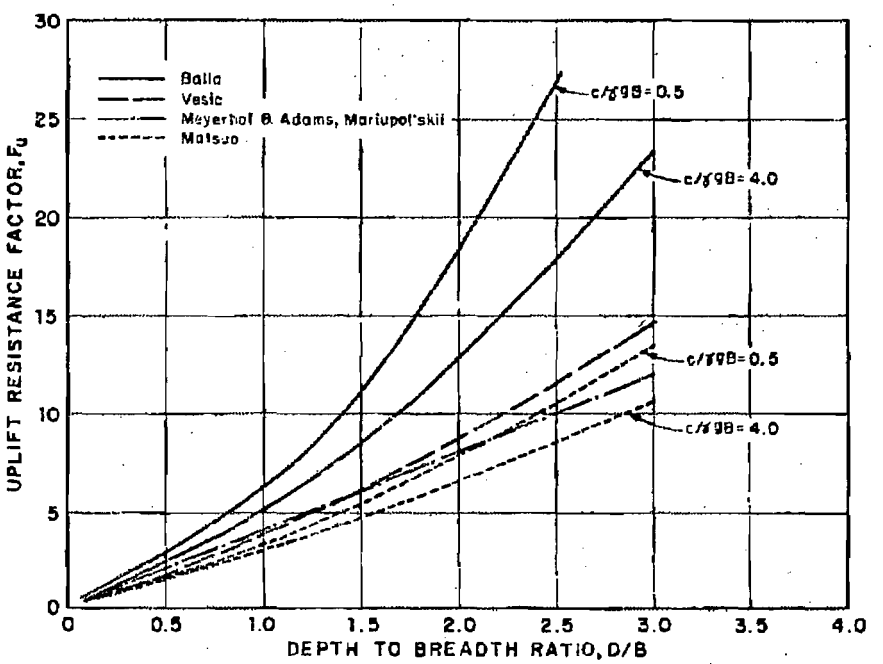

Figure 2.12 Comparison of shallow anchor theories for uplift in clay (Davie and Sutherland, 1977)

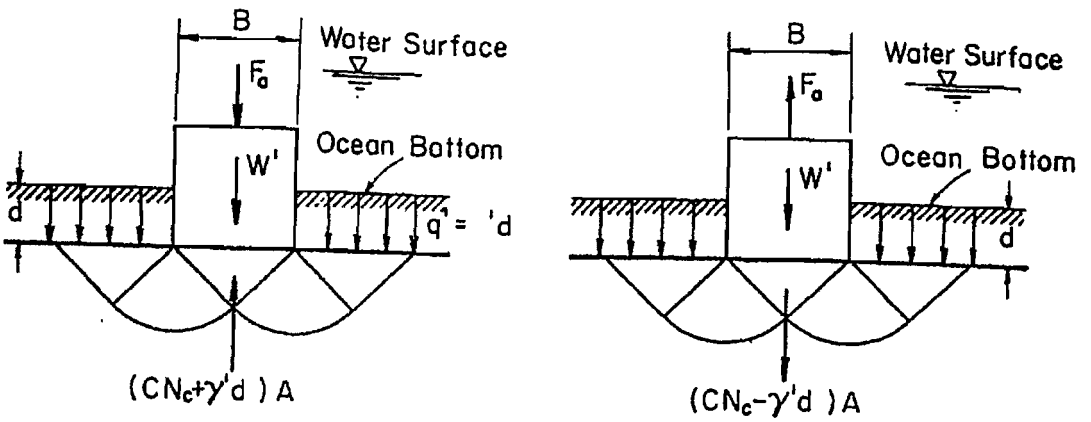

Conventional bearing capacity failure

Uplift capacity failure

Figure 2.13 Failure mechanisms for bearing and uplift of shallow embedded foundations in clay (Finn and Byrne, 1972)

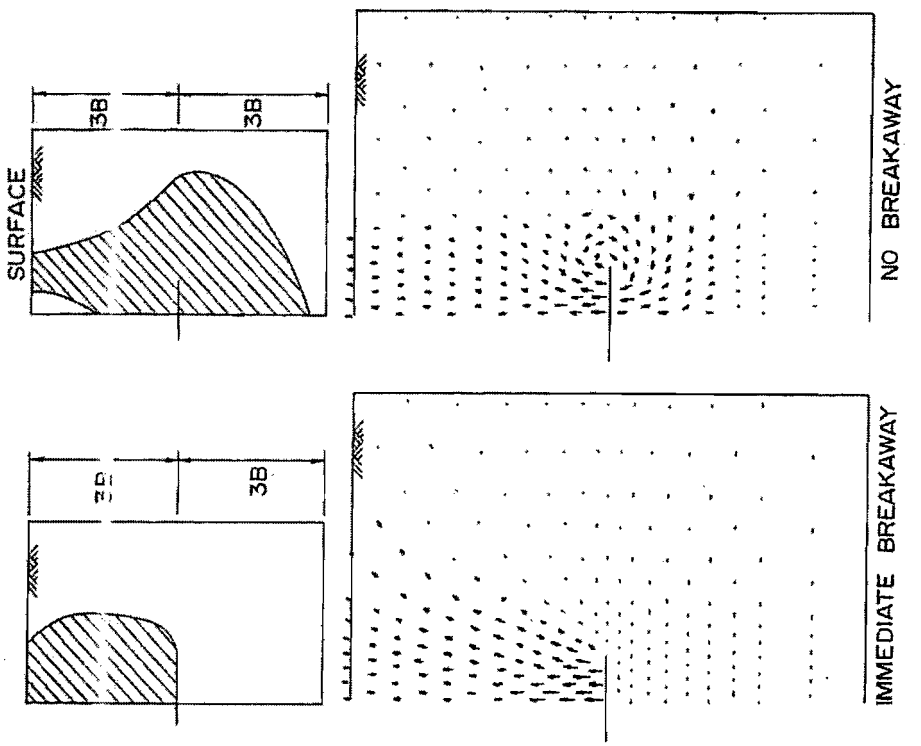

Figure 2.14 Plastic regions developed at failure for breakaway and fully bonded anchor behaviour (Rowe and Davis, 1982)

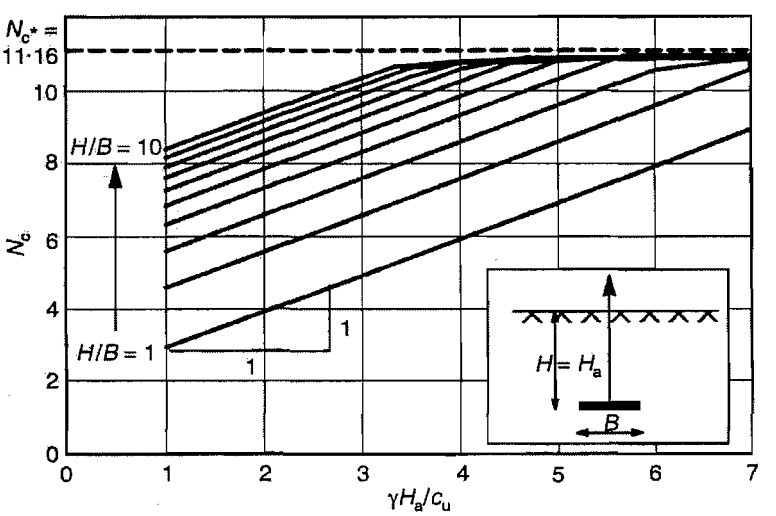

Figure 2.15 Variation of N_{uc} with overburden pressure for anchors in clay (Merifield et al. 2001)

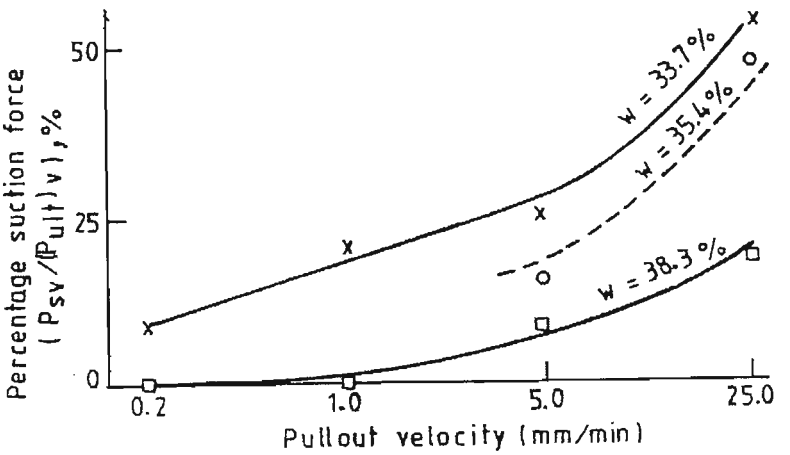

Figure 2.16 Variation of suction force with pullout velocity (Baba et al. 1989)

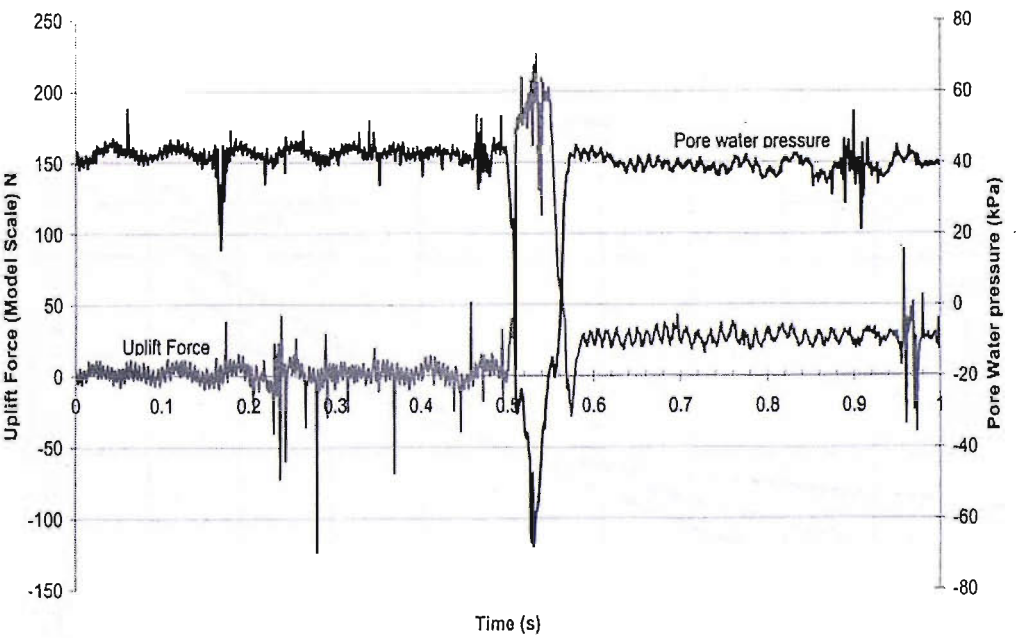

Figure 2.17 Load and pore pressure response for fast uplift test on model transmission tower footing in clay (Richards, 2002)

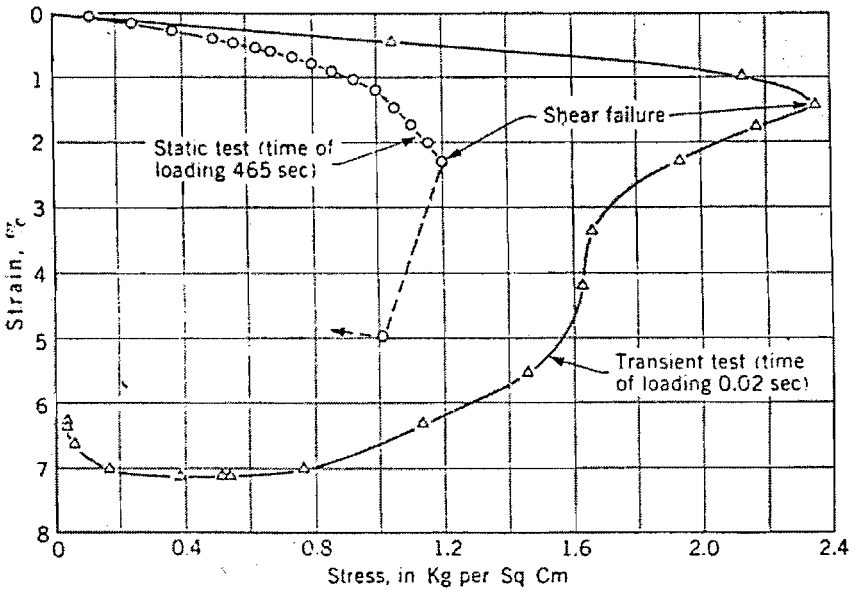

Figure 2.18 Stress-strain response of Cambridge clay in unconfined compression (Casagrande and Shannon, 1949)

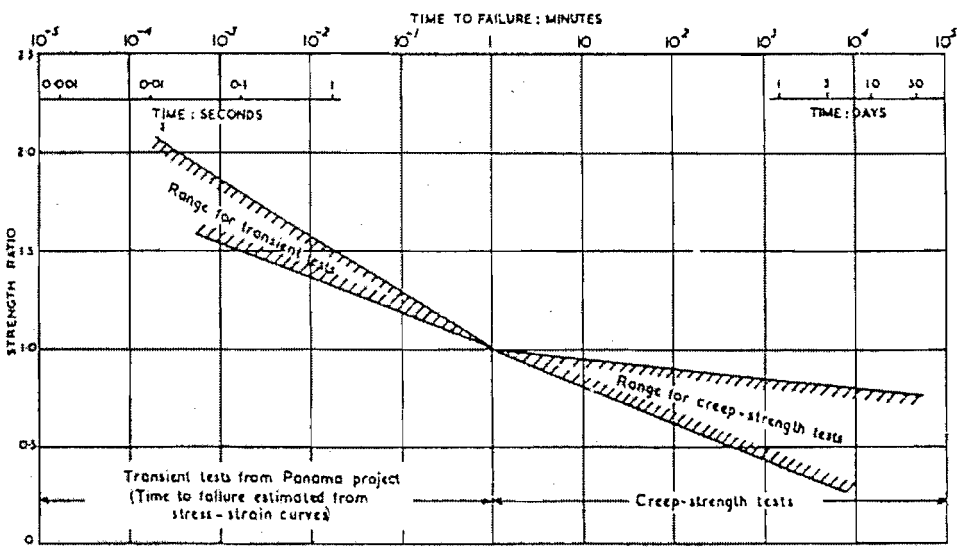

Figure 2.19 Variation in strength ratio with time to failure of Cucaracha shale (Casagrande and Wilson, 1951)

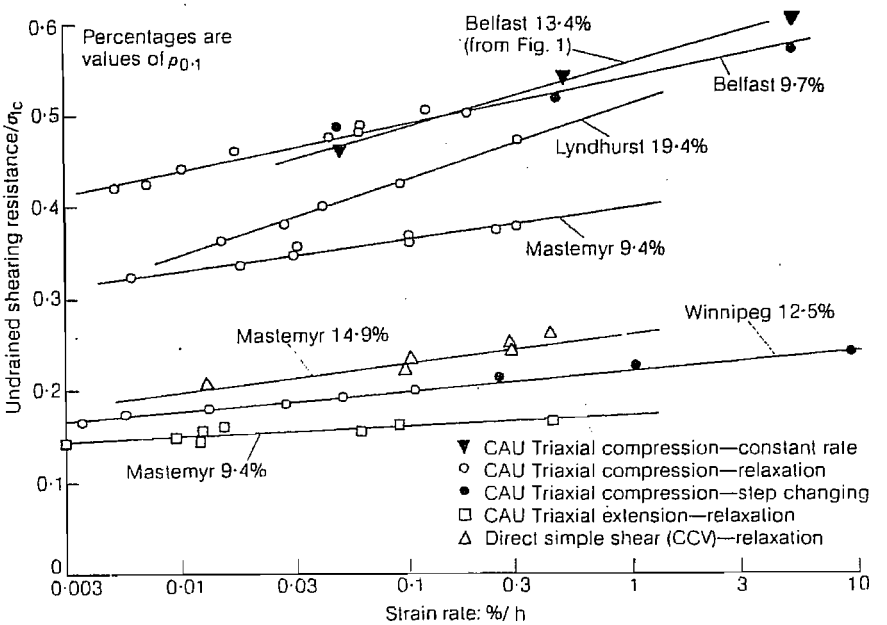

Figure 2.20 Variation of undrained shear strength ratio with strain rate (Graham et al. 1983)

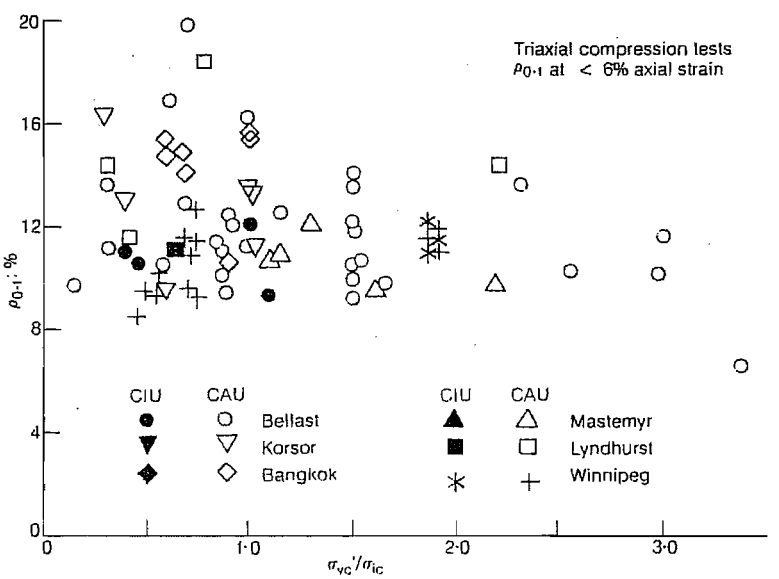

Figure 2.21 Effect of the overconsolidation ratio on $\rho_{0.1}$ (Graham et al. 1983)

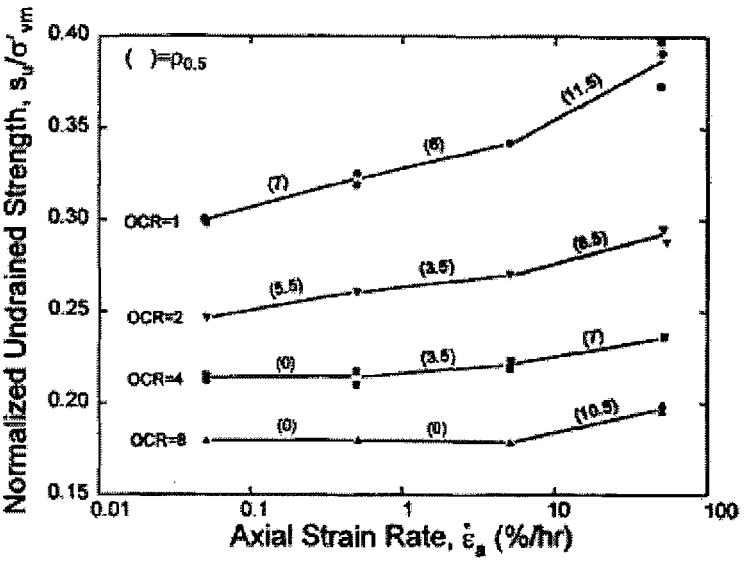

Figure 2.22 Variation of the undrained shear strength ratio with axial strain rate for Boston Blue clay (Sheahan et al. 1996)

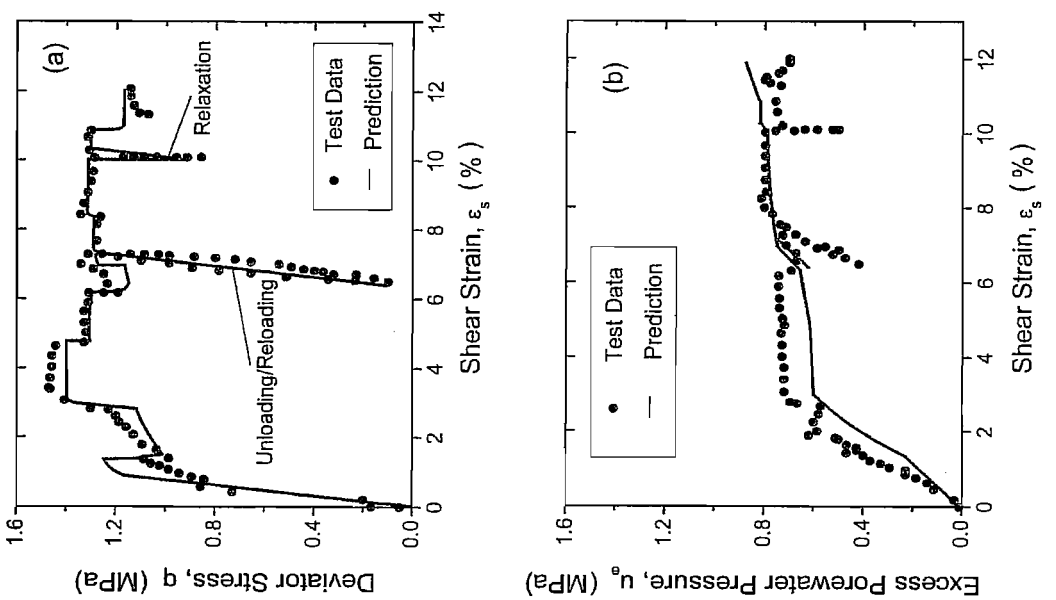

Figure 2.23 Measured and predicted stress-strain and excess pore pressure variation (Yin and Graham, 1999)

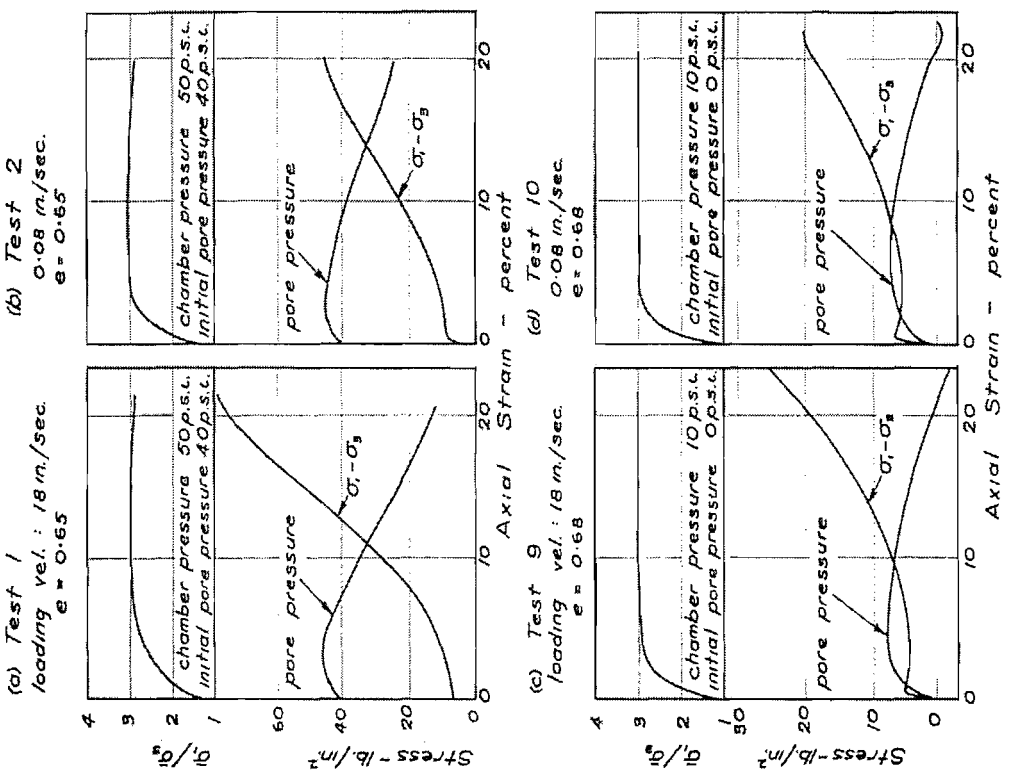

Figure 2.24 Variation in the stress-strain response of loose saturated Ottawa sand. (Whitman and Healy, 1962)

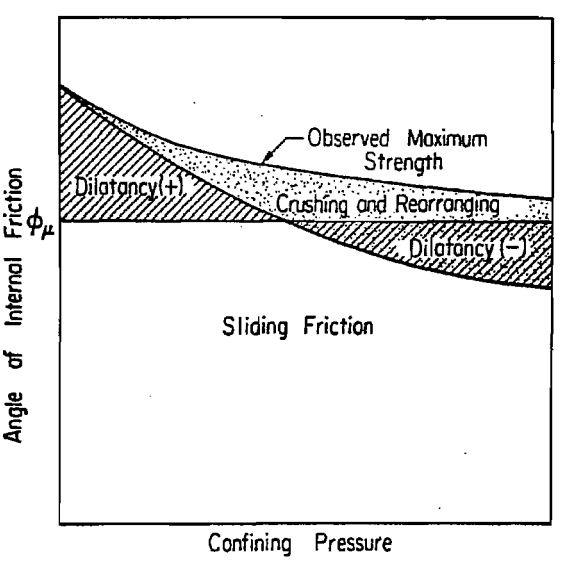

Figure 2.25 Components of shear strength in drained compression (Lee et al. 1969)

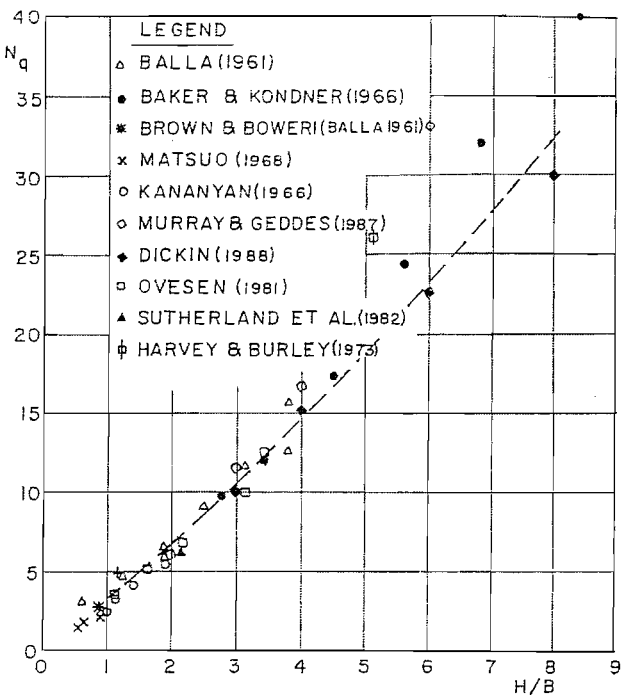

Figure 2.26 Comparison of published uplift capacity factors for square and circular plates in dense sand (Frydman and Shaham, 1989)

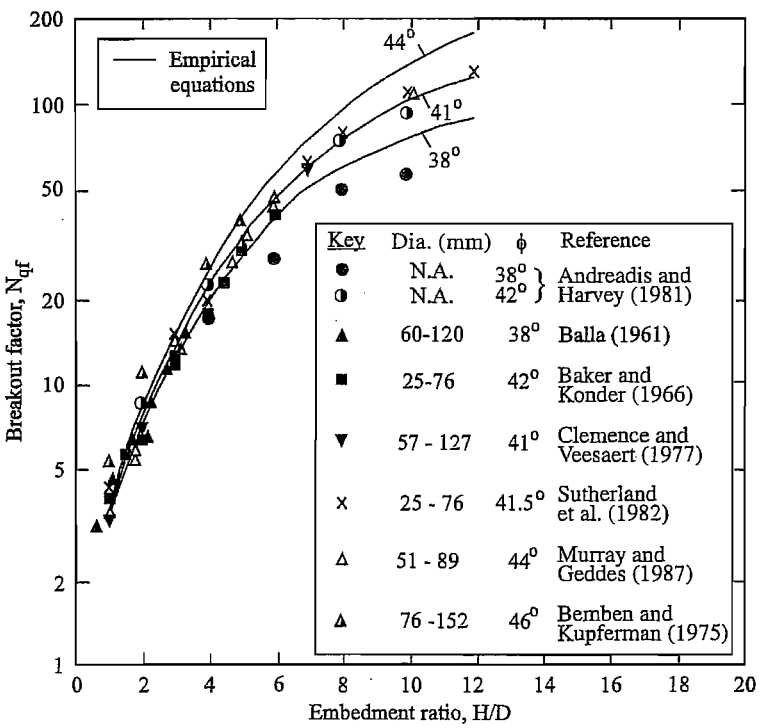

Figure 2.27 Comparison of uplift capacity factors for circular plates in medium dense to dense sand (Ilamparuthi et al 2002)

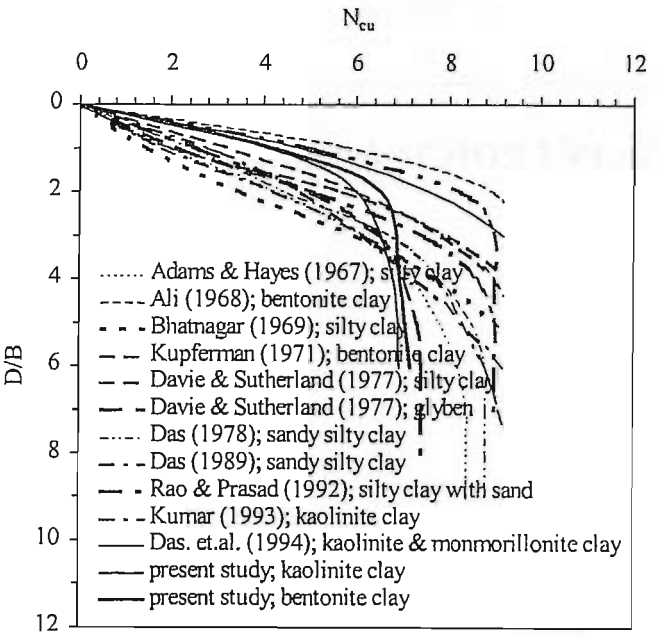

Figure 2.28 Comparison of experimental breakout uplift capacity factors for anchors in clay (Rao and Datta, 2001)

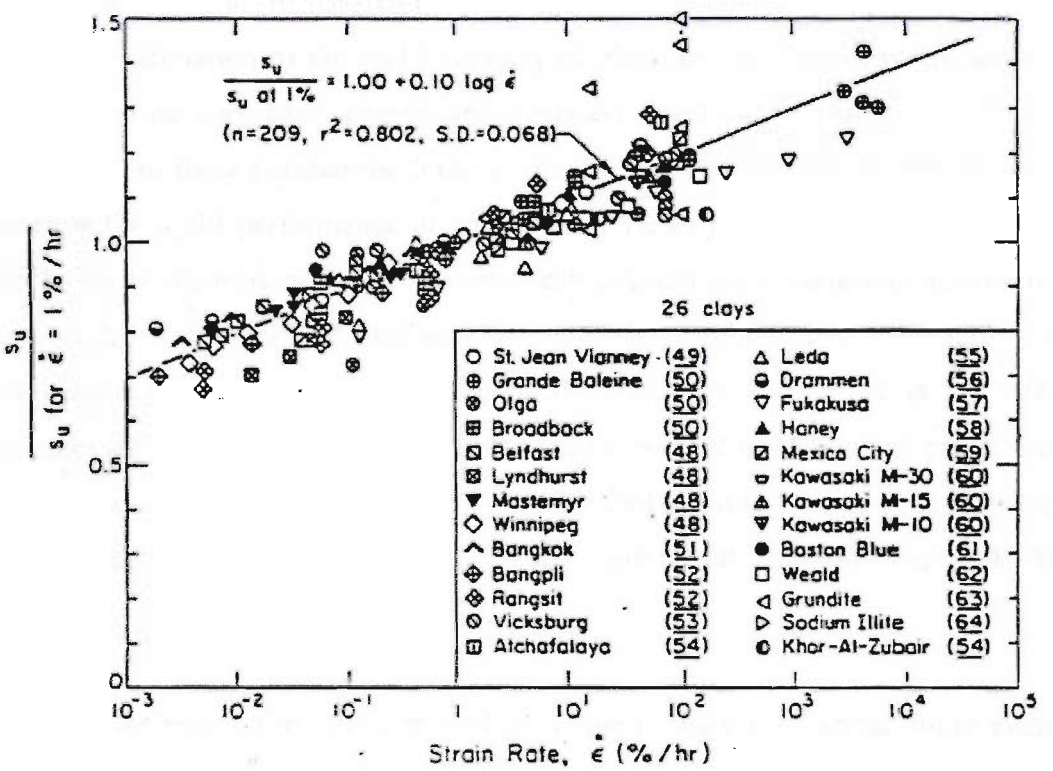

Figure 2.29 Comparison of the strain rate dependence of s_u for a range of clays (Kulhawy and Mayne, 1990)

Chapter 3

FE SOLUTIONS FOR ANCHOR UPLIFT CAPACITY

3.1 Introduction

It was seen in Chapter 2 that a considerable amount of investigation has been conducted in to the uplift capacity of anchors, principally in granular material. The large majority of this work has involved the use of approximate techniques, limit equilibrium formulations and empirical derivations. While these methods provide a reasonable estimation of the uplift capacity of plate anchors and related foundations they tend to be very case specific and generally overlook various aspects of uplift behaviour. For these reasons the finite element method has become a popular way of assessing the uplift performance of anchors in a range of soils e.g. Rowe and Davis (1982). More rigorous numerical analysis can account for a variety of factors often excluded from other methods and several authors have published broad ranging 2 and 3 dimensional investigations e.g. Merifield *et al.* (2003), Thorne *et al.* (2004), Merifield *et al.* (2006). The use of a simple finite element model, which can be easily calibrated against the results of previously published studies, is therefore thought to be an important element for consideration in the commercial design of shallow anchors and related foundations.

This Chapter presents results obtained from preliminary total stress finite element analyses using the commercially available software SAFE (OASYS, 2002). Uplift capacity factors obtained from these model scale analyses of plate anchors in sand and clay are compared with those obtained from limit equilibrium solutions, experimental investigations and more recent numerical studies.

3.2 The Finite Element Model

The finite element (FE) model developed for the preliminary total stress analyses is described and details of mesh geometry and method of analysis are presented. The numerical analyses were performed using the SAFE finite element program (SAFE, OASYS, 2002).

3.2.1 OASYS SAFE – Finite element program

"OASYS SAFE is an FE program designed to carry out finite element computations for geotechnical problems. The program enables the user to study the soil stresses and strains and deformations through one or more sequences of events. SAFE provides for two-dimensional Finite Element computations in plane stress, plane strain, or axial symmetry." (SAFE, OASYS, 2002)

SAFE uses 8-noded quadrilateral elements, each element having 3 nodes on every side. The sides of the element may be straight, or they may have quadratic or cubic shapes in order to adequately model irregular boundaries. For an 8-node element, the displacement variation within the element is quadratic and a linear strain and stress variation is given. Stresses and strains are computed at sampling points within each element, termed 'Gauss points', from which the program carries out integration over the area of the element. The 8-node element with 4 Gauss points is particularly reliable and is used frequently in many finite element codes. The positions of the Gauss points within each element used in SAFE are computed as described by Zienkiewicz and Cheung (1967).

3.2.2 Definition of the FE model

The preliminary FE analyses described in this Chapter were undertaken in order to assess whether the model scale conditions used in the centrifuge testing programme (Chapter 5) could be replicated in a Finite Element analysis. These analyses also provide an indication of the uplift capacities expected for the model anchors used during the centrifuge test programme. In order to assess the effect of the centrifuge model scaling and the model anchor geometry used in the centrifuge test series the FE analyses were conducted using the model anchor dimensions shown in Figure 3.1. The

FE model used was axisymmetrical and hence the square model anchors and stems used in the centrifuge, shown in Figure 3.1(a), were modelled as circular sections, Figure 3.1(b), in the analyses. Previous numerical analyses undertaken by Merifield *et al.* (2003) for anchors in clay and Merifield *et al.* (2006) for anchors in sand indicate that the capacities derived for circular anchors may be around 10-15% greater than those of an equivalent square anchor for embedment ratios less than 2-3. The anchor was assumed to be perfectly rigid in all cases.

The boundary conditions imposed in the FE analysis are shown in Figure 3.2. Rigid boundaries were specified at a distance of six anchor diameters in the horizontal direction and a distance of five anchor diameters plus the embedment depth of the anchor (H) in the vertical direction. A typical finite element mesh developed for the anchor problem is shown in Figure 3.3 and consisted of between 580-960 quadrilateral elements, depending on the embedment depth of the plate anchor. The elements were biased to provide a significantly higher mesh density in the regions around the anchor where the greatest changes in stress would occur during the imposed displacement. The mesh density was verified by conducting several analyses using the same mesh geometry but with double the number of elements. These analyses indicated no significant variation in the computed output compared with that obtained using the mesh shown in Figure 3.3. Separate meshes were created for anchors with embedment ratios between 0 and 4.

3.2.3 Soil model and the anchor interface

Each analysis employed an isotropic linear elastic-perfectly plastic constitutive model for the sand and clay, which was assumed to have a Mohr-Coulomb failure criterion. Each material was characterised by the total stress parameters: shear modulus, unit weight, Poisson's ratio and either shear strength (for clay) or friction angle (for sand). The parameters specified for both sand and clay soils are listed in Table 3.1. The plate anchor was modelled as a linear elastic material with a shear modulus, Poisson's ratio and unit weight representative of the aluminium material used to fabricate the model anchors used in the centrifuge study. As the FE analyses were performed to replicate centrifuge model scale tests all analyses were undertaken with the unit weights (for both soil and anchor) adjusted to account for the scale representation of the model. Each unit weight was factored by n=50 to correspond with the centrifugal acceleration

applied in the centrifuge model tests (Chapter 5). A fully rough interface was assumed between the anchor and the soil. Some analyses undertaken using a reduced frictional component at the soil anchor interface indicated that the differences in ultimate anchor capacity and load displacement behaviour were minimal. This observation is also noted in the numerical studies of Rowe and Davis (1982) and Thorne *et al.* (2004).

Table 3.1 Total stress parameters used for sand and clay

	sand	**clay**
γ	900 kN/m^3	800 kN/m^3
E	20 MPa	20 MPa
μ	0.15	0.49
s_u	0 kPa	50 kPa
ϕ	30°, 40°	0°
ψ	$0 \leq \psi \leq \phi$	0°
K_0	1	1

It was described in Chapter 2 that two limiting cases of anchor behaviour may occur during uplift. For anchors founded on sand and those founded on clay where no tension (due to the generation of negative pore water pressure) is possible at the soil-anchor interface, immediate separation of the anchor and the soil beneath it will occur during uplift. Where tension is possible at the anchor base, separation of the soil and anchor will not take place during uplift and shear failure will occur in the soil below the anchor. The former case is not well represented in a general FE model as the soil-anchor interface consists of a single set of nodes and an artificial attachment occurs between the two materials. It is possible that separation of the soil and anchor could be achieved by specifying duplicate nodes along the soil-anchor interface. This solution however will lead to problems in achieving an initial equilibrium where no vertical stress is possible across the interface and the soil below the anchor may yield under the resulting high horizontal stress. Given these problems, the most favourable solution involved assigning a significantly reduced stiffness to the layer of elements directly below the anchor base as shown in Figure 3.4. In this way stresses are allowed to act across the interface during initial equilibrium, whilst minimal tensile resistance to movement is provided by the elements during uplift of the anchor. It should be noted that although this solution is satisfactory up to ultimate failure the residual uplift behaviour will not be adequately modelled (which would still be the case had this solution not have been employed). For each analysis the value of the ratio of the

horizontal and vertical (total) stresses ($K_0 = \sigma_h/\sigma_v$) was taken to be equal to 1. In reality higher values of the *in-situ* K_0 would lead to higher initial horizontal stresses and a greater capacity in the soil above the anchor to accept the horizontal stress reductions leading to tensile failure. In this way a greater value of K_0 will lead to higher uplift capacities and the analyses may be assumed to slightly underestimate the uplift capacity at each anchor embedment depth.

3.3 Results for Anchors in Sand

Finite element analyses were undertaken to estimate the variation of the uplift capacity factor for model circular plate anchors embedded in sand (N_{us}) with increasing embedment ratio (H/D). The derivation of N_{us} was discussed in Chapter 2 in relation to the results of previously published experimental and analytical studies. Where possible the N_{us} values derived from the FE analyses described here are compared with those from these previous investigations divided into three categories: (i) theoretical solutions, involving limit equilibrium and cavity expansion methods, (ii) numerical studies involving FE analyses and (iii) experimental investigations involving 1*g* (chamber) and centrifuge model tests.

Table 3.2 Overview of theoretical studies for anchors in sand

Author(s), year	Anchor type	Method of Analysis	Relationship
Meyerhof & Adams (1968)	square circular	Limit equilibrium	$N_{us} = 1 + \left[1 + m\left(\frac{H}{B}\right)\right]\left(\frac{H}{B}\right)2K_u \tan\phi$
Vesic (1971)	circular	Cavity expansion	Table of capacity factors for H/D and ϕ are given by Das and Singh (1995)
Murray and Geddes (1987)	square circular	Limit equilibrium	$N_{us} = 1 + 2\frac{H}{B}\left(\sin\phi + \sin\frac{\phi}{2}\right)\left(1 + \frac{2}{3}\frac{H}{B}\tan\frac{\phi}{2}(2 - \sin\phi)\right)$
Sarac (1989)	square circular	Limit equilibrium	Results presented for ϕ'=0-50°

Table 3.3 Overview of Finite Element studies for anchors in sand

Author(s), year	Anchor type	Method of Analysis	Relationship
Tagaya *et al.* (1988)	circular	Finite Element	Limited FE results for ϕ'=35.1°, no relationship given
Koutsabeloulis & Griffiths (1989)	circular	Finite Element (initial stress)	Results presented for ϕ'=20-40°
Merifield *et al.* (2006)	square circular	3D numerical limit analysis/ Finite Element	Results presented for ϕ'=20-40°

As this review deals primarily with axisymmetrical analyses, limited plane strain analyses were undertaken and previously published results are considered for square and circular anchors only. Overviews of the published investigations, relating to anchor behaviour in sand, selected for comparison are given in Tables 3.2, 3.3 and 3.4.

Table 3.4 Overview of experimental studies for anchors in sand

Author(s), year	Anchor type	Type of test	Friction angles
Murray and Geddes (1987)	circular	1*g* (chamber)	dense =44°, medium =36°
Tagaya *et al.* (1988)	circular	Centrifuge	medium =35.1°
Ilamparuthi *et al.* (1999)	half-cut circular	1*g* (chamber)	loose =33.5°
Ilamparuthi *et al.* (2002)	circular	1*g* (chamber)	dense =43°

The variation of N_{us} with embedment ratio (H/D) calculated using the SAFE finite element analyses is shown in Figure 3.5 for analyses assuming fully associated and non-associated soil. It is observed that the value of N_{us} increases non-linearly with increasing embedment ratio with a maximum value of 18.5 for ϕ'=40° at an embedment ratio of 4. It was seen in Chapter 2 that anchor capacity may be expected to reach a constant value at the critical embedment ratio, $(H/D)_{cr}$, which marks the

transition from shallow to deep anchor failure as shown in Figure 3.6. For the FEA undertaken, the largest increase in N_{us} in each case occurs between an embedment ratio of 3 and 4 indicating that for the range of embedment depths used in the analysis shallow failure of the representative anchor will occur. The results of lower-bound analyses presented by Merifield *et al.* (2006) indicate that for square and circular anchors $(H/D)_{cr}$ is likely to be greater than 10 for values of ϕ' larger than 30°.

The values of N_{us} predicted in Figure 3.5 for non-associated soil are significantly lower than those for fully associated soil at the same value of ϕ'. Although this observation is similar to that recorded by Rowe and Davis (1982), the ratios of fully associated capacity to non-associated capacity (i.e. the correction factor R_ψ given by Rowe and Davis) observed here are around 50-60% above those specified in their study. The values of R_ψ given by Rowe and Davis are however related to strip anchors and it is not clear whether they are directly applicable to circular or square anchors; given the discrepancy observed in the results it would be inferred that they are not although further investigation is obviously required. The effect of soil dilatancy on the failure mechanism developed during uplift for shallow anchors is clearly shown in Figure 3.7 which plots the velocity fields for associated and non-associated soil at H/D=1. During uplift of the anchor in associated soil, a much wider failure surface is developed above the anchor as dilatancy will cause the soil in this zone to lock together. As described in Chapter 2 the angle made by the failure surface with the vertical will be associated with the angle of dilatancy (ψ) of the soil. The failure surface observed to develop for a non-associated soil consists primarily of the soil vertically above the anchor alone and, although this has been assumed in some earlier design methods (Majer, 1955), it is considered to be conservative in all but very loose sands. In subsequent sections the results of FE analyses using associated soil are compared with previously published theoretical and numerical studies. For comparison with previous experimental studies, values of ϕ' and ψ are selected to best match (where specified) the experimental soil properties.

3.3.1 Comparison with theoretical solutions

Figure 3.8 compares the N_{us} values estimated from the model representative FE analyses (for fully associated soil, $\psi=\phi$) with the results of the previously published

theoretical solutions presented in Table 3.2. Reasonable agreement is observed between the SAFE analysis and the solutions of Meyerhof and Adams (1968) and Sarac (1989) particularly at H/D values less than about 3. The limit equilibrium solution of Murray and Geddes (1987) is seen to be up to 50% greater than the SAFE analysis at $\phi' = 30°$ and significantly higher than the other published data. For $\phi' = 40°$ however the solution is much improved and good agreement is shown with the other data, particularly the SAFE analysis where the two solutions yield very close results. The cavity expansion solution presented by Vesic (1971) provides reasonable agreement with the SAFE analysis at H/D ≤ 2 for $\phi' = 30°$ but is seen to underestimate the value of N_{us} compared with other solutions in all other cases, particularly for $\phi' = 40°$.

It should be noted that in the model representative finite element analysis the anchor is modelled as weightless in line with the limit equilibrium assumption of an infinitely thin, rigid anchor. In effect, as with the general limit equilibrium solution, only the contribution to uplift resistance of the displaced soil is considered in the calculation of N_{us}.

3.3.2 Comparison with numerical data

It is evident from Table 3.3 that there is a scarcity of published data relating to the uplift capacity of square and circular anchors determined through numerical modelling, with the study of Merifield *et al.* (2006) providing possibly the only rigorous investigation into the area. The selected available data is plotted in Figure 3.9 where it is compared with the results of the SAFE analysis for friction angles of 30 and 40 degrees. As seen previously for theoretical solutions the best agreement between all the data sets is observed at the most shallow embedment ratios (H/D ≤ 2). This is not surprising given that various different assumptions regarding initial stresses, soil dilatancy, and distribution of stresses along the failure surface will have less influence on anchor capacity at shallow embedment where the zones of plastic failure developed are smaller than for larger embedment depths. Koutsabeloulis and Griffiths (1989) presented the results of axisymmetrical FEA assuming non-associated soil behaviour but providing a correction factor to account for the effects of dilation during soil deformation. This correction factor has been applied to their results to

obtain comparative data for fully associated soil. As observed in Figure 3.9 there is reasonable agreement between the results of Koutsabeloulis and Griffiths (1989) and the SAFE analysis for $\phi' = 40°$. At $\phi' = 30°$ however the estimated N_{us} values are up to 40% above those of the SAFE analysis. The data presented by Tagaya *et al.* (1988) is limited and although good agreement is seen with the SAFE analysis at the embedment ratio provided it is not possible to comment on any overall trend.

Merifield *et al.* (2006) investigated the uplift capacity of square and circular anchors using 3-dimensional numerical limit analysis to provide a lower bound solution to the problem. Their results showed good agreement with axisymmetrical displacement finite element analysis and assume fully associated soil behaviour to accurately predict the collapse load. It is encouraging therefore to note that the results of the model representative SAFE analysis are within 4-15% of the N_{us} values reported by Merifield *et al.* (2006) for circular anchors as shown in Figure 3.10. The agreement is particularly good for $\phi' = 30°$ and at embedment ratios less than or equal to 2.

3.3.3 Comparison with experimental data

The results of the experimental studies shown in Table 3.4 are plotted with embedment ratio in Figure 3.10. Also plotted are the results of representative SAFE analyses using similar soil properties to those provided in each of the experimental studies. Where the angle of dilation for the soil was not specified directly in the published study it has been taken as equal to $\phi'/3$. The comparison provided between the experimental data and the results of the SAFE analyses will provide a good insight into the capability of the FE analysis to predict the uplift resistance measured from laboratory tests. This is also an important factor for replicating the results of centrifuge model anchor tests (presented in Chapter 5).

The uplift factors determined by Murray and Geddes (1987) for $\phi' = 36°$ display a large amount of scatter compared to other experimental data but generally appear to be fairly well represented by the SAFE analysis where $\phi' = 35°$. Better agreement is observed for the results of Tagaya *et al.* (1988), particularly for values of H/D between 2 and 4, where the parameters used in the SAFE analysis appear to be more representative of those detailed in the experimental study. For embedment ratios

greater than or equal to 4 results from both Murray and Geddes (1987) and Tagaya *et al.* (1988) appear to plot below the expected trend observed from the SAFE analysis. The experimental results of Ilamparuthi et al. (1999), where ϕ'=33.5°, are higher than those predicted by the SAFE analysis, although given the slight reduction in friction angle for the sand used it might be expected that they should be lower. The results of Ilamparuthi *et al.* (1999) are taken from uplift tests on half-cut anchors where the principle aim was to investigate the failure mechanism developed by the anchor during uplift. For this reason the apparent enhanced uplift capacity may be a result of some frictional component mobilised at the half-cut anchor viewing window interface which is not corrected for in the presented results.

In comparison, for the denser sands shown in Figure 3.10(b), the agreement between experimental data and the results of the SAFE analyses is extremely good. The experimental results of Murray and Geddes (1987), for which ϕ'=44°, and Ilamparuthi *et al.* (2002), for which ϕ'=43°, are both remarkably well represented by the SAFE analysis where the angle of dilation (ψ) is assumed to be equal to $\phi'/3$. Such close agreement between experimental data and the results of the representative FEA is very encouraging and demonstrates the potential of the finite element analyses to adequately model specific experimental conditions.

3.4 Results for Anchors in Clay

Previous sections have described the results of representative finite element analyses undertaken to estimate capacity of anchors embedded in sand. Similar analyses were also undertaken to assess the variation in uplift capacity with increasing embedment ratio (H/D) for anchors in clay. As discussed in Chapter 2, and particularly in relation to the numerical investigation of Rowe and Davis (1982), the upper and lower limits to the problem of anchor behaviour in clay may be represented by two distinct mechanisms of failure, the 'fully bonded' and 'breakaway' conditions. In the fully bonded case it is assumed that tension is possible at the soil-anchor interface and the anchor remains in contact with the soil at all times during uplift. This condition is related to the generation of suction at the anchor base and is discussed in detail in later

chapters in relation to the results of the centrifuge testing programme. For these preliminary total stress FE analyses the fully bonded case is modelled assuming full cohesion at the soil anchor interface. In the breakaway case it is assumed that no tension is possible at the interface and the anchor immediately separates from the soil as the vertical stress below the anchor reduces to zero during uplift. As discussed in section 3.2.3 the breakaway case was modelled by specifying interface elements with a reduced stiffness value directly below the anchor base. For these analyses the interface elements were also assigned to be non-cohesive in order to ensure immediate separation of the soil and anchor. The derivation of anchor capacity in each case is discussed in Chapter 2 (Section 2.3.7) in relation to the results of previously published experimental and analytical studies.

Total stress analyses were undertaken using SAFE in order to model both the fully bonded and breakaway failure conditions and the results of these analyses are compared with previously published numerical and experimental data. Comparisons are provided in terms of the uplift capacity factors N_u (for fully bonded behaviour) and N_{ub} (for breakaway behaviour) as shown in Table 3.5 where $F_{u(t)}$ is the uplift capacity for the fully bonded case, $F_{u(b)}$ is the capacity for the breakaway case and A is the area of the anchor base.

Table 3.5 Uplift capacity factors for anchors in clay

Component of uplift resistance	Factor	Normalisation
Total uplift capacity (fully bonded at anchor base)	N_u	$N_u = \frac{F_{u(t)}}{s_u A_b}$
Breakout resistance (separation at anchor base)	N_{ub}	$N_{ub} = \frac{F_{u(b)}}{s_u A_b}$

Values of N_u and N_{ub} estimated from the model FE analyses are compared with those from these previous investigations divided into two categories: (i) theoretical and numerical studies, involving cavity expansion methods and finite element analyses and (ii) experimental investigations.

Table 3.6 Overview of theoretical studies for anchors in clay

Author(s), year	Anchor type	Method of Analysis	Failure condition
Vesic (1971)	circular	Cavity expansion	Breakaway
Rowe and Davis (1982)	circular (using correction)	Finite Element	Breakaway and fully bonded
Yu (2000)	circular	Cavity expansion	Breakaway
Merifield *et al.* (2003)	square circular	3D numerical limit analysis	Breakaway

The analyses undertaken in SAFE are axisymmetrical and as such previously published results are considered for circular anchors only. Overviews of the published investigations, relating to anchor behaviour in clay, selected for comparison are given in Tables 3.6 and 3.7.

Table 3.7 Overview of experimental studies for anchors in clay

Author(s), year	Anchor type	Type of test	Failure condition
Kupferman (1971)	circular	1*g* (chamber) in bentonite clay	Breakaway
Kumar (1993)	circular	1*g* (chamber) in kaolin clay	Breakaway, fully bonded
Das et al. (1994)	circular	1*g* (chamber) in kaolin clay	Breakaway, fully bonded
Rao and Datta (2001)	circular	1*g* (chamber) in kaolin & bentonite clay	Breakaway, fully bonded

The uplift capacity factor N_u estimated from the SAFE finite element analyses is plotted with embedment ratio (H/D) in Figure 3.11 for fully bonded and immediate breakaway anchor behaviour. As shown previously in Figure 3.6 the critical embedment ratio marks the transition from shallow to deep anchor behaviour, the latter case being the point at which failure is localised around the base of the anchor and the capacity is not appreciably affected by the depth of embedment. It is seen in Figure 3.11 that in the fully bonded case anchors exhibit deep anchor behaviour at an

embedment ratio of approximately 3. Velocity fields for shallow and deep anchor behaviour are shown in Figure 3.12 for the fully bonded case and illustrate the localisation of the failure mechanism at deep anchor embedment. For the breakaway case the transition to deep anchor behaviour is not reached at the range of embedment ratios used in the SAFE analyses and the critical embedment ratio is evidently greater than 4.

The differences between the failure mechanisms developed during uplift in each case are further highlighted in Figure 3.13 where the velocity fields for the fully bonded and breakaway conditions are compared for an H/D value of 3. It is apparent that the adhesion between the anchor and the soil below it has a significant effect in mobilising the deep anchor failure mechanism where the upwards movement of the soil below the anchor evidently promotes the flow of soil from above the anchor. As mentioned previously in Chapter 2 the transition from shallow to deep anchor behaviour will also be significantly effected by the overburden ratio ($\gamma H/s_u$) as illustrated by Merifield *et al.* (2001).

3.4.1 Comparison of the breakaway behaviour case

Estimates of the anchor capacity factor N_{ub} derived from the SAFE analyses are plotted in Figure 3.14(a) and compared with results from the theoretical and numerical studies shown in Table 3.6. It is observed that the cavity expansion solutions presented by Vesic (1971) compare well at embedment ratios less than approximately 1, but become very un-conservative compared to other solutions at all other values of H/D. In contrast the finite element solutions of Rowe and Davis (1982) are conservative at all embedment ratios apart from about 1, where they are in good agreement with other solutions. The solutions of Rowe and Davis (1982) are however based on a concept which allows for a serviceability limit to be placed on the ultimate load such that failure is defined at a displacement equal to four times the value which would have been reached under entirely elastic conditions. For the breakaway case, at large values of H/D, the failure mechanism involves the formation of large plastic regions, shown partially in Figure 3.13(a), and large displacements are required to reach ultimate failure. For H/D values greater than about 2 the failure loads presented

by Rowe and Davis are limited by the imposed serviceability criteria and are hence ultimately conservative.

The values of N_{ub} predicted from the SAFE analyses are well represented by the solutions of Yu (2000) and Merifield *et al.* (2003) with the latter being within less than about 5-6% of the SAFE results at all values of H/D. This level of agreement between data is encouraging particularly as the results of Merifield *et al.* (2003) are derived from 3-dimensional numerical limit analyses which provide a lower bound solution to the problem. The solutions of Yu (2000) are based on cavity expansion methods which account for the effect of soil dilation during anchor deformation. It should be noted that while there is reasonable agreement with the solution of Yu (2000) no account is made for the effect of dilation in the SAFE analyses for anchors in clay.

The results of the experimental investigations shown in Table 3.7 are plotted in Figure 3.14(b) for the breakaway case where they are compared with N_{ub} values predicted from the SAFE analyses. It is observed that the experimental results of Kupferman (1971) and Das et al. (1994) are in reasonable agreement with the results of the SAFE analyses at all embedment ratios. Evidently for both of these studies the value of N_{ub} reaches a limiting value at an embedment ratio of between 3 and 4. There is less agreement observed with the results of Kumar (1993) which appear to fall below that of the FEA at all values of H/D. It is possible that the sample preparation procedure employed by Kumar (1993) may have resulted in the model anchors being tested in an inhomogeneous clay sample. In this case the actual shear strength of the clay above the anchor (at shallow depth) may have been lower than the value used to calculate the breakout factor N_{ub} resulting in the conservative values seen in Figure 3.14(b).

The values of N_{ub} reported by Rao and Datta (2001) appear to agree relatively well with the SAFE analyses at shallow embedment ratios ($H/D \leq 2$) but fall somewhat below the numerical data at higher values of H/D. It would appear from the data shown in Figure 3.14(b) that a limiting value of N_{ub} is reached at an embedment ratio between 2 and 3 and that after this value deep anchor behaviour occurs. This value of the critical embedment ratio, $(H/D)_{cr}$, is significantly less than has been inferred for the breakaway case by Merifield *et al.* (2003) and other authors and is most likely related to the overburden ratio ($\gamma H/s_u$). The value of undrained shear strength used is

not given by Rao and Datta (2001) however, their study is related to soft offshore clays and it is assumed (given the water content of the clay used) that the value of s_u might be sufficiently small that the overburden ratio would be large even given the relatively small overburden pressures generally obtained in laboratory $1g$ chamber testing. Should this inference prove correct, the large overburden ratio would serve to promote the localised failure mechanism associated with deep anchor behaviour to occur at a smaller value of H/D, as is evident in Figure 3.14(b).

3.4.2 Comparison of the fully bonded behaviour case

Estimates of the anchor capacity factor N_u derived from the SAFE analyses are plotted in Figure 3.15 where they are compared with results from the numerical and experimental studies shown in Tables 3.6 and 3.7 for fully bonded anchor behaviour.
It is evident from Figure 3.15(a) that previous theoretical and numerical investigation into fully bonded anchor behaviour is rather limited. This is mostly due to the uncertainty regarding the magnitude of suction forces developed at the anchor base during fully bonded anchor behaviour. In reality anchor capacity in clay is likely to fall between the bounds of fully bonded and breakaway behaviour and will be a function of many parameters such as embedment ratio, undrained shear strength, loading rate, permeability and the overburden ratio. For this reason it is difficult to assess the anchor capacity factor N_u outside of a total stress analysis such as that presented by Rowe and Davis (1982) and it is also difficult to provide meaningful comparison between the results. It would appear though that the analyses presented by Rowe and Davis (1982) tend to overestimate the value of N_u for all values of H/D compared to the SAFE analyses. It might be expected however that, assuming a similar failure mechanism in fully bonded uplift as would be developed under compression loading, the N_u value obtained for a surface anchor would be similar to that for a the same anchor under compression loading. Difficulties such as those outlined above provide the motivation for the centrifuge testing programs described in Chapters 5 and 6.

A number of previous experimental studies (e.g. Ali, 1968) have attempted to make allowances for the estimated suction force developing between the anchor and soil and correct the results of anchor uplift tests accordingly. This assessment of anchor capacity is rather arbitrary and hence the results of such studies are not considered

here. The results of the experimental investigations shown in Table 3.7 are plotted in Figure 3.15(b) for the fully bonded case where they are compared with N_u values predicted from the SAFE analyses. It is observed that the experimental results generally fall below those of the SAFE analyses at all embedment ratios with the greatest variation occurring at H/D values greater than about 3. As seen previously for the breakaway anchor condition this variation could be explained due to the soft nature of the clay used in each of the selected experimental studies and the resulting (probably) high values of overburden ratio. It is also worthwhile to note that while in the SAFE analyses a perfect contact between the soil and anchor is maintained throughout deformation this may not always be true of the experimental model tests. Cavities developing below the anchor or in the backfill material during uplift may result in the lower capacities observed in comparison with the FE analyses, which should really be viewed as the 'perfectly bonded' condition. A reasonable degree of scatter is observed in the experimental data shown in Figure 3.15(b) however the results of Das *et al.* (1994) and Rao and Datta (2001) are in relatively good agreement and consistent in terms of the critical embedment ratio. Unsurprisingly, given the reasons outlined above, the upper bounds of the experimental data provide the best agreement with the SAFE analyses. The results of Kumar (1993) lie between 7%-40% below those estimated from the SAFE analyses, with the best agreement in the data occurring for H/D values above 3.

3.5 Summary

The uplift capacity of circular plate anchors in undrained clay and cohesionless soil has been investigated using axisymmetrical displacement finite element analyses. These analyses have been undertaken in order to assess whether the model scale conditions used in the centrifuge testing programme (Chapter 5) could be replicated in a Finite Element analysis. Consideration has been given to the effects of embedment ratio (H/D), anchor roughness, dilatancy and the separation condition at the soil anchor interface on the uplift capacity of model scale plate anchors.

The results obtained from the SAFE finite element analyses have been presented in the form of uplift capacity factors and compared with those from previously published experimental, theoretical and numerical studies. The following conclusions are drawn from the results of these analyses:

i. Uplift capacity factors obtained for model scale anchors embedded in both sand and clay generally compare favourably with those presented in a number of previously published investigations. The highest degree of overall agreement is observed at lower values of embedment ratio (H/D $\leq$1.5).

ii. Reduced scale modelling using the same model anchor dimensions and related scale factors for unit weight (soil and anchor) as for the centrifuge testing programme (Chapter 5) has little effect on the uplift capacity factors obtained from the FE analyses when compared to the results of previously published investigations.

iii. Although previously published numerical data for the fully bonded anchor condition is limited, the results of the SAFE FE analyses compare reasonably well with existing experimental data.

iv. The uplift capacity of plate anchors with a horizontal axis is not significantly affected by the degree of anchor roughness at the soil anchor interface for either sand or clay soil.

v. The effect of soil dilation is significant and can result in large increases in anchor uplift capacity at shallow embedment ratios for all values of ϕ' investigated. Previously published experimental data for anchors in sand is well replicated by the results of the SAFE FE analyses using the values of ψ and ϕ' reported in each study.

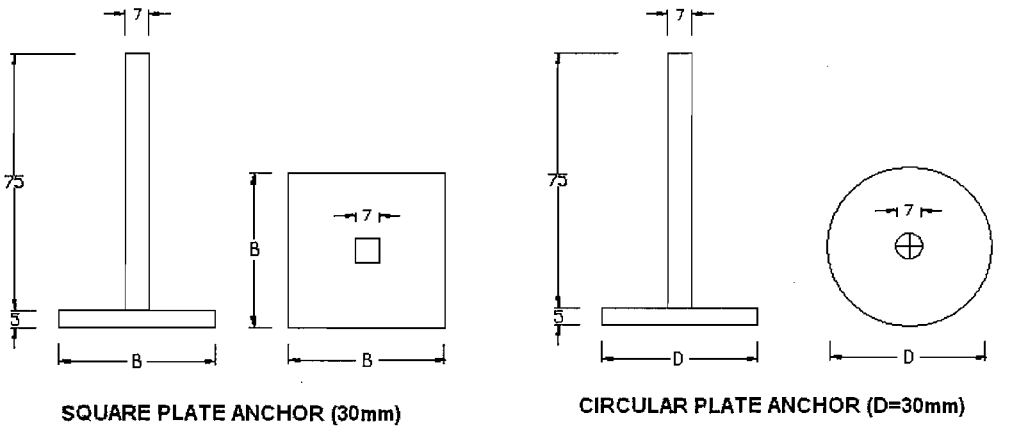

(a) (b)

Figure 3.1 Model anchor geometry

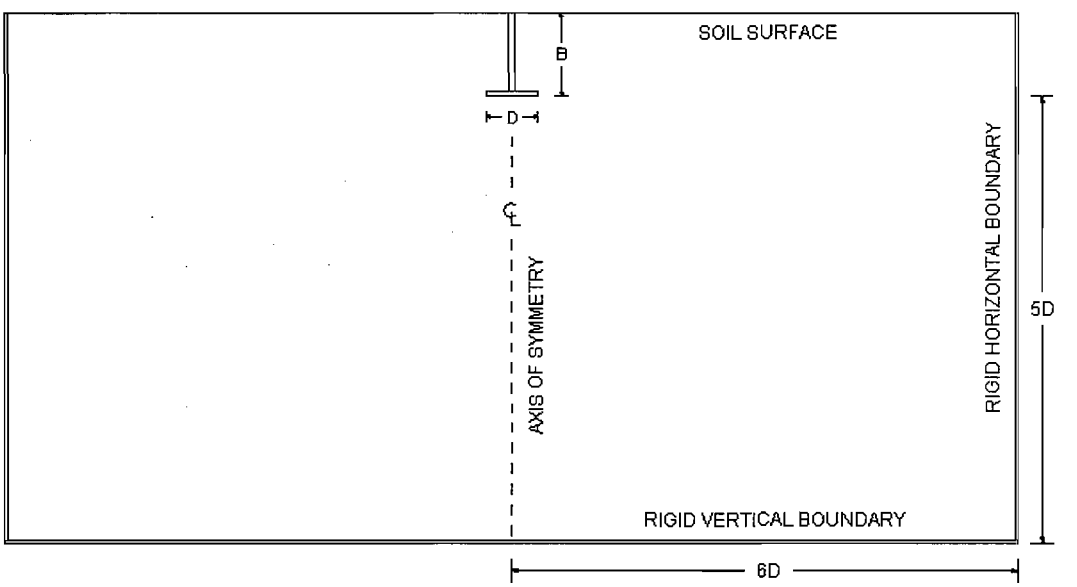

Figure 3.2 Problem boundaries for Finite Element analyses (not to scale)

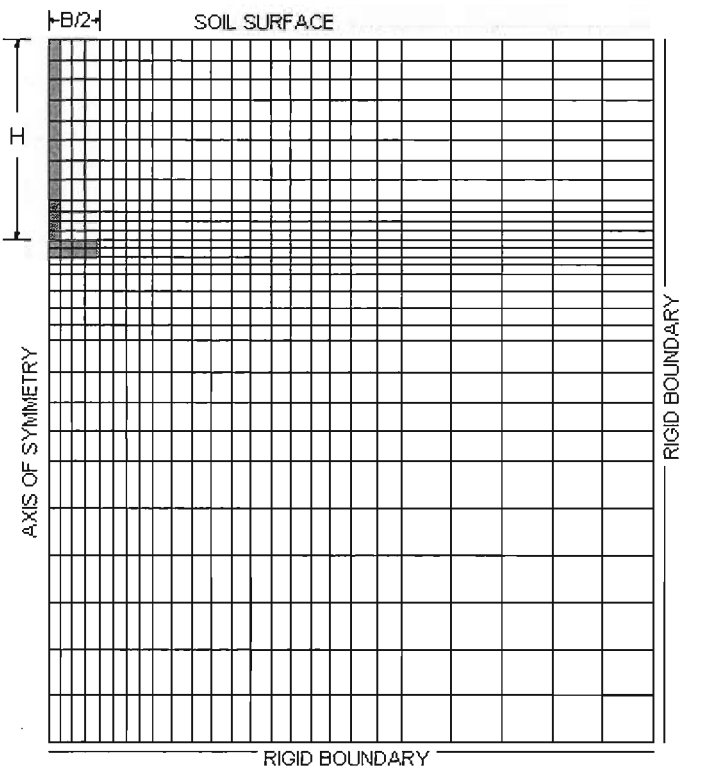

Figure 3.3 Typical Finite Element mesh for total stress analyses

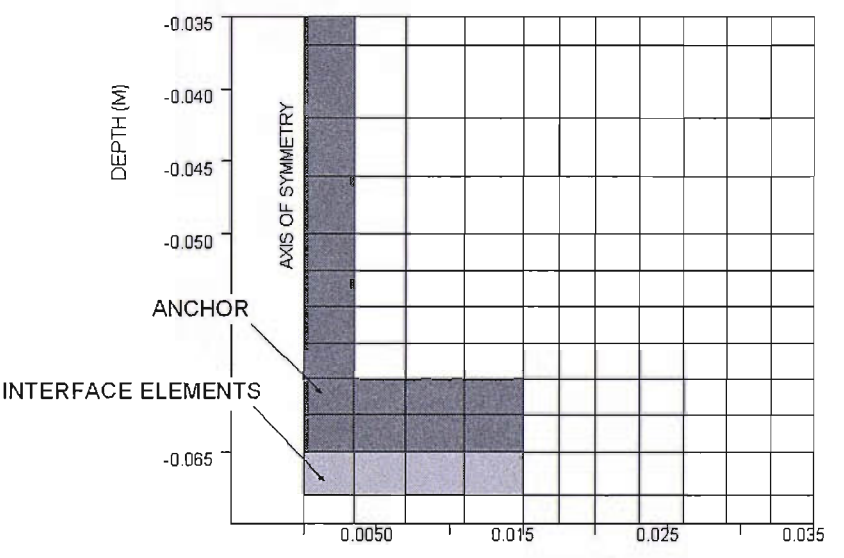

Figure 3.4 Anchor interface using elements with reduced stiffness

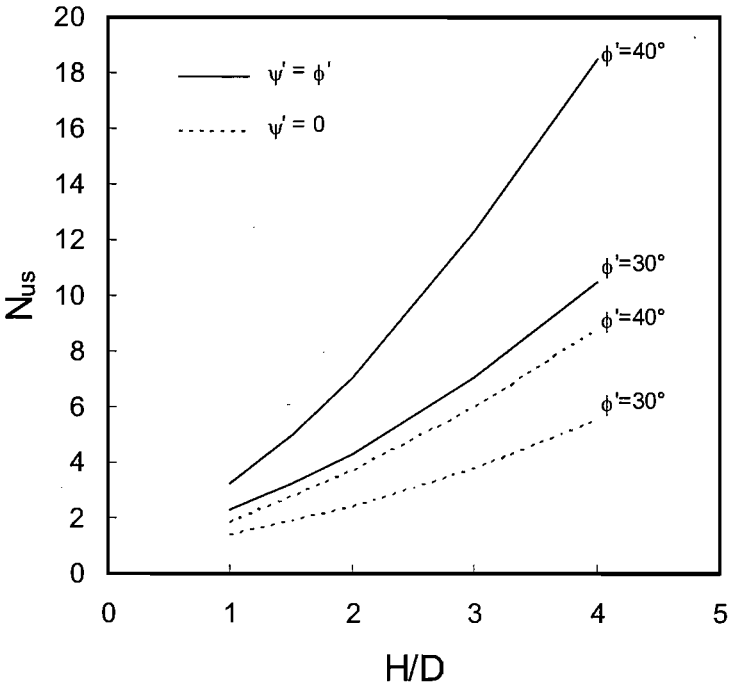

Figure 3.5 Uplift capacity factors for circular anchors in sand from SAFE analyses

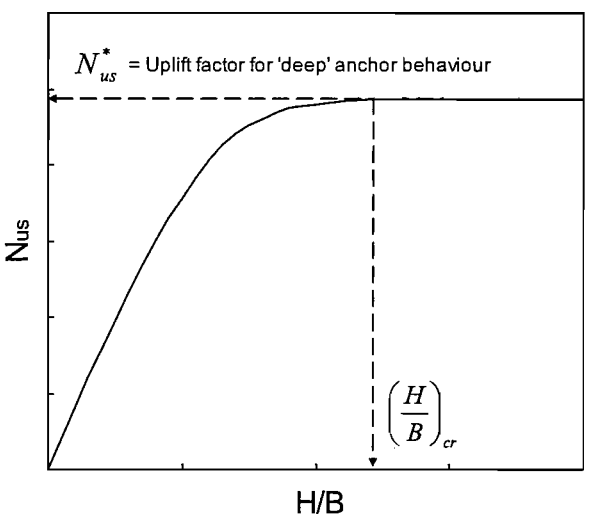

Figure 3.6 Representation of the critical embedment ratio

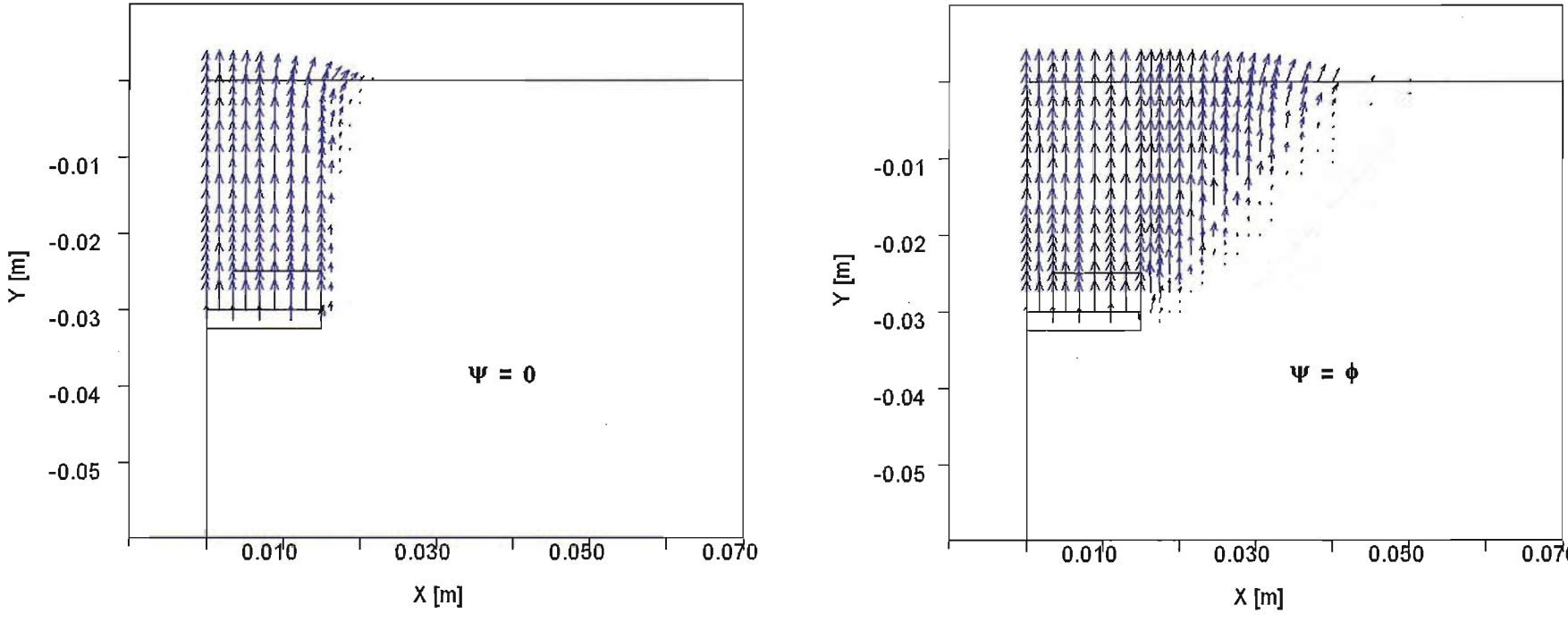

(a) No soil dilatancy

(b) Fully associated soil

Figure 3.7 Effect of soil dilatancy on the uplift failure surface, H/D = 1

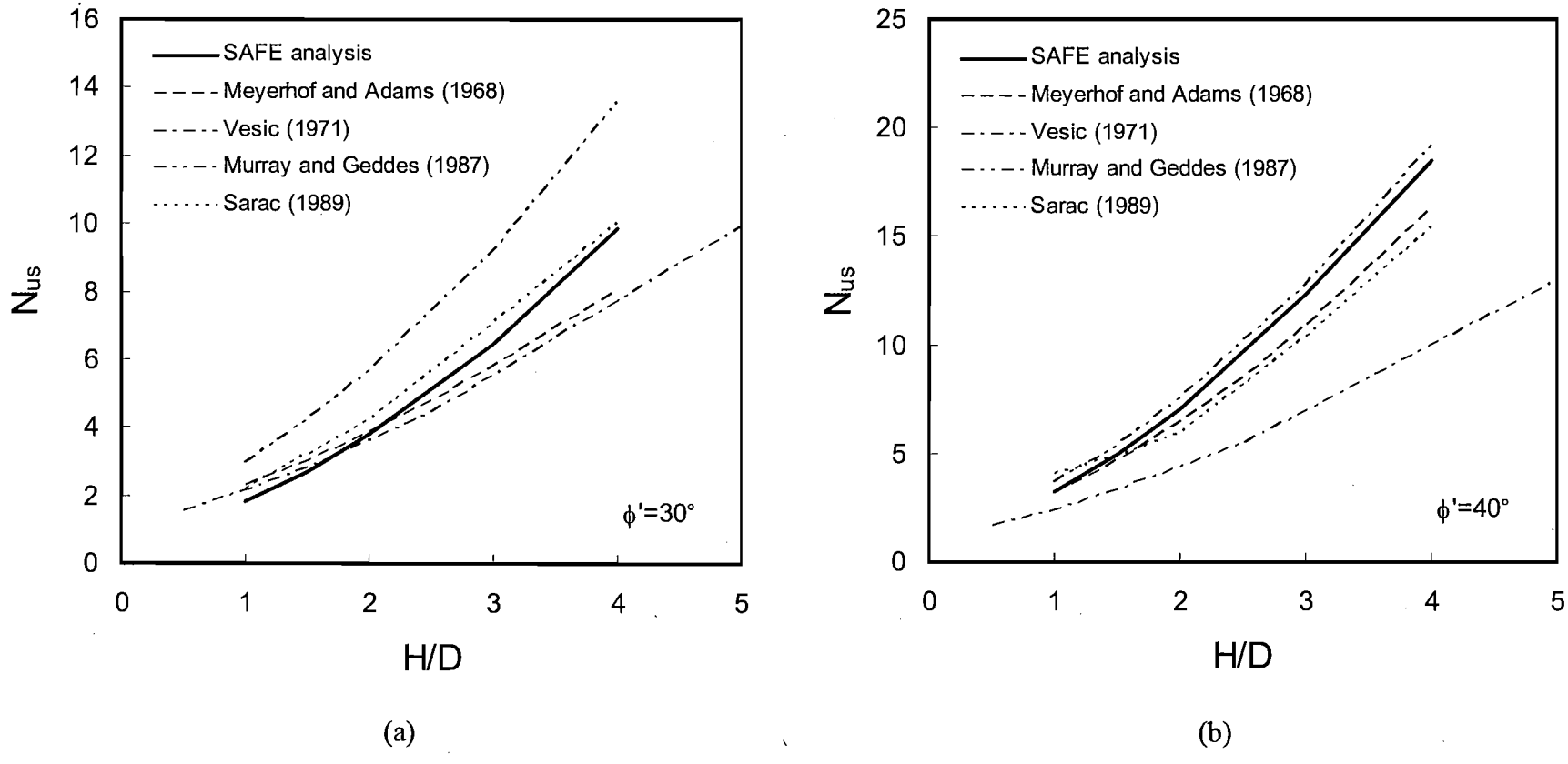

Figure 3.8 Comparison of SAFE uplift factors with existing theoretical solutions for ϕ'=30-40°

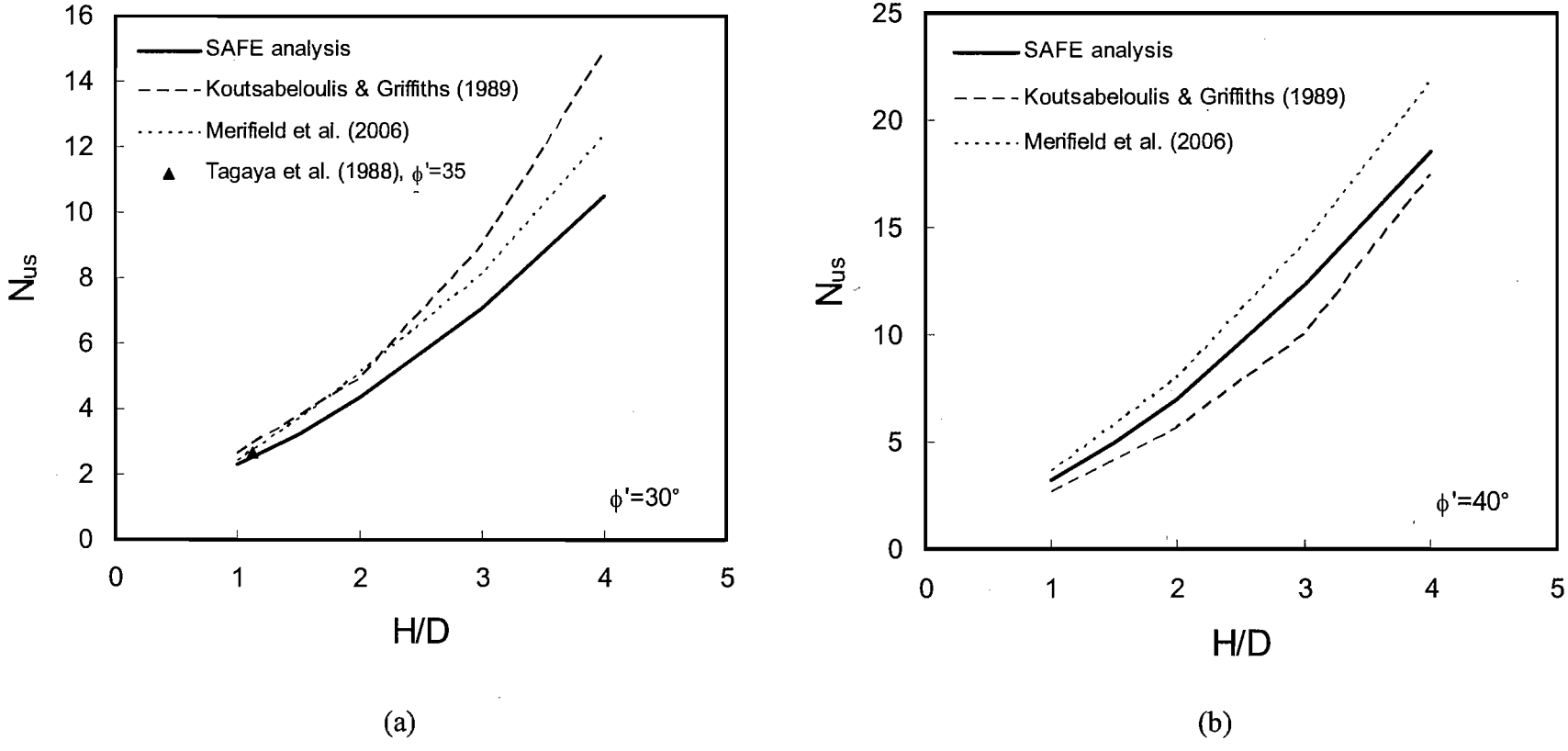

Figure 3.9 Comparison of SAFE uplift factors with existing numerical solutions for ϕ'=30-40°

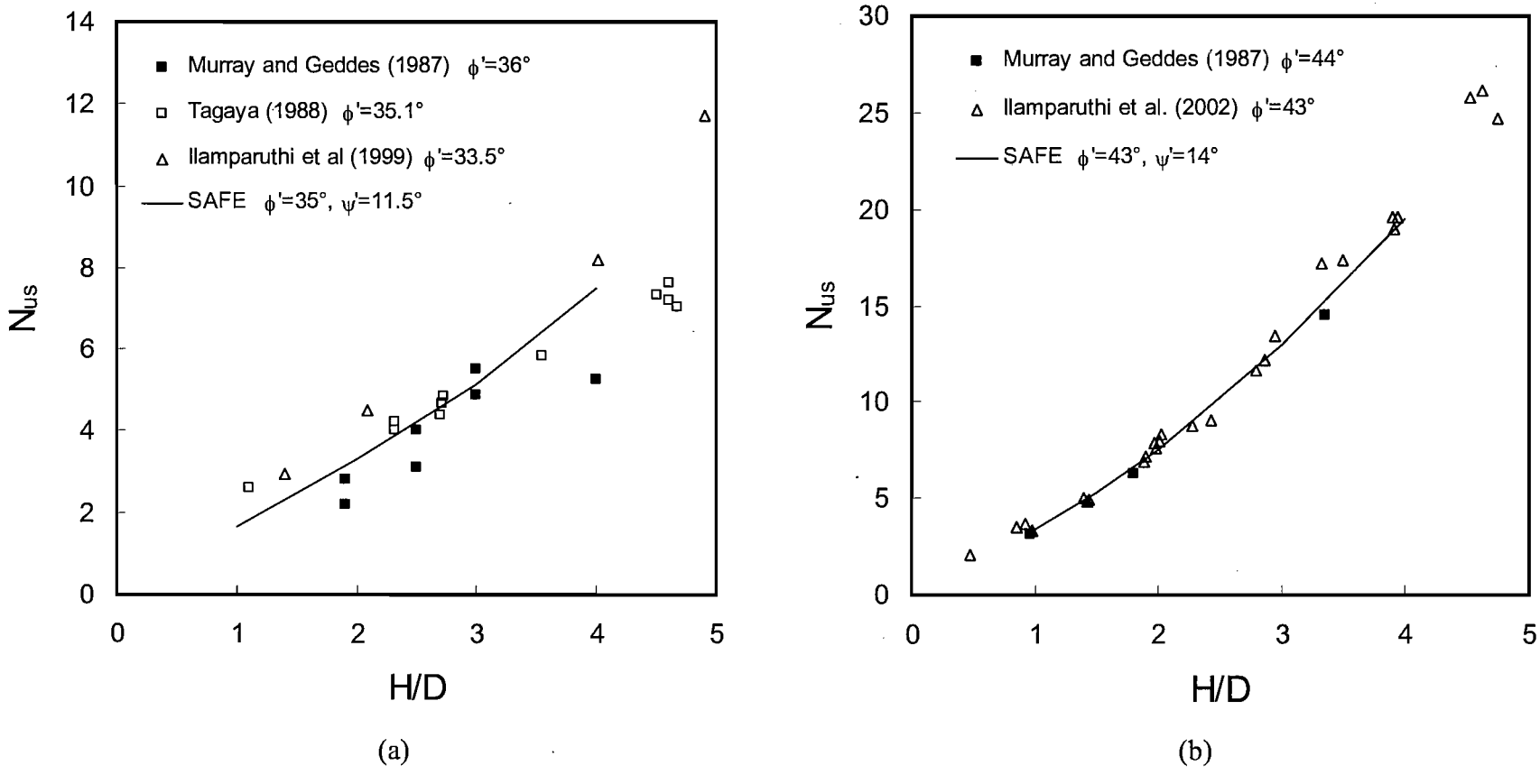

Figure 3.10 Comparison of SAFE uplift factors with existing experimental data for circular anchors in sand

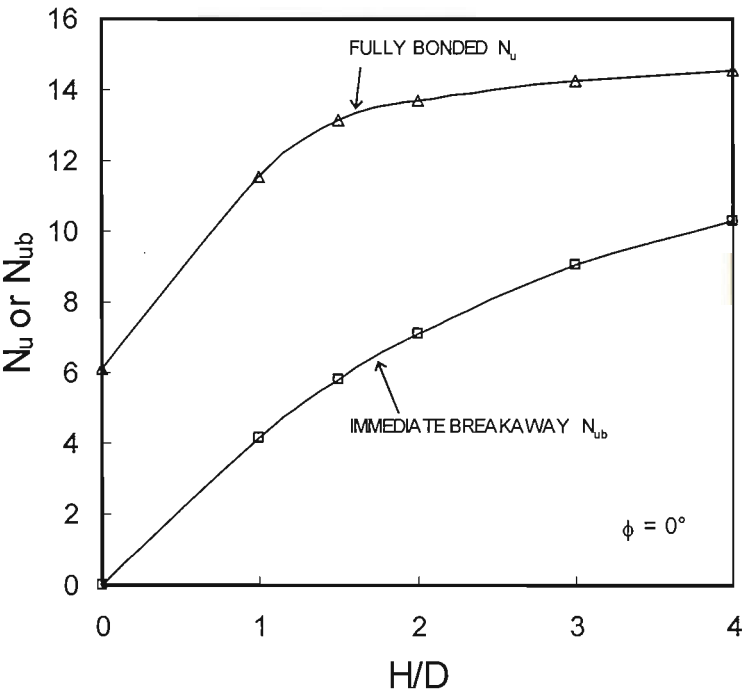

Figure 3.11 Uplift capacity factors for circular anchors in clay from SAFE analyses

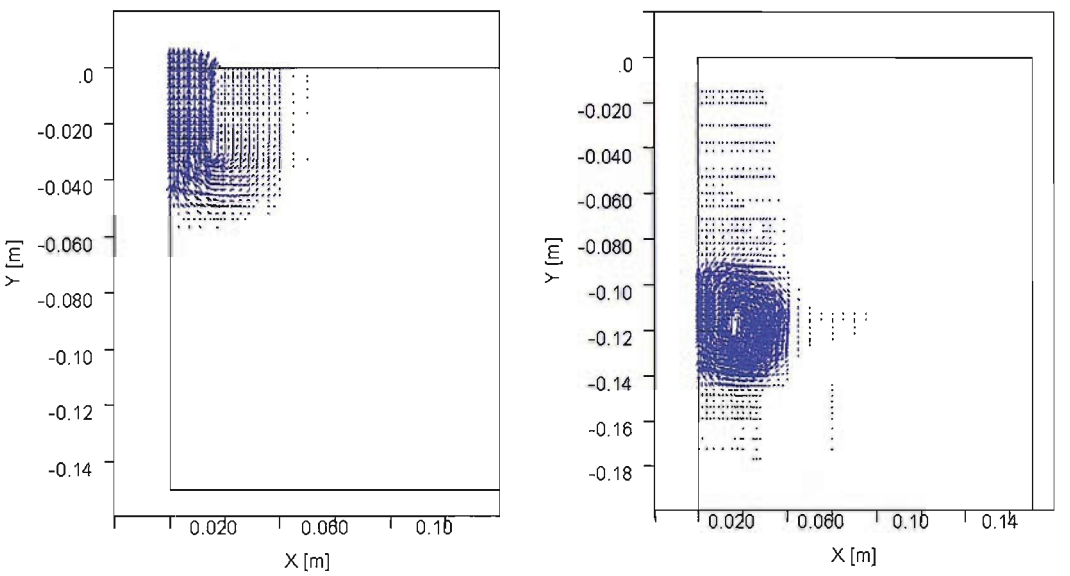

(a) Shallow anchor behaviour H/D=1 (b) Deep anchor behaviour H/D=4

Figure 3.12 Velocity fields at failure for the fully bonded anchor case

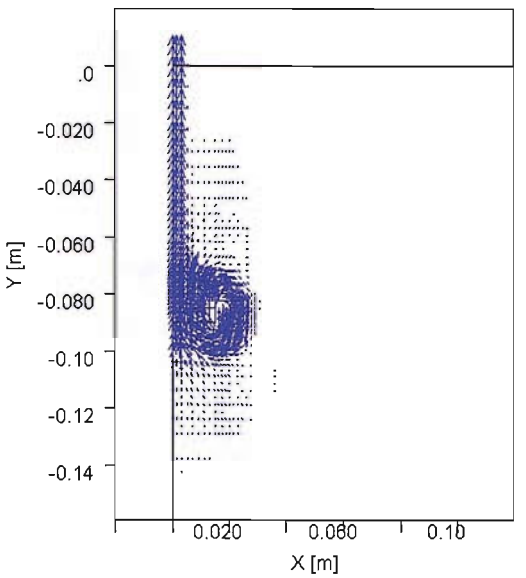

(a) Fully bonded anchor behaviour

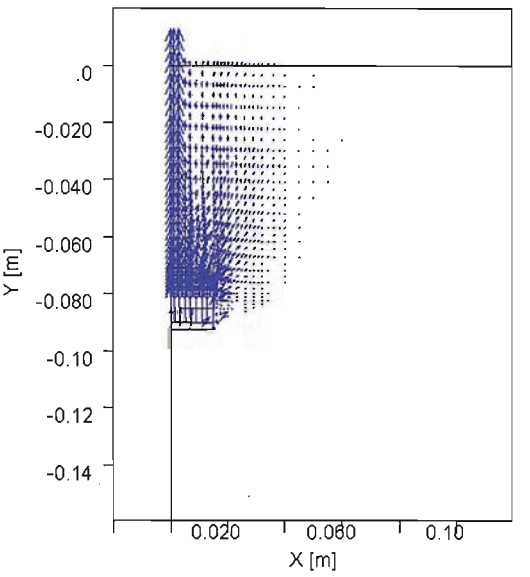

(b) Breakaway anchor behaviour

Figure 3.13 Velocity fields for circular anchors in clay, H/D=3

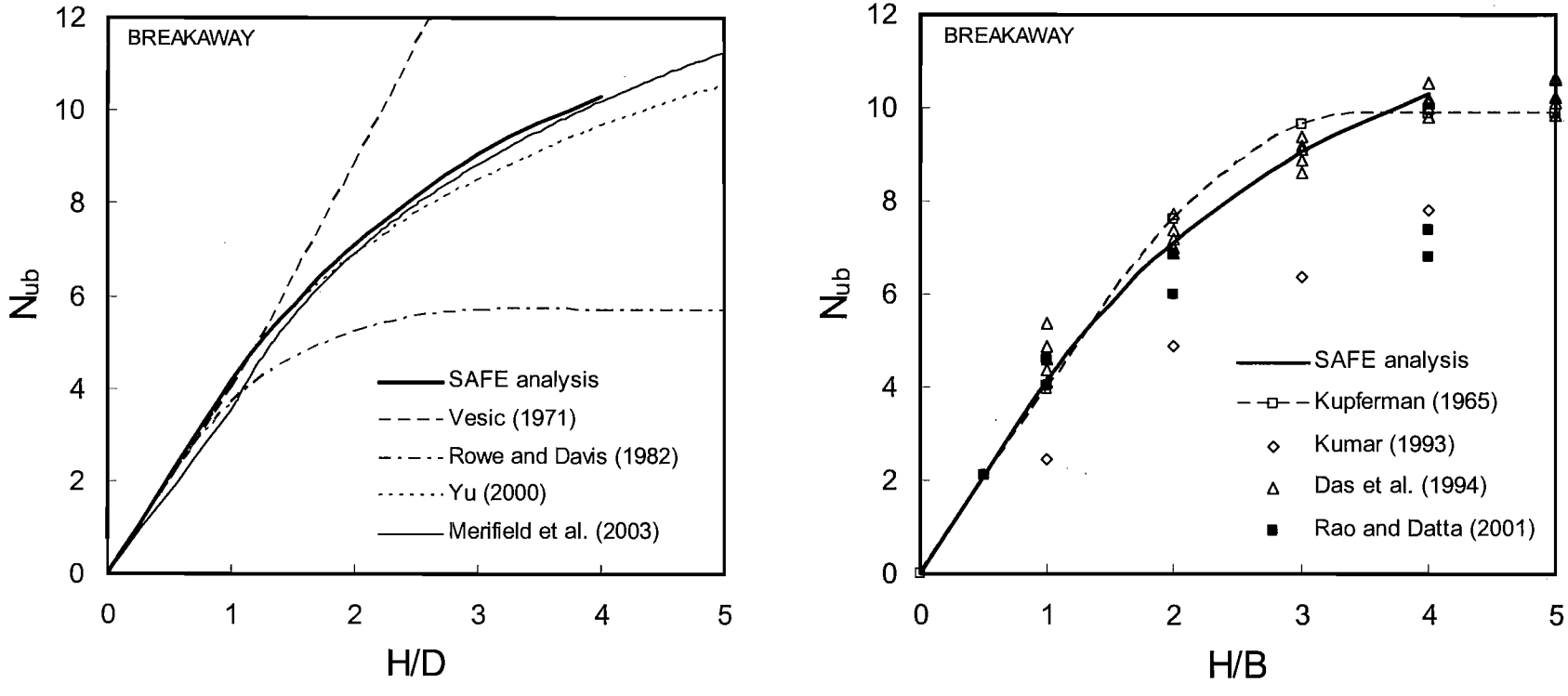

(a) Comparison with theoretical and numerical values

(b) Comparison with existing experimental data

Figure 3.14 Uplift capacity factors for the breakaway anchor case

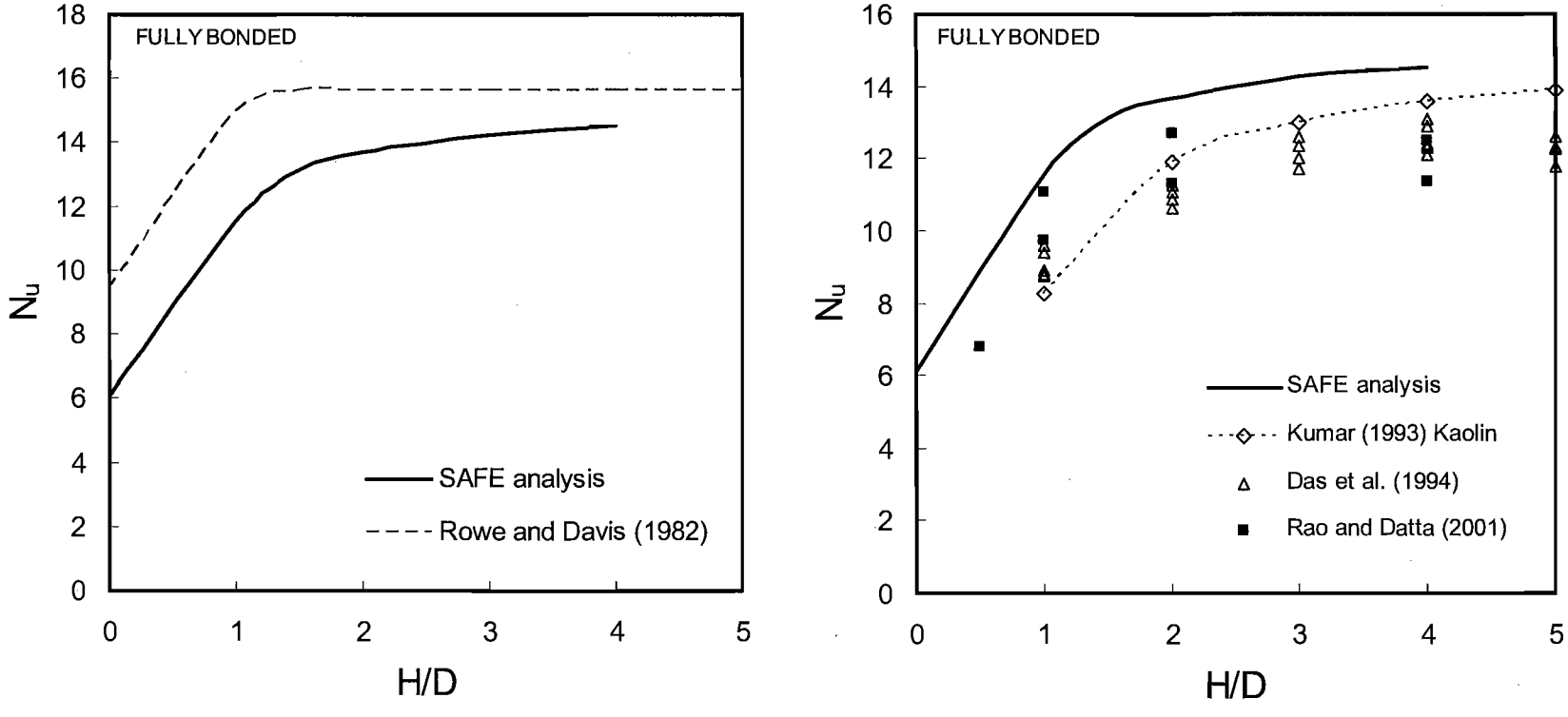

(a) Comparison with theoretical and numerical values

(b) Comparison with existing experimental data

Figure 3.15 Uplift capacity factors for the fully bonded anchor case

Chapter 4

SOIL PROPERTIES AND LABORATORY TESTING

4.1 Introduction

This chapter describes the various materials used throughout the centrifuge testing program. Soil properties for each material are given where currently available and additional laboratory testing is discussed. Details of laboratory testing undertaken on kaolin clay and silica sand are presented and parameters derived for the Finite Element analyses, described in Chapter 7, are discussed.

4.2 Kaolin Clay (type 'B')

Kaolin 'B' clay is used extensively during all forms of centrifuge model testing at the University of Western Australia (Stewart, 1992) and is the principal foundation soil used for the majority of the centrifuge testing described in this thesis (Chapters 5, 6 and 8). In order to clearly understand the results of the centrifuge study it is important to have an understanding of the properties of kaolin clay and its behaviour under the range of test conditions used in the centrifuge testing described later.

The relevant soil properties of kaolin B clay are presented in Table 4.1 and the particle size distribution is shown in Figure 4.1.

Table 4.1 Properties of Kaolin 'B' (after Stewart, 1992)

Liquid limit (LL)	*61%*
Plastic limit (PL)	*27%*
Plasticity Index (PI)	*34%*
Specific gravity (G_s)	*2.60*
Compression index (C_c)	*0.7*
Critical state friction constant (M)	*0.92*
e at 1 kPa on CSL (e_{cs})	*2.14*
Slope of NC line (λ)	*0.205*
Slope of OC line (κ)	*0.044*
Coefficient of consolidation (c_v)	*$\approx 3–5 \times 10^{-8}$ m^2/s*

4.2.1 Existing laboratory data

Despite the widespread use of kaolin clay as a representative fine grained soil in many experimental studies, extensive investigation of its mechanical properties is limited to relatively few studies (e.g. Al-Tabbaa and Wood, 1987; Lin and Penumadu, 2005 and Prashant and Penumadu, 2005).

In general, the kaolin clay used during centrifuge testing is mixed under vacuum at a moisture content of approximately 120% (i.e. around twice the liquid limit) to form a homogeneous slurry. It is then either poured into a strongbox and consolidated using a pressing machine and/or placed into a geotechnical centrifuge and consolidated under an increased centrifugal gravity. The consolidation characteristics of kaolin clay were investigated in some detail by Al-Tabbaa and Wood (1987) and further oedometer testing has been undertaken by Bhattarai (2002) and Toh and Fahey (2000). Values of the coefficient of consolidation (c_v) for normally consolidated kaolin samples obtained from some of these investigations are plotted in Figure 4.2(a) along with some limited data presented by Stewart (1990). The relationship of vertical permeability (k_v) with increasing void ratio (e) inferred from the results of Bhattarai (2002) is plotted in Figure 4.2(b) where it is compared with that observed by Al-Tabbaa and Wood (1987). While a similar relationship is predicted between the studies, the values of permeability measured by Al-Tabbaa and Wood (1987) appear to be some way above the other experimental data. It should be noted that the values reported by Al-Tabbaa and Wood are for tests conducted on kaolin 'A' clay rather than the kaolin 'B' clay

used in centrifuge testing at UWA. Al-Tabbaa and Wood (1987) also measured the horizontal permeability (k_h) of kaolin and concluded that at a given void ratio it could be a much as 3 times higher than the value of k_v for a vertically consolidated sample.

Stewart (1990) and Bhattarai (2002) conducted isotropically consolidated undrained triaxial compression tests and simple shear tests on samples of the kaolin B clay used in the UWA centrifuge investigations. The results of these investigations are summarised by Lehane *et al.* (2007) and are reproduced in Figure 4.3, which shows the variation of the undrained shear strength ratio (s_u/σ'_v) with overconsolidation ratios (OCR) between 1 and 4. The results of these tests are evidently reasonably well represented using the equation (e.g. Ladd, 1974) for which:

$$\frac{s_u}{\sigma'_v} = \left(\frac{s_u}{\sigma'_v}\right)_{nc} OCR^m \qquad (4.1)$$

where a value for the parameter m of 0.8 provides a best fit to the experimental data. The normally consolidated (OCR=1) undrained strength ratios, $(s_u/\sigma'_v)_{nc}$, are shown with increasing vertical effective stress in Figure 4.4 for triaxial compression and simple shear tests. The ratio for triaxial compression lies between about 0.26 and 0.28 at low vertical effective stresses with more limited data presented at higher stresses. These values are in broad agreement with those obtained by Ladd *et al.* (1999) for samples of Boston Blue clay and may be considered to be representative of a soft natural clay. Significant scatter is observed in the data from simple shear tests shown in Figure 4.4 although an average value of the undrained strength ratio just below that for triaxial compression may be inferred (in the range 0.25-0.27). This is again in broad agreement with, if a little higher than, that observed by Ladd *et al.* (1999) for Boston Blue clay.

Given the data presented in Figures 4.3 and 4.4 the following form of Equation 4.1 may be taken to provide a reasonable representation of the undrained strength ratios of UWA kaolin clay in compression and simple shear:

$$\frac{s_{uss}}{\sigma'_v} \approx \frac{s_{utc}}{\sigma'_v} = 0.26.OCR^{0.8} \qquad (4.2)$$

where s_{uss} and s_{utc} are the undrained strengths in simple shear and triaxial compression respectively. While Equation 4.2 is based on the available results for kaolin clay alone, in reality the undrained strength ratio for clay in simple shear is likely to be around 70-80 % of the ratio for triaxial compression (Ladd *et al.* 1999).

One focus of the centrifuge test program outlined in Chapter 5 was to quantify the variation in capacity of anchors founded on clay subject to increasing uplift velocity. Where high uplift velocities give rise to the fully bonded anchor behaviour discussed in Chapters 2 and 3 it is thought that the effect of the increased uplift velocity on the undrained shear strength of the clay will also have a significant influence on the uplift capacity of the anchor. Although no specific investigation of the rate dependence of kaolin's undrained shear strength has been previously undertaken, trends discussed in Chapter 2 and summarised by Leroueil & Hight (2003) suggest that the following relationship may be used to assess the influence of the axial strain rate ($\dot{\varepsilon}_a$) on the undrained shear strength under triaxial conditions:

$$s_u = s_{uref}\left(\frac{\dot{\varepsilon}_a}{\dot{\varepsilon}_{ref}}\right)^{0.04} \quad with\ \dot{\varepsilon}_{ref} > 0.0001\ \%/s \tag{4.3}$$

where $\dot{\varepsilon}_{ref}$ is the reference strain rate and s_{uref} is the undrained shear strength at $\dot{\varepsilon}_a = \dot{\varepsilon}_{ref}$. This inferred relationship corresponds to an increase in shear strength of approximately 10% per log cycle increase in strain rate. Triaxial data presented by Sheahan *et al.* (1996) suggest that the exponent in Equation (4.3) reduces with OCR and is reported to be approximately equal to 0.02 for Boston Blue clay at moderate to high OCR values when strain rates are less than 0.01 %/s.

4.2.2 Triaxial extension tests

For a foundation subjected to rapid uplift the stress path experienced by the clay below the foundation centre will be substantially similar to that imposed on a clay sample in an undrained triaxial extension test. It has been mentioned previously that at very high uplift velocities separation of the foundation from the underlying clay may not occur and that under these circumstances strain-rate dependent increases in the

undrained shear strength of the clay may further enhance the uplift capacity of the foundation. In order to assess the strain-rate dependence of the shear strength of kaolin clay and therefore assist interpretation of the centrifuge tests outlined in Chapter 5, a series of triaxial extension tests were performed. The test series comprised of six consolidated undrained triaxial extension tests on reconstituted 50mm diameter kaolin samples tested at four axial strain rates that were constant throughout shearing. Four tests were conducted with an initial mean effective stress (p'_0) of 20 kPa and two tests were undertaken with p'_0 equal to 50 kPa. An overview of the triaxial testing program is given in Table 4.2.

Table 4.2 Overview of triaxial test program

Test	$\dot{\varepsilon}_a$	p'_0	σ'_{vc}
	%/s	kPa	kPa
UE-1	0.00045	20	180
UE-2	0.033	20	180
UE-3	2	20	180
UE-4	19.8	20	180
UE-5	0.00045	50	250
UE-6	19.8	50	250

The triaxial apparatus used in each test was a 5Hz cyclic triaxial machine with a 40kN maximum ram capacity. The machine, shown in Figure 4.5, uses a balanced ram which allows for the free flow of water into and out of the cell during shearing in order to maintain the specified cell pressure. The axial displacement is measured outside of the cell at the base of the ram while the axial load is measured using a 2kN load cell installed inside the triaxial cell at the top of the clay sample. The pore pressure in the sample was measured during shearing at the base platen and also at the mid-plane of each sample. The mid-plane probe used was the same modified transducer, developed by Take and Bolton (2003), as that used in the centrifuge test series, described later in Chapter 5 (Section 5.5.4). The response time of the mid-plane pore pressure transducer was assessed in each test during B-value checks and in each case a full response (a B-value of >95%) was recorded within less than 1 second. For the same check the response time of the base pore pressure measurement was approximately 15-20 seconds. All load, displacement and pore pressure data was

logged using a central cyclic control system modified in order to perform single stage dynamic ramps in either compression or extension. The system enabled the application of an axial strain rate of up to 20% per second; this rate is approximately 1000 times faster than the fastest rate employed by Sheahan *et al.* (1996) in their study of strain rate effects on Boston Blue Clay.

The kaolin clay sample was mixed under vacuum (with an initial water content of 120%), placed carefully into a consolidation strongbox and then consolidated one-dimensionally and incrementally in a pressing machine to a maximum vertical effective stress (σ'_{vy}) of 250 kPa (which equates to a maximum mean effective stress, p'_y, of about 180 kPa, assuming K_0=0.6). The sample was then allowed to swell back to vertical effective stress of 50 kPa over a period of about one week to attain a one-dimensional overconsolidation ratio of 5. Thin walled samplers with an internal diameter of 50mm were employed to retrieve the samples for triaxial testing. Moisture contents derived from trimmings around each of the samples confirm that the soil was uniform with depth with a value of 41.4% ± 1% being observed in each case. Two of the samples were re-consolidated to $\sigma'_v = p'_0 = 50$ kPa and as such had an OCR of 5 prior to undrained shearing (assuming minimal loss in effective stress during sampling). Four other samples were allowed to swell isotropically from $\sigma'_v = p'_0 = 50$ kPa to a value of 20 kPa prior to shearing. In this latter case the OCR is taken as the isotropic value = p'_y/p'_0=180/20 = 9, since the K_0=1 condition imposed during isotropic swelling differs from the larger K_0 values that would be exist during 1-D unloading at this level of overconsolidation. A relatively high back pressure of 300 kPa was employed in all tests and ensured that the B value was in excess of 0.95 prior to shearing of all samples. For each test the recommendations of Head (1982) were employed to correct the recorded deviator stress (q) for the effect of membrane stiffness.

The deviator stress and mid-plane pore pressure relationships with axial strain for samples with p'_0=20 kPa measured at the four axial strain rates ($\dot{\varepsilon}_a$) of 0.00045, 0.033, 2 and 19.8 %/s are shown in Figure 4.6. It is apparent that both the stiffness and strength are rate dependent and increase with an increase in axial strain rate. The axial strain required to attain peak strength increases with the strain rate and specimen

failure occurs at less than 10% axial strain (ε_a) for the slowest rate only. For all the tests except that at the slowest strain rate, localised shear planes were apparent in the top half of the specimen at an axial strain of about 15-20% (approximately 2-5% beyond ε_f in each case). In all cases the pore pressure measured by the mid-plane probe decreases progressively with continued shearing and the change in pore pressure at the axial strain at failure (ε_f) increases with increasing strain rate. The initial reduction of the pore pressure at equivalent values of ε_a (<10%) would appear to be greater at slower axial strain rates indicating the possibility of some induced dilation in the samples tested at high strain rates. This behaviour may also be attributed partly to the localised shear failure observed as mentioned previously. Undrained strengths, s_{ute} ($=q_{max}/2$) at $\dot{\varepsilon}_a$=19.8 %/s are over 70% higher than those for $\dot{\varepsilon}_a$=0.00045 %/s for both p'_0 values investigated. An overview of these results is presented in Table 4.3.

Table 4.3 Overview of triaxial extension test results

Test	$\dot{\varepsilon}_a$	p'_0	OCR	q_{max}	Δu_{min}	ε_f	$(\phi')_{peakq}$
	%/s	kPa		kPa	kPa	%	
UE-1	0.00045	20.1	9	-30.8	-25.3	-9.4	28.5
UE-2	0.033	19	9	-41.1	-31.3	-13.7	31.9
UE-3	2	18.9	9	-45.7	-34.2	-17	35.2
UE-4	19.8	21.1	9	-53.6	-49	-19.1	32.3
UE-5	0.00045	50.4	5	-53.7	-35.6	-10.7	29.5
UE-6	19.8	51.0	5	-86.3	-76.5	-16.1	31.6

The stress paths (in q-p' space) obtained for tests on all samples are presented in Figure 4.7. The values of peak friction angle, $(\phi')_{peak}$ shown in Table 4.3 and Figure 4.7 were assessed at peak deviator stress rather than at the peak stress ratio (q/p'), where the mobilised friction angles are observed to be much larger. It is apparent that the value of $(\phi')_{peakq}$ mobilised by each sample is relatively independent of the axial strain rate with a value of approximately 32°. This trend is consistent with that reported by Sheahan *et al.* (1996) for triaxial compression tests on reconstituted Boston Blue clay at high OCR values and the value of the friction angle is the same as that reported by Lin & Penumadu (2005) for kaolin in triaxial extension. The friction

angles mobilised at peak shear stress for tests where $\dot{\varepsilon}_a$ is equal to 0.00045 %/s are plotted with OCR in Figure 4.8, where they are compared with the friction angles in triaxial compression and simple shear from Bhattarai (2002) as reported by Lehane *at al.* (2007). There is significant scatter in the data for triaxial compression, particularly at low values of OCR however an average value for ϕ'_p of approximately 26 ± 2° may be obtained from the data. The peak friction angles at maximum stress recorded in simple shear are higher than those in triaxial compression but are in better agreement with those measured in the triaxial extension tests. The increase in undrained shear strength with axial strain rate noted from Table 4.3 is evidently due to the increased tendency for dilation (i.e. greater reduction in pore pressure) as the rate increases. Although the mid-plane pore pressure measurements should perhaps be treated with more caution at the higher strain rates of 2 and 19.8 %/s, it is interesting to note that they are compatible with the peak friction angles measured at lower strain rates.

The undrained strength ratios in undrained triaxial extension at $\dot{\varepsilon}_a$ = 0.00045 %/s are plotted with OCR in Figure 4.9. The results of Stewart (1990) and Bhattarai (2002), as presented previously, are also plotted. It is evident that the strength ratios in triaxial extension are well represented by the relationship:

$$\frac{s_{ute}}{\sigma'_v} = 0.13.OCR^{0.8} \qquad (4.4)$$

where s_{ute} is the undrained shear strength in triaxial extension. The derived value for the normally consolidated undrained shear strength ratio of 0.13 is just over half that for kaolin in triaxial compression values and is comparable to that reported for reconstituted Boston Blue clay in triaxial extension by Ladd *et al.* (1999).

The rate dependence of the undrained strength in extension (s_{ute}) is illustrated on Figure 4.10 where is it seen that s_{ute} increases by approximately 12.5% per log cycle increase in strain rate. The variation in undrained strength ratio in extension provided by Equation 4.4, is shown in Figure 4.10 and provides a good fit to the observed rate dependence of the undrained shear strength measured in all 6 undrained triaxial extension tests.

$$s_{ute} = s_{uref}\left(\frac{\dot{\varepsilon}_a}{\dot{\varepsilon}_{ref}}\right)^{0.05} \quad with\ \dot{\varepsilon}_{ref} = 0.0001\ \%/s \tag{4.5}$$

Equation (4.5) implies a normally consolidated undrained strength ratio in extension of approximately 0.17 at a typical 'quick undrained' testing rate of 1% per minute.

Comparisons between the secant undrained modulus (E_u) assessed from the triaxial extension tests at increasing strain rate are presented in Figure 4.11(a). It is clear that specimens tested at higher strain rates display increased values of E_u, particularly at axial strains less than 10%. The highest rate dependence is seen to occur in the region of 0.2-2% ε_a, with increases in the value of E_u of up to 100% being observed between the fastest and slowest strain rates. In general, changes in the pore pressure measured at the mid-plane of the specimen, shown in Figure 4.6, are relatively low at axial strains less than about 4%. For this reason changes in effective stress in the region of highest observed increase in E_u are relatively small (typically within 10% of p'_0 at axial strains less than 1%) and therefore increases in stiffness are thought to arise due to viscosity and not due to changes in effective stress at higher strain rates. At high axial strains greater reductions in the measured pore pressure occurs, resulting in a greater change in the effective stress and stiffness becomes relatively independent of strain rate. Values of E_u are normalized by the undrained shear strength of the respective samples (s_{ute}) and are plotted against axial strain in Figure 4.11(b). Apart from the test where $\dot{\varepsilon}_a$ =0.00045 %/s with p'_0=50 kPa, it may be seen that E_u is generally proportional to s_{ute} at a given strain with E_u/s_{ute} reducing from a value of approximately 300 at ε_a=0.1 % to about 75 at ε_a=1 % and a value of 20 at ε_a=10 %.

4.3 Cemented and un-cemented silica sand

In the centrifuge study (Chapter 5) a range of foundation backfill materials including kaolin clay (as described in section 4.2) and superfine silica sand are investigated. The benefits of backfill stabilisation, using cement treated silica sand are also investigated (Chapter 9) and the properties of cemented and un-cemented silica sand are discussed

here. The relevant soil properties of the (un-cemented) silica sand used during centrifuge testing at UWA are presented in Table 4.4.

Table 4.4 Properties of superfine silica sand

Specific gravity G_s	2.67
D_{50}	0.18 mm
Min. saturated density $\rho_{s,min}$	1.94×10^3 kg/m^3
Min. saturated density $\rho_{s,max}$	2.06×10^3 kg/m^3
Permeability k	$1.1 - 3.6 \times 10^{-4}$ m/s

The silica sand is a non-plastic uniform fine quartz sand with a mean effective particle size (D_{50}) of 0.18 mm and minimum and maximum void ratios of 0.52 and 0.75 respectively.

The properties of cemented sand were investigated for sand samples modified by the addition of 1%, 3% and 5% (by dry weight) of early strength Portland cement (Type III). This cement is more finely ground and includes a higher proportion of blast furnace slag than ordinary Portand cement, and has a setting time of approximately 3 hours. Given the fast gain in strength with time exhibited by this cement a reasonably short curing period of 20 hours was able to be adopted for each test specimen. The specific gravity of the cement grains is 3.15.

4.3.1 Laboratory testing programme

All laboratory tests were carried out using a very loose consistency of backfill sand with a void ratio of approximately 0.74 for un-cemented sand and in the range of 0.73 to 0.68 for cement contents of 1% to 5% respectively. The soil samples were prepared first by hand-mixing the dry sand and cement and then adding water to a moisture content of 12%. The strength and stiffness of the cement treated sand was measured in direct shear and unconfined compression tests whilst direct shear tests were performed on the un-treated sand. Isotropic compression tests with shear wave velocity measurements using bender elements were undertaken for measurement of the very small strain shear modulus (G_0).

The moulded soil samples used in the G_0 determinations and the unconfined compression tests were prepared by hand-mixing dry sand and water. The samples were statically compacted in three layers into an 80 mm diameter by 160 mm high split mould according to the undercompaction process (Ladd, 1978) to ensure a homogenous sample. The specimens moulded for the direct shear tests were statically compacted in a single layer into a 71 mm diameter by 35 mm high shear box. For the isotropic compression tests with bender elements the specimens were installed in the triaxial chamber immediately after preparation and were left to cure for 20 hours under an isotropic effective stress of 20 kN/m^2. The samples tested in unconfined compression (UC) were cured for 16 hours following mixing and then submerged in a water tank (maintained at 23 $\pm 3^{\circ}$C) for a further 4 hours for saturation to minimize suction effects. Excess surface water was removed using an absorbent cloth prior to testing. A similar curing and saturation regime to that of the UC tests was adopted for the samples subjected to direct shear which were left to cure for 20 hours under effective normal stresses of 50, 150 and 300 kN/m^2.

Unconfined compression tests have been used in the majority of previously published experimental studies (e.g. Stefanoff *et al.* 1983 and Consoli et *al.* 2003) in order to verify the effectiveness of cement stabilization or to access the importance of influencing factors on the strength of cemented soils. An automatic loading machine, with a maximum capacity of 50kN and proving rings with capacities of 10kN and resolution of 0.005kN were used for each unconfined compression tests. The maximum load was recorded for each test sample. Acceptance criteria stipulated that the individual strengths of three specimens, moulded with the same characteristics, should not deviate from the mean strength by more than 10%.

The direct shear tests were carried out under a controlled displacement rate of 0.5 mm/minute. The execution of the shear box tests followed the general procedures described by BS 1377 (1990). Each specimen was fully immersed throughout the test in order to ensure full saturation.

The bender element test procedure was introduced by Shirley and Hampton (1977) and is now a standard technique for deriving the small strain shear modulus of a soil.

The velocity of a shear wave propagating across the sample (V_s) is measured and G_0 is determined from the relationship:

$$G_0 = \rho V_s^{\,2} = \rho\left(\frac{L^2}{t^2}\right) \tag{4.6}$$

where ρ is the density of the soil, L is the distance between the elements and t is the travel time of the shear wave trough the sample. Bender element tests were carried out in a stress path apparatus. The test procedures and methods of interpretation followed those of Jovicic *et al.* (1996), using a single shot sine wave with measurement of the wave velocity at the first arrival, taking care to use sufficiently high frequencies to avoid near field effects. For each reading a range of frequencies were used, ensuring that the measured arrival time was not frequency dependent.

4.3.2 Laboratory test results

The results of the laboratory testing for un-cemented sand and samples with 1%, 3% and 5% cementation are summarised in Table 4.5. The average unconfined compressive strengths (q_{uc}) are indicative of a weakly to moderately cemented soil, depending on the classification considered (e.g. Beckwith and Hansen 1982; Rad and Clough 1985 or Hardingham 1994).

Table 4.5 Overview of laboratory test results for un-cemented and cemented sand

Sample	Unconfined compressive strength q_{uc} (kPa)	Peak friction angle ϕ'_p (degrees)	Shear strength at zero effective stress c' (kPa)	Elastic shear modulus[1] G_0 (MPa)
Un-cemented	-	34.7	0	50
1% cement	25	35.3	17.7	249
3% cement	87	39.8	28.2	566
5% cement	365	41.5	57.4	973

[1] At a mean effective stress of 20 kPa

The peak strength envelopes obtained from direct shear tests with normal stresses of 50 kPa, 150 kPa and 300 kPa are shown on Figure 4.12(a) and the corresponding

values of c' and ϕ'_p are listed in Table 4.5. It is apparent that the cement content has a marked effect on the value of c', increasing from zero for un-cemented sand to 57 kPa for sand with a cement content of 5%. The relationship between c' and cement content is clearly shown in Figure 4.12(b) and is observed to be approximately linear at the cementation ratios investigated. The cement content is also observed to have a slight effect on the value of ϕ'_p which is thought to be principally due to the higher densities of the cemented sand and/or modest differences between respective samples. Typical shear stress-displacement curves measured in the direct shear tests are shown in Figure 4.12(c), for a normal stress of 50 kPa. These highlight the brittle nature of the cemented sand and the tendency, after large relative displacement, for the shear strength to reduce to close to that of the un-cemented sand.

The measured G_0 values are listed in Table 4.5, which indicates that the cemented sand specimens were about 5, 11 and 20 times stiffer than the un-cemented sand for 1%, 3% and 5% cement contents respectively. The relationship between G_0 and cement content is shown in Figure 4.13 where, similarly to that between c' and cement content, a near proportional relationship is observed.

4.4 Summary

The foundation and backfill materials to be used in the centrifuge model studies seen in subsequent chapters have been investigated. Results from previous laboratory studies of kaolin clay have been reviewed and compared to the results of a recent series of undrained triaxial extension tests. It is apparent that:

i. The vertical permeability (k_v) of kaolin clay increases with void ratio (e) and, based on the available evidence, is within the range $3 - 4.6 \times 10^{-9}$ at e =2. The horizontal permeability (k_h) may be up to 3 times higher than k_v at a given value of e.

ii. The stress path experienced by the clay beneath a foundation subject to rapid uplift is likely to be broadly similar to that imposed on a clay sample in an undrained extension test. The undrained strength ratio for kaolin clay in

triaxial extension is well represented by the equation (e.g. Ladd and Foott, 1974) in the form:

$$\frac{s_{ute}}{\sigma_v'} = 0.13.OCR^{0.8} \qquad (4.4)$$

iii. The peak effective stress friction angle $(\phi')_{peakq}$ for kaolin in triaxial extension is equal to approximately 32°.

iv. The observed rate dependence of the undrained shear strength in triaxial extension is well represented by:

$$s_{ute} = s_{uref}\left(\frac{\dot{\varepsilon}_a}{\dot{\varepsilon}_{ref}}\right)^{0.05} \quad with\ \dot{\varepsilon}_{ref} = 0.0001\ \%/s \qquad (4.5)$$

v. The stiffness of kaolin clay increases with increasing axial strain rate ($\dot{\varepsilon}_a$) and these increases are related to viscous effects at axial strains less than about 2%.

Laboratory testing of un-cemented sand and sand modified by the addition of 1%, 3% and 5% (by dry weight) of Portland cement have shown that:

i. For the cement ratios tested the increase in the value of the Mohr-Coulomb c' varies approximately linearly with the cement content.

ii. The shear stress-displacement behaviour observed from direct shear tests indicates a brittle response of cemented sand where the shear strength may reduce to that of un-cemented sand at large displacements.

iii. Cemented sand samples may be up to 20 times stiffer than un-cemented sand and the value of G_0 also varies approximately linearly with cement content.

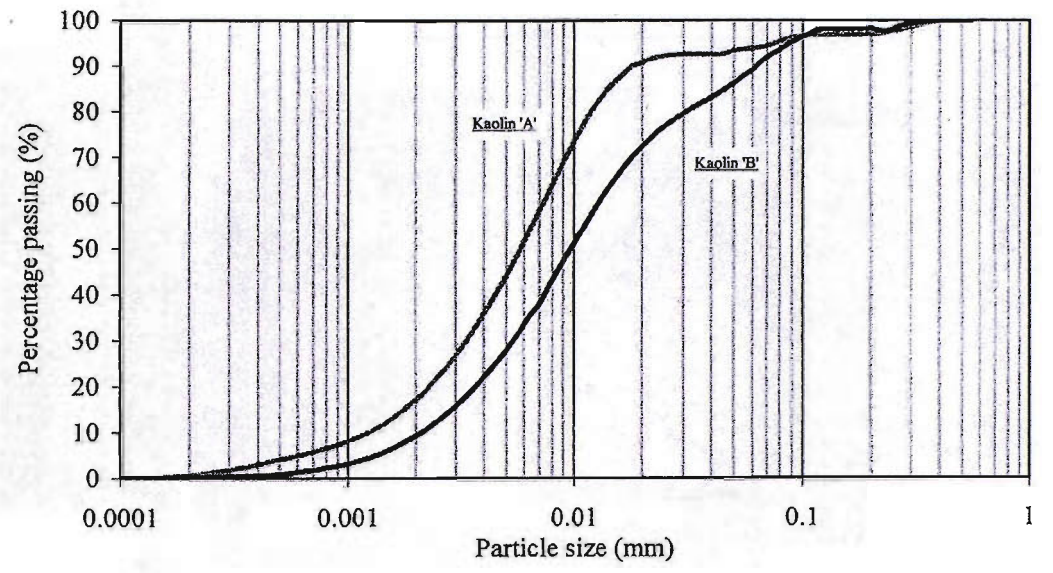

Figure 4.1 Particle size distribution for Kaolin B clay

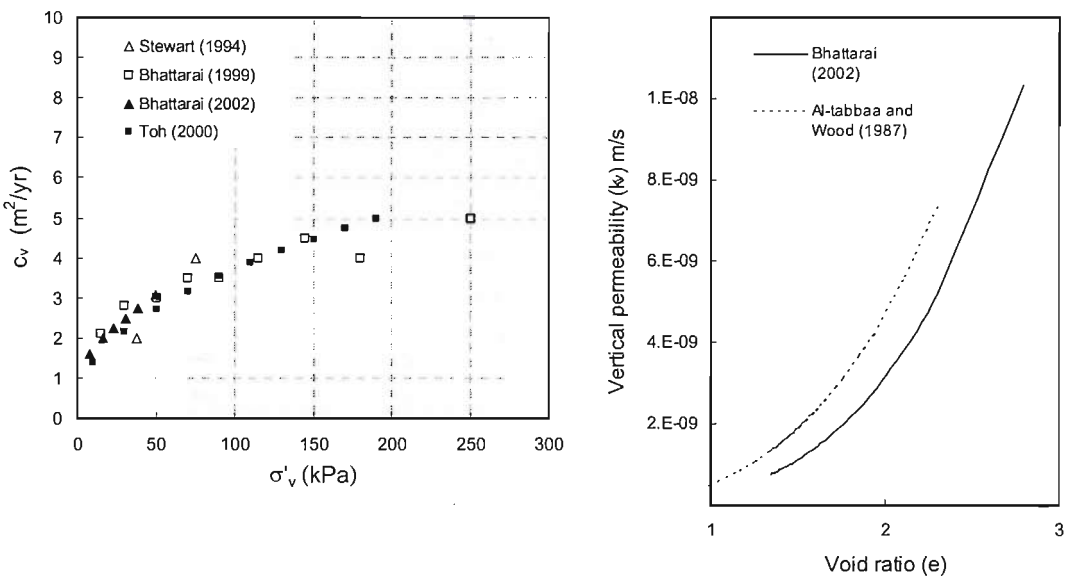

(a) coefficient of consolidation (b) vertical permeability

Figure 4.2 Consolidation characteristics of kaolin clay

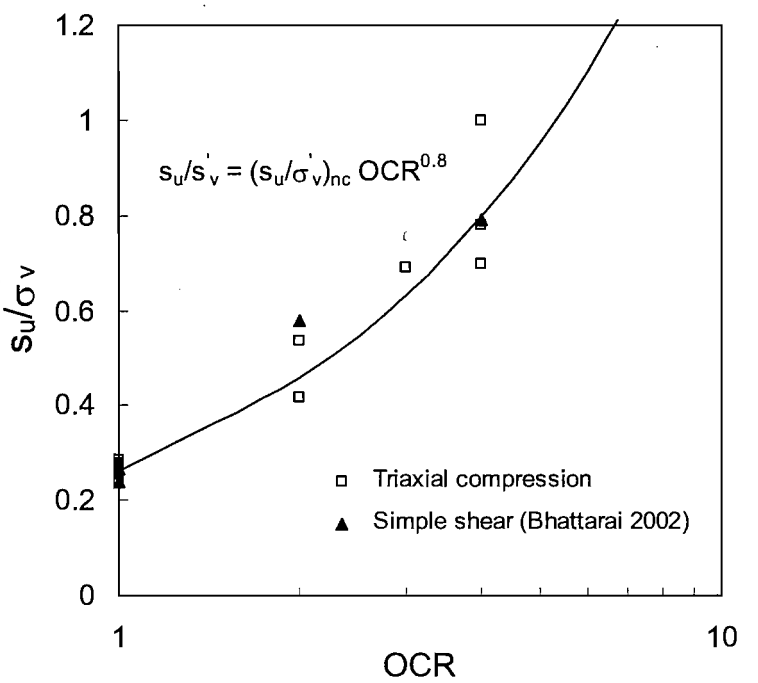

Figure 4.3 Variation of undrained strength ratio with OCR (Lehane et al. 2007)

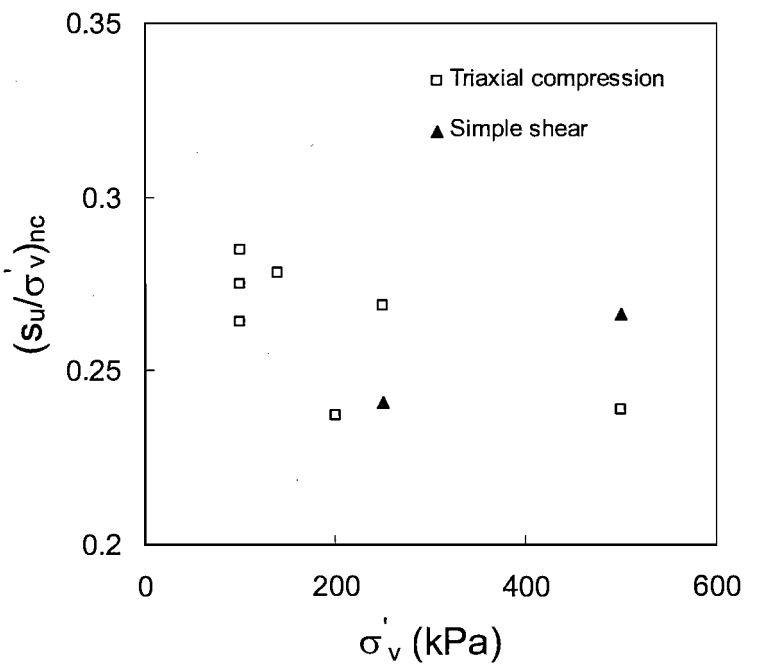

Figure 4.4 Normally consolidated strength ratio with vertical effective stress, OCR=1 (Lehane et al. 2007)

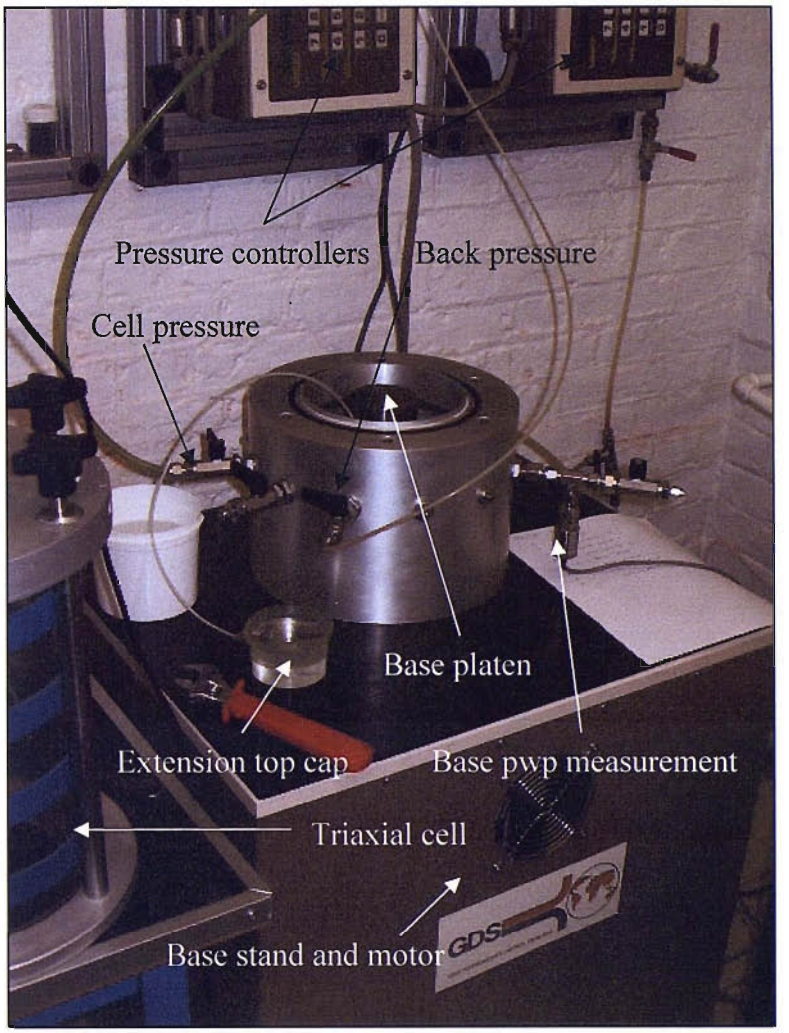

Figure 4.5 The GDS (5Hz) cyclic triaxial apparatus

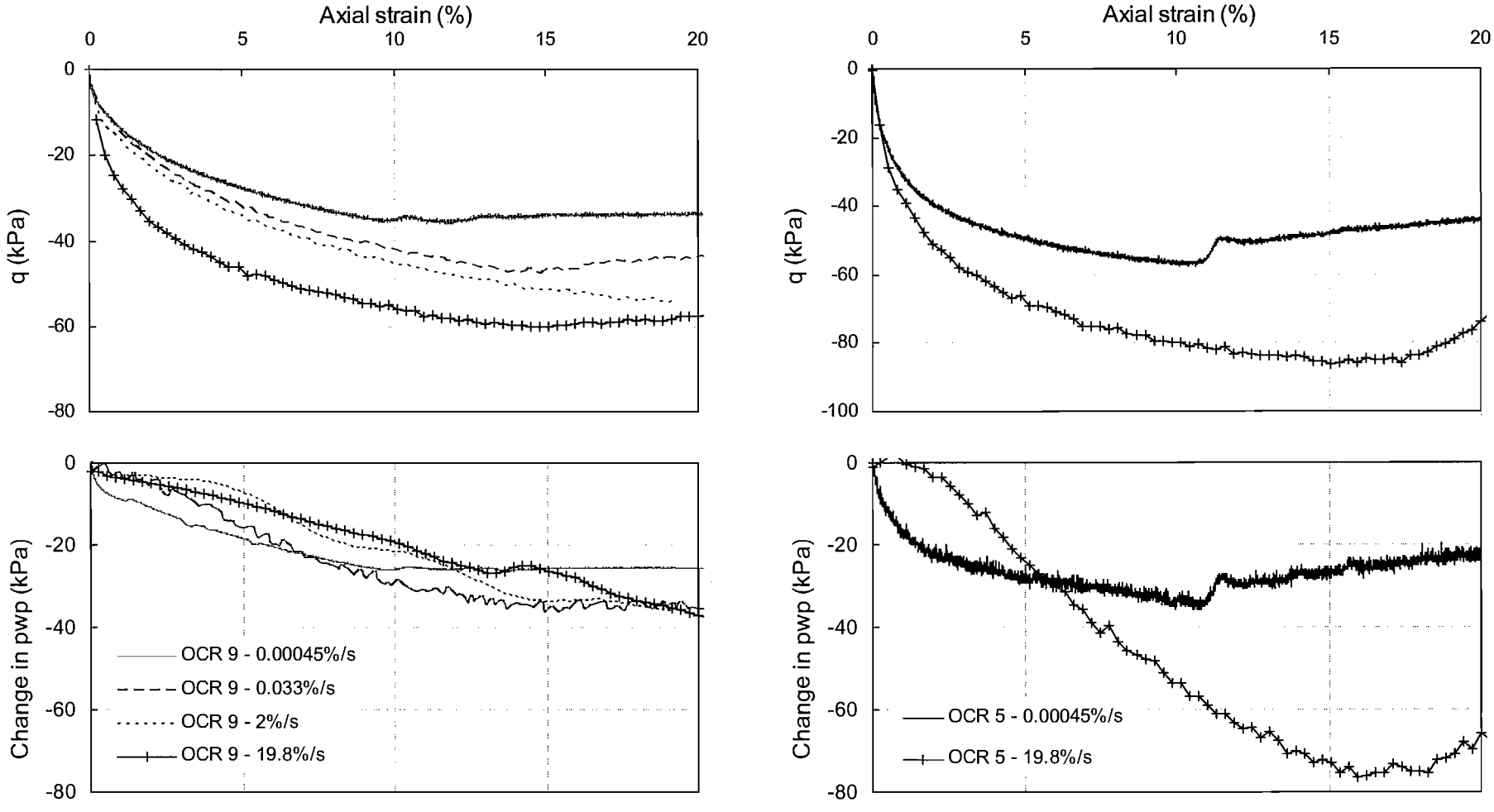

Figure 4.6 Variation of deviator stress and mid-plane pore pressure for undrained triaxial extension tests

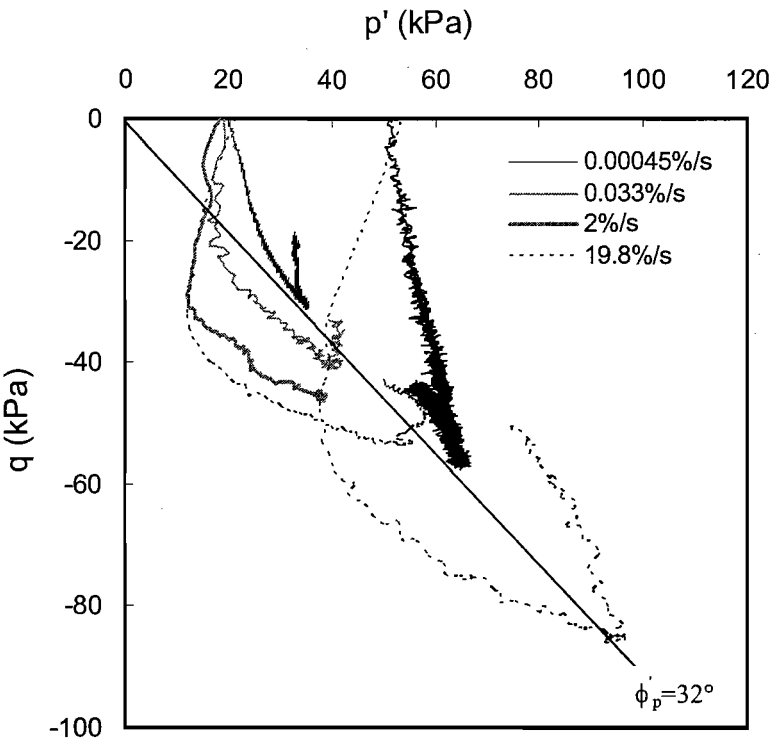

Figure 4.7 Stress paths for kaolin clay in undrained triaxial extension (OCR 5 and OCR 9)

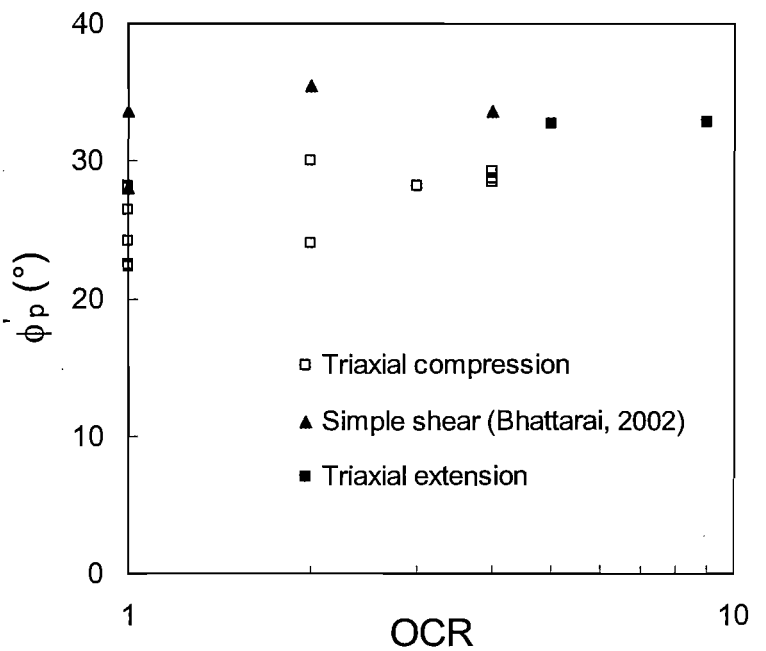

Figure 4.8 Variation of peak friction angle with OCR (Lehane et al. 2007)

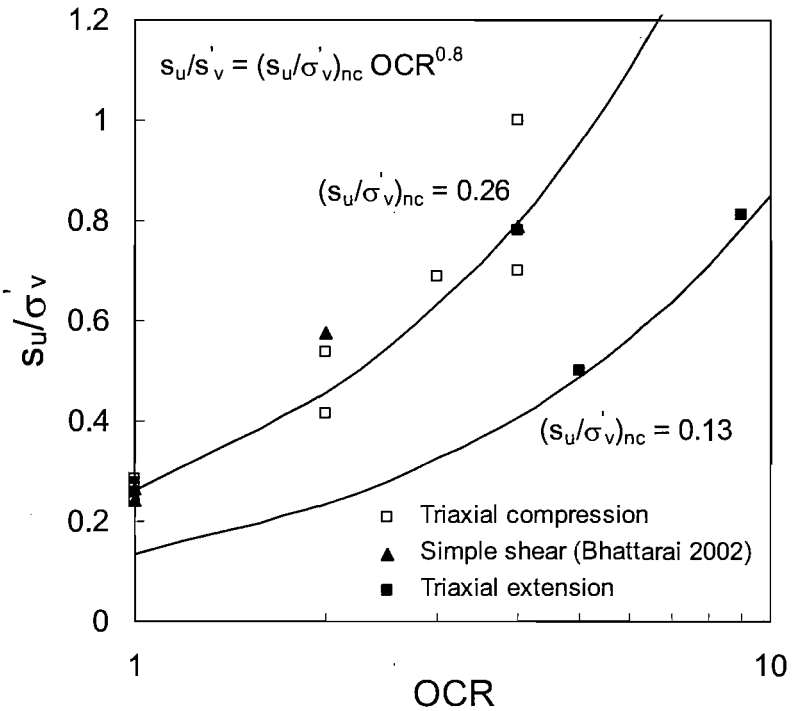

Figure 4.9 Comparison of undrained strength ratios with OCR from laboratory testing of kaolin (Lehane et al. 2007)

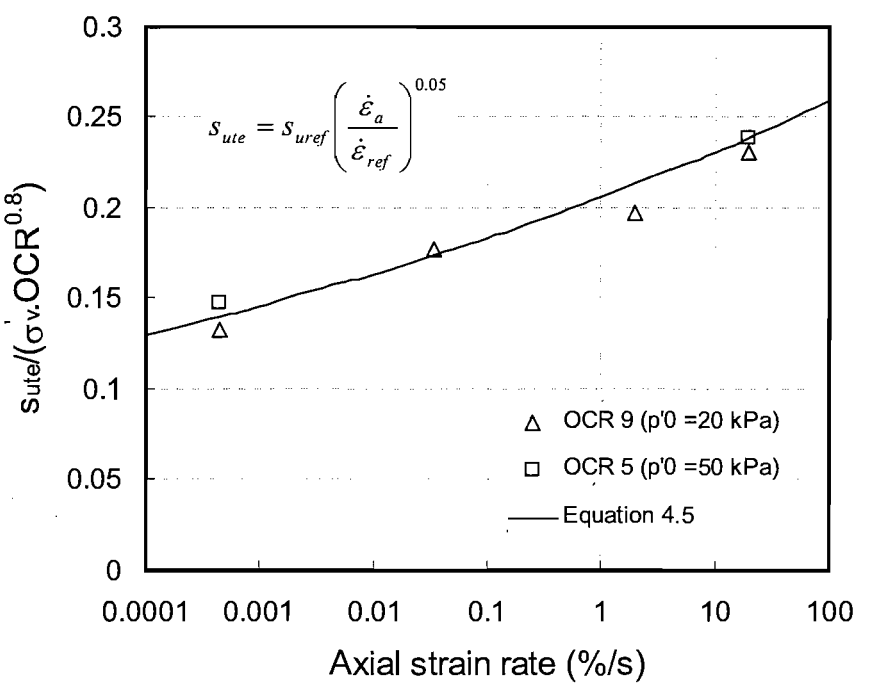

Figure 4.10 Rate dependence of the undrained strength of kaolin in triaxial extension

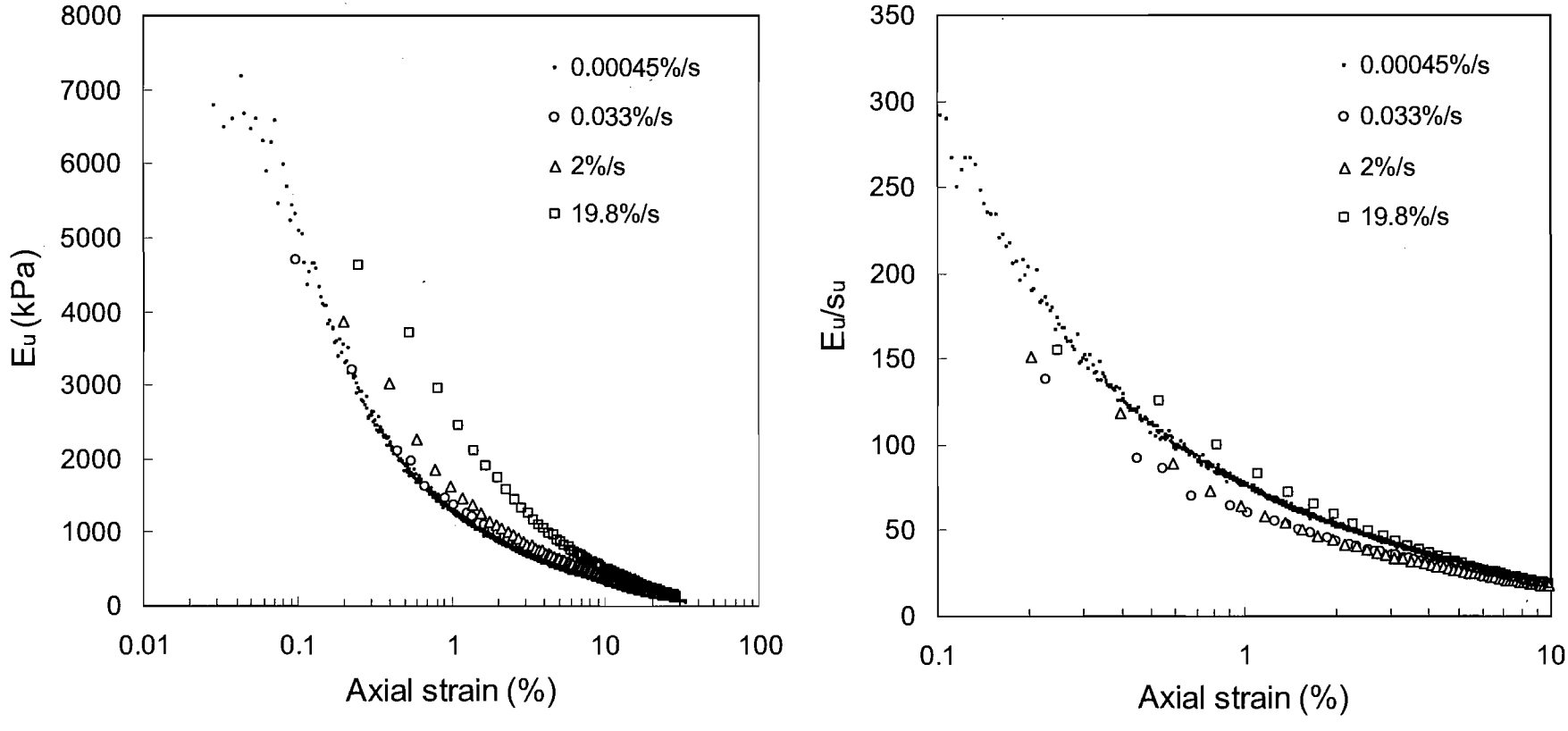

(a) variation of the secant undrained modulus with axial strain

(b) variation of the normalised undrained modulus with axial strain

Figure 4.11 Influence of axial strain rate on the secant undrained modulus of kaolin in triaxial extension

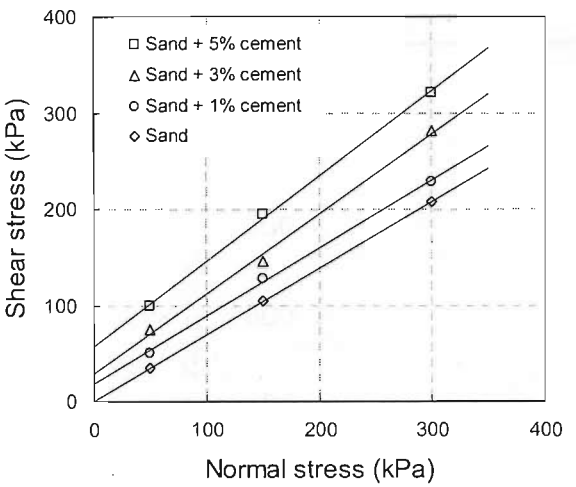

(a) peak strength envelopes

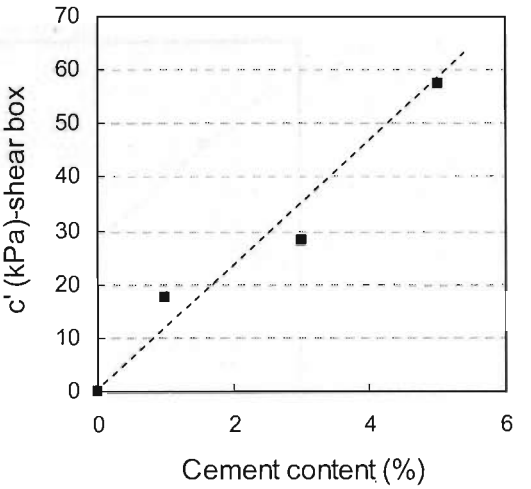

(b) variation of c' with cement content

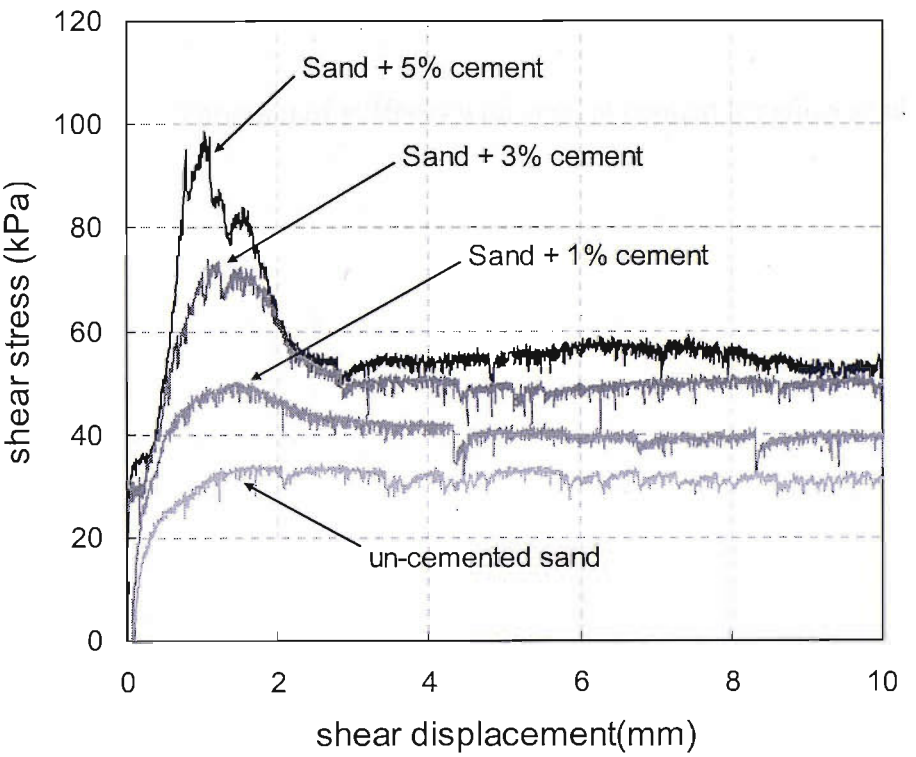

(c) shear stress-displacement variation at σ'_n=50 kPa

Figure 4.12 Direct shear test results for cemented and un-cemented silica sand

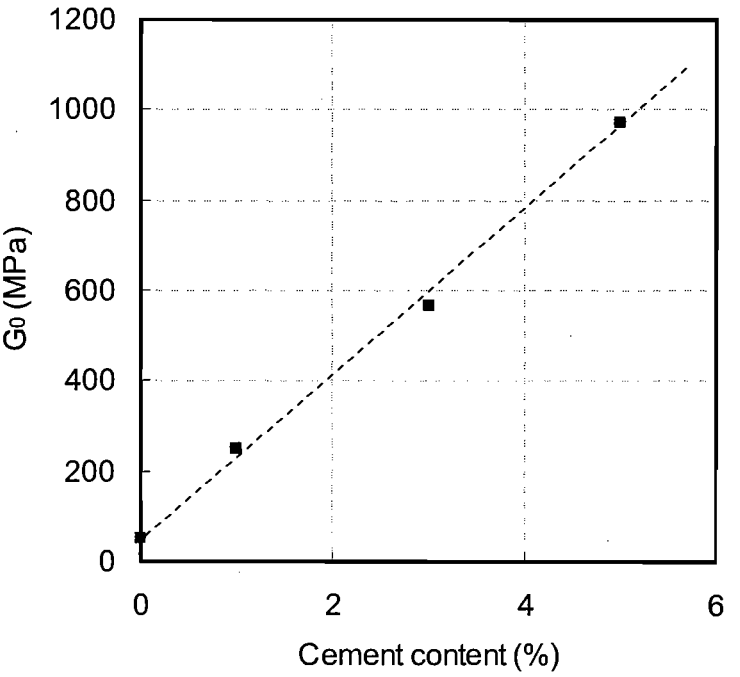

Figure 4.13 Variation of stiffness with cement content for silica sand

Chapter 5

CENTRIFUGE EXPERIMENTAL DETAILS

5.1 Introduction

As highlighted in Chapter 2, investigations into the dynamic uplift resistance of transmission tower footings to uplift (Richards, 2002) identified a number of aspects of footing behaviour that required further research. These investigations had recommended that centrifuge modelling be undertaken in order to further classify dynamic tension effects in the backfill soil overlaying the footings. The magnitude of uplift pressure and corresponding resistance of the footing preceding failure could be usefully determined by means of additional centrifuge tests. Moreover it is thought that further analysis of negative pore pressure at the base of shallow anchors would be of significant use in classifying the ability of such suctions to resist longer term uplift forces.

Preliminary centrifuge modelling studies involving the uplift of shallow plate anchors, founded on both clay and sand, at various rates have been undertaken (Lehane and Goodwin, 2003). These studies concluded that the uplift capacity of shallow foundations increased significantly with uplift rate. Further tests to investigate the influence of uplift rate, variation of backfill soil, footing width and load inclination on the uplift resistance of shallow plate anchors have been undertaken and are detailed here. A further series of tests has also been carried out to directly measure negative pore pressures generated below model transmission tower footings during fast uplift. This chapter provides a brief introduction to centrifuge modelling and scaling laws

and a description of the experimental facilities used for each test series in addition to detailing the overall centrifuge testing program.

5.2 Objectives

The objectives of the centrifuge test program were:

1. To identify the response of shallow anchors to increasing uplift velocity.
2. To identify the contribution of suction to the overall uplift resistance and examine the effect of increasing uplift rate on this contribution.
3. To identify and evaluate the primary parameters governing the development of suction.
4. To provide a parametric study on parameters such as the inclination of the applied load and the width of the anchor.

In addition to the objectives outlined above which are principally concerned with the behaviour of shallow anchors further testing, specific to transmission tower foundations, was undertaken. The aims of this testing were:

1. To identify the response of transmission tower style footings to increasing uplift velocity
2. To directly measure suctions generated below model transmission tower footings during rapid uplift.
3. To assess the potential for using in-situ soil improvement techniques to increase the uplift capacity of existing transmission tower foundations.

5.3 Centrifuge Modelling

Difficulties arise in small-scale physical modelling in relating the stress-strain relationship of the soil in a way that is appropriate to field conditions. If we imagine an element of soil at some depth, z, below the soil surface, the effective vertical

confining stress is dependent upon the unit weight of the overlying soil and is related, in general terms, to the overburden pressure ρgz, Figure 5.1. In a small-scale physical model at normal gravity the overburden pressure is reduced by the model factor, n and stress-strain behaviour in the model will not replicate the behaviour under field conditions. The use of an appropriately scaled model in a geotechnical centrifuge is a well-established and convenient physical modelling technique for all types of geotechnical problem (Schofield, 1980). The process involves applying an increased gravitational acceleration to physical models, through the development of centrifugal acceleration. In this way the reduction in overburden pressure due to a reduction in the physical dimension, z is balanced by an equal increase in the local acceleration field, g and identical self-weight stresses are produced in the model as in the field. A $1/n$ scale model in a centrifuge is subjected to a radial acceleration field of n times the normal gravity.

5.3.1 Scaling relationships

In conversion from model to prototype, considerable thought must be given to the scaling relationships involved. In a $1:n$ scale centrifuge model linear dimensions are reduced by a factor of n, areas by a factor of n^2 and volumes by a factor of n^3. Stresses, strains, and pore pressures are the same at relating depths in the model at ng and in the prototype. Thus, given these relationships, it follows that forces and bending moments are reduced in the model by factors of n^2 and n^3 respectively. Scaling relationships relevant for testing undertaken during this research are presented in Table 5.1.

Consolidation times are reduced in centrifuge modelling by a factor of n^2. This reduction is a consequence of scaling of linear dimensions, not of the increased acceleration, as time for consolidation scales in proportion to the square of the drainage path length. The timescale of rapid tests is an additional factor which needs to be considered in the interpretation of centrifuge test result and subsequent scaling and application to prototype conditions. Where the pore fluid used during testing is water, the loading frequency in the model should be n times greater than the frequency to be represented in the prototype. Where failure is reached under a constant assigned

displacement rate, as in the tests considered later, the time for dynamic events in the model is reduced by a factor of n.

Table 5.1 Centrifuge Modelling Scale Factors

Parameter	**Value in Prototype**	**Value in Model Scale 1:*n***
Acceleration	a	a/n
Linear dimension	l	l/n
Area	A	A/n^2
Volume	V	V/n^3
Stress	σ	σ
Strain	ε	ε
Force	F	F/n^2
Moment	M	M/n^3
Consolidation time	t_c	t_c/n^2
Frequency (for dynamic tests)	f_d	nf_d
Time (for dynamic tests)	t_d	t_d/n

5.4 Model Footings

Three distinct test series have been undertaken and are reported in detail in the following chapters. The first series involves a study of the effects of pull-out velocity, footing width and load inclination on the capacity of shallow plate anchors. The second series addresses the direct measurement of negative pore pressures generated below model transmission tower footings during uplift. The third series examines the potential for using soil improvement techniques to enhance the uplift capacity of existing foundations. The following sections provide an overview of the model footings used in each of the studies. Each of the footing geometries were important in developing the test apparatus described in subsequent sections. The model footing scale for all centrifuge tests undertaken was 1:50.

5.4.1 Plate anchors

The model anchors were fabricated from aluminium. The footings are of plate anchor type, comprising a 5 mm thick square base with a width (B) of 30, 45 or 60 mm square. A 75 mm long, 7 mm square shaft is attached at the centre of each anchor. The depth of embedment (H) for all anchor widths was 45 mm from the anchor base corresponding to a range for the embedment ratio (H/B) of between 0.75 and 1.5.

These parameters are considered to be generally representative of pad and chimney footings used for transmission tower footings in the UK where the embedment ratio is typically between 1 and 2. It has been shown in a number of experimental and numerical studies (e.g. Rowe and Davis, 1982; Shin *et al.* 1994; Rao and Datta, 2001 and Thorne *et al.* 2004) that an embedment ratio between 0.75 and 1.5 will result in a shallow anchor condition during uplift whereby the failure plane mobilised above the anchor will extend to the soil surface. Under 50*g* acceleration the test anchors model prototype square shallow plate anchors between 1.5 and 3 m in width buried at a depth of 2.25 metres below the soil surface. A number of 30 mm anchors were also fabricated where the fixed anchor shaft was inclined at an angle between 0 and 20 degrees. A small head attachment, designed to fit a hook arrangement mounted on the bearing rail of the fast pull actuator, was screwed into the top of the shaft and allowed each anchor to be caught in flight for testing without stopping the centrifuge channel. The plate anchor geometry is shown in Figure 5.2.

5.4.2 Transmission tower footings

A number of foundation tests were undertaken using a National Grid type D12 transmission tower foundation, which is used for a large number of transmission tower foundations in the UK. This foundation is shown in Figure 5.3. Three 1:50 scale model footings were fabricated from aluminium for use in the centrifuge. Each footing comprised a truncated pyramid (40 mm wide at the base) and chimney and is detailed in Figure 5.4. One model footing represents a reproduction of the D12 type footing incorporating a chimney which rises from the centre of the truncated pyramid base at an angle of 9.3°. Two model footings were also fabricated each with a vertical chimney and were identical except for a modification to one of the model footings to allow a pore pressure transducer to be installed at the centre of the base of the footing.

The need for a model footing with a vertical chimney, as opposed to the inclined chimney used in practice, is related to some extent to subsequent modelling concerns but also to the connection between the centrifuge actuator and the footing head. During to the footing setup stage of the test the centrifuge was stopped to allow installation of the footing. Once the footing is in place the centrifuge was spun back to the test acceleration and re-consolidation will occur within the sample. At this stage the clay will consolidate causing the model footing to move downwards relative to the

central tool table on which the fast uplift actuator was mounted. The use of a fixed connection between the footing head and the fast actuator would therefore prevent the footing from moving with the clay base during the re-consolidation phase and may cause the footing to separate from the clay base. Typically, a floating connection between the actuator and footing head was used to accommodate these movements. However, the use of such a connector with footings incorporating an inclined chimney was thought to lead to footing base rotations during uplift (rotation could occur at the head) which in turn could affect the magnitude of the suctions generated.

For the footing incorporating a pressure transducer, as shown in Figures 5.4 and 5.5, the transducer cable was threaded up through the centre of the chimney and exited at the top of the footing head to enable connection to the on-board computer via a junction box positioned on the central actuator table. To ensure that the suctions generated at the footing base during uplift could not be vented through the chimney, the head attachment contained two separate o-rings installed between the head and the connector and the connector and the top lock-bolt respectively. The opening for the pressure transducer wire was also sealed with a silicone sealant prior to installation of the footing in the excavation.

For a number of later tests, the footing was subjected to a range of cyclic load events prior to uplift to failure. At this stage the footing head connector was modified to allow tensile and compressive loads to be imposed on the footing through appropriately controlled vertical displacements.

5.5 Test Apparatus

The apparatus developed to apply rapid uplift to scaled model anchors is described together with a brief description of the centrifuge facility at the University of Western Australia (UWA), Perth. Details of existing apparatus are included where necessary.

5.5.1 Geotechnical centrifuge facility

The centrifuge tests were undertaken in the geotechnical drum centrifuge at UWA. A complete description of this facility is given by Stewart *et al.* (1998) and a brief description of the centrifuge and equipment associated with this test program is presented here. The UWA geotechnical drum centrifuge, Figure 5.6(a) is one of a number of drum centrifuges manufactured by Thomas Broadbent and Partners. The drum centrifuge comprises an outer channel for sample containment 300 mm wide (measured vertically) and 200 mm in radial depth, with a diameter of 1.2 metres. A horizontal centrifugal acceleration field, acting down into the channel, is generated as the channel rotates about the central vertical axis. The centrifuge allows for a peak effective acceleration of 400*g* corresponding to a maximum rotational speed of 850 rpm.

The drum centrifuge features a central tool table, Figure 5.6(b), which may be stopped and started independently of the outer channel. This is achieved through the use of two concentric and independent drive shafts which may be operated separately or clutch engaged to rotate together. Independent movement of the central tool table enables test apparatus to be placed, removed or modified without stopping the channel.

5.5.2 Actuators

Three electric actuators fitted on the tool table enable movement of attached experimental apparatus in the vertical, radial and circumferential directions. Movement of these actuators is directed remotely, via power slip rings and specially designed computer software, from the adjoining control room. During sample saturation water is directed to the channel in flight via nozzles at both the top and bottom edges of the channel. In this way water may also be added to the sample during a test period to balance any in-flight evaporation which may occur. The sample is visually monitored from the control room during testing through use of miniature video cameras mounted at various locations on the central tool table.

5.5.3 Fast pull out actuator

Prior to this research, the maximum applied loading rate achievable using the drum centrifuge actuator, described above, was limited to 3 mm/s. The testing programme

developed for this research called for the application of much faster displacement rates in order to produce loading rates similar to those measured during load events replicated in transmission tower field tests (Clark *et al.* 2006). Loading rates inferred from these tests required a new 'fast pull' actuator to be developed at UWA, Figure 5.7(a), to apply fast rates of displacement to footings at varied angles of pull-out.

The fast pull actuator is driven by a 12V DC Maxton motor coupled to a 66:1 gear box. The motor is connected to a rack and pinion that slides on a bearing rail with a maximum stroke of 100 mm. The displacement of the actuator is measured by an encoder mounted on the motor. The output voltage given by the encoder is directly proportional to the rotation of the motor and hence, the linear displacement of the pinion rack. Inclination is achieved through mounting the whole system on a rotating platform which is attached to the existing actuator. The system allows for application of loads of up to 500 N under an acceleration of 50*g* at a loading rate of 100 mm/s with inclinations ranging from 0-35 degrees. A holder designed for catching footing heads in flight and a 2 kN load cell, to measure uplift resistance, are connected at the top of the bearing rail, Figure 5.7(b). The fast pull actuator is mounted on the drum centrifuge actuator as shown in Figure 5.8.

Software has been developed at UWA to control the fast pull actuator and to allow the specification of any pull out rate between 0.01 and 100 mm/s. During fast uplift phenomena associated with the development of uplift resistance may occur extremely rapidly. In order to acquire sufficient data to allow a thorough interpretation of the results a new data acquisition system was implemented, capable of logging continuous output from two channels at a rate of 25 kHz per channel via an in-flight computer. Data can be subsequently filtered according to the displacement rate in order to minimise the presence of noise in the data resulting from the fast acquisition rate. At slower uplift rates, the test data is captured via the usual data acquisition system which records over 16 channels at a logging rate of 5 Hz.

5.5.4 The pore pressure and tension transducer

One of the objectives of the centrifuge testing program (Section 5.2) is to directly measure suctions developing below a model transmission tower footing during rapid pull-out. Richards (2002) performed a preliminary series of footing uplift tests in a

beam centrifuge using a Druck PDCR81 transducer combined with a 1 bar ceramic stone embedded in the footing base to measure suction. The tendency for these devices to cavitate when footings on clay were subjected to fast uplift rates prompted the use here of a pore pressure and tension transducer (PPTT) recently developed by Take and Bolton (2003) for use in reduced scale physical modelling. The PPTT, which is shown in Figure 5.9, has a low volume and employs an 'Entran EPB' transducer which Take and Bolton (2003) show is more suitable for measurement of tension than the Druck PDCR81. The performance of the PPTT may be modified through the use of a ceramic stone filter with different air entry values. A ceramic stone with a 3 bar air entry value rating was used in all of the relevant tests reported in this thesis.

The recommended procedure for the saturation of the PPTT is a two stage process consisting of an initial saturation of the (oven dried) porous filter with water followed by pre-pressurisation of the device (Take and Bolton, 2003). This process is discussed in more detail in Section 5.8.7.

5.5.5 General instrumentation and apparatus

Additional apparatus used in the test program included:

- Druck PDCR-81 miniature pore pressure transducers: Three such pressure transducers are installed in the drum channel at depths of 50, 75 and 100 mm from the base of the channel. These were used to measure the pore water pressure generation and dissipation in the soil sample during consolidation and to monitor the pore pressure during the test period.
- Load cell: A 2 kN load cell (manufactured by the University of Western Australia) was used to measure the axial resistance of the footing during pull out, Figure 5.7(b).
- Penetrometers: T-bar and cone penetrometers were used to characterise the strength of each soil sample. This process is described in more detail in Section 5.10.

5.6 Experimental Arrangement

An overview of the experimental arrangement used during the test series, including details of each of the test geometries is discussed.

5.6.1 Plate anchor series

In relation to the behaviour of transmission tower foundations, the focus of the plate anchor test program was primarily to identify the response with increasing uplift velocity of shallow anchors founded on clay. In practice transmission tower foundations are formed in excavations which, subsequent to footing construction, may be backfilled with a range of soil types. Sand and clay backfills are considered here in two separate series of tests, with particular emphasis placed on the former. The potential for using backfill soil improvement to increase transmission tower footing uplift capacity is also investigated.

Series 1 - Sand backfill

Configurations for plate anchor tests with sand backfill are shown in Figure 5.10. As shown in Figure 5.10(b), some anchors were founded on loosely placed sand backfill to assist in interpretation of the influence of clay at the base of most of the test anchors, which had the geometry shown in Figure 5.10(a).

Series 2 - Clay backfill

Configurations for plate anchor tests with clay backfill are shown in Figure 5.11. As described above some anchors were founded on loosely placed sand backfill as shown in Figure 5.11(b).

Series 3 - Cemented backfill

The configuration for plate anchor tests with cemented backfill is shown in Figure 5.12. Since the influence of clay at the base of the anchor is not investigated during this test series, each anchor was founded on loosely placed sand backfill as shown.

5.6.2 Transmission tower footing test series

The transmission tower footing test series was undertaken specifically to model the response of replica transmission tower footings to increasing uplift velocities. The footing embedment was consistent with that recommended by routine design for the D12 type foundation modelled. In each test sand was used as a representative backfill material although the study focused on behaviour at the base of the footing during uplift. Configurations for the transmission tower footing test series are shown in Figure 5.13. As described previously for the plate anchor test series some footings were founded on loose sand, shown in Figure 5.13(b), in order to assess the influence of clay at the footing base.

5.7 Experimental Program

This section presents the experimental program for each series of centrifuge tests described in this thesis. All tests were performed at a model scale of 1:50 and a corresponding centrifuge acceleration of 50*g*.

5.7.1 Plate anchor series 1 – Sand backfill

The most extensive of the test series described in this thesis was plate anchor series 1, using sand backfill. The series comprised a total of 57 footing uplift tests in 5 centrifuge samples. Uplift tests relating to this series are prescribed the notation PASB followed by the sample number and test number; thus test number 8 from sample 3 would be denoted PASB-S3-8 and so on. The uplift tests conducted in each centrifuge sample are presented in Tables 5.2-5.6. The soil at the anchor base given in the tables refers to the test configurations shown in Figure 5.10. Where sand is specified the entire thickness of clay at the excavation base was removed and replaced with sand, Figure 5.10(b). The test configuration within the centrifuge channel is presented for each sample in Figure 5.14(a)-(e).

Table 5.2 Experimental program PASB – 1st Sample

Test No.	Anchor Width, B (mm)	Soil at Anchor Base	Uplift Inclination (°)	Uplift Rate, v_f (mm/s)
S1-1	30	Clay	0	3
S1-2	30	Clay	0	3
S1-3	30	Sand	0	3
S1-4	30	Clay	5	3
S1-5	30	Clay	10	3
S1-6	30	Clay	15	3
S1-7	30	Sand	15	3

Table 5.3 Experimental program PASB – 2nd Sample

Test No.	Anchor Width, B (mm)	Soil at Anchor Base	Uplift Inclination (°)	Uplift Rate, v_f (mm/s)
S2-1	30	Clay	0	0.03
S2-2	30	Clay	0	0.3
S2-3	30	Clay	0	60
S2-4	30	Clay	0	100
S2-5	30	Sand	0	30
S2-6	45	Clay	0	30
S2-7	45	Sand	0	3
S2-8	30	Clay	15	3
S2-9	30	Clay	15	30
S2-10	30	Sand	10	3
S2-11	30	Sand	5	3
S2-12	45	N/A	CPT test location	

Table 5.4 Experimental program PASB – 3rd Sample

Test No.	Anchor Width, B (mm)	Soil at Anchor Base	Uplift Inclination (°)	Uplift Rate, v_f (mm/s)
S3-1	30	Clay	0	100
S3-2	30	Clay	0	60
S3-3	30	Clay	0	30
S3-4	30	Clay	0	3
S3-5	30	Clay	0	0.3
S3-6	30	Clay	0	0.03
S3-7	60	Clay	0	100
S3-8	60	Clay	0	60
S3-9	60	Clay	0	30
S3-10	30	Sand	0	3
S3-11	60	Clay	0	3
S3-12	60	Clay	0	0.3
S3-13	60	Clay	0	0.03
S3-14	60	Clay	0	30
S3-15	60	Sand	0	3

Table 5.5 Experimental program PASB – 4th Sample

Test No.	Anchor Width, B (mm)	Soil at Anchor Base	Uplift Inclination (°)	Uplift Rate, v_f (mm/s)
S4-1	30	Clay	0	0.3
S4-2	45	Clay	0	3
S4-3	30	Clay	0	100
S4-4	30	Clay	0	30
S4-5	30	Clay	0	0.03
S4-6	30	Clay	0	3
S4-7	30	Clay	0	30
S4-8	30	Clay	0	60
S4-9	60	Clay	0	3
S4-10	30	Clay	15	3
S4-11	30	Clay	0	30
S4-12	60	Clay	0	3
S4-13	30	Clay	0	100

Table 5.6 Experimental program PASB – 5th Sample

Test No.	Anchor Width, B (mm)	Soil at Anchor Base	Uplift Inclination (°)	Uplift Rate, v_f (mm/s)
S5-1	45	Clay	0	3
S5-2	60	Clay	0	0.03
S5-3	60	Clay	0	0.3
S5-4	60	Clay	0	3
S5-5	30	Clay	5	3
S5-6	30	Clay	10	3
S5-7	30	Clay	15	3
S5-8	30	Clay	20	3
S5-9	30	Sand	15	3
S5-10	60	Sand	0	3

5.7.2 Plate anchor series 2 – Clay backfill

Plate anchor series 2, using clay backfill comprised a total of 11 footing uplift tests in 1 centrifuge sample. Uplift tests relating to this series are prescribed the notation PACB followed by the sample number and test number; thus test number 5 from sample 1 would be denoted PACB-S1-5. The uplift tests conducted in the sample are presented in Table 5.7. The test configuration within the centrifuge channel is presented for the sample in Figure 5.15.

Table 5.7 Experimental program PACB – 1st Sample

Test No.	Anchor Width, B (mm)	Soil at Anchor Base	Uplift Inclination (°)	Uplift Rate, v_f (mm/s)
S1-1	30	Clay	0	3
S1-2	30	Clay	0	30
S1-3	30	Clay	0	100
S1-4	30	Clay	0	0.03
S1-5	30	Sand	0	3
S1-6	60	Clay	0	3
S1-7	45	Sand	0	3
S1-8	45	Clay	0	3
S1-9	30	Clay	5	3
S1-10	30	Clay	10	3
S1-11	30	Clay	15	3

5.7.3 Plate anchor series 3 – Cemented backfill

Plate anchor series 3, using cemented backfill comprised 4 footing uplift tests in 1 centrifuge sample. Uplift tests relating to this series are prescribed the notation PAIB followed by the sample number and test number as seen previously. The uplift tests conducted in the sample are presented in Table 5.8. The test configuration within the centrifuge channel is presented for the sample in Figure 5.16.

Table 5.8 Experimental program PAIB – 1st Sample

Test No.	Anchor Width, B (mm)	Soil at Anchor Base	Backfill cement ratio (%)	Uplift Rate, v_f (mm/s)
S1-1	30	Sand	0	0.3
S1-2	30	Sand	1	0.3
S1-3	30	Sand	3	0.3
S1-4	30	Sand	5	0.3

Testing detailed in tables 5.2 to 5.8 comprises a thorough experimental examination into the effect of loading rate, inclination and backfill type on the behaviour of shallow embedded plate anchors (spread foundations).

5.7.3 Transmission tower footing test series

The transmission tower footing test series involved a total of 10 uplift tests in 1 centrifuge sample. Uplift tests relating to this series are given the notation TTFS followed by the sample number and test number. The uplift tests undertaken in the series are detailed in Table 5.9. As noted in Table 5.9, 2 tests were also undertaken on

footings to assess the development of suction under cyclic loading conditions. In each case after a period of cyclic loading was applied, each footing was uplifted to failure at the given rate. PPTT relates to the installation of a pore pressure transducer for measurement of suction at the base of the footing as described in Section 5.4.2. The test configuration within the centrifuge channel is presented for the sample in Figure 5.17.

Table 5.9 Experimental program TTFS – 1st Sample

Test No.	Anchor Width, B (mm)	Soil at Footing Base	Uplift Inclination (°)	Uplift Type	PPTT	Uplift Rate, v_f (mm/s)
S1-1	40	Sand	9.3	Fast	NO	3
S1-2	40	Clay	0	Fast	YES	30
S1-3	40	Clay	9.3	Fast	NO	30
S1-4	40	Sand	0	Fast	NO	3
S1-5	40	Clay	0	Fast	YES	3
S1-6	40	Clay	0	Slow	YES	0.1
S1-7	40	Clay	9.3	Fast	NO	3
S1-8	40	Clay	0	Fast	YES	100
S1-9	40	Clay	0	Cyclic	YES	1/30
S1-10	40	Clay	0	Cyclic	YES	1/30

5.8 Sample Preparation and Setup

This section details the process for the preparation of each centrifuge sample and provides details of the footing installation procedure for each series of tests.

5.8.1 Overview of sample preparation

The sample preparation procedure outlined below is a general overview of the method used to prepare the clay sample in the drum centrifuge for each test series. For the transmission tower footing (TTF) test series, the sample preparation procedure was significantly modified. These modifications and the specific procedures used there are discussed in later sections.

For plate anchor series 1 and 2 (sand and clay backfill) the clay at the base of the anchor was required to be overconsolidated so as to be representative of the type of clay state encountered in field conditions for transmission tower foundations. The sample preparation procedure outlined below was formulated to achieve this whilst

being repeatable and (where more than one sample was required in the test series) resulted in samples which exhibited similar strength and stiffness properties.

A sand layer, 15 mm thick, was placed at the bottom of the drum channel to create a drainage layer. For sand placement, a specially designed actuator was fitted to the central shaft of the centrifuge in place of the multi-axis loading actuator. A hopper was positioned overhead and attached to the sand placement actuator via a rotating coupling and 40 mm diameter hose. The sand was introduced via the hose, under an acceleration of 20*g*, into the channel which had been filled with water to a depth of approximately 30 mm, selected so as to ensure a low to medium density of the placed sand. The water was then drained from the channel leaving a partially saturated sand layer and the centrifuge stopped. The sand layer was scraped to a uniform thickness then spun back to 20*g* where water was introduced to the sample channel to a height approximately 20 mm above the surface of the sand.

The kaolin clay sample was then prepared in two stages. The kaolin was mixed under a vacuum, at a moisture content approximately 120% (twice the liquid limit), for one day to form an homogeneous slurry. The slurry was transferred to a hopper and, by using the drum actuator and a modified delivery nozzle, was placed above the existing sand layer in a self-levelling and non-erosive manner. The clay was subsequently consolidated under its self-weight at an acceleration of 250*g*. Full consolidation was achieved once the pore pressures recorded by the transducers located at various depths within the clay layer became constant. Two layers of clay were necessary to achieve the target sample depth for the test geometry. The second clay layer was placed using the same process to that of the first to ensure the same unit weight in both layers. During the placement of each clay layer, the delivery nozzle height was adjusted to maintain a constant drop height, according to the depth of the nozzle in the channel.

Following this procedure, the clay sample was overconsolidated. An overconsolidation ratio (OCR) of 5 was obtained by first consolidating the sample at an acceleration level of 250*g* (n_{max}=250) and then at an acceleration of 50*g* (n=50). This OCR value was selected as the clay on which transmission tower footings are generally founded is usually moderately to heavily overconsolidated.

Subsequent to preparation and full consolidation of the test sample for each series, as outlined above, installation of the anchors was carried out. This installation process, detailed in the following sections, varied depending on the backfill soil used in each sample.

As mentioned previously a number of tests have been undertaken in each test series where anchors were placed on a sand base rather than on clay. This set up is shown in Figure 5.10(b) and 5.11(b) for the sand and clay backfill series respectively. A comparison of the uplift resistance measured for anchors founded on sand with those founded on clay is used to estimate the magnitude of base suction developed during uplift. It is expected that no suction effects will occur for anchors founded on sands due to the increased drainage and hence fast dissipation of negative pore pressures at the anchor base.

5.8.2 Anchor installation in sand backfill

A number of different methods were considered in order to achieve the most suitable technique with which to carry out the experimental setup. This process included forming the excavation for the anchor, reconstituting the sand drain underneath the anchor base (where required), placing the anchors and backfilling the excavation. The following process, described here and summarised in Table 5.9, appeared to be the most efficient and repeatable and was adopted for all tests undertaken in the sand backfill series.

Following preparation of the clay layer the centrifuge was stopped to facilitate the formation of a series of excavations in which each anchor was placed. In each case the anchor was founded directly onto the base of the excavation and held in place using the pull-out actuator while partially saturated sand was manually backfilled around the anchor. A method trialled previously, whereby sand was rained into the excavation to form the backfill in-flight, encountered problems with the sand nozzle disturbing the anchor.

The base of each excavation was formed to be 5 mm wider than the overall anchor width both to facilitate placement and to ensure good contact between the anchor base and the clay. To ensure that failure for each anchor occurred within the backfill soil,

the side slopes of the excavation were formed at an angle of approximately 50 degrees. The selection of the excavation angle for this purpose assumed an inverted truncated cone failure mechanism where the angle of failure to the vertical is equal to the dilatancy angle of the soil (Vermeer and Sutjiadi, 1985; Murray and Geddes, 1987). The experimental arrangement (mid-set up) for placing the anchor and backfilling the excavation is shown in Figure 5.18. Where the base of the excavation was sand rather than clay, Figure 5.10(b), the clay base sample was removed down to the drainage layer and then replaced with free-draining loose backfill sand prior to footing installation.

Following anchor installation the centrifuge acceleration was increased back to the test level of 50g and the water level was returned to 10 mm above the surface of the clay. Uplift tests were conducted after a period of at least 3 hours was allowed for consolidation under the weight of the anchor and backfill. The full setup process for plate anchor series 1 is shown in Table 5.10.

Table 5.10 Setup process for sand backfilled anchor

Stage	Action	Centrifuge @	Tool used	Comments
1	Reconstitute bottom drain sand layer	20*g*	Sand placement tool	
2	Reconstitute clay sample	20*g*	Actuator with clay delivery nozzle	The clay sample needed to be reconstituted in two layers
3	Consolidation	250*g*	-	
4	Drain the channel, stop the centrifuge	No	-	The actuator was removed at this stage
5	Form the excavation	No	-	For anchors resting on sand, the entire thickness of clay was removed below the anchor
6	Place the plate anchor	No	Actuator	The actuator was used to place the anchor to ensure correct position and a perfect contact with the soil, Figure 5.18
7	Backfill the excavation with moist sand	No		The operation was carried out while the anchors were held by the actuator
8	Ramp up, introduce water	50*g*		The water level was set and maintained using PPTs located in the channel
9	Pull out the anchors	50*g*	Fast pull out actuator	A period of around 3 hours was allowed prior to uplift

5.8.3 Anchor installation in clay backfill

Plate anchor test series 2 (PACB) was undertaken to model anchor behaviour in clay backfill and a modified sample preparation procedure was used to form the test sample in this case. The preparation procedure was initially identical to that described in Section 5.8.1 however only one clay layer was poured initially resulting in a reduced sample height. After the initial consolidation stage (Stage 3, Table 5.9) anchors were placed 'in-flight' (at 20*g*) directly onto the surface of the clay layer using the pull-out actuator. Each anchor was then discharged from the actuator hook and the actuator driven upwards, clear of the spinning channel, where another anchor was placed in the holder arrangement and installed on the surface of the clay in the same manner. This process is shown schematically in Figure 5.19. At two test sites (as required) the clay base below the anchor was removed down to the sand drainage layer and backfilled with sand as shown in Figure 5.11(b) prior to the footing installation process. The two anchors located at these sites were installed directly onto the surface of the sand layer.

Following placement of the plate anchors a second layer of clay slurry was poured at 20*g*. At this stage, care was taken to allow the clay to self level over the anchors in order to minimise any possible disturbance. The sample was then consolidated at an acceleration of 150*g* before reducing the centrifuge acceleration to the test acceleration value of 50*g* for a period of 1 day prior to commencing the uplift tests. At this stage the height of the backfill clay layer was 45mm above the base of the anchor.

5.8.4 Anchor installation in cemented backfill

The anchor installation process for plate anchor test series 3 (PAIB) was initially identical to that described in Section 5.8.2 for sand backfill. As shown in Figure 5.12(a) and Figure 5.16 each anchor was founded on loose, free draining sand to ensure that no suctions were generated at the anchor base during uplift. Once each anchor was positioned and held in place using the pull-out actuator, sand or cement treated sand was manually backfilled around the anchor.

Table 5.11 Setup process for clay backfilled anchor

Stage	Action	Centrifuge @	Tool used	Comments
1	Reconstitute bottom drain sand layer	20*g*	Sand placement tool	
2	Reconstitute clay sample	20*g*	Actuator with clay delivery nozzle	The clay sample was reconstituted in one layer
3	Consolidation	250*g*	-	
4	Drain the channel, stop the centrifuge	No	-	
5	Place the plate anchor (in-flight)	20g	Actuator	The actuator was used to place the anchor in-flight and to ensure correct position, Figure 5.19
6	Reconstitute backfill clay layer	20g	Clay nozzle	The clay was allowed to self level over the anchors
7	Consolidation	150g	-	
8	Pull out the anchors	50*g*	Fast pull out actuator	A period of around 3 hours was allowed prior to uplift

For cement treated sand, early strength Portland cement (Type III) was used as the cementing agent. This cement was selected as it has a setting time of approximately 3 hours and the majority of its strength gain takes place within 20 hours. This meant that the curing time required in the centrifuge tests did not need to be excessive. The soil specimens for centrifuge and element tests were prepared by first hand-mixing the dry sand and cement and then adding water to a moisture content of approximately 12%. The void ratio of un-cemented sand was 0.74 and that of the cement treated sand was in the range of 0.73 to 0.68 for cement contents of 1% to 5% respectively.

Four additional excavations were also backfilled with sand or cement treated sand (at ratios 1, 3 and 5%) to allow for cone penetration tests to be performed during testing. These excavations are shown in Figure 5.12(b).

Subsequent to backfilling each of the four anchors and the four excavations allowed for cone penetrometer testing, the centrifuge acceleration was brought up to the test level of 50g and a time period of 20 hours was allowed for curing of the cement treated backfill. During this period the water level was maintained at 10 mm above the soil surface.

5.8.5 Transmission tower footing sample preparation

The sample preparation procedure detailed in Section 5.8.1 was devised as the most efficient way in which to prepare a moderately overconsolidated clay sample in the drum centrifuge. Although the resulting strength of the sample may not necessarily be representative of that encountered in field conditions, comparison is shown later to be valid through normalisation of the anchor capacities measured in each sample. In the TTF test series an extended sample preparation procedure was introduced to achieve an undrained shear strength in the test sample which more closely represented that which might be found in the field. The resulting sample preparation process was similar to that presented in Section 5.8.1, but with some modifications applied during the consolidation stages. The modified sample preparation and reconstitution process is described herein.

After the formation of a drainage layer as detailed in Section 5.8.1, kaolin clay slurry, previously mixed under a vacuum to a moisture content of approximately 120%, was placed in-flight onto the sand. The centrifuge drum speed was then increased to allow the clay to consolidate at an acceleration of 250*g* for a period of approximately 2 days. After this initial period of consolidation, the sample had sufficient strength to allow the centrifuge to be stopped and a layer of geo-textile was applied to the surface of the clay. The centrifuge acceleration was subsequently reduced to 20*g* and a 50 mm thick layer of dry sand was placed in flight on top of the geo-textile. The sand layer was added in order to surcharge the underlying clay and as stated previously, increase its strength to a level more typical of field applications. The centrifuge acceleration was then increased to 250*g* and the sample was consolidated for three days.

After full consolidation under the sand surcharge, the centrifuge was stopped and the sand layer and geo-textile were removed. A second clay layer (in which excavations for footings would be made) was then added, in-flight at 20g, on top of the first layer and then consolidated at an acceleration of 150*g* over a period of 3 days. The acceleration level was then reduced to the test level of 50*g* and the complete sample was allowed to swell for a further 2 days, under a continued supply of water.

This extended consolidation procedure led an overconsolidation ratio greater than that previously seen for samples in the plate anchor test series. The sample OCR is discussed in relation to sample characterisation and strength in Section 5.11.

5.8.6 Transmission tower footing installation

The footing installation method for the TTF series was similar to that described in Section 5.8.2 for the plate anchor tests series. Each footing was founded directly onto the base of a prepared excavation and held in place using the pull-out actuator while partially saturated sand was manually backfilled around it. Where measurement of suction at the base of the footing was specified during the test a modified footing, including the PPT transducer shown in Figure 5.5, was installed. In this case, due to restrictions on the lateral movement of the actuator during testing caused by protrusion of the PPTT wire from the top of the footing, only one footing was installed and subsequently tested at a time. The process for the saturation, pre-pressurisation and installation of the PPTT in the modified footing is described in Section 5.8.7 below.

Subsequent to the footing installation process the centrifuge acceleration level was increased back to the test level of 50g and the water level was returned to 10 mm above the surface of the clay. Uplift tests were conducted after a period of at least 3 hours was allowed for consolidation under the weight of the footing and backfill. The full setup process for the TTF test series is shown in Table 5.12.

5.8.7 PPTT saturation, calibration and installation

Prior to installation of the footing in the excavation it was essential that the PPTT was fully saturated in order to accurately measure suction. The procedure employed for the saturation of the tensiometer followed that described by Take and Bolton (2003) and involved initial saturation of the (oven dried) porous filter with water followed by the application of cycles of positive and negative absolute pressure (between 600 kPa and -100 kPa) to the device when submerged in water. Apparatus specifically designed for the purpose of replicating this saturation procedure was fabricated at UWA and is shown in Figure 5.20. The PPTT is shown undergoing saturation in Figure 5.21.

Following the saturation procedure the PPTT was calibrated for positive pressure up to 300 kPa as shown in Figure 5.22. During this process, particular attention was paid to the lower range of pressures the transducer would be measuring during testing. The negative pressure response of the device was assessed by the sudden application of a vacuum pressure that varied in direct proportion to the time required to apply the vacuum pressure using a needle valve. The vacuum was maintained for a period of time to ensure that no drift occurred in the sustained negative pressure measurement before being released as the chamber was vented. An example of the pressure measurements logged from the PPTT during such a calibration exercise is presented in Figure 5.23. Where the response time of the device was judged to be unacceptable or where the negative pressure was seen to deviate before a maximum value was recorded this was considered to be evidence that the porous stone was not fully saturated. In such cases, further pressurisation cycles were applied to the transducer to ensure full saturation.

The entire saturation and calibration procedure was carried out prior to every test involving use of the PPTT. After each test the ceramic filter stone was cleaned and oven dried at 50°C in order that the initial degree of saturation was consistent prior to each saturation procedure. The device was installed into the footing base (as shown in Figure 5.5) underwater and a thin layer of saturated clay was placed onto the exposed surface of the filter stone to prevent de-saturation during placement of the footing within each excavation.

5.9 Experimental Procedure

Details of the experimental procedure adopted for each test series are presented. In general this procedure is consistent across each plate anchor test series reported in this thesis. For the transmission tower footing series (TTFS) the direct measurement of suction required the use of a modified experimental procedure detailed separately.

Table 5.12 Setup process for the transmission tower footing

Stage	Action	Centrifuge @	Tool used	Comments
1	Reconstitute bottom drain sand layer	20*g*	Sand placement tool	
2	Reconstitute clay sample	20*g*	Actuator with clay delivery nozzle	The clay sample needed to be reconstituted in two layers
3	Consolidation	250*g*	-	
4	Drain the channel, stop the centrifuge	No	-	The actuator was removed at this stage
5	Apply a layer of geo-textile at sample surface	No	-	
6	Place dry sand surcharge	20*g*	Sand placement tool	
7	Consolidation	250*g*	-	3 days allowed
8	Stop the centrifuge, remove sand surcharge and geo-textile layer	No	-	
9	Reconstitute upper clay layer	20*g*	Clay delivery nozzle	
10	Consolidation	150*g*	-	3 days allowed + 2 days for swelling @ 50*g*
11	Drain the channel, stop the centrifuge	No	-	
12	Form the excavation	No	-	
13	Where required, install saturated PPTT in footing base	No	-	The PPTT was installed underwater
14	Place the footing	No	Actuator	The actuator was used to place the footing
15	Backfill the excavation with moist sand	No	-	The operation was carried out while the footing was held by the actuator
16	Ramp up, introduce water	50*g*	-	The water level was set @ 10 mm above the sample surface
17	Pull out the footing	50*g*	Fast pull out actuator	A period of at least 3 hours was allowed prior to uplift

5.9.1 Plate anchor test series (PASB, PACB and PAIB)

The experimental procedure followed for testing on all samples was as follows:

1. Prepare the samples and install the anchors as described in detail previously in Section 5.8.
2. Mount the T-bar (and cone penetrometer when used) and carry out penetration tests to determine the soil properties within the sample.
3. Mount the fast actuator on the drum actuator and connect the load cell and the holder at the end of the bearing rail.

4. Spin up the channel and actuator to an acceleration of 50*g*, saturate the sample and allow re-consolidation. For cement backfilled anchors 20 hours spinning time was allowed for curing of cement treated sand at this stage. During this period the water table was located and maintained at a depth 10 mm above the soil surface.
5. Wait for equilibrium of the pore pressure recorded by the Druck transducers situated in the drum channel. Equilibrium of the pore pressure is assumed to represent full re-consolidation.
6. In-flight, adjust the position of the actuator and engage the head of the selected anchor with the holder arrangement.
7. Pull out the anchor while recording the uplift load and vertical displacement of the anchor.
8. Stop the actuator (while the channel is still spinning and test conditions of 50*g* are maintained in the sample) and drive upwards, clear of the channel, in order to remove the uplifted anchor.
9. Spin up the tool table to 50*g* and adjust the position of the actuator to allow the connector to engage with the next anchor.
10. Repeat sequences 7 to 9 for each anchor in the sample.
11. Perform cone penetrometer tests in backfilled excavations provided.
12. Stop the centrifuge, dismantle the sample and take a sample to deduce the final moisture content.

5.9.2 Transmission tower footing test series (SFSB)

The experimental procedure followed for testing on the TTF sample was as follows:

1. Prepare the sample as described previously in Section 5.8.
2. Where required, saturate and calibrate the PPTT and install it into the footing base.
3. Install the footing in the test excavation and backfill with moist sand.

4. Spin up the channel and the tool table to 50*g*, saturate and allow at least 3 hours for consolidation of the sample. The water table was located at 10 mm above the soil surface in every test.
5. Wait for equilibrium of the pore pressures recorded by the Druck PDCR81 transducers and the PPTT where available.
6. Carry out T-bar penetration tests to determine the soil properties within the sample.
7. Pull out the footing while recording uplift load, vertical displacement of the footing and, where required, change in pore pressure at the footing base.
8. Stop the centrifuge, remove the footing. Repeat steps 4-7 or steps 3-7 where necessary for tests involving direct suction measurement using the PPTT

For each test series (PASB, PACB, PAIB and TTFS) the uplift force and vertical displacement of the anchor/footing were recorded in every test. Suctions were measured where specified in the TTF test series. The three Druck pressure transducers located at various depths within each sample clay layer registered minimal pore pressure change during each series of uplift tests indicating that each test sample was fully consolidated.

5.10 In-Situ Sample Characterisation

A T-bar penetrometer and a cone penetrometer were used to estimate the characteristics of the soil sample and in particular to provide the shear strength profile of the clay. The results of these characterisation tests provide an outline of the soil strength between each centrifuge sample and facilitate the normalisation of footing capacity and comparison of results from uplift tests performed in each sample. Details of the characterisation tests undertaken are provided.

5.10.1 The T-bar penetrometer

The T-bar penetrometer was first introduced for centrifuge application in determining the undrained strength of normally consolidated clay by Stewart and Randolph (1991). It was later used at field scale in order to improve the accuracy of strength profiling in soft soils for both onshore (Stewart and Randolph, 1994) and offshore environments (Randolph *et al.* 1998). The T-bar comprises a cylindrical bar which is attached to a vertical shaft, the bar having a projected area of 5 to 10 times the shaft area. A sensitive load cell is located along the shaft, behind the T-bar, and is used to measure the pressure required to penetrate the T-bar into the soil. The principle of this, and other penetrometers, is to force the soil to flow around the probe and hence facilitate analysis and interpretation of the test. The model T-bar developed for the drum centrifuge comprises a 5 mm diameter cross bar, 20 mm long, attached at right angles to the end of a vertical shaft, which narrows to 4.5 mm diameter behind the T-bar, Figure 5.24.

The measured bearing pressure (q_{ct}) of the T-bar is related to the undrained shear strength, $s_{uT\text{-}bar}$, of the penetrated soil by the equation

$$s_{uT-bar} = \frac{q_{ct}}{N_{T-bar}} \tag{5.1}$$

Where $N_{T\text{-}bar}$ is a well established parameter determined through plasticity analysis of a laterally displaced cylinder in cohesive soil (Randolph and Houlsby, 1984). The true value of $N_{T\text{-}bar}$ varies between 9.14-9.66 for a fully smooth interface and 11.9 for a fully rough interface with a transitional value of 10.5 recommended by Stewart and Randolph (1991) for correlation of results in general use.

5.10.2 The cone penetrometer

The cone penetrometer adopted for use in the drum centrifuge has a diameter of 6 mm and a 60 degree cone tip giving an end area of about 28.3 mm^2, as shown in Figure 5.24. A load cell, attached inside the penetrometer rod directly behind the tip of the cone, is used to measure the tip pressure developed as the cone is penetrated through the soil. During penetration of the cone a profile of tip pressure (q_c) is recorded which may be assessed to provide a measure of the strength and relative density (D_r) for

sands. The tip pressure may also be interpreted in order to determine the profile of undrained shear strength of clay soils using methods detailed by Lunne *et al.* (1997) (for Norwegian sensitive soils) and by Mesri (2001) (for other soft clays).

Both penetrometers are mounted on the drum actuator, after the sample is consolidated, and can be used in-flight at any radial position in the channel. In a standard penetration test, they are pushed in and pulled out at a rate of 1 mm/s sufficient to obtain an undrained response of the soil. This penetration rate is related to a normalised velocity V in excess of 30 as outlined by Finnie and Randolph (1994),

$$V = \frac{vD}{c_v} \tag{5.2}$$

where, v is the penetration velocity, D is the equivalent diameter and c_v is the coefficient of consolidation. In the case of the T-bar, extended tests were performed at penetration rates ranging from 0.03 mm/s to 100 mm/s, the results of which are discussed in following sections.

5.11 T-bar Soil Strength

An overview of the soil strength for each sample as measured using the T-bar is presented. Also included are the results of a series of T-bar tests performed at increasing velocities and a reflection on the effect of penetration rate on the undrained strengths measured in these tests. The value of undrained strengths measured using the T-bar and their application in the normalisation of anchor capacity is also discussed.

5.11.1 Plate anchor series 1 – Sand backfill

A number of T-bar penetration tests were undertaken throughout the test period for each sample in order to characterise the soil and determine the undrained strength profile of the clay. Summaries of the undrained shear strength profiles recorded during the test period at various locations within each of the five samples are presented in Figures 5.25-5.29 inclusive. For each sample the average T-bar strength profile is

inferred from the individual measured profiles and a comparison of the average profile from each of the samples is presented in Figure 5.30.

For logistical reasons and to facilitate the development of ancillary apparatus, the first sample was left to spin for a period of about 3 weeks before the anchor uplift tests were performed. The T-bar tests for this first sample were therefore performed at various intervals over a period of one month both after sample preparation and during the test period. This being the case however, no significant change in the initial shear strength (T-bar tests 1 and 2, Figure 5.25a) is observed over the test period when compared to the strength profile for subsequent T-bar tests performed on sample 1. For all following samples T-bar tests were performed throughout the test period. The following observations may be made from the profiles presented:

- Within each sample reasonable agreement is observed between the measured strength profiles from T-bar tests performed at different locations during the test period. This demonstrates that the sample preparation procedure adopted produced samples in each case with a high level of homogeneity.
- The undrained shear strength observed in all samples ranges from 0 at the surface of the sample to 24 kPa at the extent of the T-bar penetration and varies approximately linearly with depth from the sample surface.
- The undrained shear strength of the first sample is significantly lower than that of the other four samples. At a model depth (z_m) of 45 mm (prototype depth (z_p) of 2.25), corresponding to the embedment depth of the anchors, the undrained shear strength of the first sample is approximately 25% lower than that measured in each other case (5.7 kPa versus 7.3-7.9 kPa). As mentioned previously the increased test period for preparation, development of apparatus and anchor installation may have contributed to this variation in the strength of the sample. In later sections this difference in strength will be considered through the normalisation of results from each sample. It should also be noted however that in sample 1 only one pull out test of an anchor founded on an entirely clay base is undertaken at a displacement rate of greater than 3mm/s, at which point the clay shear strength is thought to have a more significant effect on the measured pull out capacity.

- The overall depth the fourth sample is significantly larger than that of the other three samples. The average strength profile for this sample, as presented in Figure 5.30, is however, similar to that of the other samples (with the exception of sample 1 as noted) and reasonable agreement is observed in the undrained shear strengths at the base of the anchor with each of the other samples, Table 5.13.

The average undrained shear strength at the base of the anchor for each sample is presented in Table 5.13. Where the anchor uplift velocity (v_f) is such that partial separation or fully bonded behaviour occurs at the anchor base, the contribution to uplift resistance provided by the reverse bearing capacity mechanism developed will be a function of the undrained shear strength of the clay. If it is assumed that this reverse bearing mechanism is similar in its development to the conventional bearing mechanism (e.g. Finn and Byrne, 1972), then for a simplified case the failure mechanism would be expected to extend approximately one anchor width (B) in depth below the anchor base. Where normalisation of the uplift capacity is required to obtain the appropriate uplift capacity factor, the average undrained shear strength may be conveniently taken as the average value within this zone, at a depth B/2 below the anchor base. These values are also presented in Table 5.13 and are used later for calculation of the uplift capacity factor N_{uc}.

Table 5.13 Undrained shear strength at anchor base, averaged from T-bar tests

	1st sample	2nd sample	3rd sample	4th sample	5th sample
$s_{uT\text{-}bar}$ (kPa)	5.7	7.5	7.4	7.3	7.9
$s_{uT\text{-}bar}$ at depth B/2 below anchor base (kPa)	8.0	9.3	9.4	9.0	9.3

In reality if a reverse bearing capacity mechanism is assumed to develop, then by inference from conventional bearing capacity theory the effect of vertical strength heterogeneity, corresponding to a dimensionless strength gradient (kB/s_{u0}, where k is the linear strength gradient and s_{u0} is the undrained strength at the anchor base) will be to either increase or reduce the zone of influence below the anchor. In such cases a

modified bearing capacity factor N_c^* (which is greater than Nc for a homogenous clay and is a function of kB/s_{u0}) may be applied to s_{u0} to calculate the foundation capacity (Davis and Booker, 1973). Alternatively, Skempton (1951) recommended that where the undrained shear strength was observed to vary by less than ± 50% of the average value within a depth of 2/3B, the mean value over this depth should be used (i.e. the value of s_u at B/3 for a linear strength profile). As the exact uplift failure mechanism below an anchor founded on clay is largely unknown and there is no available guidance with regard to a modified uplift capacity factor to account for strength heterogeneity, it is thought that the use of an undrained strength at depth B/2 below the anchor will provide a conservative approach at this stage. Given the profiles shown in Figure 5.30 the average value of $s_{uT\text{-}bar}$ at B/2 below the anchor base is a maximum of 5% higher than the value of $s_{uT\text{-}bar}$ at B/3 below the anchor base.

The average linear undrained strength profiles and mean undrained shear strength ratios at the base of the anchor, defined as the undrained shear strength divided by the effective stress at embedment depth ($s_{uT\text{-}bar}/\sigma'_v$), are given in Table 5.14. The effective unit weight (γ') of each sample was assessed from sample cores taken after testing and an average value for γ' of approximately 6.1 kN/m^3 was obtained, yielding undrained strength ratios ranging between 0.42 and 0.58 according to the sample.

Table 5.14 Undrained shear strength ratios at anchor base

	1st sample	2nd Sample	3rd Sample	4th sample	5th sample
	z_m = 45-80mm depth (z_p = 2.25-4m)				
$s_{uT\text{-}bar}$ (kPa)	5.7 + 3.7 z	7.5 + 3.3 z	7.4 + 4.4 z	7.3 + 3.8z	7.9 + 4.2z
$s_{uT\text{-}bar}/\sigma'_v$ (at the base of the anchor)	**0.42**	**0.55**	**0.54**	**0.53**	**0.58**

The values of undrained shear strength ratio obtained from the T-bar test results are much lower than those observed in Chapter 4 for kaolin B clay in either triaxial compression or direct simple shear but, (for OCR=5) are reasonably well represented the undrained strength ratios for triaxial extension shown in Figure 4.9. The average of the values given in Table 5.14 (for samples 2-5) may be expressed using the

normalised strength equation (Equation 2.18, Ladd and Foott, 1974) where, for the sample overconsolidation ratio of 5:

$$\frac{s_u}{\sigma_v'} = 0.15.OCR^{0.8} \qquad (5.3)$$

This result is in broad agreement with the recommendations of Watson (1999) where a value for the normally consolidated undrained shear strength ratio of between 0.15 and 0.2 (just above that for kaolin clay in triaxial extension where $(s_u/\sigma'_v)_{nc}$ =0.13) is generally observed.

5.11.2 Plate anchor series 2 – Clay backfill

A summary of the undrained shear strength profiles recorded during the test period at various locations within the clay backfill sample is presented in Figure 5.31(a). As previously for plate anchor series 1, the average T-bar strength profile is inferred from the individual measured profiles and the average profile is presented in Figure 5.31(b). The sample was prepared using a modified 2-stage procedure, as detailed in section 5.8.3, the effect of which is seen in the layered nature of the profile. As a result of previous testing undertaken, the initial clay layer (at $z_p > 2.2$ m) was subject to a much longer period of consolidation at accelerations of 50*g* and 250*g* prior to placement of the backfill layer. A number of observations may be made from the T-bar profiles presented in Figure 5.31:

- T-bar profiles measured at different locations within the sample during the test period are similar, illustrating the homogeneity of the sample.
- The undrained shear strength profile of the sample ranges from 0 kPa at the surface of the sample to 22 kPa at the base.
- As a result of the 2-stage preparation procedure, the undrained shear strength profile was not uniform throughout the sample depth and a significant increase is observed between the two layers.

As observed in Figure 5.31 the distinction between the backfill and base clay layer profiles occurs at approximately the embedment depth of the anchor and there is a significant variation in the T-bar undrained strength at this depth. The average undrained shear strength and mean undrained shear strength ratios at the base of the

anchor for each clay layer are given in Table 5.15. At the embedment depth of the anchor the undrained strength ratio is between 0.68 and 0.98 due to the layered profile of the sample. For the purpose of normalisation of measured anchor uplift capacities and to provide the corresponding uplift capacity factors, the undrained strength is taken at a depth of B/2 below the anchor base (as described in Section 5.11.1) where there is no variation in the T-bar undrained strength profile.

Table 5.15 Undrained shear strengths for the backfill and base clay layers and undrained strength ratios at the anchor base

	Backfill layer	Base layer
$s_{uT\text{-}bar}$ (kPa)	**9.5**	**13.6**
$s_{uT\text{-}bar}$ at depth B/2 below anchor base (kPa)	-	**16.0**
$s_{uT\text{-}bar}/\sigma'_v$ (at the base of the anchor)	**0.68**	**0.98**

The mean undrained strength ratio observed in the base clay layer, at an OCR of 5, is approximately 0.81 and is higher than that observed at the same OCR for the clay samples in plate anchor series 1 (PASB). For the PACB sample the mean undrained strength ratios are well represented by Equation 2.18 in the form:

$$\frac{s_u}{\sigma'_v} = 0.22.OCR^{0.8} \qquad (5.4)$$

where the value of the OCR is equal to 3 for the backfill clay and equal to 5 for the clay below the anchor base. In this case the undrained strengths predicted by Equation 5.4 are broadly similar to those measured in triaxial compression tests on kaolin as presented in Chapter 4 and shown in Figure 4.9. Given the variation with OCR of the T-bar undrained shear strength predicted by Equation 5.3 for the kaolin samples in plate anchor series 1 and the values of $(s_u/\sigma'_v)_{nc}$ presented by Watson (1999) it would appear that the undrained strengths measured in the PACB kaolin sample are a little higher than expected.

5.11.3 T-Bar rate effects

The influence of the penetration velocity on the undrained strength ratio obtained from T-bar penetration tests was investigated in samples two and three of plate anchor test series 1. The rate dependence of T-bar undrained shear strength is highlighted in Figure 5.32 where the shear strength ratio ($s_{uT\text{-}bar}/\sigma'_v$) is plotted with the penetration velocity (v). It is apparent that a strong rate dependence exists in the undrained strength at penetration velocities greater than between 0.3 and 1 mm/s and that this dependence is most significant at velocities greater than 10 mm/s. It is expected that at penetration velocities less than 0.3–1 mm/s the undrained shear strength ratio would increase steadily as a higher degree of consolidation is possible during penetration. The value of the undrained strength ratio would reach a maximum at a penetration velocity such that fully drained conditions arise and thereafter remain constant with decreasing velocity (Lehane *et al.* 2007). The rate dependence at high penetration velocities, such as those shown in Figure 5.32, may be attributed to an increased viscous effect which governs the increase in undrained shear strength where reduced consolidation effects are minimal. Above 10 mm/s, the penetration velocity is evidently fully undrained and a rate of increase in strength of approximately 10-15% per log cycle increase in velocity is consistent with strength increases reported for a large number of published previously studies on a variety of clays in triaxial compression (Chapter 2).

In following sections, it will be assumed that the T-bar tests performed at 1 mm/s provide a reference undrained shear strength ($s_{uT\text{-}bar(ref)}$).

5.11.4 Transmission tower footing test series

A summary of the undrained shear strength profiles and the average T-bar strength profile (inferred from the individual test profiles) for the transmission tower footing test sample is presented in Figure 5.33. As result of the sample preparation procedure two distinct clay layers are evident in the sample, with a much higher strength measured in the base clay layer due to the sand surcharge applied to the clay during consolidation (Section 5.8.5). A number of observations may be made from the T-bar profiles presented in Figure 5.33:

- As observed previously for series PASB and PACB the results of T-bar tests performed at different locations during the test period are similar and demonstrate the homogeneity of the sample. The undrained strength does however, become noticeably less uniform with increasing depth. This may be a result of small fluctuations in the depth of the sand surcharge and specified water level for the base clay layer during the consolidation period.
- The undrained shear strength profile achieved in both samples ranges from 0 at the surface of the sample to approximately 39 kPa at the base.
- The undrained shear strength varies approximately linearly with the depth from the sample surface to 45 mm (2.25m prototype) depth. After this depth there is a sharp increase in strength indicating the top of the more heavily overconsolidated clay base layer and the effect of the sand surcharge provided on the top of this layer during consolidation.
- The undrained shear strength does not vary linearly with depth. A fluctuation in the strength profile is observed at a sample depth of approximately 56 mm where the undrained shear strength reduces by about 12%. From 65 mm depth the undrained shear strength profile once again increases roughly linearly with depth.

In order to overcome the fluctuation in shear strength within the base clay layer below the footing approximately 10 mm of clay was removed from the top of the sample. For the same footing embedment (65 mm) this resulted in the footing being founding at a depth such that the shear strength profile was uniform below the footing. The undrained shear strength profile measured below the footing embedment depth is shown in Figure 5.34 and varies from approximately 21 kPa at the footing base to 39 kPa at the extent of T-bar penetration. It should be noted that the maximum penetration depth of the t-bar is approximately 30 mm above the base of the clay layer.

The overconsolidation ratio for the clay sample used in the transmission tower footing test series is plotted with depth in Figure 5.35(a). The effect of the sand surcharge is seen to increase the OCR at the top of the base clay layer to a value of about 10 while the top clay layer (in which the excavations were formed) was consolidated to an OCR of 3. At the embedment depth of the footing the OCR is reduced to a value of

approximately 9. The undrained shear strength profile of the sample may be reasonably well represented using the form of the normalised strength equation using a value for the normally consolidated shear strength ratio of 0.18:

$$\frac{s_u}{\sigma_v'} = 0.18.OCR^{0.8} \qquad (5.5)$$

where the value of the OCR in the sample varies with depth as shown in Figure 5.35(a). The undrained shear strength profile predicted using Equation 5.5 is compared in Figure 5.35(b) with the average undrained shear strength profile measured using the T-bar. It is apparent that (given the fluctuation in the measured T-bar strength at z_m = 55–65 mm) the measured T-bar profile is in broad agreement with that predicted using Equation 5.5 and that the best fit value for $(s_u/\sigma'_v)_{nc}$ of 0.18 is within the range of values predicted from previous investigation (e.g. Watson, 1999 and Lehane *et al.* 2007). It may therefore be assumed that the relationship predicted by Equation 5.5 and shown in Figure 5.35 is compatible with the stress history imposed on the centrifuge test sample.

5.11.5 Measurement of undrained strength

While the T-bar penetration test was selected as the most convenient method of determining the in-situ undrained shear strength (s_u) of the kaolin sample in each centrifuge test series, estimates of s_u may also be obtained from the triaxial compression, triaxial extension and direct simple shear data compiled for kaolin clay in Chapter 4. As mentioned earlier the undrained shear strength of the clay beneath the anchor will have a significant effect on the ultimate uplift capacity where the uplift velocity is of a magnitude whereby full or partial adhesion occurs between the anchor and the underlying clay. Under such circumstances the most appropriate mode of deformation under which to determine the undrained shear strength will depend on the stress path experienced by the clay at the anchor base. In general, where fully bonded behaviour or where only partial separation of the anchor and underlying clay occurs, the stress path will be broadly similar to that imposed on a clay sample in triaxial extension. It was shown in Chapter 4 that the normally consolidated undrained shear strength ratio obtained from undrained triaxial extension tests is just over half the

value assessed in triaxial compression or simple shear. For this reason the use of an undrained shear strength determined in triaxial compression (s_{utc}) in the generalisation of uplift test data may result in conservative estimates of the uplift capacity factor N_{uc}. While the above assumptions are adequate for the zone of soil directly below the anchor (i.e. the passive zone for a reverse bearing mechanism) they may not be representative of the complete failure mechanism where (if similarity with bearing capacity theory is assumed) the undrained strength in the zone of soil below each side of the anchor, where the soil is deforming differently (i.e. the active zone), may be more closely represented by the undrained shear strength determined in triaxial compression. The normally consolidated undrained strength ratio assessed from the T-bar penetration tests undertaken in each centrifuge sample has been observed to lie in the region 0.15-0.2 and as such will fall between that generally assessed from triaxial compression and triaxial extension tests in Chapter 4. Furthermore the strain rate dependence exhibited by T-bar tests undertaken at increased penetration rates is similar (in terms of relative increase per log cycle) to that derived from the series of triaxial extension tests described in Chapter 4. Considering that the T-bar also provides an in-situ assessment of the undrained shear strength it is thought that uplift capacity factors derived using the T-bar measurement of shear strength ($s_{uT\text{-}bar}$) will be relevant to the majority of design cases.

5.12 Cone Penetrometer Test Results

In the test series PASB, PAIB and TTFS sand was used as the foundation backfill material for each uplift test. In order to characterise the sand backfill, cone penetrometer tests (CPTs) were performed in backfilled excavations in which no anchor was founded, similar to that shown in Figure 5.12(b). An overview of the measured CPT profiles and derived parameters and a comparison of the behaviour of sand modified with the addition of Portland cement are presented.

5.12.1 Plate anchor series 1 – Sand backfill

Three cone penetrometer tests were performed for fully sand-backfilled excavations with no anchors for samples 1, 2 and 3 in plate anchor series 1. In each case the

excavation was made with a sand base (with the base clay layer removed and backfilled with sand) and backfilled in the same manner as would an anchor have been present. The profiles, each corrected as recommended by Lunne *et al.* (1997), for net cone resistance q_{cnet} are presented in Figure 5.36. It is apparent that the corrected cone resistance is low ($\approx$1.5 MPa at the embedment depth of the anchors), and indicative of a loose consistency/relative density for the backfilled sand. Typical CPT correlations for normally consolidated un-aged sands, as given in Lunne *et al.* (1997), indicate a backfill relative density (D_r) of approximately 38%. Tip resistance profiles of the three CPTs performed in different samples are in broad agreement and demonstrate a satisfactory level of repeatability in the adopted backfill method. Tip resistance profiles for CPTs undertaken in sand backfilled excavations in the transmission tower footing test series are shown in Figure 5.37. As expected the results obtained are similar at similar depth to those seen in the plate anchor test series 1, although a generally more linear increase in tip resistance with depth (z_p < 45 mm) is observed in the latter case.

5.12.2 Plate anchor series 3 – Cemented backfill

In plate anchor series 3 a distinction was made between un-cemented and cemented sand backfill and cone penetrometer tests were undertaken in four excavations backfilled with un-cemented sand and cemented sand at 1, 3 and 5% cement content. A curing period of at least 20 hours was allocated prior to undertaking each CPT and no significant lapse of time was allowed between tests, so as to maintain a similar state of curing in each cemented sand backfill. The cone resistance profiles measured in each test are plotted in Figure 5.38 from which it is observed that:

- In each case the cone resistance (q_c) reaches a maximum at depths between 15mm and 40mm then reduces due to the presence of the kaolin clay (i.e. the base of the excavation shown in Figure 5.12b) located at a depth of 60mm.
- The net cone resistance for the un-cemented sand is low with a relative density (D_r) of approximately 30% in the upper 40mm of the sample. This value is broadly in line with the target void ratio of 0.74 employed in the laboratory tests but is slightly lower than that observed for similar sand backfilled excavations in plate anchor series 1.

- The value of q_c increases with increasing cement content of the backfill sand up to a maximum of around 6.3 MPa at a cement content of 5%. The highest relative gain in q_c is observed between a cement content of 1 and 3%.

The ratio of the q_c value measured in the backfill at a cement content of 3% to that at a cement content of 1% is similar to the that observed in the unconfined compressive strengths (q_{uc}) at the same cement contents presented in Chapter 4 (Table 4.2). The value of q_c measured at a cement content of 5% however is relatively low compared to its q_{uc} value and may underestimate the respective gain in strength between 3% and 5% cement content. Given the data presented in Table 4.2 for laboratory testing of cemented sand samples, there appears to be no simple general correlation between q_c and either the effective stress strength parameters (c' and ϕ'_p) or with the unconfined compressive strength (q_{uc}).

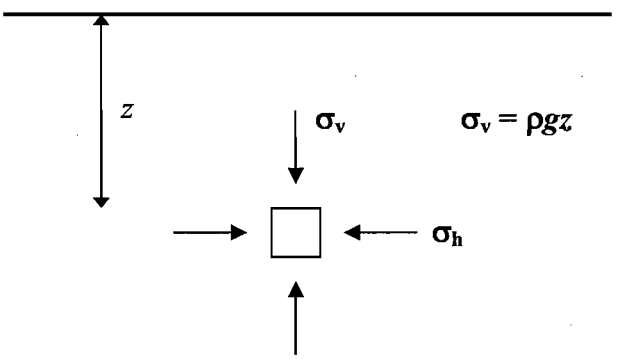

Figure 5.1 General 2-dimensional stress state for an element of soil at a depth z

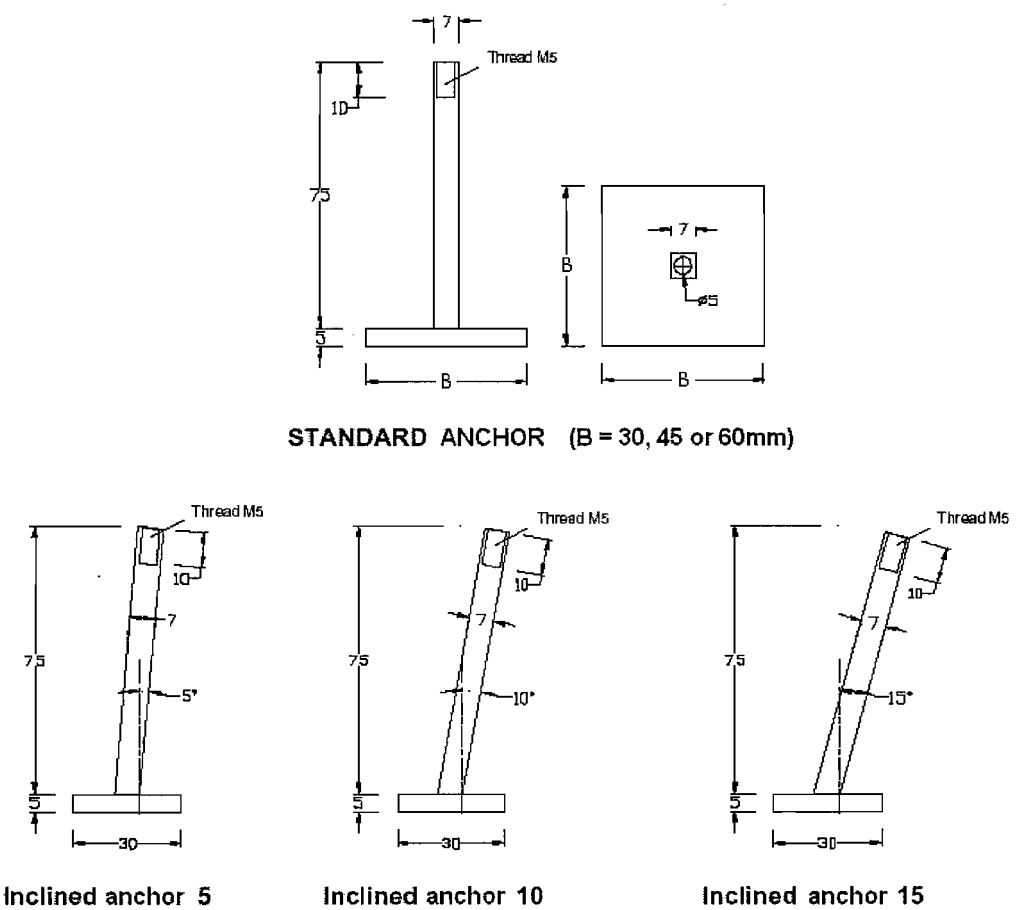

Figure 5.2 Model footing geometry

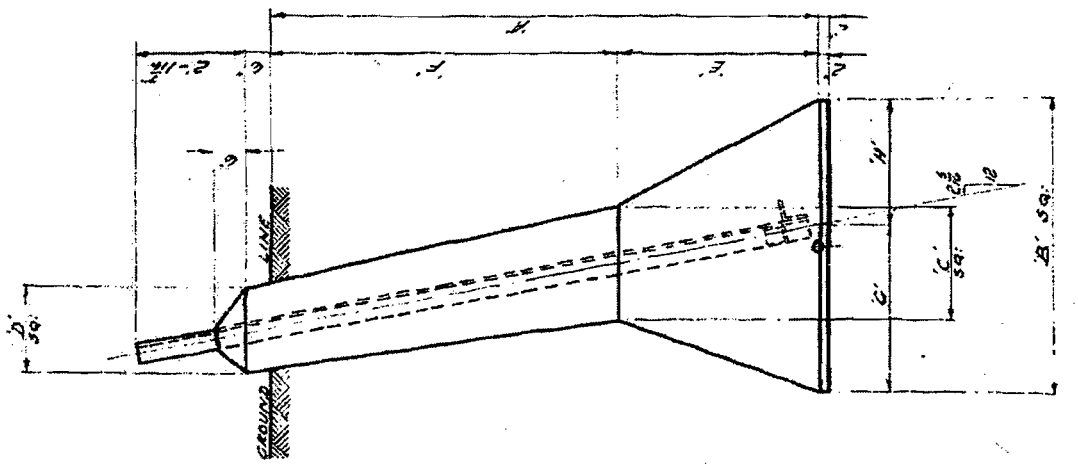

Figure 5.3 Type D12 transmission tower footing

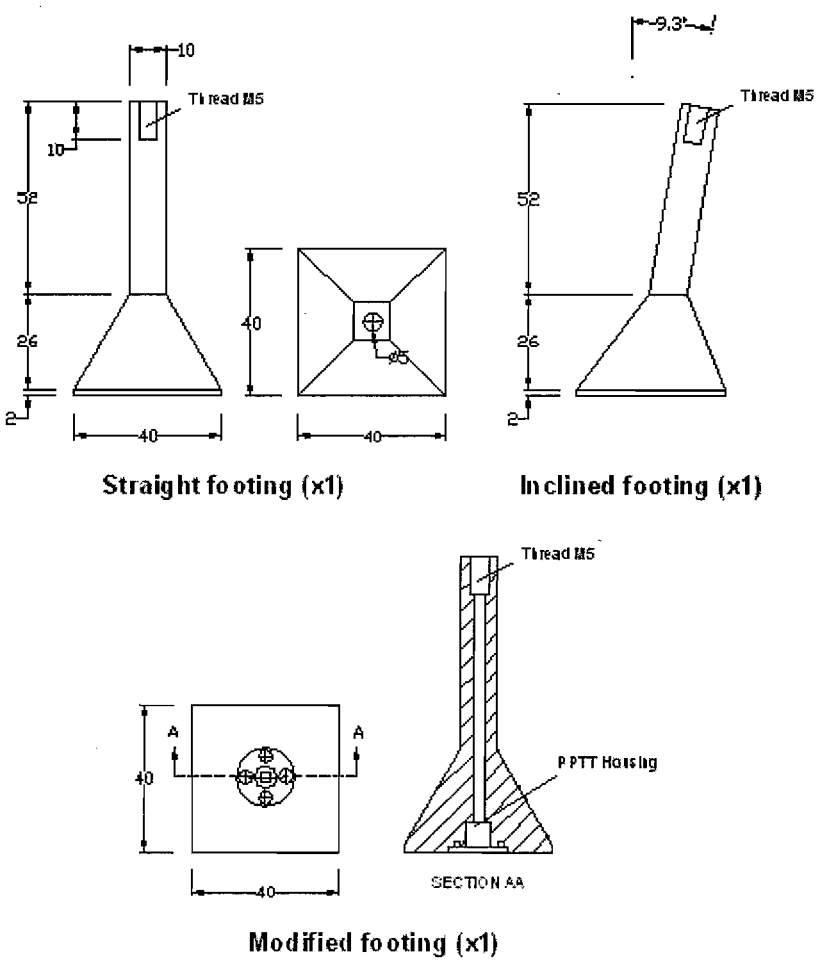

Figure 5.4 Type D12 model footing geometry

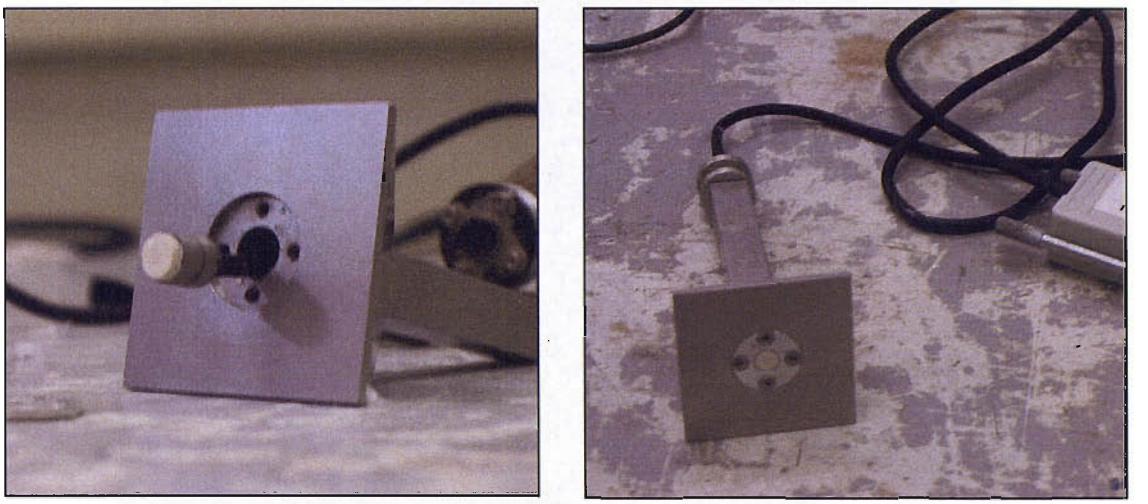

Figure 5.5 Pore pressure transducer (PPTT) installation in the model footing base

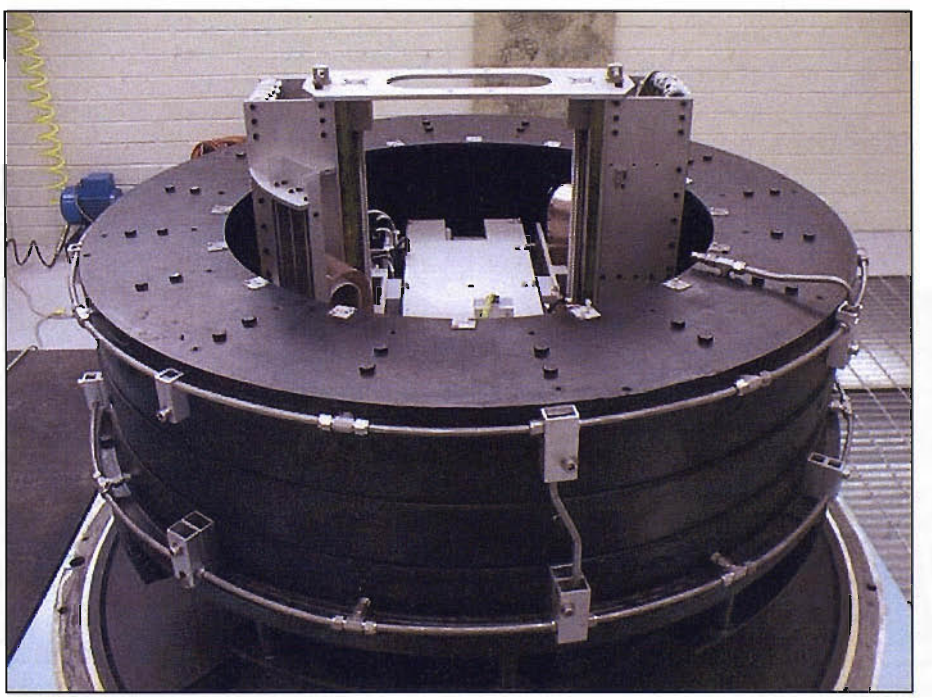

Figure 5.6(a) UWA drum centrifuge

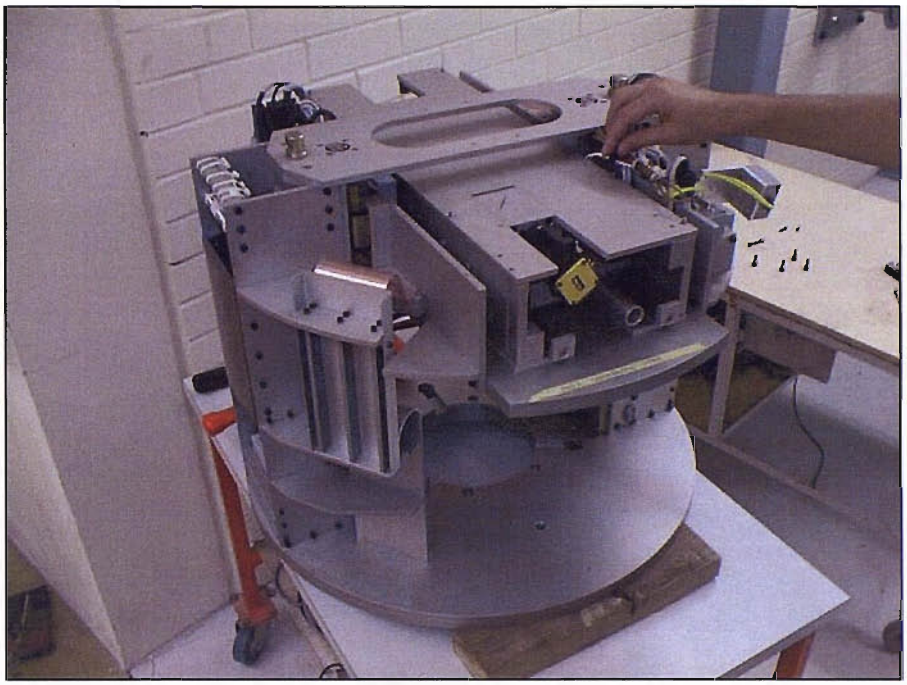

Figure 5.6(b) Centrifuge tool table and actuator

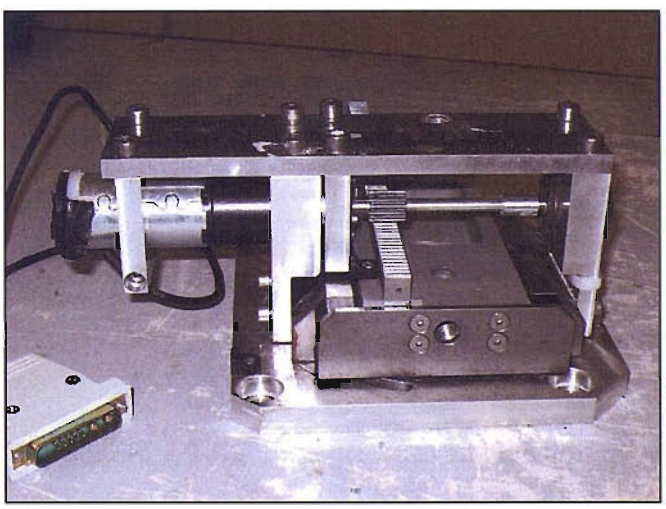

(a) Fast pull actuator with base plate

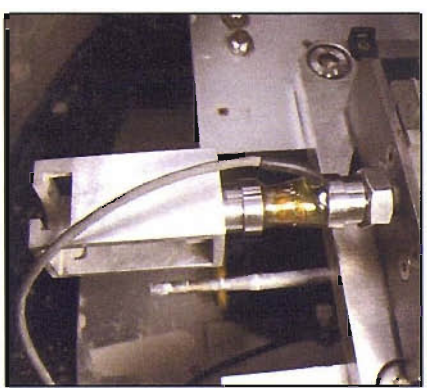

(b) Load cell and hook arrangement

Figure 5.7 Fast pull actuator

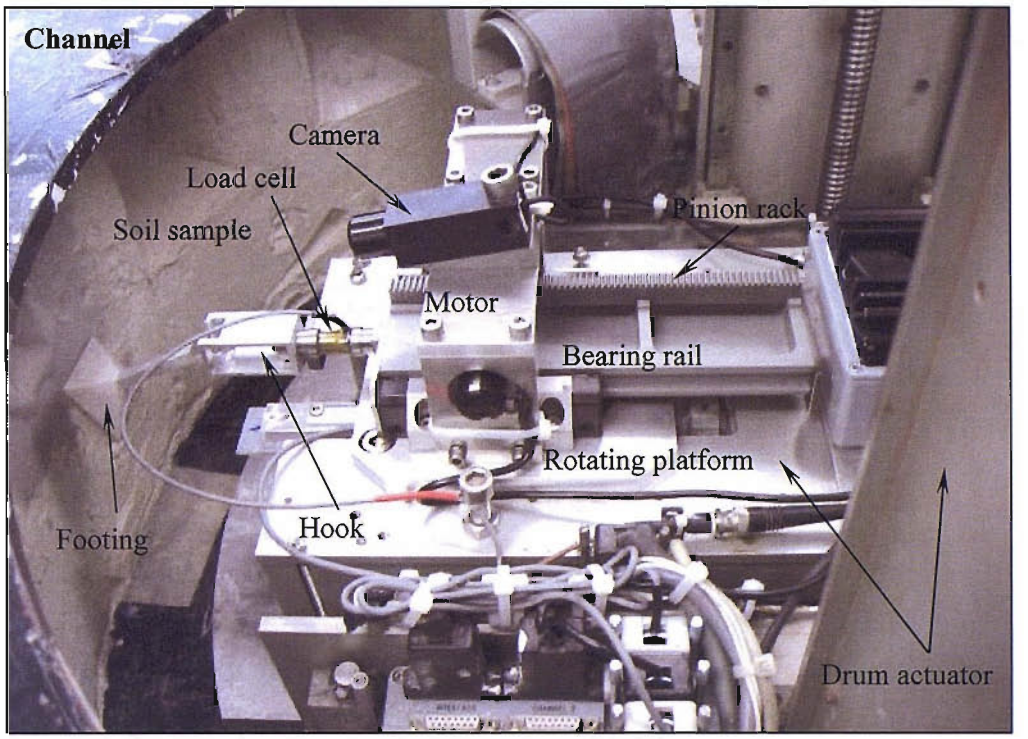

Figure 5.8 Fast pull actuator mounted on the main centrifuge actuator

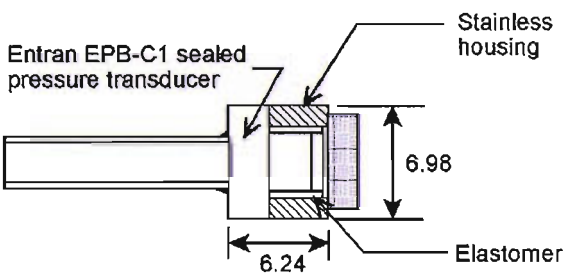

Figure 5.9 Pore pressure and tension transducer (Take and Bolton, 2003)

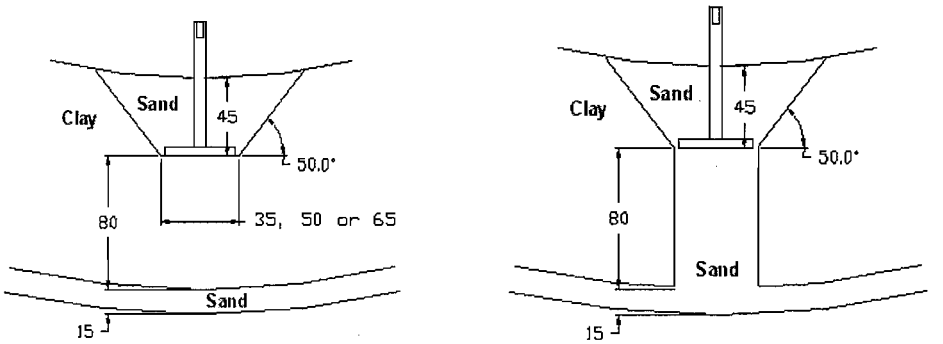

a) Anchor on clay base b) Anchor on sand base

Figure 5.10 Test geometries of plate anchor series 1 – sand backfill

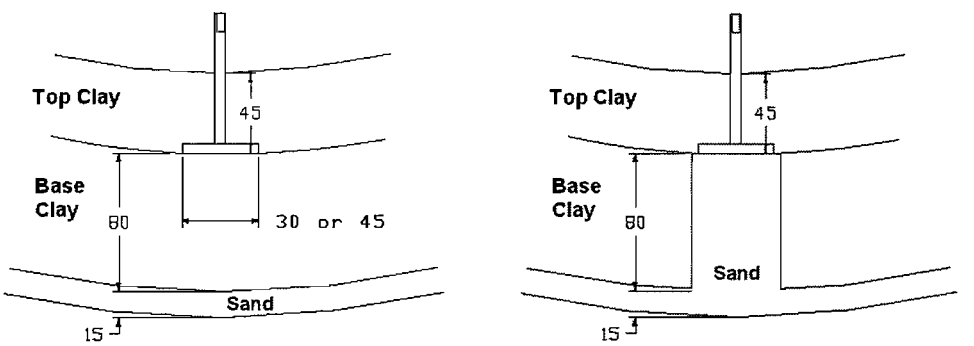

a) Anchor on clay base b) Anchor on sand base

Figure 5.11 Test geometries of plate anchor series 2 – clay backfill

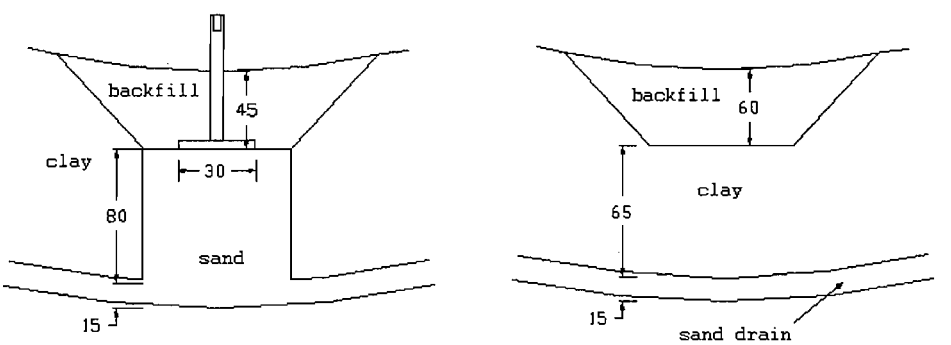

a) Anchor on sand base b) Excavation for CPT

Figure 5.12 Test geometries of plate anchor series 3 – cemented backfill

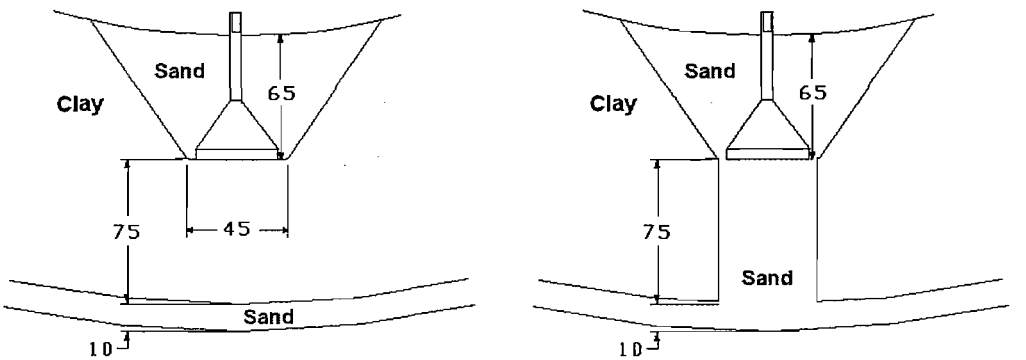

a) Footing on clay base b) Footing on sand base

Figure 5.13 Test geometry of transmission tower footing test series

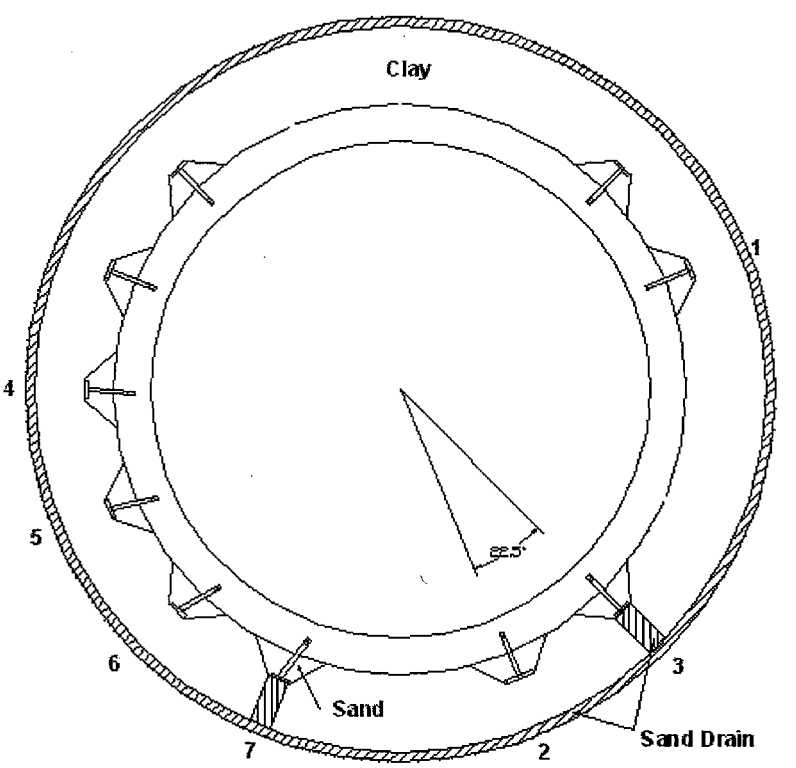

Figure 5.14(a) Test configuration – PASB Sample 1

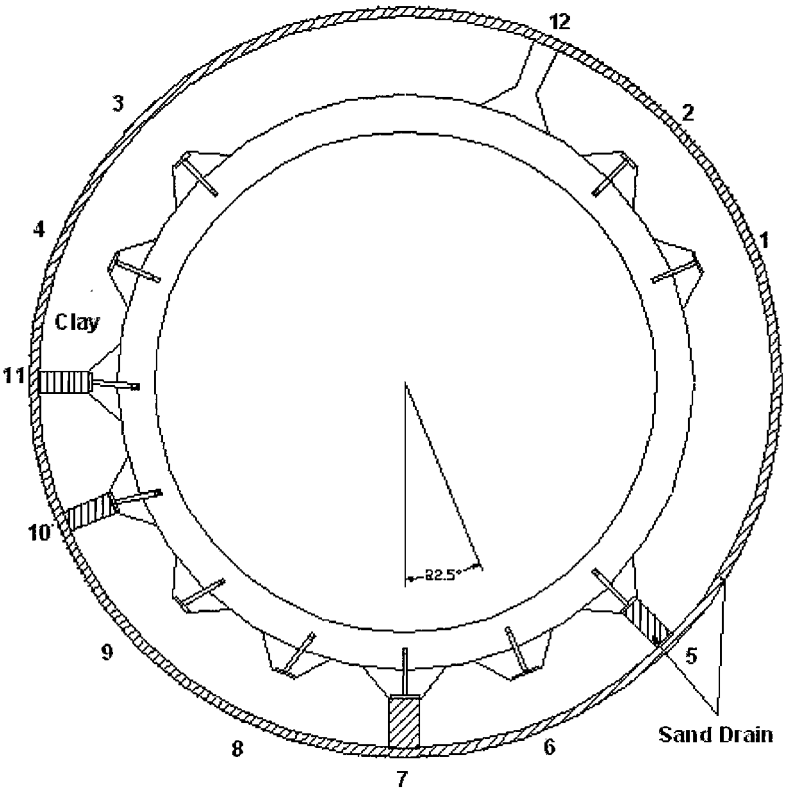

Figure 5.14(b) Test configuration – PASB Sample 2

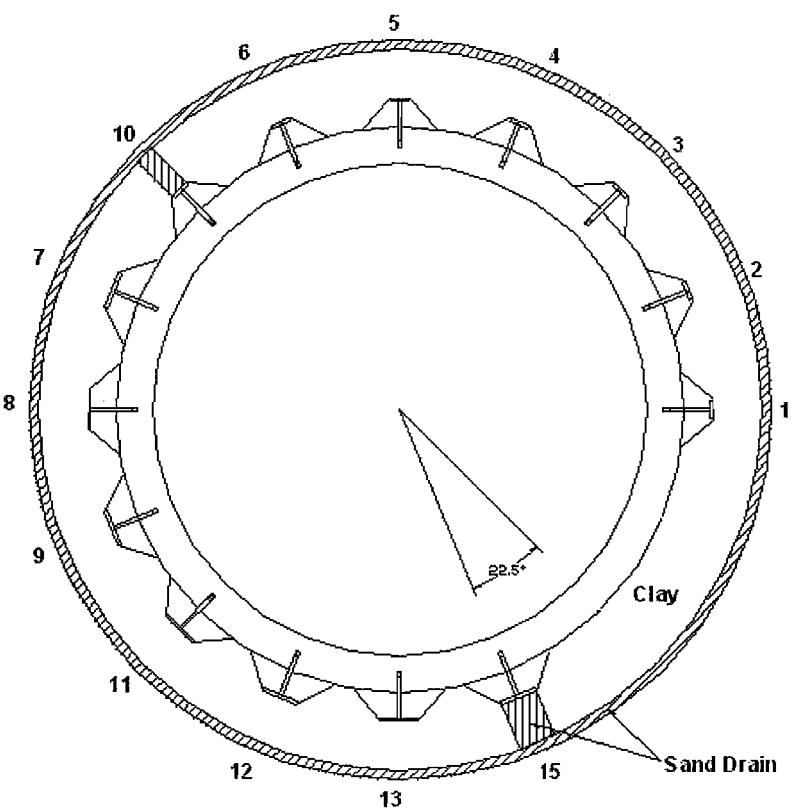

Figure 5.14(c) Test configuration – PASB Sample 3

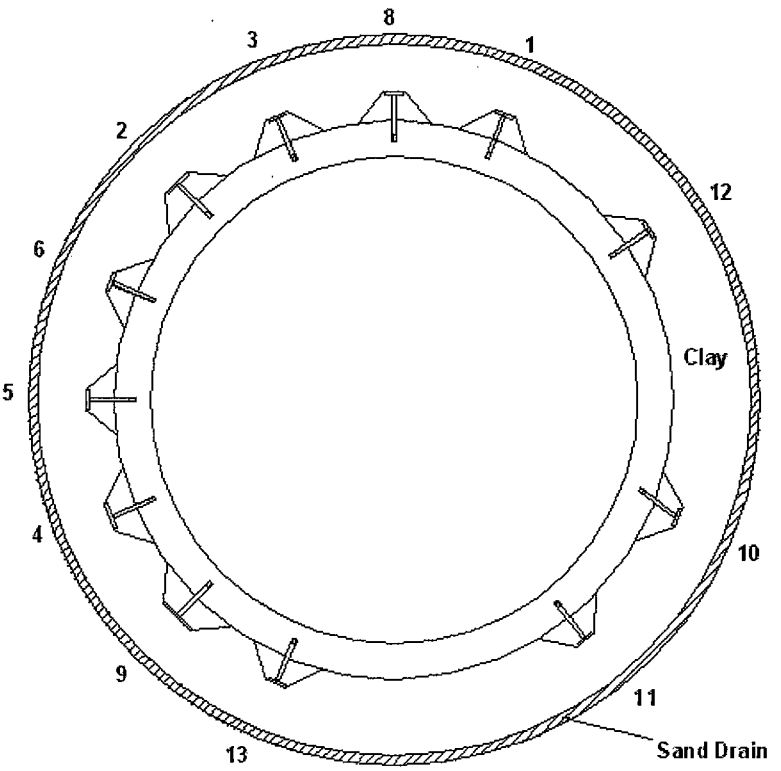

Figure 5.14(d) Test configuration – PASB Sample 4

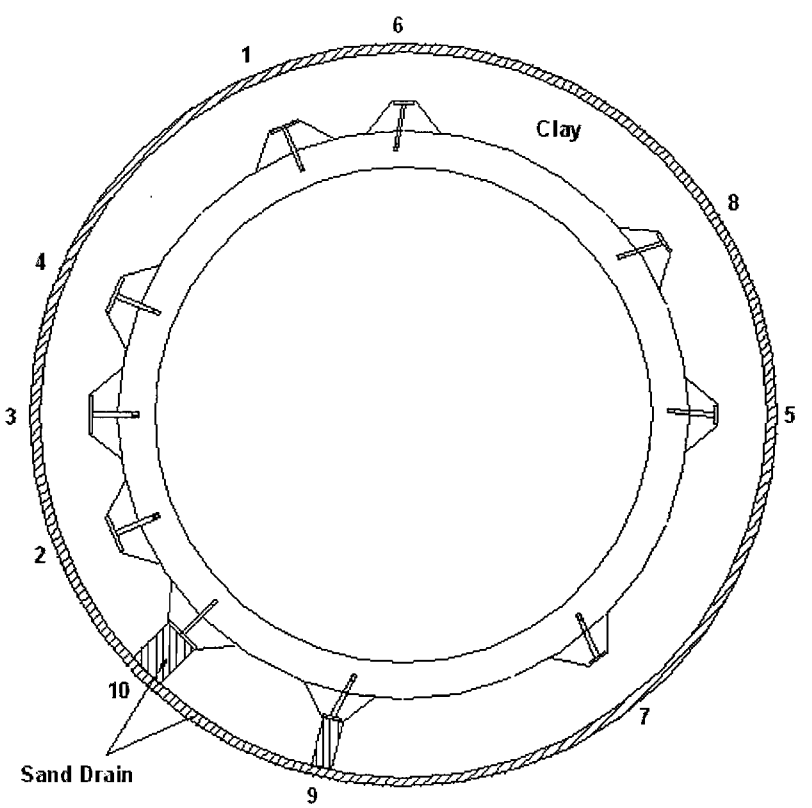

Figure 5.14(e) Test configuration – PASB Sample 5

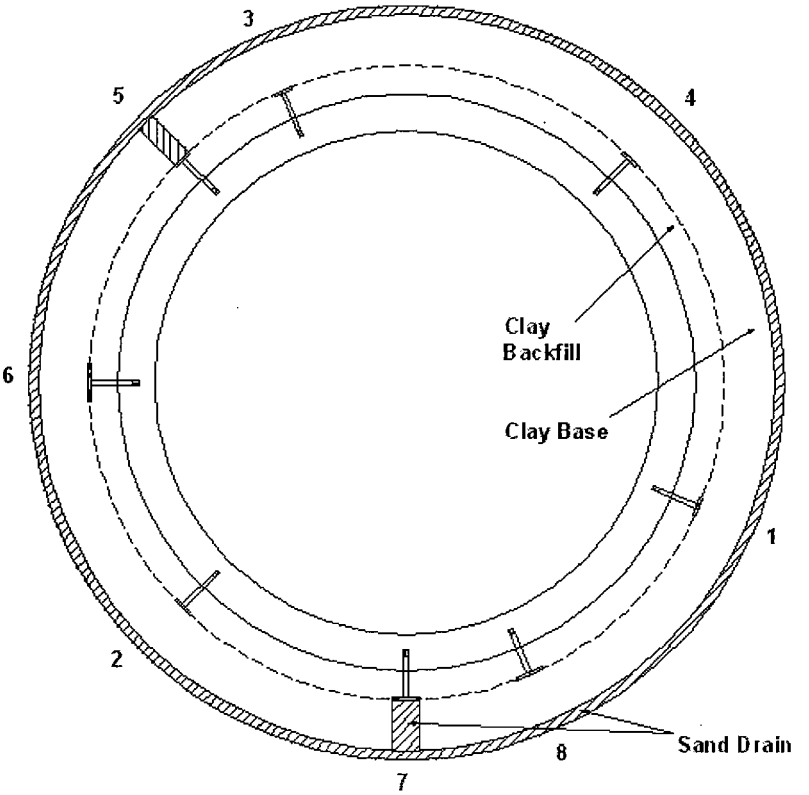

Figure 5.15 Test configuration – PACB Sample 1

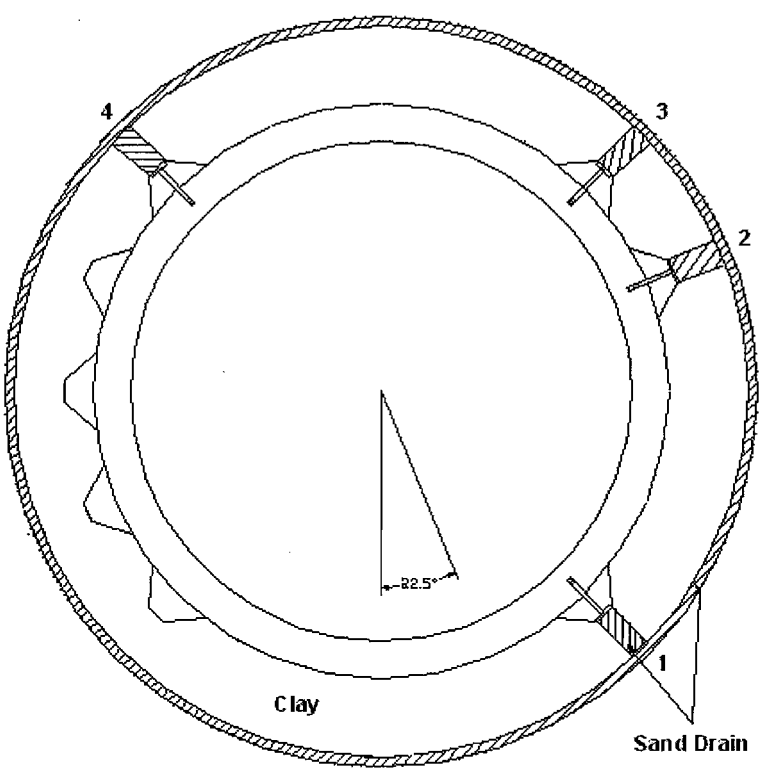

Figure 5.16 Test configuration – PAIB Sample 1

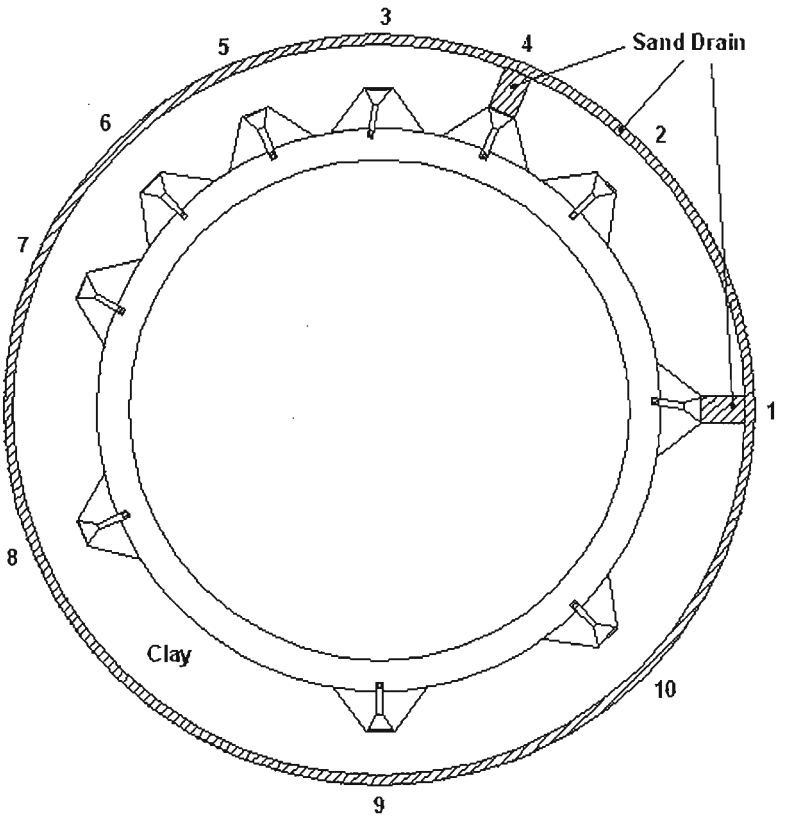

Figure 5.17 Test configuration – TTFS Sample 1

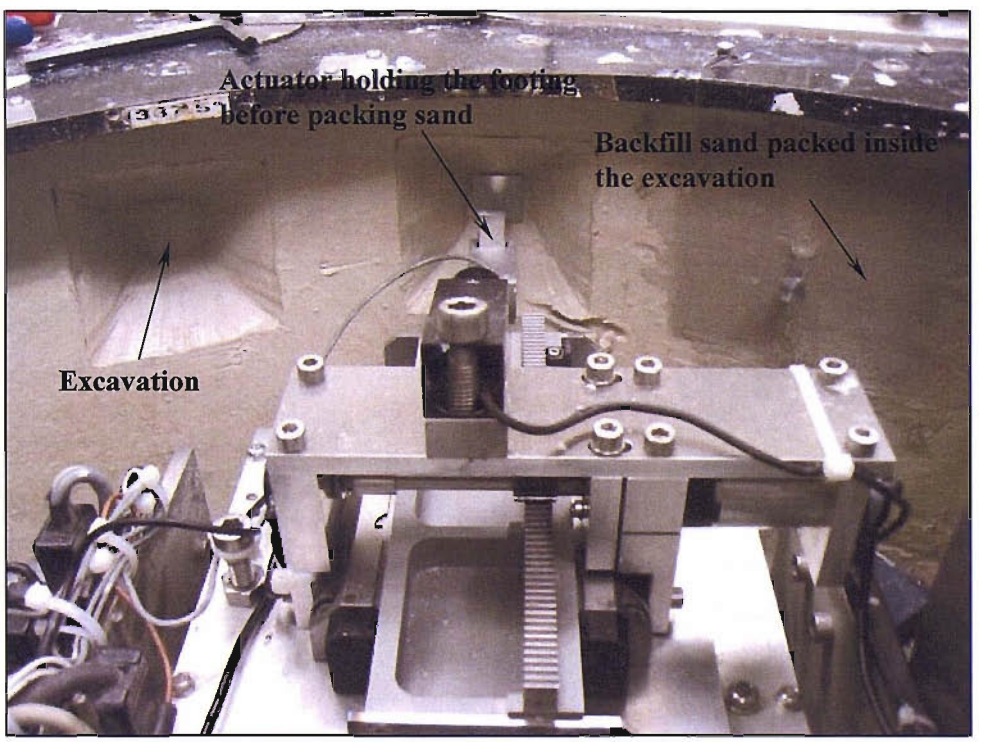

Figure 5.18 Anchor installation in sand backfill test series

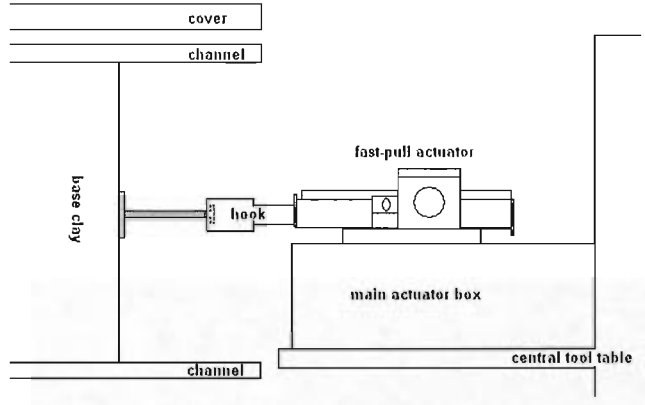

(a) 1st anchor placed in flight on clay surface

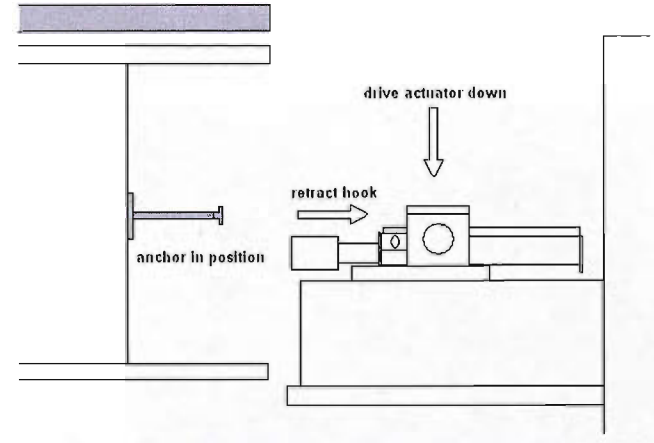

(b) Discharge anchor and retract hook attachment

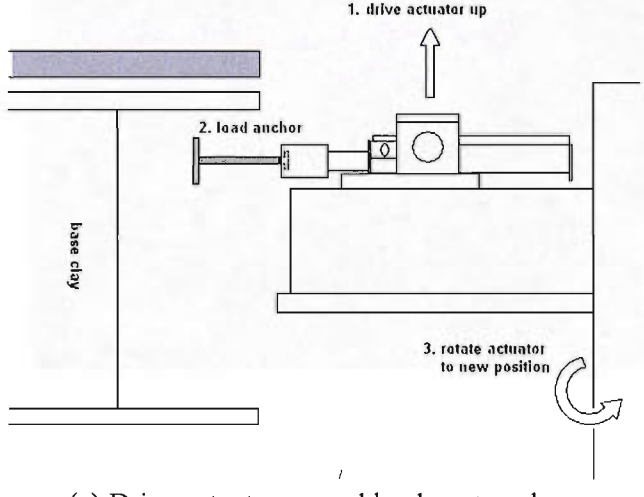

(c) Drive actuator up and load next anchor

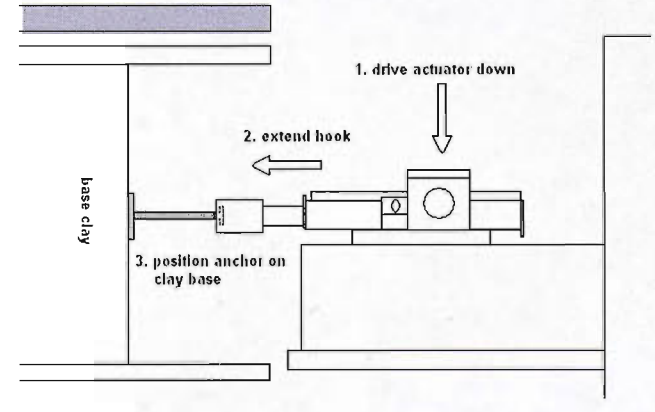

(d) Drive actuator down and position anchor

Figure 5.19 Anchor installation in clay backfill test series (not to scale)

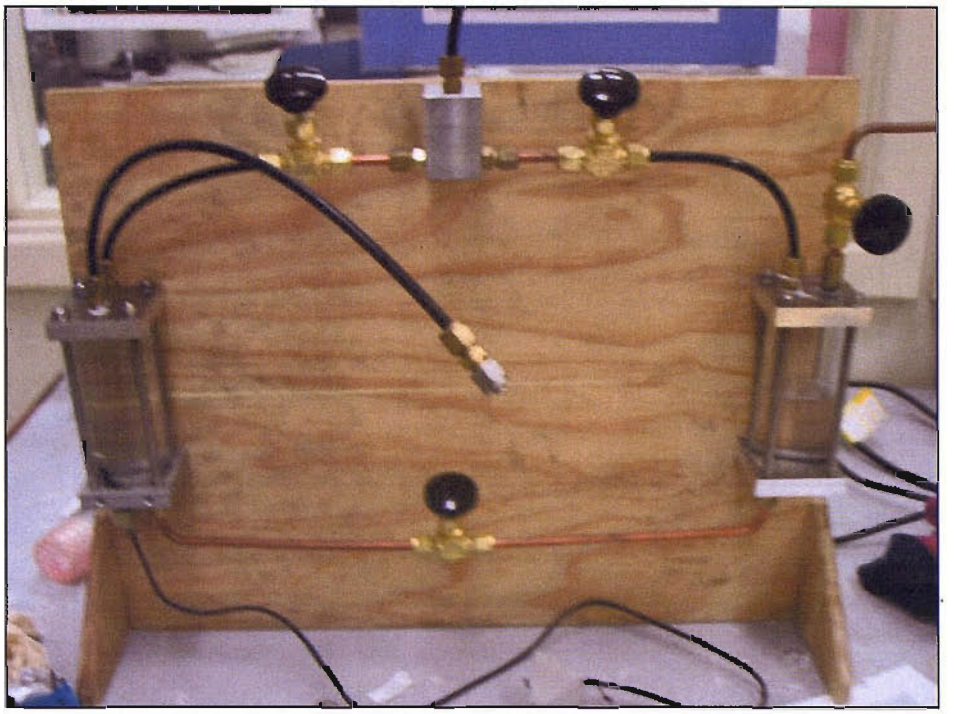

Figure 5.20 The PPTT saturation apparatus, replicated from Take and Bolton (2003)

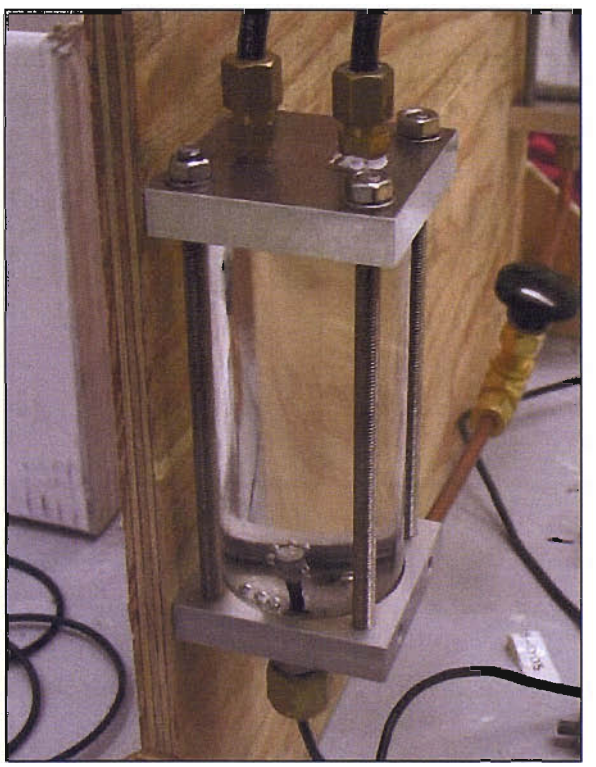

Figure 5.21 The PPTT during initial saturation under vacuum

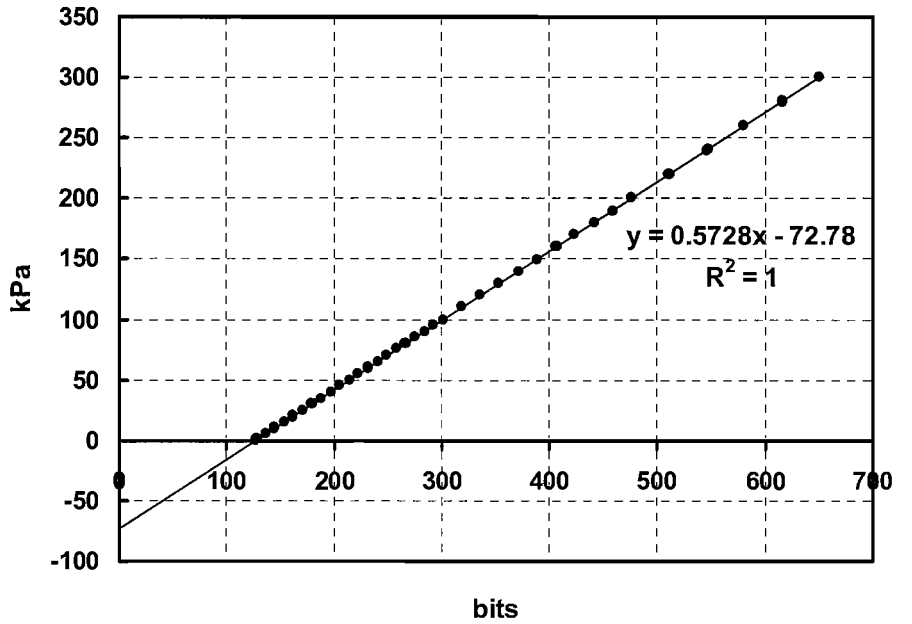

Figure 5.22 PPTT calibration for positive pressure

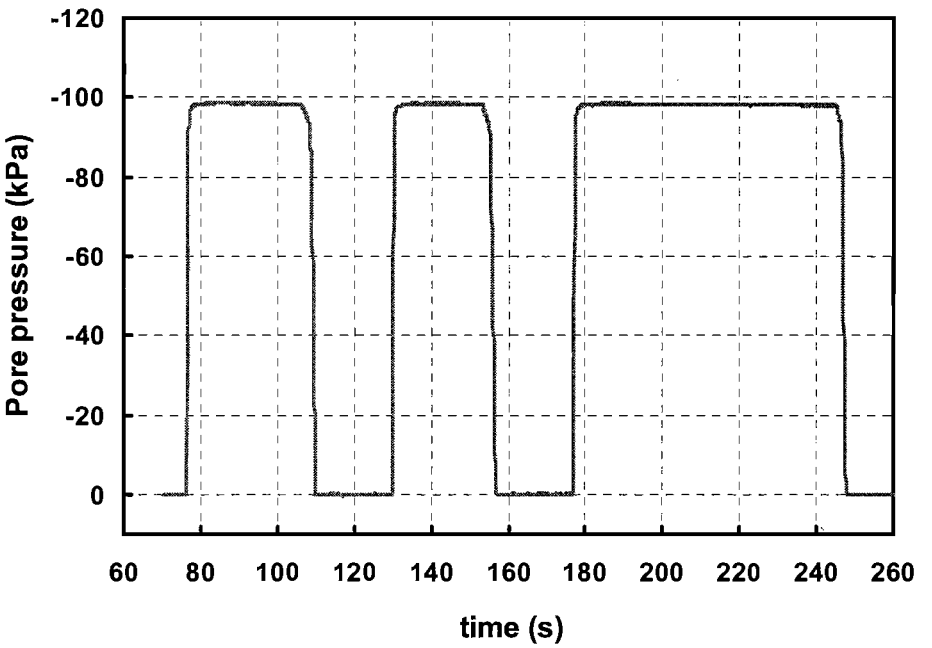

Figure 5.23 Negative pressure response of PPTT to applied vacuum (99 kPa)

Figure 5.24 T-bar and cone penetrometer

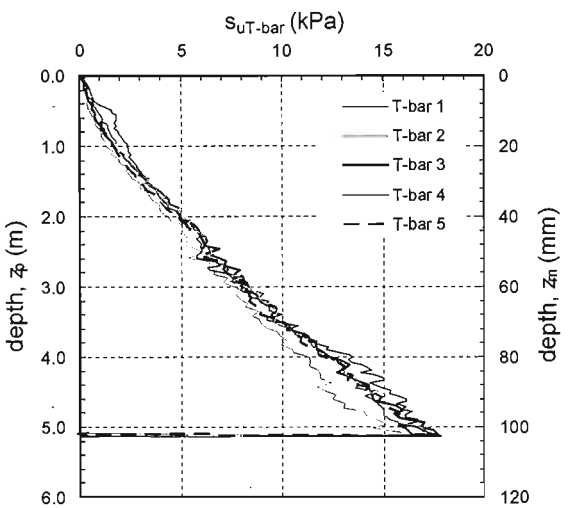

(a) T-bar profile summary

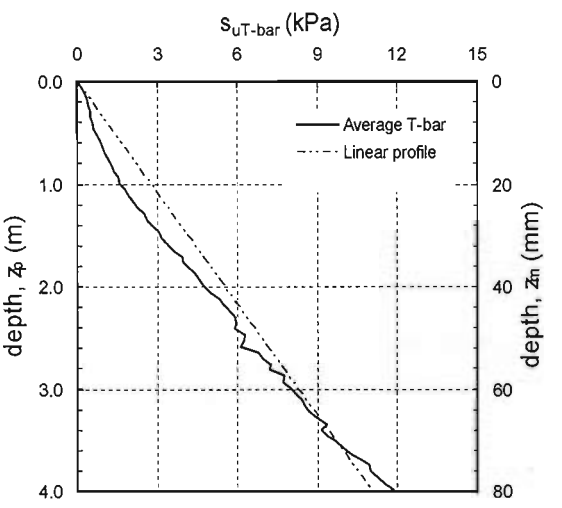

(b) Average T-bar profile

Figure 5.25 T-bar characterisation – PASB sample 1

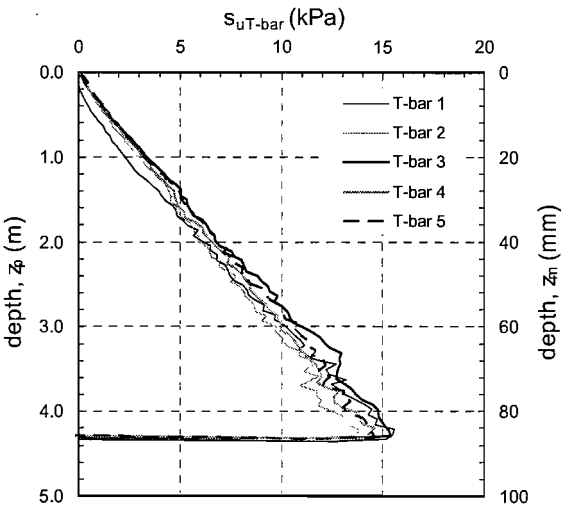

(a) T-bar profile summary

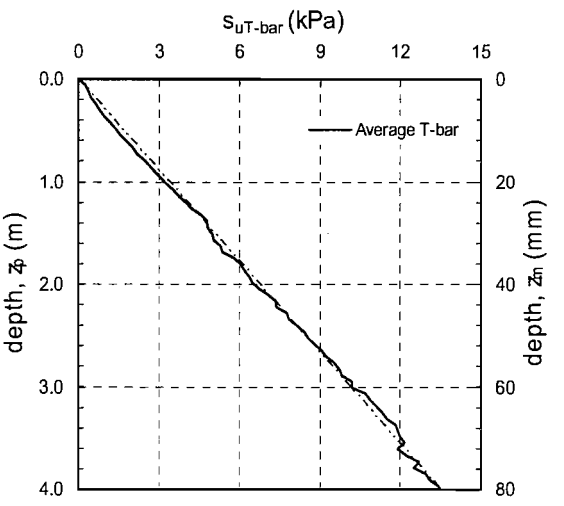

(b) Average T-bar profile

Figure 5.26 T-bar characterisation – PASB sample 2

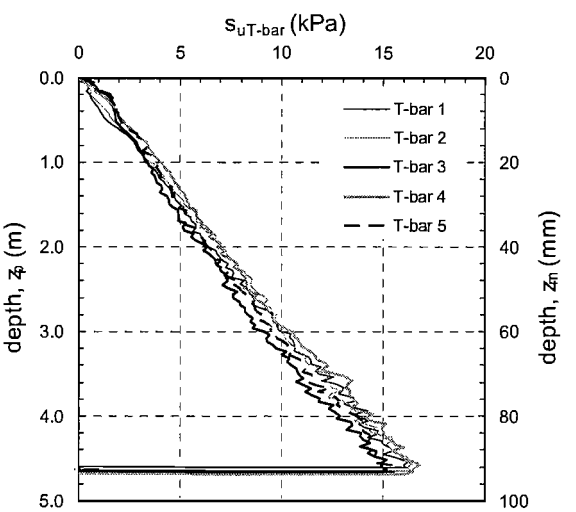

(a) T-bar profile summary

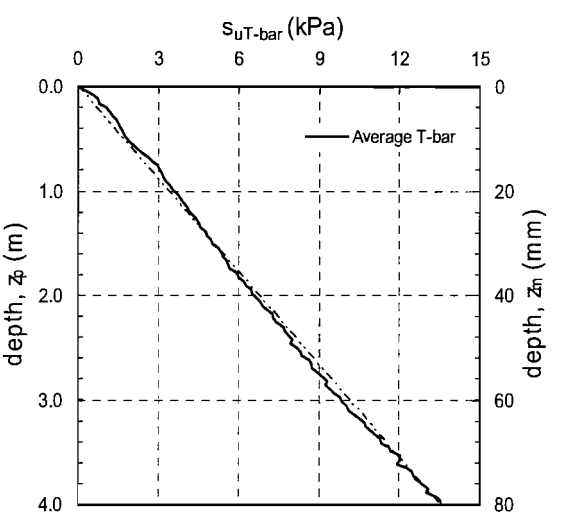

(b) Average T-bar profile

Figure 5.27 T-bar characterisation – PASB sample 3

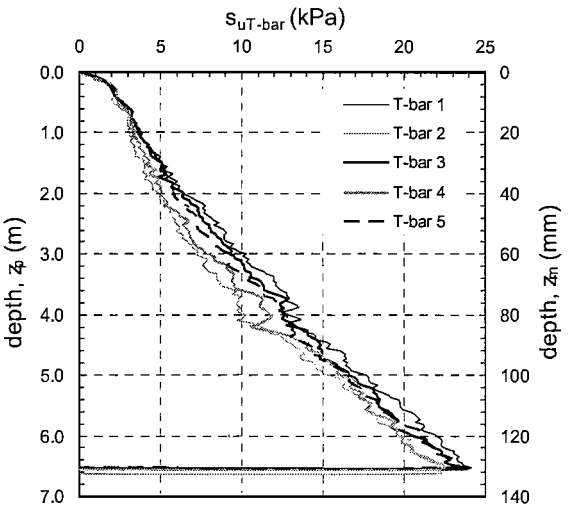

(a) T-bar profile summary

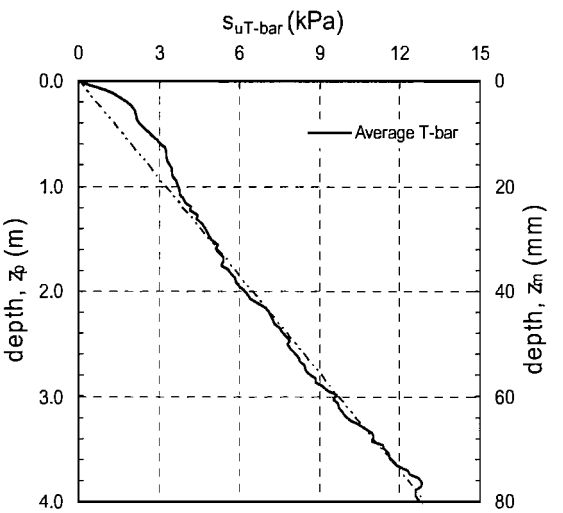

(b) Average T-bar profile

Figure 5.28 T-bar characterisation – PASB sample 4

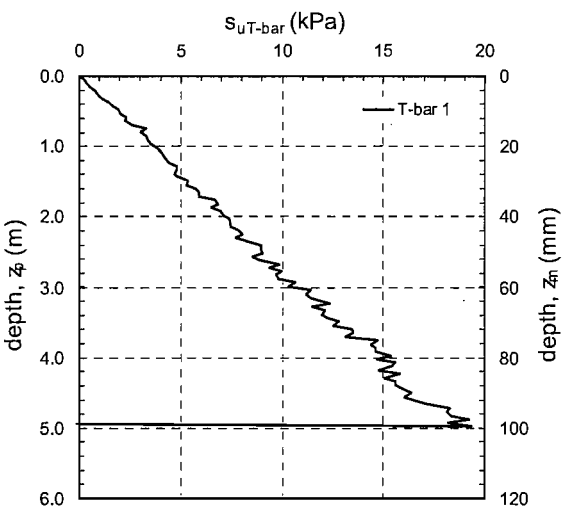

(a) T-bar profile summary

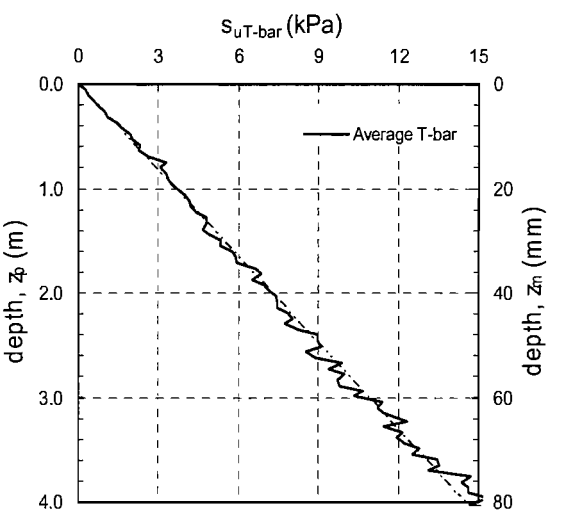

(b) Average T-bar profile

Figure 5.29 T-bar characterisation – PASB sample 5

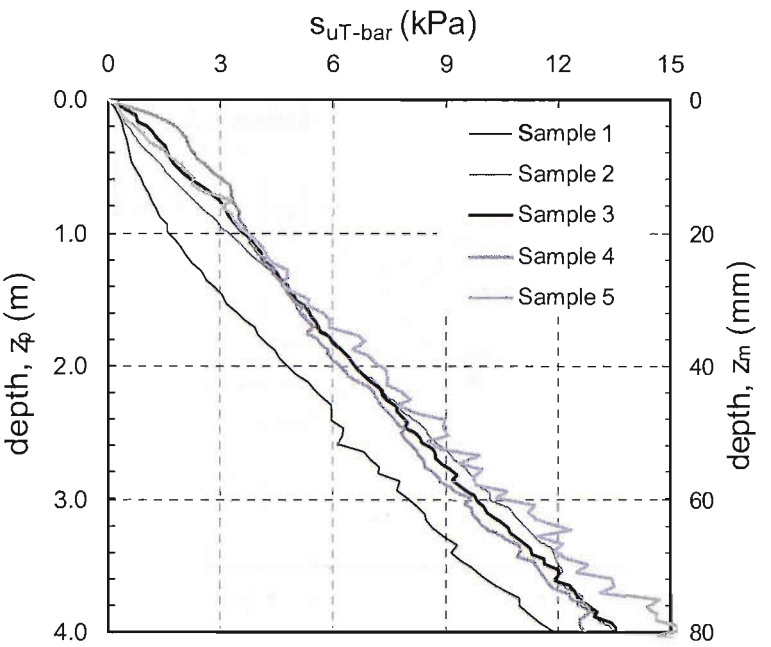

Figure 5.30 Comparison of average T-bar profiles for PASB samples 1-5

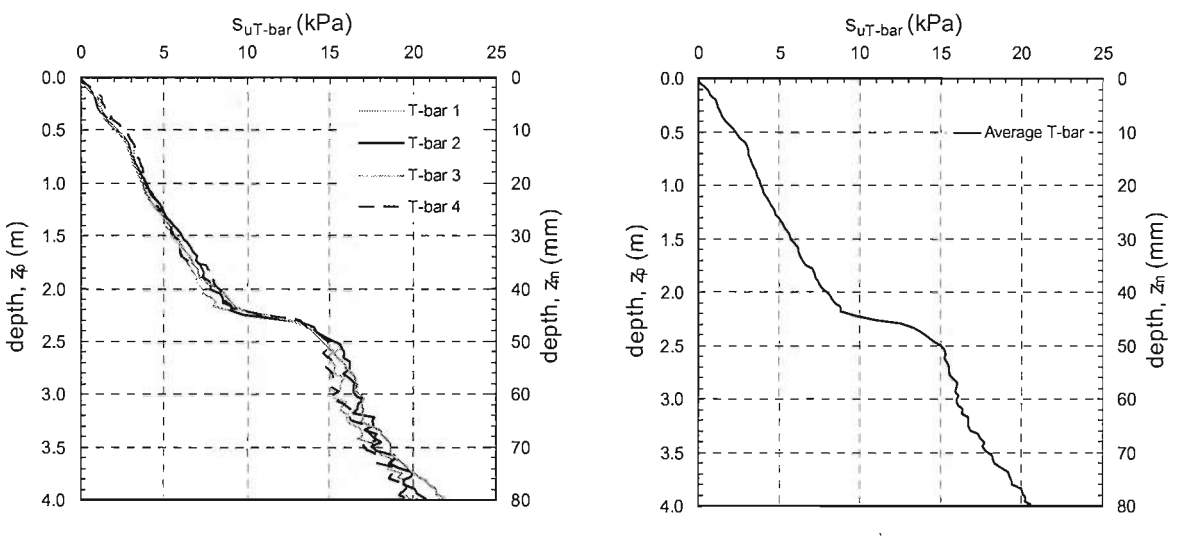

(a) T-bar profile summary (b) Average T-bar profile

Figure 5.31 T-bar characterisation – PACB sample 1

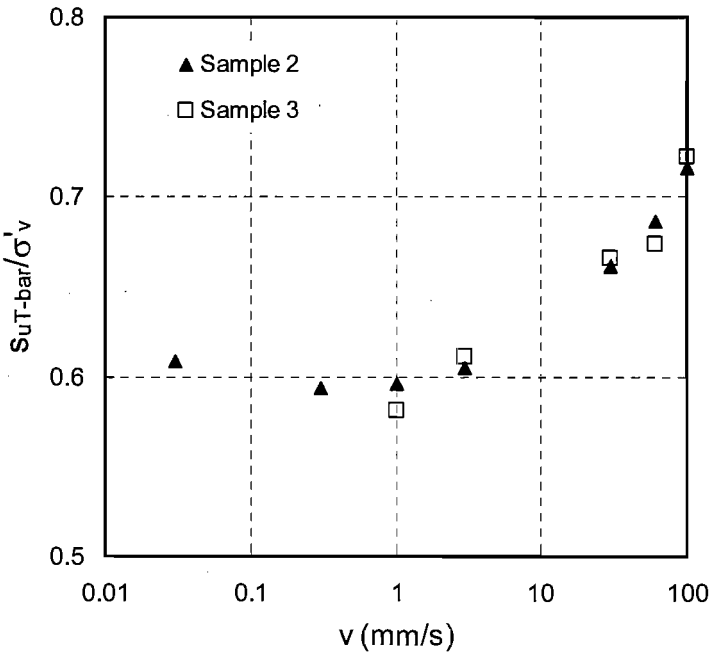

Figure 5.32 Evolution of shear strength ratio with increasing penetration rate for T-bar tests in samples 2 and 3

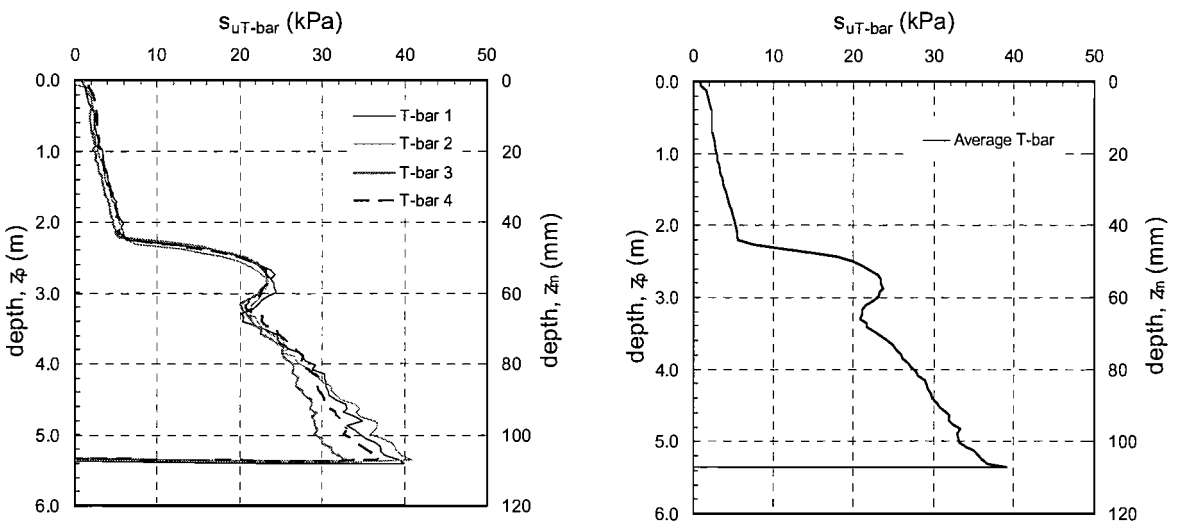

(a) T-bar profile summary (b) Average T-bar profile

Figure 5.33 T-bar characterisation – TTFS sample 1

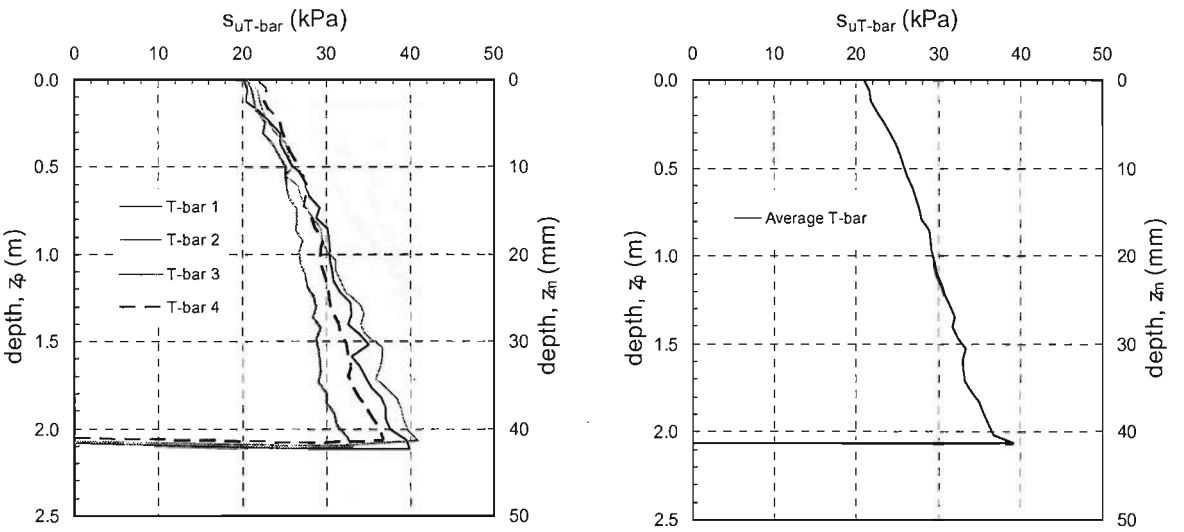

(a) T-bar profile summary (b) Average T-bar profile

Figure 5.34 T-bar profile below footing embedment depth – TTFS sample 1

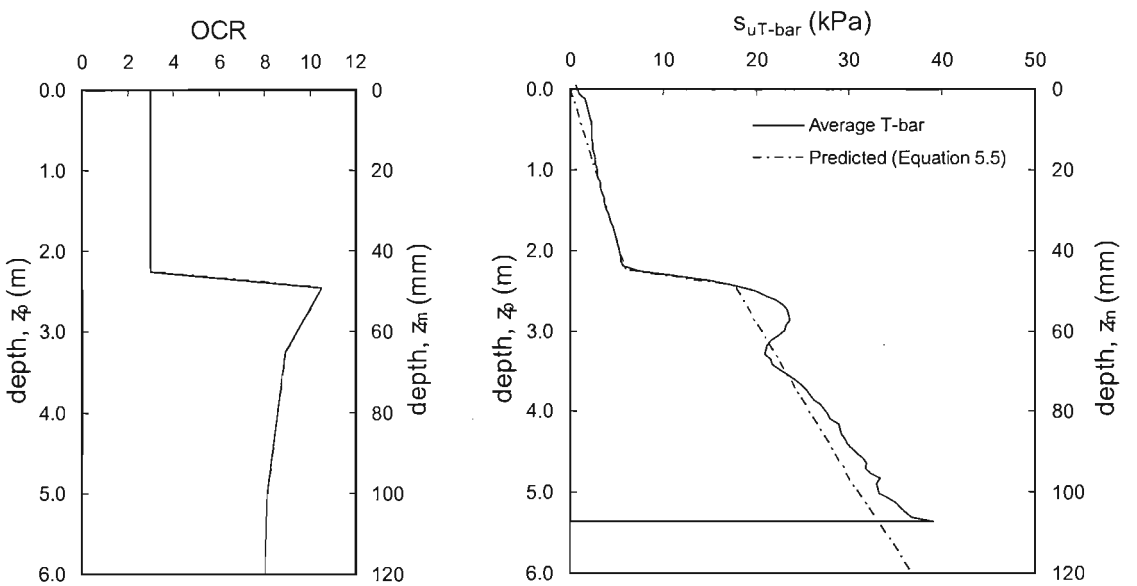

(a) Sample OCR (b) Comparison of average and predicted profile

Figure 5.35 Sample OCR and predicted undrained strength profile using Equation 5.5 – TTFS sample 1

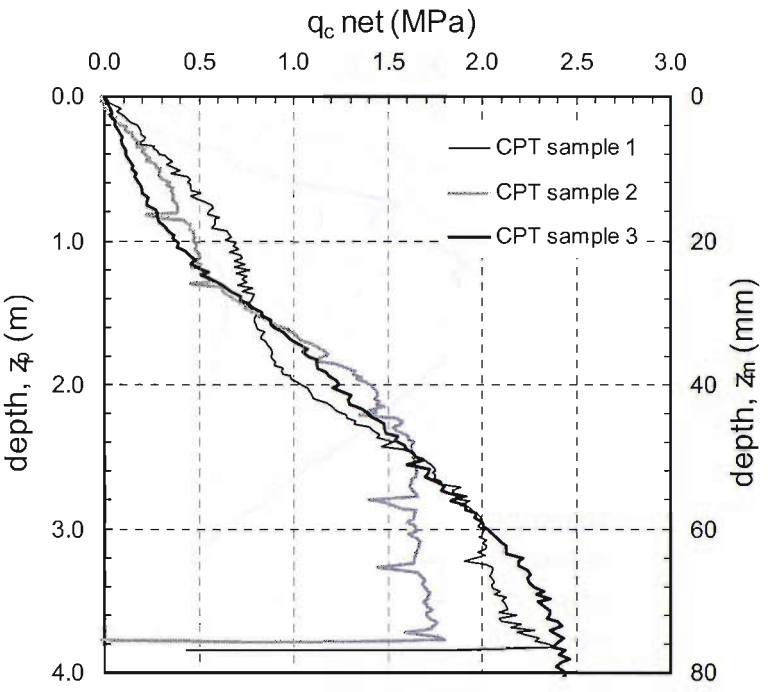

Figure 5.36 CPT tip resistance profile for fully backfilled excavation and sand base layer – PASB

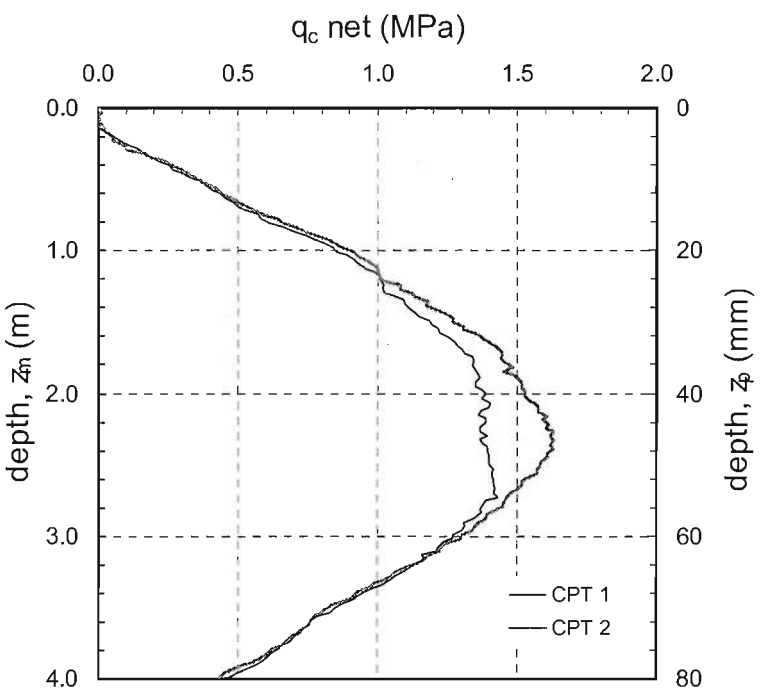

Figure 5.37 CPT tip resistance profile for fully backfilled excavation – TTFS

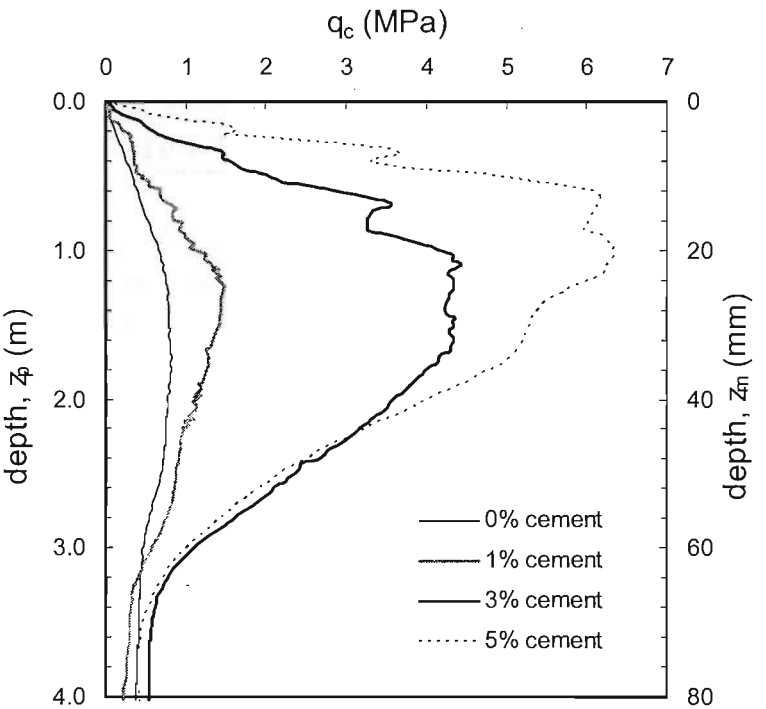

Figure 5.38 CPT tip resistance profiles for un-cemented and cemented backfill sand – PAIB

Chapter 6

UPLIFT OF PLATE ANCHORS (A centrifuge study)

6.1 Introduction

This chapter presents the results of a rigorous experimental investigation into the rate dependant uplift behaviour of shallow embedded plate anchors. The overall performance of these plate anchors were assessed over a range of uplift velocities from 0.03 to 100 mm/s. A particular aspect of these tests is the role of the negative pore water pressures in providing additional uplift resistance that may be generated at the base of the anchors. A parametric study to assess the effect of anchor width, inclination and backfill soil type was undertaken. The results of the centrifuge testing programme provide upper (undrained) and lower (drained) limits to uplift capacity which are compared with existing theoretical solutions and the results of previously published experimental studies. Anchor behaviour between these bounds (partially drained) is assessed in terms of the development of negative pore pressure approximated at the anchor base during uplift.

6.2 Plate Anchor Series 1 – Sand Backfill

The results of plate anchor series 1 are presented and anchor response in sand backfill examined. Tests have been conducted according to the experimental programmes outlined in Chapter 5 (Section 5.7).

6.2.1 Assessment of uplift capacity

The two test configurations used for plate anchor series 1 were presented previously in Figure 5.10. As described in Chapter 2, for anchors founded on saturated sand, as shown in Figure 5.10(b), the ultimate uplift capacity (F_u) may be expressed as:

$$F_u = q_{fu} A \text{ , with } q_{fu} = N_{us} \gamma' H \qquad (6.1)$$

where γ' is the sand's effective unit weight (= γ-γ_w). In the centrifuge experiments presented the unit weight is taken as the bulk density of the sand multiplied by the imposed centrifuge acceleration n (in this case n = 50). N_{us} is the uplift capacity factor for an anchor in sand which has been shown to be a function of H/B and the sand's peak friction angle (ϕ'_p). The results of total stress Finite Element analyses presented in Chapter 3 for anchors in sand indicate that for a loose sand with $\phi'_p \approx 32 \pm 2°$, the value of N_{us} varies from approximately 1.5 for an H/B of 0.5 to about 5 for an H/B of 2.

For the configuration shown in Figure 5.10(a) the ultimate uplift capacity may be assessed from Equation 6.1 only if tension cannot develop at the base of the anchor. If the anchor-clay interface is able to sustain suction however, tension is possible in the underlying clay during uplift and no published methods are available to assist in the calculation of the uplift capacity. In this case the failure mechanism is likely to be either one involving an inverted bearing capacity failure or a breakout contraction type mechanism discussed in Chapter 2. Previously reported results relating to these failure types have involved uniform clay above and below the anchor and are not directly applicable to the geometry shown in Figure 5.10(a). The anchor capacity will be dependant on both the peak strength of the sand and the undrained shear strength of the clay, and may be estimated as:

$$q_{fu} = N_{us} \gamma' H + N_{uc} s_u - \alpha \gamma' H \qquad \text{with } \alpha = f(N_{uc}) \qquad (6.2)$$

where the coefficient α varies between 1, for a full reverse bearing capacity failure mechanism and zero where a cavity contraction failure occurs at the anchor base. If similarity is assumed in the limit equilibrium state between failure mechanisms

developed in uplift and bearing then a value of N_{uc} may be approximated from comparison with published solutions for downward loading. In this case the value might be assumed to lie between $N_{uc} \approx 5$ when $\alpha = 0$ (Yu, 2000) and $N_{uc} \approx 7$ (approximately half the value suggested by Martin (2001) for a full flow around bearing failure) when $\alpha = 1$. Equation 6.1 is based upon the assumption that the peak resistance mobilised in the sand and clay are coincident and may therefore result in an over-estimation of the ultimate uplift capacity.

Equations 6.1 and 6.2 predict the lower and upper limits to the expected uplift capacity of an anchor with the configuration shown in Figure 5.10(a). For anchor behaviour between these bounds, the capacity will be affected by the degree of pore pressure dissipation taking place at the anchor base during load application as well as the ability for suction to develop at the clay-footing interface. Although the boundary conditions differ, a preliminary assessment of the anchor displacement rates at which fully undrained, partially drained and drained responses occur may be obtained from the solution (for a foundation of consolidating soil) given by Booker & Small (1986) and reproduced in Figure 6.1. This figure shows the variation of the average degree of consolidation (U) of an impermeable, rigid circular plate on a clay surface as a function of a time factor (T), which is defined as:

$$T = \frac{4c_v t}{D^2} \tag{6.3}$$

where c_v is the coefficient of consolidation of the clay, t is the time and D is the plate diameter. For values of T less than approximately 0.02, the plot indicates that the degree of consolidation will be less than 10% (i.e. conditions are essentially undrained) and for values of T greater than 30, at least 90% consolidation is inferred to have taken place (i.e. conditions are close to being fully drained). Finnie & Randolph (1994) used the normalised velocity (V) as a means to define drainage conditions where V is defined as:

$$V = \frac{vD}{c_v} \tag{6.4}$$

It may be shown that, if failure is considered to require a footing movement of at least 10% of the anchor diameter, the time factors (T) of 0.02 and 30 presented by Booker & Small (1986) correspond to respective normalised velocities of 20 and 0.01 (marking the transition points for fully undrained and fully drained behaviour respectively). The inclined boundary (and hence the greater drainage path) for the configuration shown in Figure 5.10 is expected to reduce both of these limits to V, although similar normalised velocity limits were deduced by Finnie & Randolph (1994) from centrifuge tests on embedded circular anchors in normally consolidated kaolin.

6.2.2 Uplift test results

Post processed load and displacement data for each anchor uplift test conducted is collected in Appendix B, Figures B1-B5 for samples 1-5 respectively. These figures show the development of uplift force and vertical displacement with time for each test conducted in the five drum centrifuge samples.

From general test observations and the data presented in Appendix B several points regarding the performance of the fast pull actuator and data acquisition system and the experimental procedures employed throughout the test series are noted:

- For anchor widths of 45 mm or less the vertical displacement varies linearly with time implying that the uplift rate was constant during the loading and did not depend on the uplift force generated. For tests on 60 mm wide anchors, it is seen that the uplift rate (v_f) is significantly less up to the maximum recorded load indicating the magnitude of uplift force was in excess of the actuator uplift capacity at high rates of loading. Re-calculated loading rates for the pull out of 60 mm anchors are shown in Table 6.1.

- In some cases, uplift resistance data displayed a relatively high degree of noise due to the fast data acquisition rate and electronic noise generated by the slip ring system. For each sample a signal filtering routine was initially employed to remove noise from the data although this was limited where the initial response of the anchor may have been artificially altered by the application of too stringent a filter. In such cases the maximum uplift force was selected as the average of the two extreme curves as indicated in Figure 6.2.

- During the fastest uplift test (v_f = 100 mm/s), the maximum uplift resistance was reached in less than 50 ms. The 25 kHz data acquisition system meant that about 1250 data points were recorded up to the peak load. The acquisition system is considered to be sufficient to capture the full behaviour of anchors subject to these very fast rates of uplift.

Table 6.1 Corrected uplift rate for 60 mm anchors, PASB - Sample 3

Test No.	Anchor Width, B (mm)	Soil at Anchor Base	Intended Uplift Rate, v_f (mm/s)	Achieved Uplift Rate (mm/s)
S3-7	60	Clay	100	43.2
S3-8	60	Clay	60	34.6
S3-9	60	Clay	30	28.7
S3-11	60	Clay	3	3
S3-12	60	Clay	0.3	0.3
S3-13	60	Clay	0.03	0.03

Peak uplift resistance (F_{up}) and the anchor displacement at peak resistance (w_p) for uplift tests in each centrifuge sample are assembled in Tables 6.2 to 6.6. A preliminary summary of these results shows that:

i. Regarding the increase in anchor capacity; anchors founded on clay uplifted at increasing velocities may have an uplift capacity up to 2.7 times greater than an equivalent anchor founded on sand.

ii. Regarding anchor capacity at the lowest uplift velocity; the average, the uplift capacity of a 30 mm wide anchor on clay loaded at a rate of 0.03 mm/s is only 6% higher than that of an anchor founded on sand. It may therefore be inferred that this rate of 0.03 mm/s is close to that which leads to drained behaviour and therefore an absence of base suction.

iii. Regarding the anchor displacement; the vertical displacement corresponding to the peak uplift force for 30 mm wide anchors ranged from 0.3 to 3.3 mm and generally increased with the pull out rate.

Table 6.2 Summary of results for PASB – 1st Sample

Sample 1							
Test	**B**	**θ**	**v_f**	**Soil at base**	**F_{up}**	**q_{fu}**	**w_p**
(-)	**mm**	**°**	**mm/s**	**-**	**(N)**	**(kPa)**	**(mm)**
S1-1	30	0	3	Clay	68	75.6	0.8
S1-2	30	0	3	Clay	61	67.8	0.95
S1-3	30	0	3	Sand	43.8	48.7	0.9
S1-4	30	5	3	Clay	55	61.1	1
S1-5	30	10	3	Clay	46	51.1	1
S1-6	30	15	3	Clay	60	66.7	1.2
S1-7	30	15	3	Sand	35	38.9	1

Table 6.3 Summary of results for PASB – 2nd Sample

Sample 2							
Test	**B**	**θ**	**v_f**	**Soil at base**	**F_{up}**	**q_{fu}**	**w_p**
(-)	**mm**	**°**	**mm/s**	**-**	**(N)**	**(kPa)**	**(mm)**
S2-1	30	0	0.03	Clay	49	54.4	0.3
S2-2	30	0	0.3	Clay	53	58.9	0.55
S2-3	30	0	60	Clay	104.5	116.1	3.3
S2-4	30	0	100	Clay	93	103.3	2.5
S2-5	30	0	30	Sand	40.5	45.0	2.8
S2-6	45	0	30	Clay	211	104.2	2.6
S2-7	45	0	3	Sand	89	44.0	1.8
S2-8	30	15	3	Clay	50.5	56.1	1.1
S2-9	30	15	30	Clay	73	81.1	2.7
S2-10	30	10	3	Sand	45	50.0	1.2
S2-11	30	5	3	Sand	40	44.4	1

Table 6.4 Summary of results for PASB – 3rd Sample

Sample 3 (corrected)							
Test	**B**	**θ**	**v_f**	**Soil at base**	**F_{up}**	**q_{fu}**	**w_p**
(-)	**mm**	**°**	**mm/s**	**-**	**(N)**	**(kPa)**	**(mm)**
S3-1	30	0	100	Clay	104.4	116.0	3.1
S3-2	30	0	60	Clay	94.4	104.9	2.4
S3-3	30	0	30	Clay	92.3	102.6	2.1
S3-4	30	0	3	Clay	83.3	92.6	1.5
S3-5	30	0	0.3	Clay	63.8	70.9	1.2
S3-6	30	0	0.03	Clay	46.6	51.8	0.6
S3-7	60	0	43.2	Clay	329.4	91.5	4.9
S3-8	60	0	34.6	Clay	309.9	86.1	3.98
S3-9	60	0	28.7	Clay	315.8	87.7	2.97
S3-10	30	0	3	Sand	45.1	50.1	1.2
S3-11	60	0	3	Clay	200.6	55.7	2.02
S3-12	60	0	0.3	Clay	161.7	44.9	1.51
S3-13	60	0	0.03	Clay	120.8	33.6	1.27
S3-16	60	0	30	Clay	300.7	83.5	2.86
S3-17	60	0	3	Sand	113.7	31.6	2.5

Table 6.5 Summary of results for PASB – 4th Sample

Sample 4							
Test	B	θ	v_f	Soil at base	F_{up}	q_{fu}	w_p
(-)	mm	°	mm/s	-	(N)	(kPa)	(mm)
S4-1	30	0	0.3	Clay	50.9	56.6	1.1
S4-2	45	0	3	Clay	120.8	59.6	1.3
S4-3	30	0	100	Clay	107.3	119.3	2.3
S4-4	30	0	30	Clay	98.0	108.9	1.9
S4-5	30	0	0.03	Clay	42.7	47.4	0.5
S4-6	30	0	3	Clay	65.3	72.6	1.2
S4-7	30	0	30	Clay	88.9	98.8	1.8
S4-8	30	0	60	Clay	104.6	116.3	2.0
S4-9	60	0	3	Clay	180.5	50.1	1.74
S4-10	30	15	3	Clay	59.6	66.2	1.33
S4-11	30	0	30	Clay	96.9	107.7	2.0
S4-12	60	0	3	Clay	203.4	56.5	2.06
S4-13	30	0	100	Clay	105.7	117.4	2.4

Table 6.6 Summary of results for PASB – 5th Sample

Sample 5							
Test	B	θ	v_f	Soil at base	F_{up}	q_{fu}	w_p
(-)	mm	°	mm/s	-	(N)	(kPa)	(mm)
S5-1	45	0	3	Clay	148.0	73.1	1.51
S5-2	60	0	0.03	Clay	128.4	30.4	0.58
S5-3	60	0	0.3	Clay	143.9	40.0	0.94
S5-4	60	0	3	Clay	239.4	66.5	1.53
S5-5	30	5	3	Clay	75.5	83.9	3.0
S5-6	30	10	3	Clay	72.9	81.0	2.37
S5-7	30	15	3	Clay	70.1	77.9	1.18
S5-8	30	20	3	Clay	89.9	89.9	2.56
S5-9	30	15	3	Sand	37.9	42.1	2.4
S5-10	60	0	3	Sand	97.3	21.8	2.1

6.2.3 Load displacement response

The typical measured load displacement response for a 30 mm anchor founded on clay is shown in Figure 6.3 where it is compared with the response of a similar anchor founded on sand. In both cases the anchor was uplifted at a rate of 3 mm/s and it is evident that a significantly higher uplift capacity is generated by the anchor founded on clay. This increase in capacity is a result of the contribution to uplift resistance provided by the generation of suction in the clay at the anchor base. At a normalised displacement (w_f/B) of approximately 2% (corresponding to the generation of peak capacity) the anchor-clay interface is no longer able to sustain the developed suction

and the proportion of uplift resistance provided by the clay at the anchor base reduces. With increasing displacement the degree of contact at the anchor-clay interface decreases until full separation occurs and the uplift capacity reduces to a value which is comparable to that of the anchor founded on sand, at a w_f/B value greater than 5%.

The typical measured uplift load-displacement responses for 30 mm and 60 mm anchors founded on clay are presented in Figure 6.4. It is observed that the general trend in the variation of the load-displacement response with increasing uplift velocity is similar for both 30 mm and 60 mm anchors. At the highest selected rates (30 mm/s and the achieved value of 43.2 mm/s for the 30 mm and 60 mm anchors respectively) much higher uplift resistances are generated by the anchors, but significantly greater displacements are required to develop the peak capacity (F_{up}). At these uplift velocities it is likely that the clay response is fully undrained and that significant suctions are developed in the clay at the anchor base. Given the change in load displacement response and increase in peak uplift capacity between v_f=3 mm/s and v_f ≥30 mm/s it is clear that the suctions developed during undrained response reach a maximum value only at large anchor displacements. During the development of these suctions a high degree of contact is maintained at the anchor-clay interface and the rate dependence of the undrained shear strength of the clay will also contribute to the observed high uplift capacity of the anchor. Although not apparent in Figure 6.3, it should be noted that the uplift resistance of all footings on clay and sand reduced to comparable values, but that anchor displacements in excess of 15 mm (w_f/B>50%) were often required to achieve this convergence in capacity.

The normalised anchor displacement (w_p/B) required to attain peak uplift capacity is plotted against uplift velocity in Figure 6.5 for all anchors founded on clay. Despite the fair degree of scatter evident in the data it is apparent that the displacement at peak capacity is strongly dependent upon the uplift velocity with an approximate 6 fold increase in w_p/B observed across the full range of v_f. The largest gain, per log cycle increase in v_f, in normalised displacement is seen to occur at high anchor velocities (v_f >3 mm/s) and w_p/B values recorded at the highest velocities are in the region of 8-10% of the anchor width. For a typical transmission tower foundation this relates to displacements in excess of around 200 mm required for the generation of the maximum available uplift resistance, a value which is well in excess of tower

serviceability limits. The requirement for such large displacement is presumably related to the generation of maximum under-base suctions at high uplift velocities and has also been observed by Houlsby et al. (2006) in uplift tests on full scale suction caissons. This has obvious implications where foundation capacity should be assessed in relation to the deflection criteria imposed by the structure above.

6.2.4 Peak uplift capacity

The variation of peak uplift capacity (F_{up}) with uplift velocity (v_f) for 30 mm wide anchors founded on clay is shown in Figure 6.6(a). A positive evolution of F_{up} with v_f is evident across the full range of uplift rates considered, with the largest gain in capacity occurring for v_f between 3 and 30 mm/s. It is observed that higher peak resistances were measured for anchors uplifted at v_f =0.3 and 3 mm/s in sample 3. Given that the T-bar derived undrained strengths measured in sample 3 (Section 5.11.1, Table 5.12) were similar to those measured in other samples this difference is likely to have been caused by an increased contribution to resistance of the backfill sand. It appears from Figure 6.6(a) and (b) that this increase is limited to only two tests in the sample indicating that some variation in backfill density may have occurred during setup for these tests.

The average gain in capacity across each log cycle increase in v_f is indicated by the trend lines shown on Figure 6.6. The slower rate of gain in capacity at v_f >30 mm/s of around 10-15% per log cycle is concurrent with expected increases due to viscous effects in the clay at the base of the anchor. This indicates that anchor behaviour is fully undrained after this point and partial drainage of suction is no longer a significant factor. A similar plot is shown in Figure 6.6(b) for 60 mm wide anchors founded on clay. It would appear from comparison of Figures 6.6 (a) and (b) that the trends associated with increasing uplift velocity are similar for both 30 and 60 mm anchors.

The rate dependency of the capacity of 30 and 60 mm anchors is further highlighted in Figure 6.7 where uplift capacity is compared for anchors founded on clay and those founded on sand. For 30 mm anchors founded on sand there appears to be no apparent rate dependence of anchor capacity at the uplift velocities presented. For both anchor

widths the capacity of anchors on sand is marginally less than that for anchors on clay uplifted at 0.03 mm/s indicating that at v_f =0.03 mm/s anchor behaviour is close to being fully drained and minimal suction is developed at the base of the anchor. Trend lines plotted through the data in Figure 6.7 indicate that the rate of gain in capacity is greatest at values of v_f between about 2 and 10 mm/s.

The uplift coefficients (N_{us}) were calculated for all tests on anchors founded on sand using Equation 6.1 assuming γ'=8 kN/m^3 and taking the depth of embedment (H) as equal to the depth to the top of the anchor base (=40 mm). The values of N_{us} obtained are plotted against the corresponding embedment ratios (H/B) in Figure 6.8. Also plotted are N_{us} values derived from total stress Finite element analyses presented in Chapter 3 using equivalent H/D values for sand with ϕ'=32° . The theoretical values of Meyerhof and Adams (1968) and limit equilibrium solutions of Murray and Geddes (1987), for which N_{us} is given for a square footing as:

$$N_{us} = 1 + \frac{H}{B}\tan\phi'\left(2 + \frac{\pi}{3}\frac{H}{B}\tan\phi'\right) \qquad (6.5)$$

are also presented for comparison in Figure 6.8. It is evident that the N_{us} factors from the centrifuge uplift tests are a little lower than those from Murray and Geddes (1987) but are reasonably well represented by those of Meyerhof and Adams (1968) for ϕ'=32°. The agreement between the factors calculated from the centrifuge tests and those predicted using Finite Element analyses (discussed in Chapter 3) with equivalent geometries however illustrate that FEA can provide more accurate assessments than other empirical approaches where specific anchor details and soil properties are not easily implemented.

6.2.5 Estimate of suction

The estimated contribution of suction force generated during uplift is inferred in Figure 6.7 as the difference between the peak capacity of a given anchor on clay (F_{up}) and that of the same anchor when founded on sand ($F_{up\text{-}sand}$). The maximum suction force (F_{su}) is therefore approximated according to the following equation:

$$F_{su} \approx F_{up} - F_{up-sand} \qquad (6.6)$$

The mean maximum suction stress (s) developed at the anchor base during uplift is given by:

$$s \approx \frac{F_{su}}{B^2} \tag{6.7}$$

Due to the difference in the relative displacements required for the mobilisation of F_{up} and $F_{u\text{-}sand}$, Equation 6.6 will, in some cases, under estimate the maximum suction force developed. This is illustrated by the typical load displacement data for a 60 mm anchor presented in Figure 6.9, where the approximated suction force is shown to be around 10% less than the actual contribution.

The maximum suction stresses derived using Equation 6.7 for anchors founded on clay are plotted with anchor velocity in Figure 6.10. Suctions developed at slow velocities are low, on average less than 5 kPa at v_f =0.03 mm/s and increase with increasing velocity up to a maximum value of just under 70 kPa at v_f =100 mm/s. These maximum values are below that at which cavitation of water occurs (85-100 kPa) and are likely to be limited by the relatively low undrained shear strength of the kaolin clay used in these experiments. Trend lines plotted through the data indicate that suction pressures generated beneath anchors of various widths are similar at equivalent velocities. As expected the variation of s seen in Figure 6.10 is similar to that observed previously for F_{up} in Figure 6.6 although a relatively high degree of scatter is displayed at higher uplift velocities. This scatter is most noticeable at v_f =3 mm/s where partial drainage is thought to have a significant effect on the variation in developed suction.

For anchors uplifted at velocities of 30 mm/s and above inspection of the anchors after uplift revealed that a wedge of clay, with a height of approximately B/3, had adhered to the base of the anchor, Figure 6.11. No clay was present on the base of anchors uplifted at values of v_f below 30 mm/s. This observation suggests that at $v_f \geq 30$ mm/s the suction developed at the anchor base is such that separation of the anchor and underlying clay does not occur. In this case an undrained inverted bearing capacity failure mechanism (discussed in Chapter 2 and Section 6.2.1) is likely to develop and

the peak uplift resistance will be controlled by the undrained shear strength of the clay. Given the variation of s assessed at $v_f \geq 30$ mm/s in Figure 6.10 it would appear that this undrained mechanism will occur when the developed suction is approximately equal to $6s_u$. At uplift velocities less than 30 mm/s partial drainage will have reduced the generated suction and hindered the development of the undrained mechanism.

6.2.6 Generalisation of uplift test data

As discussed in Chapter 2, foundation bearing capacity is often presented in terms of a bearing capacity factor (N_c) relating to the failure mechanism developed in the soil below a foundation under compressive loading. Using the same format as Equation 6.2 a reverse bearing or uplift capacity factor (N_u) for anchors founded on clay is defined as:

$$N_u = \frac{s}{s_u} \approx \frac{\left(F_{up} - F_{up-sand}\right)}{s_u B^2} \tag{6.8}$$

where $N_u = N_{uc}$ for undrained conditions. N_u factors may be calculated from the centrifuge test results assuming that the average undrained shear strength (s_u) is equal to the measured T-bar strength ($s_{uT\text{-}bar}$) at a depth of B/2 below the anchor, as given in Table 5.12 and discussed in Chapter 5 (Section 5.11.5). For uplift tests performed at velocities greater than or equal to 3 mm/s the T-bar undrained shear strength used in Equation 6.8 is corrected for strain rate dependence using Equation 5.5 (Section 5.11.3). It is inferred from Atkinson (2000) that the average operational strain rate beneath a foundation is approximately equal to $v_f/3B$ if full contact exists between the foundation base and the underlying clay. Equation 5.5 may therefore be re-written in terms of anchor uplift velocity (v_f) as:

$$s_{uT-bar} = s_{uT-bar(ref)} \cdot \left(\frac{v_f / 3B}{\dot{\varepsilon}_{ref}} \right)^{0.04} \tag{6.9}$$

where $s_{uT\text{-}bar(ref)}$ is the T-bar undrained shear strength at the reference axial strain rate $\dot{\varepsilon}_{ref}$ (taken at a penetration velocity of 1 mm/s). The values of N_{uc} calculated using

Equation 6.8 are plotted with anchor velocity in Figure 6.12. As $s_{uT\text{-}bar}$ is rate corrected (according to Equation 6.9) and based upon the available evidence, the observed variation may be considered to be independent (at high velocities) of the viscous rate dependence of the undrained shear strength of the clay at the anchor base. It is evident that:

- The rate of increase in N_{uc} with increasing velocity drops after anchor velocities in excess of about 20-30 mm/s. Although the data is more limited after this point, at these velocities anchor behaviour is assumed to be fully undrained.
- Although a reasonable amount of scatter is observed in the data, the mean value of N_{uc} at $v_f \geq 30$ mm/s lies between about 5 and 6. This range is in broad agreement with the values suggested in Chapter 2 based on the results of previous investigation and that inferred from comparison with conventional bearing capacity behaviour. Values of N_{uc} (averaged from tests at v_f >30 mm/s) are plotted with H/B in Figure 6.13 where they are compared with values inferred from 1*g* model tests in kaolin clay conducted by Kumar (1993), Shin et al. (1994) and Rao et al. (2001). It is evident that the N_{uc} values are in reasonable agreement with the results of reported 1*g* tests, given the various definitions of undrained strength employed for assessing N_{uc}. The lower N_{uc} values reported by Shin et al. (1994), with an average value of approximately 4, were approximated from stress controlled tests involving load steps during which partial dissipation of the suctions generated rapidly during uplift may have occurred.

6.2.7 Influence of anchor inclination

Investigation into the influence of anchor inclination on F_{up} for 30mm anchors founded on clay and sand is summarised in Figure 6.14, which shows the variation of anchor capacity with stem inclination (θ). There is significant scatter in the data for anchors founded on clay and no clear trend with θ is discernable. The available evidence suggests that increasing inclination affects the stability of the anchor on the clay base layer and hence its ability to develop suction.

A similar trend, or lack thereof, is observed for anchors founded on sand where, although there is less scatter in the available data, there appears to be no clear increase

or reduction in anchor capacity with inclination (θ). This may suggest that the range of inclinations used were not large enough to significantly affect the contribution to uplift resistance of the failure mechanism developed in the overlying soil (either vertical failure surface, curved slip failure surface or inverted truncated cone failure as discussed in Chapter 2) which would appear to be similar for all θ values considered.

Rotation of the anchor base may be a possible cause for the inconsistencies displayed in both sets of data, as the hook connection between the anchor head and the centrifuge actuator is not fixed and the anchor is free to pivot about this point during uplift. The scatter may also be attributed to minor misalignments of the actuator with the anchor stem (which did not occur for straight anchors where θ=0°) and future experimental study in this area should include the provision of a hinge joint at the anchor head prior to uplift loading. Generally these misalignments would tend to reduce uplift capacity and it may be inferred from this that load inclinations up to 15° do not lead to a significant reduction in uplift capacity. This tentative conclusion is in agreement with the observations of Dembicki (2005) where no effect of load inclination was observed for (model and field scale) transmission tower foundations with values of θ up to 20° when the line of action of the load was coincident with the central axis of the stem. Further tests are recommended to verify this potential trend which has important implications for transmission tower foundations and similar applications where θ is generally greater than zero.

6.3 Plate Anchor Series 2 – Clay Backfill

The results of plate anchor series 2 are presented and anchor response in clay backfill examined. Tests have been conducted according to the programmes outlined in Chapter 5 (Section 5.7).

6.3.1 Assessment of uplift capacity

The two test configurations used for plate anchor series 1 were presented previously in Figure 5.10. As described in Chapter 2, for anchors founded on saturated sand, as shown in Figure 5.10(b), the ultimate uplift capacity (F_u) may be expressed as:

$$F_u = q_{fu} A \text{, with } q_{fu} = s_u N_u + \gamma' H \qquad (6.10)$$

where γ' is the effective unit weight of the clay ($= \gamma - \gamma_w$). N_u is the uplift capacity factor for an anchor in clay which has been shown to be a function of H/B and the overburden stress ratio at the embedment depth ($\gamma H/s_u$). The results of total stress finite element analyses given in Chapter 3 were presented for the cases of fully bonded and breakaway behaviour. The uplift factor N_u for an embedment ratio of 1.5 was observed to vary from approximately 6 for the breakaway case, up to a value of approximately 13 for the fully bonded case. The difference between these two cases may be considered as the contribution to uplift resistance provided at the base of the anchor.

6.3.2 Uplift test results

Post processed load and displacement data for each clay backfilled anchor uplift test conducted is collected in Appendix C, Figure C1(a-g).

Some observations regarding the performance of the new actuator and the experimental procedures employed for the clay backfill sample may be made:

- 3 inclined anchors became unstable during the placement of the backfill clay layer and were overturned and buried. For this reason those tests (S1-9, S1-10 and S1-11) scheduled to investigate the effect of anchor inclination on uplift capacity for clay backfill were not undertaken.
- For anchor widths of 45mm or less the vertical displacement varies linearly with time implying that the velocity was constant during uplift and did not depend upon the uplift force generated. For the 60mm anchor test (S1-6), the actuator was not able to generate enough force to uplift the anchor, at even the slowest rate of loading, and the test was not completed.

Table 6.7 Summary of results for PACB – 1st Sample

Sample 1							
Test	**B**	**θ**	**v_f**	**Soil at base**	**F_{up}**	**q_{fu}**	**w_p**
(-)	**mm**	**°**	**mm/s**	**-**	**(N)**	**(kPa)**	**(mm)**
S1-1	30	0	3	Clay	112.4	124.9	
S1-2	30	0	30	Clay	118.0	131.1	
S1-3	30	0	100	Clay	121.3	134.8	
S1-4	30	0	0.03	Clay	85.2	94.7	
S1-5	30	0	3	Sand	49.8	54.7	
S1-6	60	0	3	Clay	Not completed		
S1-7	45	0	3	Sand	145.4	71.8	
S1-8	45	0	3	Clay	292.2	144.3	
S1-9	30	5	3	Clay	Not completed		
S1-10	30	10	3	Clay	Not completed		
S1-11	30	15	3	Clay	Not completed		

Peak uplift resistance (F_{up}) and the anchor displacement at peak resistance (w_p) for uplift tests in each centrifuge sample are presented in Table 6.7. The following observations are made:

i. Regarding the increase in anchor capacity; 30 mm anchors founded on clay and uplifted at increasing velocity may have up to about 2 and a half times the peak uplift capacity of an equivalent anchor founded on sand.

ii. Regarding anchor capacity at the slowest uplift velocity; the peak resistance measured for an anchor founded on clay uplifted at v_f =0.03 mm/s is just under twice that of the same anchor on sand indicating that some suction is generated at this velocity and the behaviour is partially drained. A velocity of less than 0.03 mm/s would be required for the behaviour of an anchor founded on clay to be considered fully drained.

iii. Regarding the anchor displacement; the displacement of an anchor at maximum load increases with uplift velocity.

6.3.3 Peak uplift capacity

The variation of the peak uplift capacity with velocity for 30 mm anchors founded on clay and sand is presented in Figure 6.15. Although the data are limited, a progressive increase in F_{up} with v_f is apparent across the full range of v_f values investigated. The rate of gain in capacity is greatest at uplift velocities between 0.03 and 3 mm/s, the latter representing the point at which a considerably lower increase in resistance

occurs with increasing velocity. It may be inferred that at $v_f \geq 3$ mm/s, partial drainage is not a significant factor and the strain rate dependence of the clays undrained shear strength controls increases in capacity after this point. This rate dependence will result in an increased contribution to resistance both in the backfill failure zone and for the reverse bearing failure mechanism developed at the anchor base. For an anchor founded on free draining sand, as shown in Figure 5.11(b), uplifted at a velocity of 3 mm/s and the same anchor founded on clay, Figure 5.11(a), uplifted at the same velocity the contribution to resistance provided by the backfill clay will be similar. In this case the approximation of suction force (F_{su}) given by Equation 6.6 will be valid. For comparison with an anchor on sand uplifted at 3 mm/s and the same anchor founded on clay uplifted at 30 mm/s however the approximated suction force will include some increase due to viscous effects in the backfill clay. In this case the approximation given by Equation 6.6 is likely to overestimate the suction force in relation to the strain rate dependence of the clay. While this is a valid point to note it should also be considered that, as illustrated in Figure 6.9, Equation 6.6 will also tend to underestimate F_{su} due to differences in the relative displacements at peak resistance between anchors on sand and clay.

6.3.4 Estimate of suction

The approximated suction stress (s) below anchors founded on clay, calculated from Equation 6.7, is plotted with v_f in Figure 6.16 for 30 mm anchors. The available suction is observed to increase from around 50 kPa at v_f =0.03 mm/s to a maximum value of up to 90 kPa at v_f =100 mm/s. As suggested previously for the PASB test series the maximum value was likely limited by the relatively low undrained shear strength of the kaolin clay although the values inferred are within the region of negative pressures at which cavitation of water occurs (85-100 kPa). It has been proposed (Thorne et al. 2004) that cavitation of the pore water in the underlying clay could limit the suction available at the base of the anchor. Goodwin and Lehane (2003) have however previously inferred suction stresses in excess of 200 kPa from UWA centrifuge experiments involving anchors in stiffer clay, while it is shown later in Chapter 7 that suctions measured directly at a model footing base are not limited by the cavitation pressure of water.

The mean maximum suction stress for a 45 mm anchor founded on clay and uplifted at 3 mm/s is also plotted on Figure 6.16. With only two data points with which to compare, it is perhaps inappropriate to infer any definite trend however it would appear from the results available that for anchors on clay the suction stress at the base of the anchor will remain approximately constant with anchor width. This is a similar trend to that seen previously for PASB in Section 6.1.5.

6.3.5 Generalisation of uplift test data

As previously observed for the PASB tests, inspection of the anchors after uplift revealed that a wedge of clay from the stiffer base layer, with a height of approximately B/2, had adhered to the base of anchors uplifted at v_f values of 30 and 100 mm/s (Figure 6.17). A smaller wedge was also noticeable on the base of the anchor uplifted at 3 mm/s. Again this indicates that a reverse bearing capacity failure mechanism operates at the base of the anchor at these velocities and the failure load is dependent upon the undrained strength of the clay.

To assist in the interpretation and comparison of the results the uplift resistances may be divided into three separate components and normalised factors provided for each case. These components are presented in Table 6.8.

Table 6.8 Components of uplift resistance

Component of uplift resistance	Factor	Normalisation
Total uplift capacity (fully bonded at anchor base)	N_u	$N_u = \frac{F_{up}}{s_u B^2}$
Breakout resistance (separation at anchor base)	N_{ub}	$N_{ub} = \frac{F_{up-sand}}{s_u B^2}$
Reverse bearing capacity (resistance at anchor base)	N_{uc}	$N_{uc} = \frac{\left(F_{up} - F_{up-sand}\right)}{s_u B^2}$

The total uplift capacity is taken as the uplift resistance of anchors founded on clay (i.e. where suction is allowed to develop at the anchor base) and the breakout resistance is taken as the uplift resistance of anchors founded on sand (i.e. where immediate separation of the anchor occurs and no suction develops). As approximated previously the component of resistance at the base of the anchor is assessed as the

difference between the other two components. In each case the uplift capacity factors are calculated using the strain rate corrected T-bar undrained shear strength assessed from Equation 6.9.

The total uplift coefficients (N_u) for 30 and 45 mm anchors were determined according to Table 6.8 and are plotted against their corresponding embedment ratios in Figure 6.18 where they are compared with the results of previous (a) experimental and (b) numerical studies. It is evident that:

i. The N_u value for the 45 mm (H/B=1) anchor is a little higher than the experimental data but well replicated by the results of the total stress FEA presented in Chapter 3. In contrast the N_u value for the 30 mm anchor (averaged from the results of uplift tests where $v_f \geq 30$ mm/s, H/B=1.5) is well represented by the experimental results of Rao and Datta (2001) and Das et al. (1994) but falls some way short of the FEA predicted curve.

ii. The trend for increasing N_u with H/B ratio evident in previous experimental and numerical data is not observed in the centrifuge test data. The discrepancies in the, rather limited, centrifuge data are however not so significant as to be beyond the boundaries of experimental error. Increased consolidation in the clay below the 45 mm anchor due to the increased self weight of the anchor would lead to a higher shear strength than is mobilised below the 30 mm anchor. As this increase is not accounted for in normalisation of the data, this may account for the apparent overestimation in the observed value of N_u at H/B =1.

The breakout resistance factors (N_{ub}) for the centrifuge tests are plotted with embedment ratio in Figure 6.19. As might be expected the trend with increasing embedment ratio is similar to that shown in Figure 6.18 for values of N_u from the data provided. Also plotted in Figure 6.19 are results from previous (a) experimental and (b) numerical studies. It is noted that:

iii. In general the N_{ub} values presented from previous experimental and numerical studies are a little higher than the value calculated for the 30 mm anchor and a little lower than that calculated for the 45 mm anchor. The N_{ub} values from the centrifuge tests are not well replicated by the results of the equivalent model scale (SAFE) FEA for either anchor width. It should be noted that in each case

the value of undrained shear strength ($s_{uT\text{-}bar}$) used in the calculation of N_{ub} for the centrifuge anchor tests is assessed from an inhomogeneous profile and taken as the value at the anchor base. The previous experimental and numerical data presented for comparison is all representative of anchors in homogeneous clay.

iv. As seen previously for N_u, the trend present in previous experimental and numerical data is not replicated by the N_{ub} values assessed from the centrifuge test results.

Values of reverse bearing capacity factors (N_{uc}) calculated for the centrifuge test data according to the equation shown in Table 6.8 are plotted with H/B in Figure 6.20 where they are compared with N_{uc} values assessed from previous experimental studies. There appear to be no results from previous numerical analysis to directly assess the reverse bearing capacity factor where suction is developed at the anchor base. From comparison with bearing capacity solutions, as discussed in Section 6.2.1, it would be expected that the value of N_{uc} would lie within the range 5-7. It is seen in Figure 6.20 that:

v. The N_{uc} values calculated for the centrifuge tests compare favourably to the results of model tests described by Rao and Datta (2001) and Kumar (1993). The N_{uc} values assessed from the experimental data of Das et al. (1994) appear to be significantly lower than those from the centrifuge tests and from other studies.

vi. The overall trend in N_{uc} observed from the centrifuge data indicates that the available suction, and thus development of the reverse bearing failure, will increase with H/B although the other published experimental data shows that N_{uc} may tend to decrease slightly with H/B. Generally the factor N_{uc} will be controlled by the suction available at the base of the anchor and will be limited by the undrained shear strength of the clay. For this reason it is thought to be more likely that N_{uc} would remain constant with increasing H/B up to the point at which anchor behaviour becomes deep, $(H/B)_{crit}$, and failure is entirely localised around the anchor base.

vii. Due to the normalisation shown in Table 6.8 the variation in N_{uc} with H/B will be dependent upon the trends observed previously for N_u and N_{ub}.

The N_{uc} factors calculated for each anchor width are plotted in Figure 6.21 with uplift velocity. It is apparent that:

- The rate of increase in N_{uc} with increasing velocity drops after anchor velocities in excess of 3 mm/s and corresponds to the generation of full suction at the anchor base. It should be noted that the variation of N_{uc} with velocity is thought to be independent of the effects of clay viscosity and anchor behaviour may be assumed to be fully undrained at uplift velocities greater than 3 mm/s.
- The mean value of N_{uc} at $v_f \geq 3$ mm/s is approximately 6. This value is in broad agreement with the values suggested in Section 6.1.1 based on the results of previous investigation and that inferred from comparison with conventional bearing capacity behaviour.
- The value of N_{uc} of around 3.5 at v_f=0.03 mm/s indicates that some suction is still developed at this velocity and partial drainage effects dominate. Based on the observed trend line it would be estimated that an uplift velocity below around 0.001 would be required to ensure full dissipation of suction at the anchor base.

6.4 Comparison of uplift behaviour

The trends observed in Sections 6.2 and 6.3 with regard to the variation of uplift behaviour with varying uplift velocity are compared for 30 mm anchors in clay and sand backfill soils. Differences in the limits of fully drained and fully undrained behaviour arising between the two backfill soils are discussed in relation to the respective values of normalised velocity.

6.4.1 Variation of N_{uc}

The N_{uc} values calculated for PASB and PACB for 30 mm anchors in sand and clay backfill are plotted in Figure 6.22 with (a) anchor uplift velocity and (b) the normalised velocity (V), as given by Equation 6.4, substituting the anchor width (B) in place of diameter:

$$V = \frac{v_f B}{c_v} \tag{6.11}$$

where a typical value of the coefficient of consolidation (c_v) for kaolin clay is selected from the existing laboratory data presented in Figure 4.2(a), and taken to be equal to 3 m^2/year. It is apparent that:

i. While similar values of N_{uc} are assessed between tests with clay and sand backfill at high uplift velocities ($\geq$30mm/s), there is a significant difference in the values deduced at slower uplift rates. This observation indicates that for clay backfill, dissipation of generated suctions occurs at a slower rate and the behaviour of the anchor may become fully undrained at much lower velocities (3 mm/s for clay compared to 30 mm/s for sand backfill).

ii. At the slowest rate of loading tested (0.03 mm/s) the N_{uc} value assessed for an anchor in clay backfill is considerably higher than an equivalent anchor backfilled with sand. It is therefore inferred that for anchors in clay backfill soils appreciably slower uplift rates would need to be applied to achieve fully drained, immediate breakaway behaviour.

iii. The variation of N_u with the normalised anchor velocity (V) in Figure 6.22(b) is significantly different to that shown for consolidation under compression loading in Figure 6.1. For anchors in sand backfill the V value of approximately 10000, after which conditions can be considered undrained for uplift loading, is in marked contrast to the value of approximately 100 assessed from Figure 6.1 for compression loading. For anchors subject to uplift loading in clay backfill the difference is significantly less, with a V value of 1000 being just one order of magnitude higher than that for compression loading. This highlights the effect of the backfill material on the dissipation of suctions, where granular soils evidently provide faster relief of negative pore water pressures developing at the anchor base. Over the lower range of velocity, N_{uc} is shown to be approximately zero at $V<10$ for sand backfilled anchors whereas the degree of pore pressure dissipation (U) only reaches above 0.9 at $V<0.01$ for compression loading.

It has been suggested previously that the failure mechanisms developed for bearing and uplift behaviour are essentially similar under fully undrained conditions. The variation in anchor behaviour with uplift velocity has however been shown to be markedly different within the partially drained region. The very high normalised

velocities required to attain fully undrained conditions observed in the centrifuge experiments shows that some disparity exists in the factors controlling the base resistance of a foundation loaded in compression and those controlling the uplift resistance provided by under-base suction. The absence, noted at the end of the tests, of clay adhered to the bases of sand backfilled anchors tested at $v_f \leq 3$mm/s suggests a mechanism where the generated suctions are relieved by the heave occurring during the generation of full undrained uplift and the flow of water (pulled through the adjacent sand) along the underside of the anchor. This is shown schematically in Figure 6.23 where the enhanced ability for excess pore pressure relief in uplift, compared to a an anchor loaded in compression, may be expected to arise because of the drainage path encouraged by the separation of the clay along the outside edge of the anchor. The under-base uplift capacity is related directly to the average degree of excess pore pressure (suction) dissipation, reducing to zero at full dissipation, while in compression loading, the base resistance generally increases with increased dissipation of excess pore pressures.

It is important to note that the values of the normalised velocity (V) are calculated for the centrifuge test data using a value for c_v derived from oedometer tests on normally consolidated kaolin. Randolph and Hope (2004) assume a value of c_v for overconsolidated kaolin equal to 7 m^2/year, just over twice the value adopted here. Given that the process of unloading will also cause the value of c_v to increase compared to that given from primary loading, these distinctions could be used to explain the differences in the limits of V obtained for compression loading and those derived for the centrifuge tests with clay backfill (where the lower permeability will reduce drainage through the backfill to the anchor base). It is expected that, even considering the above ideas, there will still be some degree of variation between the limits of V obtained for compression loading and those for anchors with sand backfill due to the relief mechanisms explained previously.

6.5 Summary

A series of centrifuge model tests have been undertaken on plate anchors of varying width embedded in sand and clay soil subjected to uplift over a range of velocities.

These tests have confirmed that suctions are generated at the base of anchors founded on clay during uplift and that the magnitude of these developed suctions may be estimated by comparison of the capacity of anchors founded on clay and those founded on sand (where no suctions are developed). It has been established that:

i. High uplift capacities are developed at high uplift velocities; however, displacements of up to 10% of the anchor width may be required in order to generate the full capacity at these velocities.

ii. The magnitude of developed suction increases with increasing anchor uplift velocity (v_f). This increase is related to a reduced tendency for pore water drainage during uplift at high velocity and to the strain rate related behaviour of the clay underlying the anchor.

iii. The anchor uplift capacity at high uplift velocities (leading to fully undrained behaviour) may be estimated from a reverse bearing capacity type failure mechanism with a base uplift capacity factor (N_{uc}) of approximately 6. This value of N_{uc} may be related to the undrained shear strength in triaxial extension, which has been shown to be similar, for the centrifuge test samples, to the undrained shear strength derived using T-bar penetration tests.

iv. For a given level of partial drainage, the normalised velocities (V) for sand backfilled anchors subject to uplift loading are approximately two orders of magnitude higher than estimated for an equivalent anchor under compression loading. The normalised velocities for anchors with clay backfill is only one order of magnitude higher than for compression loading, indicating the presence of a mechanism whereby the permeability of the backfill soil may effect the relief of suctions developed at the anchor base. For anchors backfilled with sand a drainage path is developed, where water is pulled through the sand to relieve negative pore pressures, and is propagated by the separation of the clay at the edge of the anchor base where the initial dissipation of suction occurs.

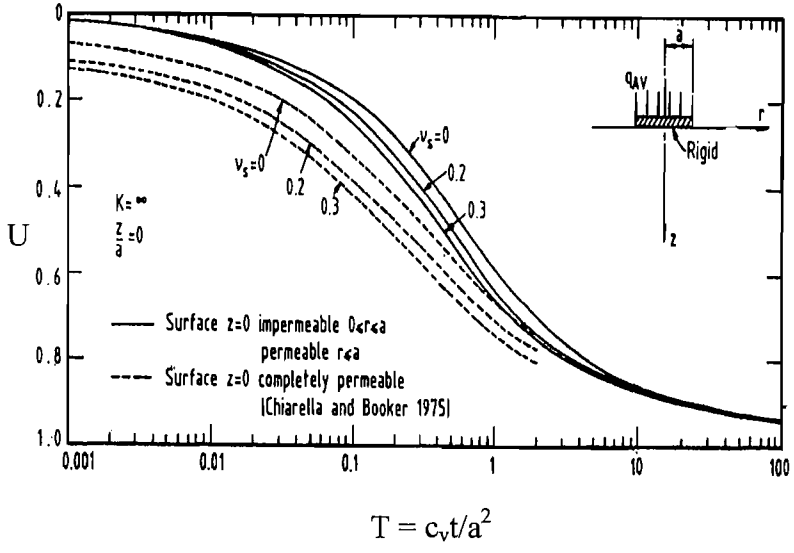

(a) Degree of consolidation with time factor for compression loading (Booker and Small, 1986)

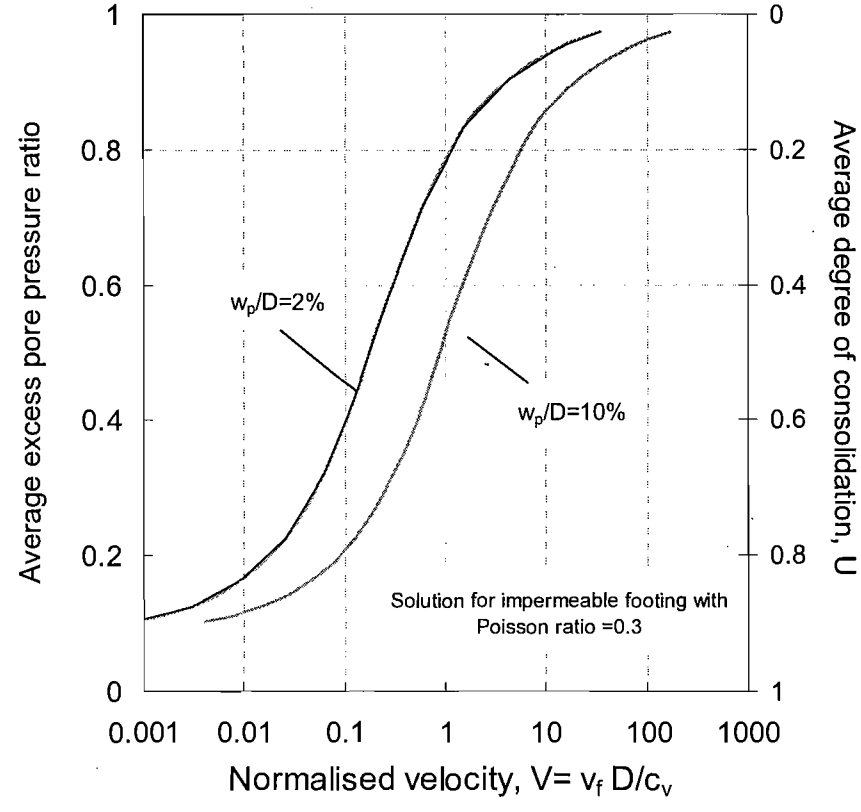

(b) Degree of consolidation with normalised velocity for compression loading

Figure 6.1 Average degree of consolidation for compression loading

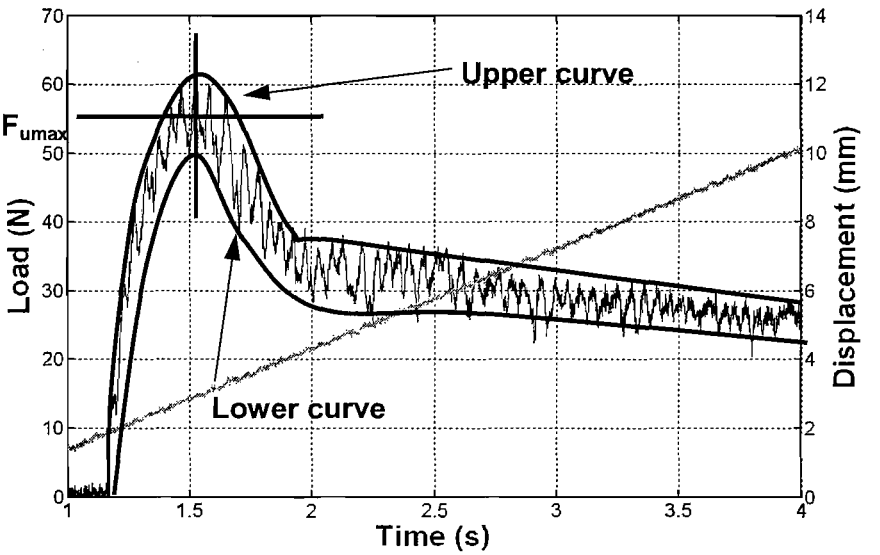

Figure 6.2 Determination of the maximum uplift force

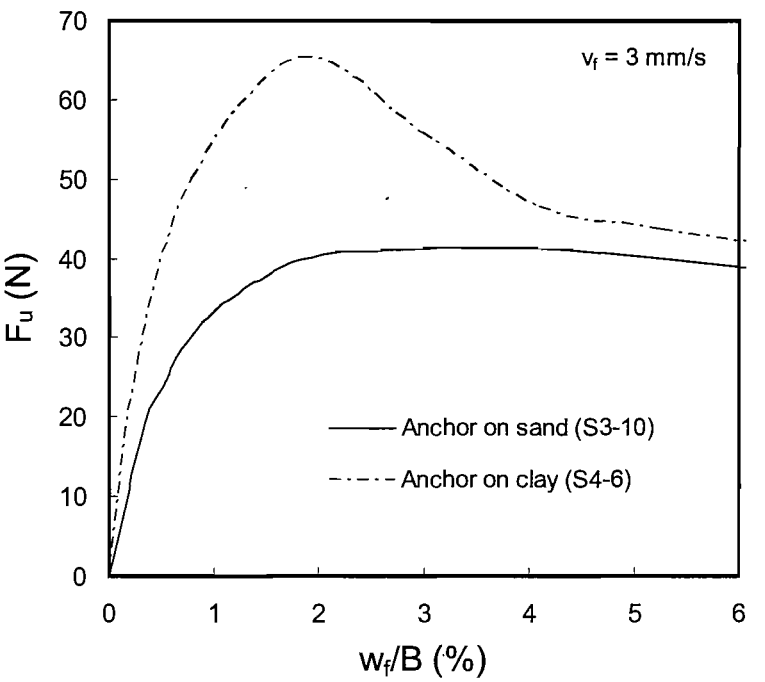

Figure 6.3 PASB – Comparison of load displacement response for 30mm anchor founded on clay and sand

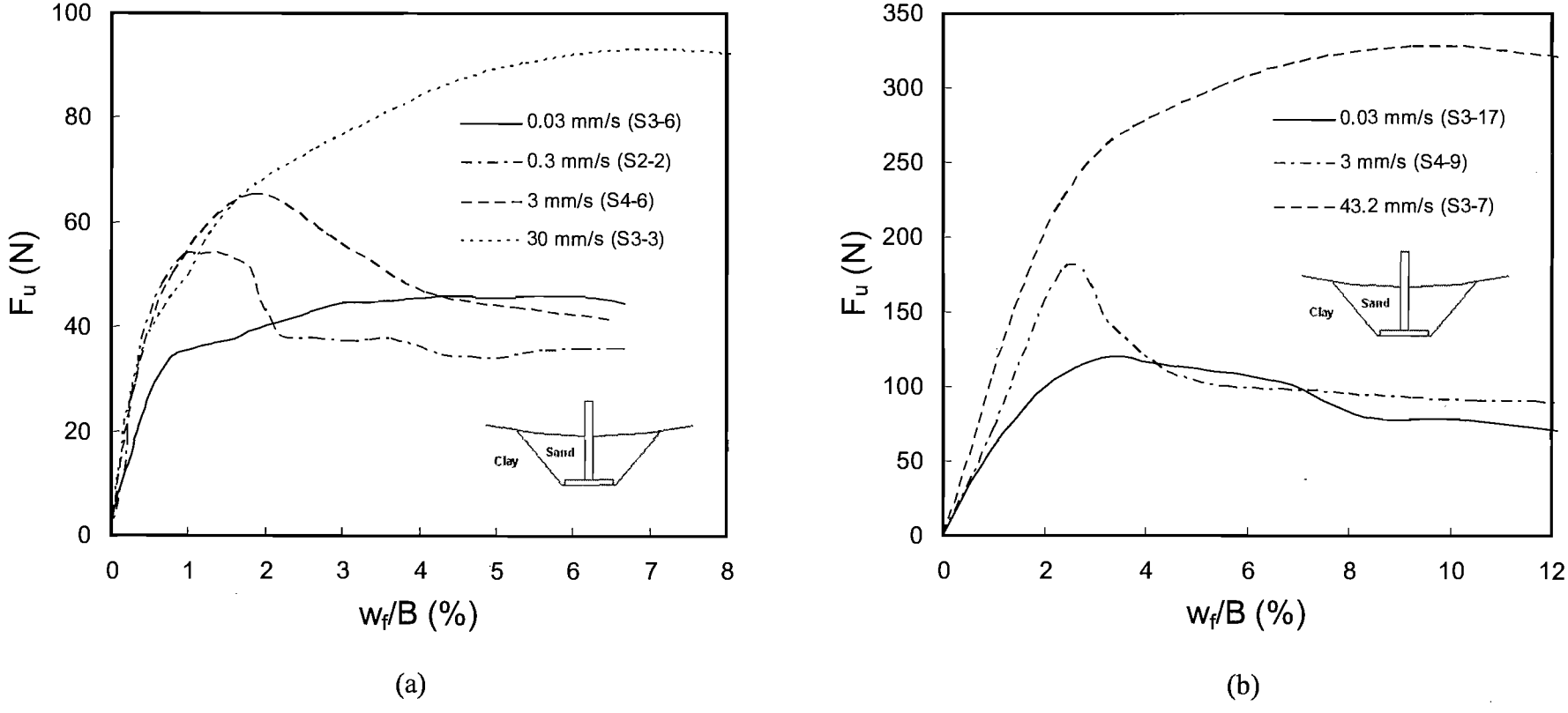

Figure 6.4 PASB – Typical load displacement response with increasing uplift velocity for (a) 30mm and (b) 60mm anchors founded on clay

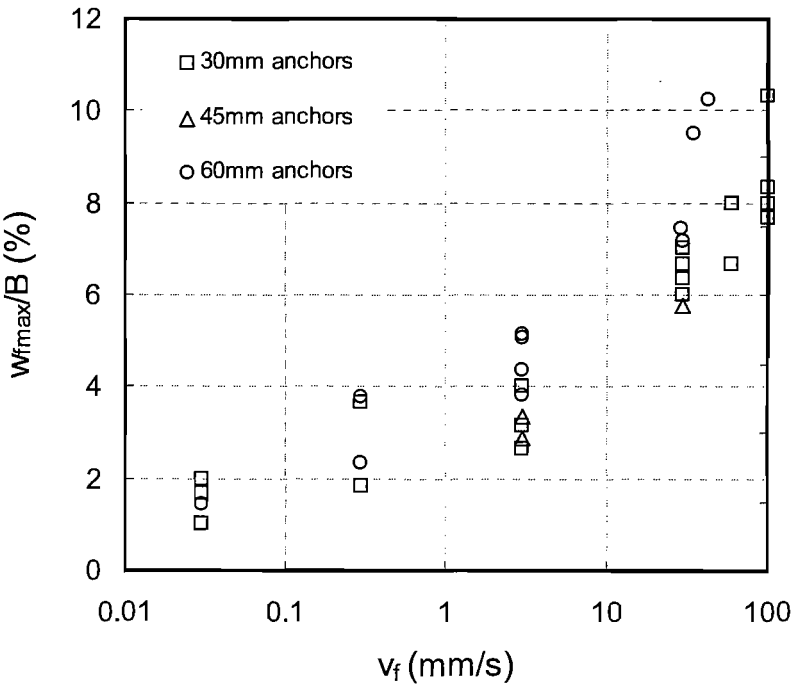

Figure 6.5 PASB - Variation of displacement at peak uplift load with uplift velocity for anchors founded on clay

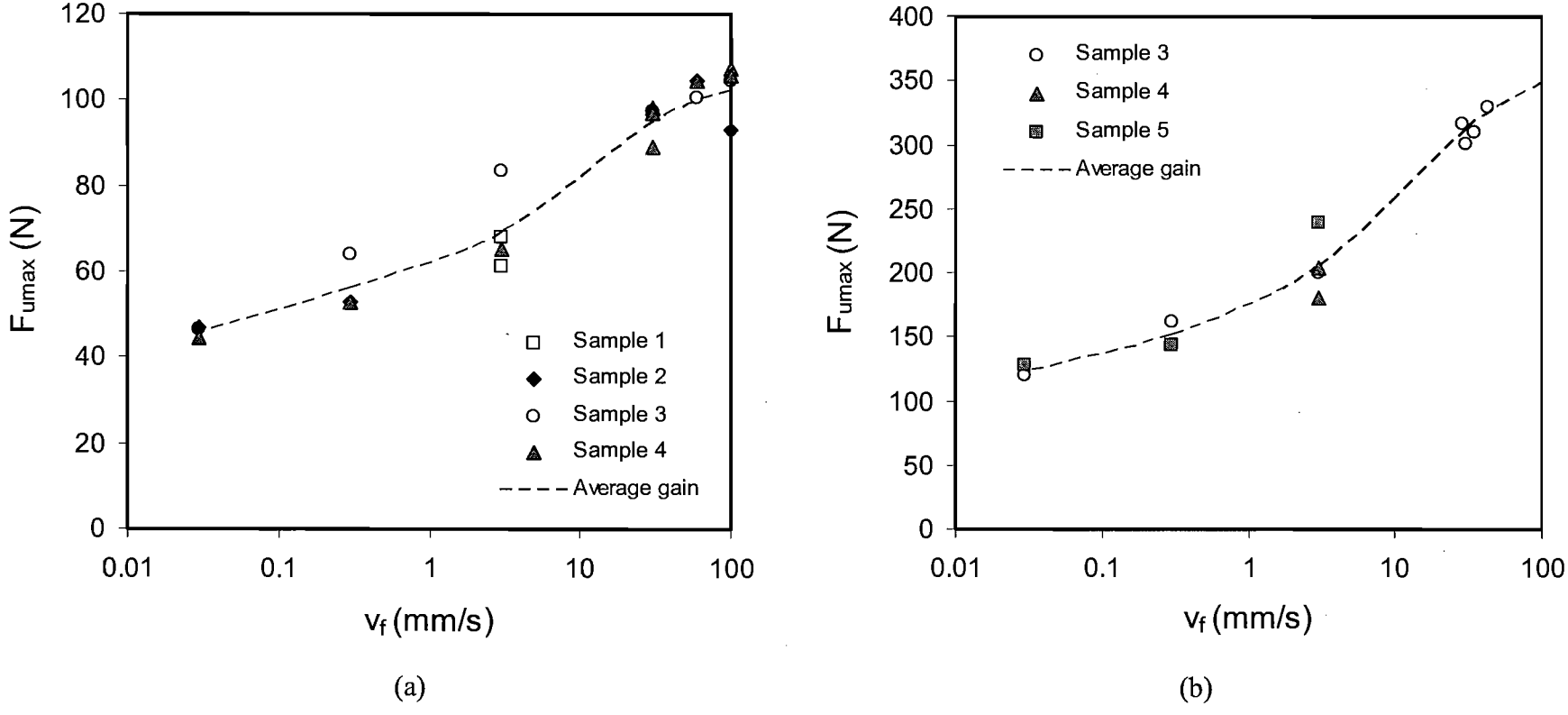

Figure 6.6 PASB - Anchor capacity with uplift velocity for (a) 30mm and (b) 60mm anchors founded on clay

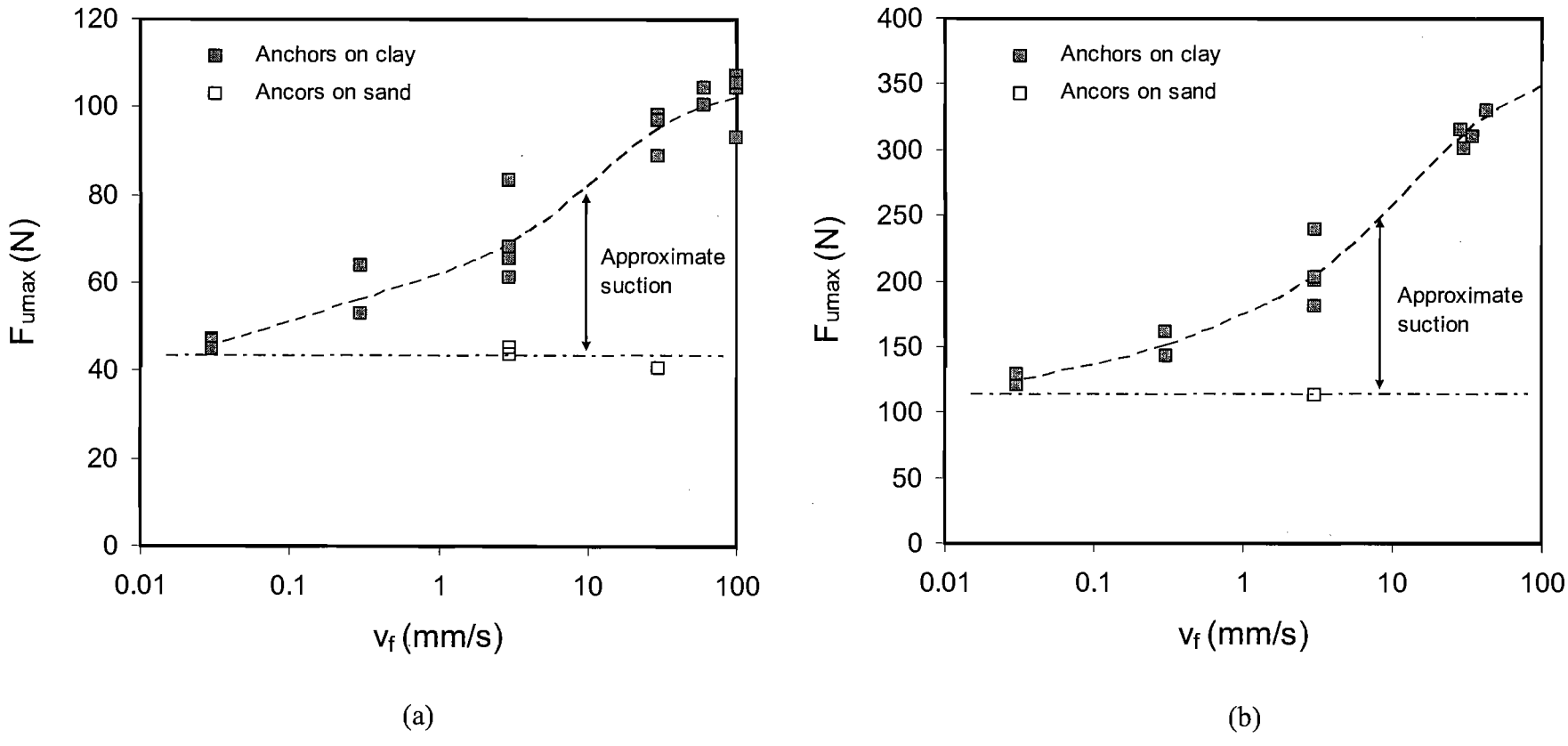

Figure 6.7 PASB - Anchor capacity and approximate gain in suction force (F_{su}) with uplift velocity for (a) 30mm and (b) 60mm anchors founded on clay and sand.

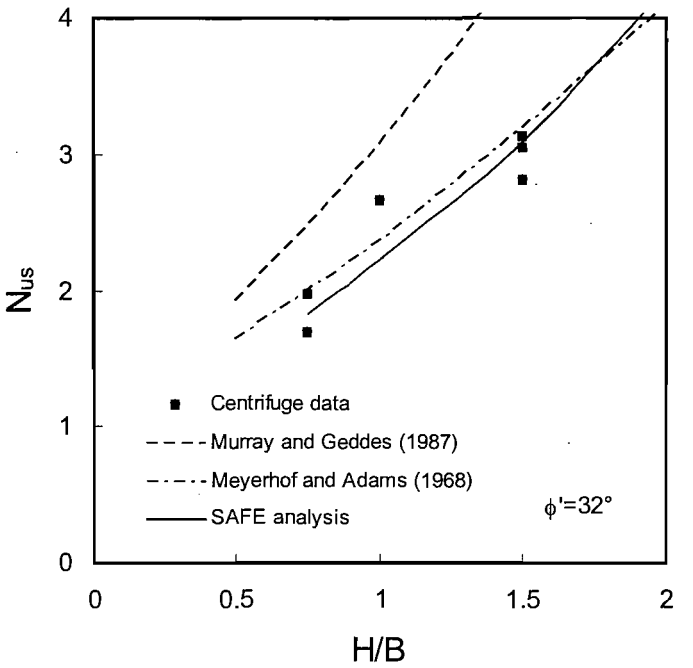

Figure 6.8 PASB – Uplift capacity factor N_{us} with embedment ratio for anchors founded on sand

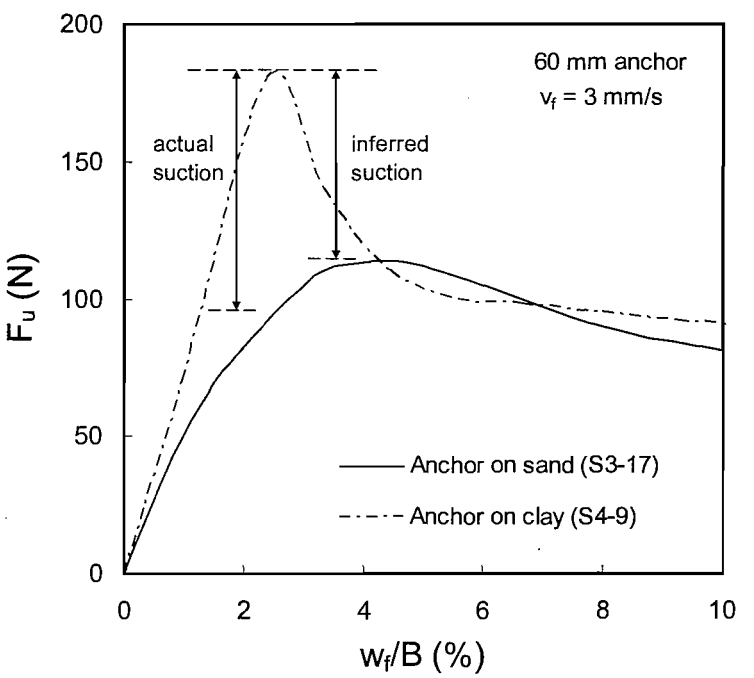

Figure 6.9 Variation in the actual suction contribution and the inferred value for a 60mm anchor

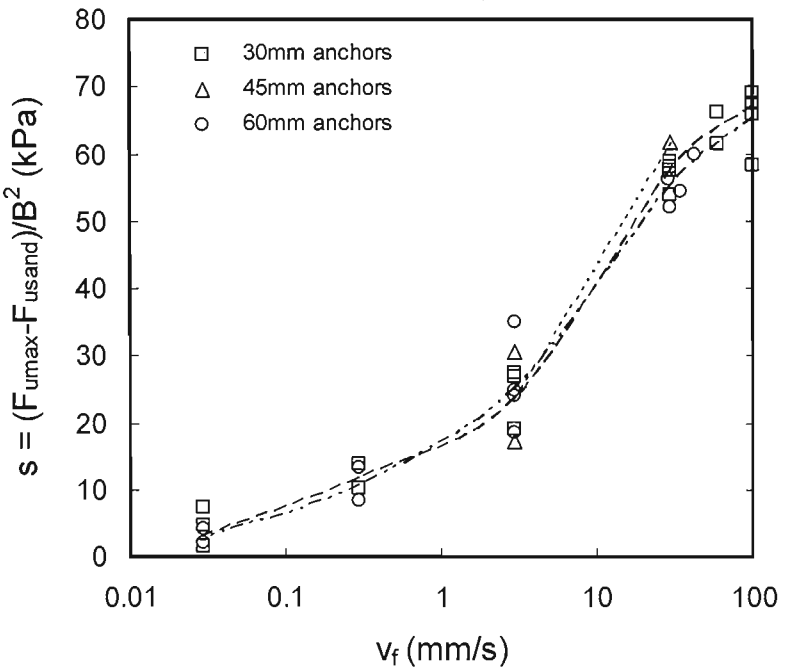

Figure 6.10 PASB - Maximum suction stress (s) with uplift velocity for anchors founded on clay

Figure 6.11 Wedge of clay adhered to anchor base after uplift ($v_f \geq 30$ mm/s)

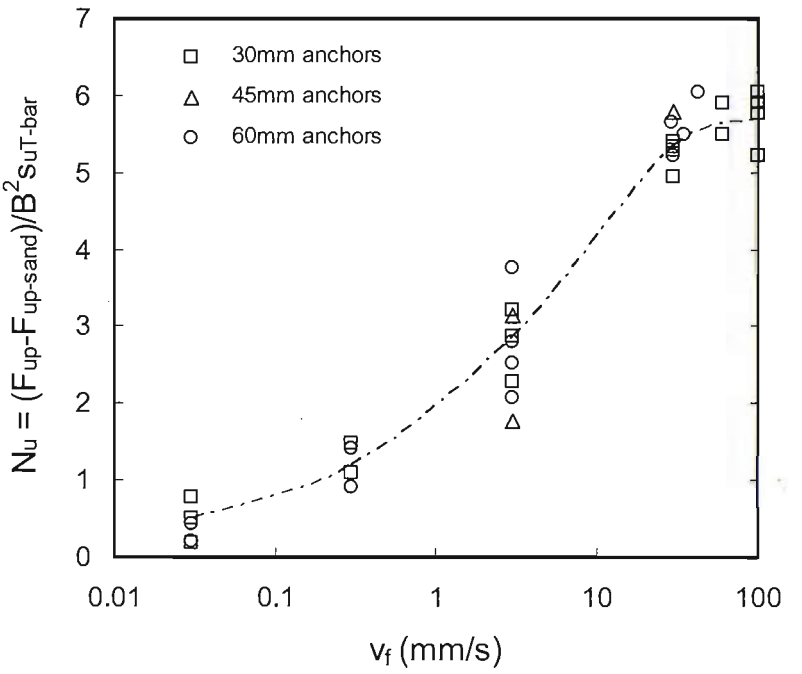

Figure 6.12 PASB - Uplift capacity factor (N_{uc}) with uplift velocity

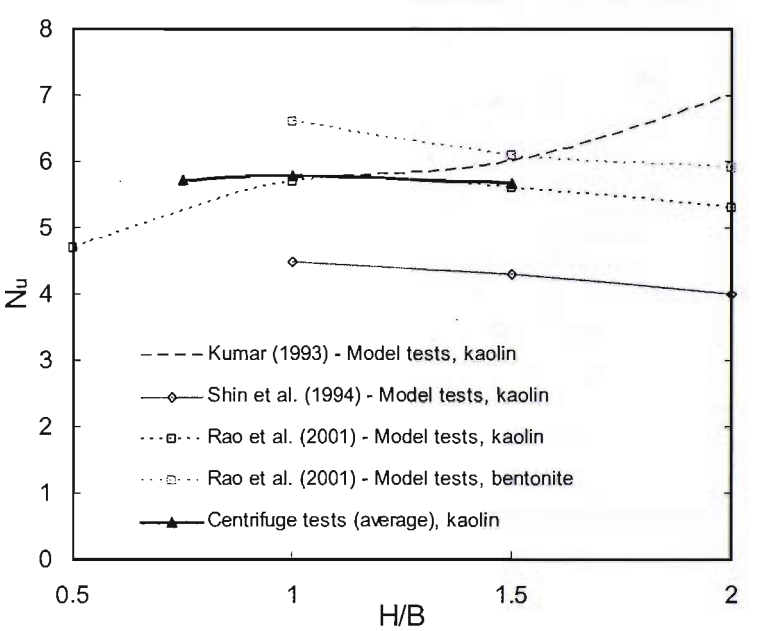

Figure 6.13 PASB - Comparison of centrifuge and previously published experimental N_{uc} factors

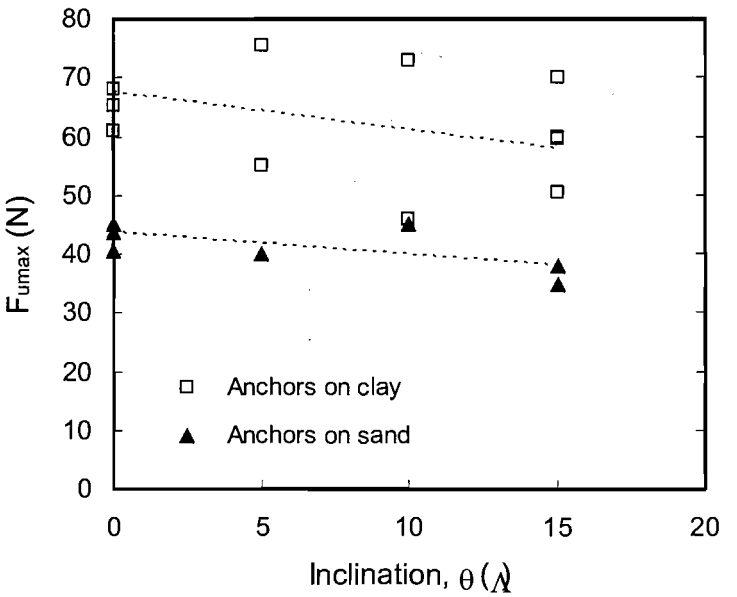

Figure 6.14 PASB - Anchor capacity with stem inclination for anchors on clay and anchors on sand

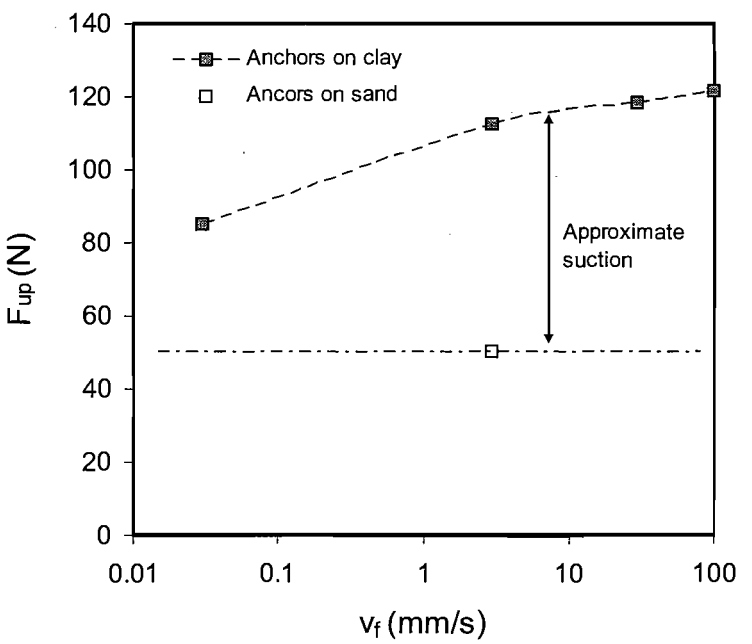

Figure 6.15 PACB - Anchor capacity and approximate gain in suction force (F_{su}) for anchors founded on clay and sand.

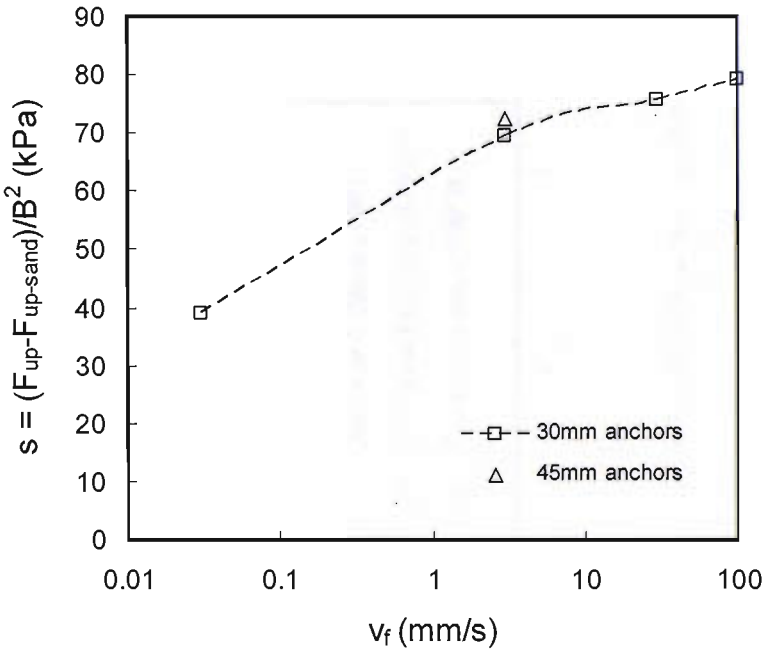

Figure 6.16 PACB - Maximum suction stress (s) with uplift velocity for anchors founded on clay

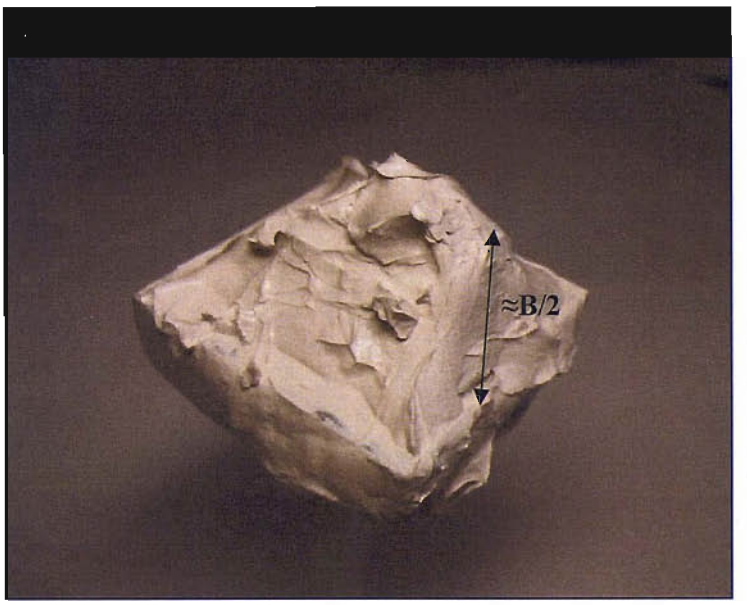

Figure 6.17 PACB - Wedge of stiffer clay adhered to anchor base after uplift (v_f ≥30 mm/s)

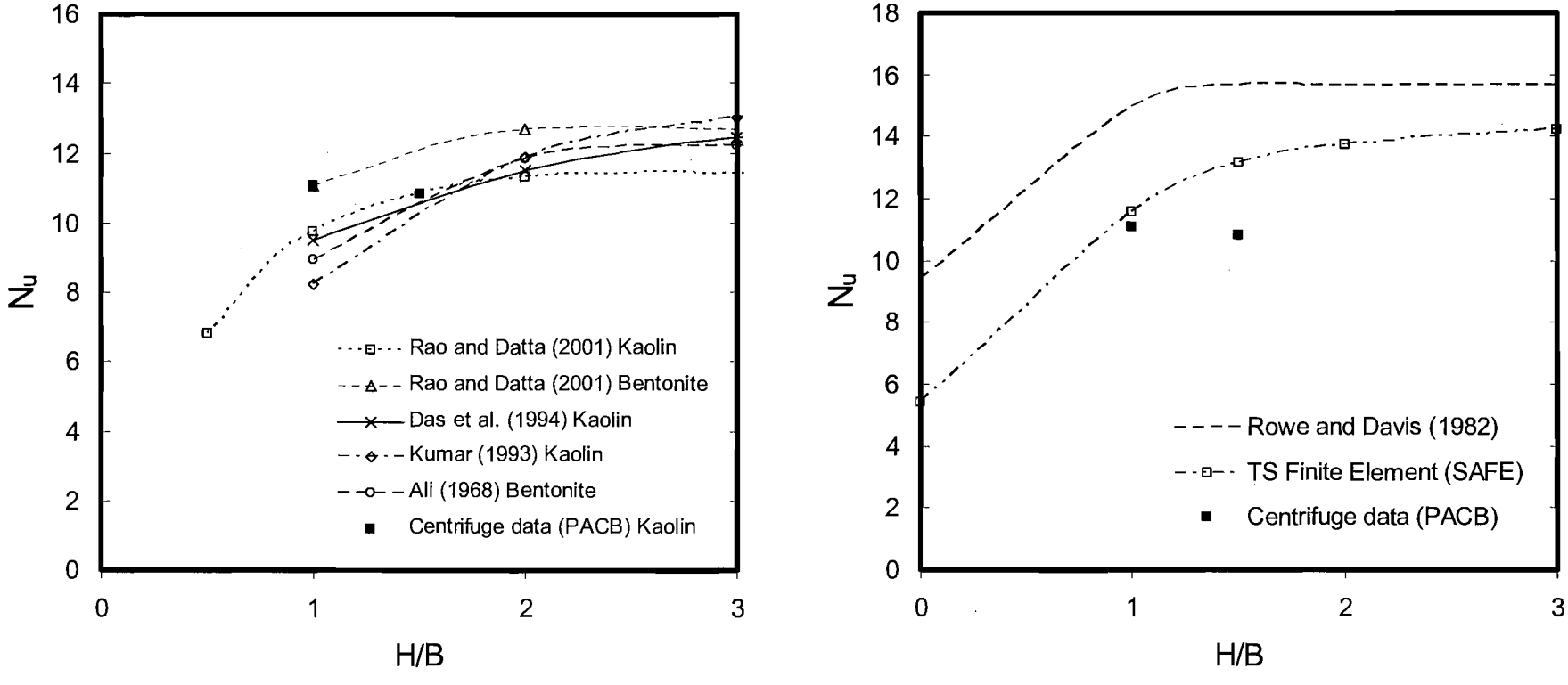

(a) Comparison with total uplift factors from experimental studies

(b) Comparison with total uplift factors from numerical studies

Figure 6.18 PACB – Total uplift factor (N_u) with embedment ratio

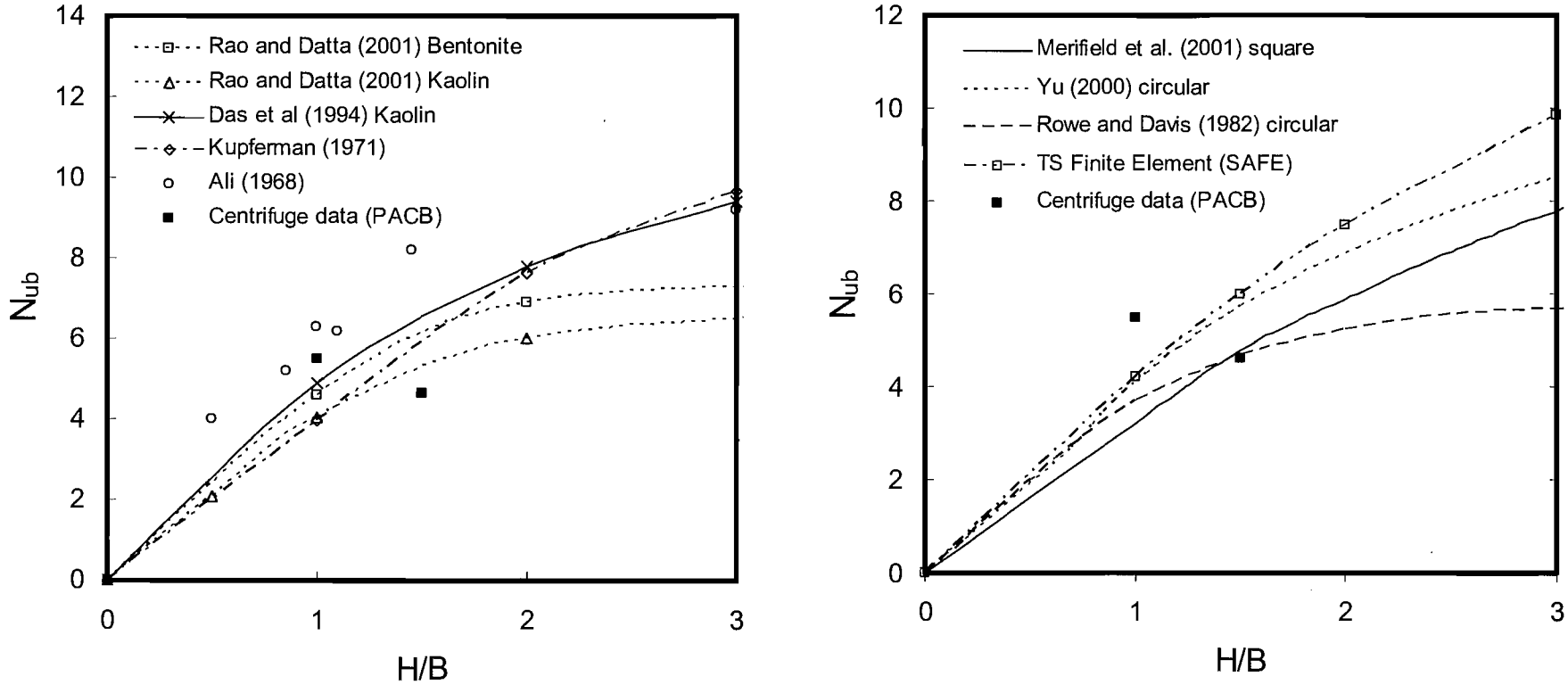

(a) Comparison with total uplift factors from experimental studies

(b) Comparison with total uplift factors from numerical studies

Figure 6.19 PACB – Breakout resistance factor (N_{ub}) with embedment ratio

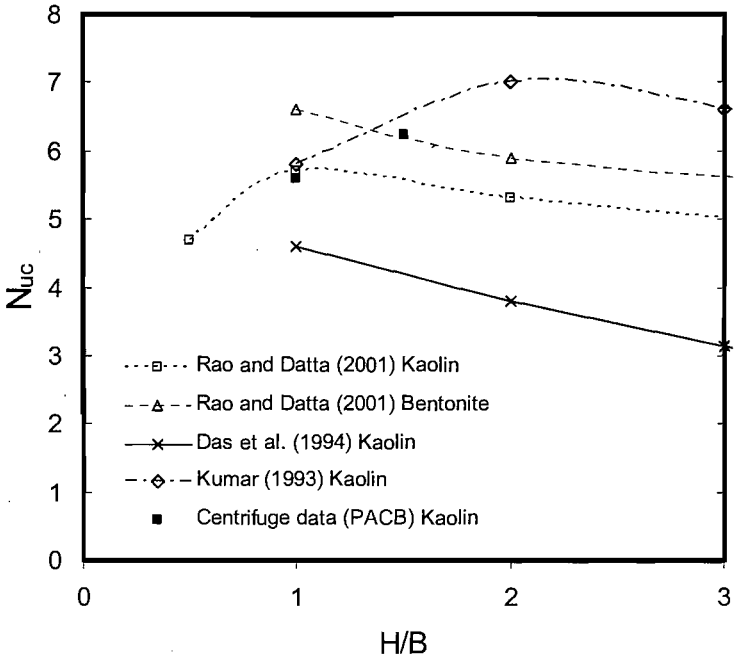

Figure 6.20 PACB – Reverse bearing factor (N_{uc}) with embedment ratio

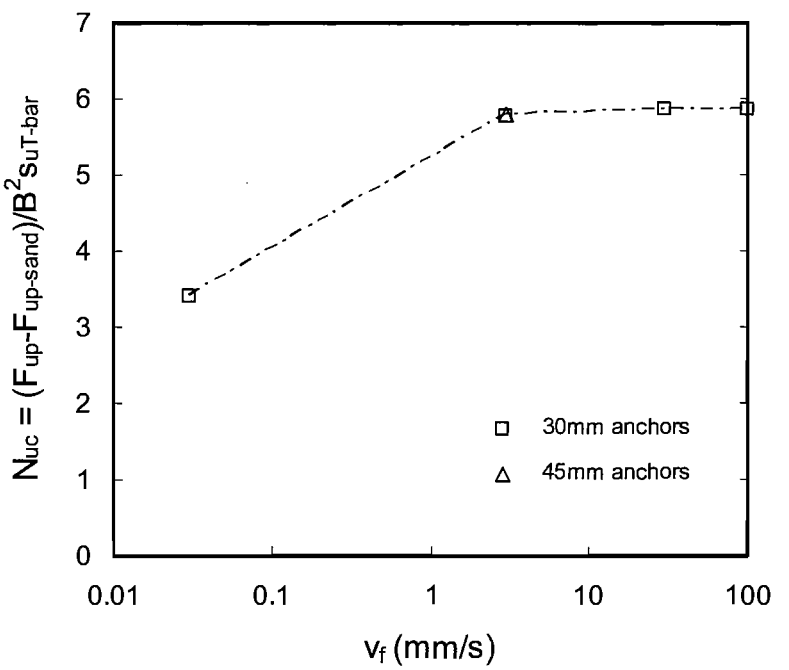

Figure 6.21 PACB – Uplift capacity factor (N_{uc}) with uplift velocity

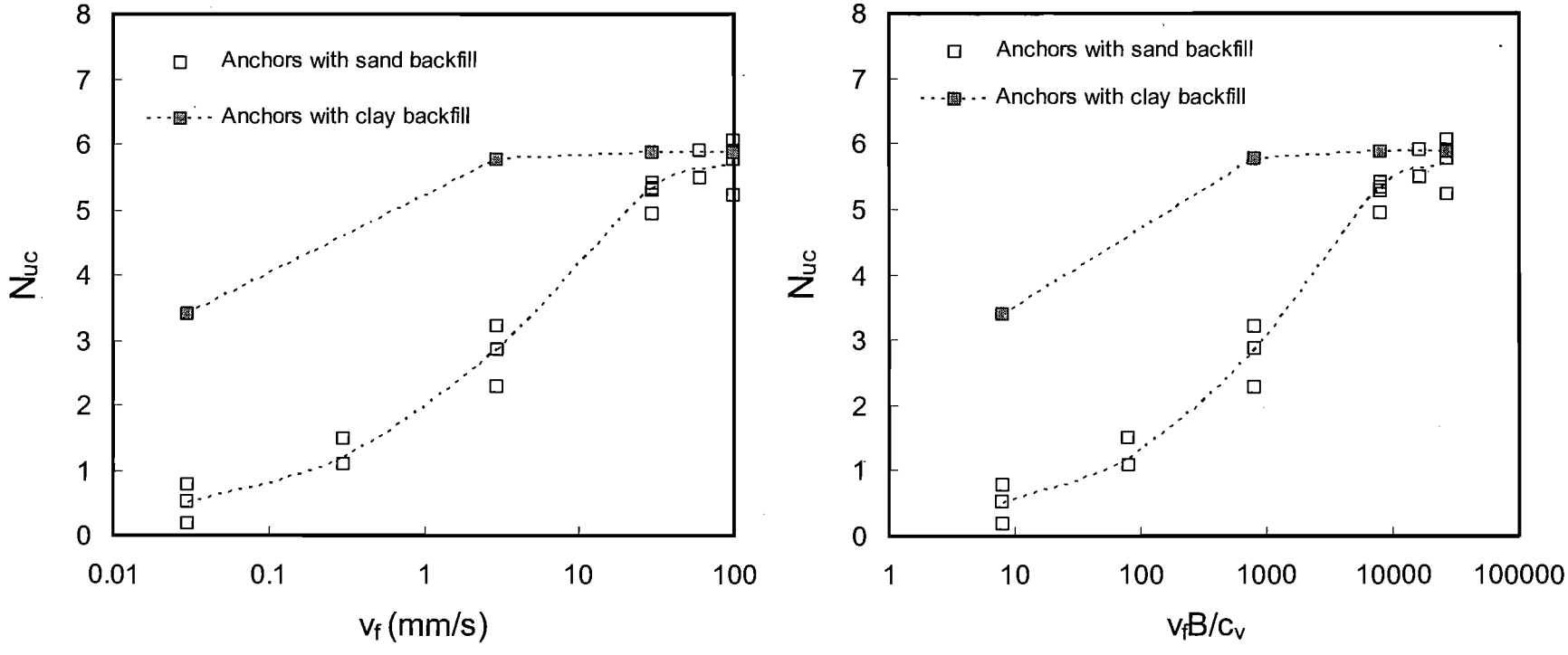

(a) Variation of N_{uc} with uplift velocity

(b) Variation of N_{uc} with normalised uplift velocity

Figure 6.22 Comparison of N_{uc} values for sand and clay backfilled anchors (30 mm)

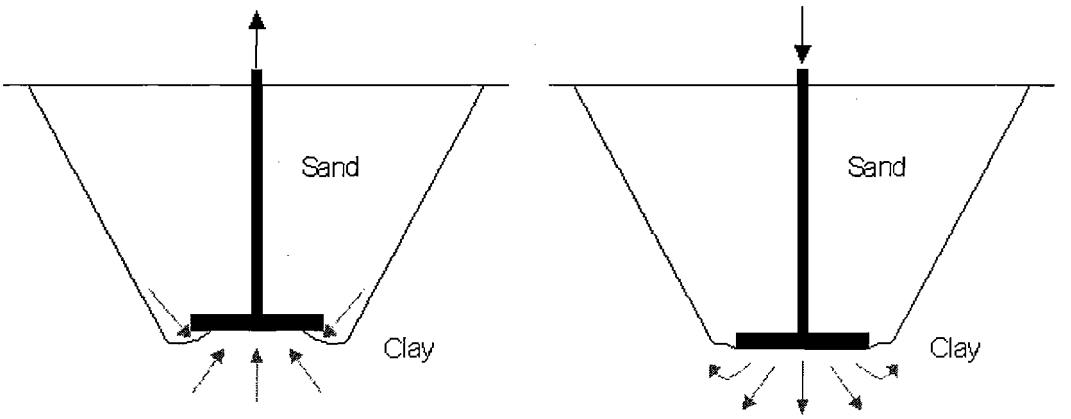

Figure 6.23 Enhanced pore pressure relief for sand backfilled anchors between uplift and compression loading

Chapter 7

FE SOLUTIONS FOR RATE DEPENDENT UPLIFT BEHAVIOUR

7.1 Introduction

The results of the centrifuge model study described in Chapter 6 have shown that the uplift behaviour of anchors founded on clay soil is significantly affected by the applied uplift velocity. The upper and lower bounds of anchor behaviour, i.e. the limiting cases of breakaway (drained) and fully bonded (undrained) behaviour, are reasonably well established and have been the focus of a number of previously published investigations (see Chapter 2). In reality the uplift behaviour of foundations in the field is likely to fall within these limits where the effects of partial drainage and the degree of adhesion between the soil and anchor base will have a considerable effect on the ultimate uplift capacity. While some limited guidance exists to estimate anchor capacity under undrained conditions (e.g. Small et al. 1998, Thorne et al. 2004) there are no published solutions for anchor capacity in a fully coupled consolidation analysis where substantial negative pore water pressures would be expected to develop. The presence of suction forces, developed during uplift at the base of an anchor founded on clay, have been investigated in a small number of experimental studies (e.g. Baba et al. 1989; Das et al. 1994; Rao and Datta, 2001) where it has been found that under undrained loading suction forces can provide a significant portion of the overall anchor capacity. No relationship has been made however between the developed suction and the loading rate of the anchor. It was shown in Chapter 6 that where uplift velocities are high enough to lead to undrained anchor behaviour, prediction of the contribution of suction may be estimated using traditional undrained

bearing capacity theory. Where the anchor uplift velocity leads to partially drained behaviour however, the prediction of uplift capacity (and the generation of suction) is complicated by the tendency for partial separation of the anchor from the underlying clay due to the propagation of a gap from the anchor edge, as shown in Figure 6.23. For the anchor geometry investigated in the centrifuge study water is subsequently drawn in to this gap, fed from the overlying granular backfill leading to more rapid dissipation of suctions closer to the centre of the anchor base. As a consequence the normalised uplift velocity ($V = v_j B/c_v$) required to attain fully undrained conditions is (for the geometries examined) between one and two orders of magnitude higher than the normalised velocity that would be expected to lead to undrained conditions for an anchor loaded in compression.

Rigorous finite element modelling of an anchor on clay subjected to uplift at partially drained rates requires continual mesh updating to track the development of the gap that forms beneath the anchor. In addition, contact/separation elements would be required to model the response at the anchor soil interface and would require tensile cut off values, which are themselves subject to extreme uncertainty. This is considered to be generally beyond the scope of routine design using numerical methods. This Chapter presents results obtained from a simplified finite element approach that involves modification of the clay's permeability to reflect the increased level of drainage that arises due to the formation of a gap at the edge of the anchor. The numerical analyses were performed using the finite element software SAFE described in Chapter 3. Results of the centrifuge testing program (Chapter 6) were back-analysed to test the validity of this single adjustment to the clay's permeability in representing the uplift behaviour over a range of uplift velocities to further characterise the magnitude of the suction forces generated under undrained and partially drained conditions.

7.2 The Finite Element Model

The finite element (FE) model developed for the numerical back analyses is described and details of the mesh geometry and soil model are presented. The numerical

analyses were performed using the SAFE Finite Element program (SAFE, OASYS, 2002) for which a general overview was given in Chapter 3.

7.2.1 Definition of the FE model

The FE analyses described in this Chapter were undertaken in order to provide a back analysis of the model anchor tests carried out during the centrifuge test program (Chapters 5 & 6). The analyses assumed axisymmetrical conditions and therefore the square model anchors and stem used in the centrifuge tests were represented as circular sections of equivalent area. The anchor was assumed to be perfectly rigid in all cases.

The boundary conditions imposed in the FE back-analyses are shown in Figure 7.1 and essentially model the centrifuge test geometry shown in Figure 5.10 (for sand backfill - PASB) and Figure 5.11 (for clay backfill - PACB). The location of the rigid lower horizontal boundary corresponded with the depth to the base of the centrifuge channel. The rigid far vertical boundary was selected, arbitrarily, as the mid-point distance between each footing position in the centrifuge tests. To assess the possible impact of these mesh boundary locations on the computed results a series of undrained analyses employing meshes with increased and reduced far vertical boundary locations were undertaken. The results of these analyses are summarised in Figure 7.2 and indicate that increasing the far horizontal or vertical boundaries has little or no effect on the computed output. The reduction in anchor capacity seen for a reduction in the lower horizontal boundary is presumably related to a limiting effect of the lower boundary on the development of negative pore pressure at the anchor base. In each case the output presented in Figure 7.2 confirms that the selected boundary locations were suitable and no unbalancing stresses were introduced at either boundary. It also confirms that the depth of the clay allowed below the anchor base in the centrifuge model tests was sufficient to fully encompass the failure mechanism developed at high uplift velocity.

The finite element mesh developed for the back-analysis is shown in Figure 7.3 and consisted of 580 8-noded quadrilateral elements each with 4 Gauss points. The elements were biased to provide a significantly higher mesh density in the regions

around the anchor where the greatest changes in stress, and therefore strain, would occur during the imposed displacement.

7.2.2 Soil model and the anchor interface

In each effective stress analysis the sand and clay were assumed to behave as isotropic linear elastic-perfectly plastic materials with a Mohr-Coulomb failure criterion. The water table was set at the soil surface and each material was characterised by the effective stress parameters: shear modulus, unit weight, Poisson's ratio and effective angle of friction (where c′ was assumed to be zero). The plate anchor was modelled as a linear elastic material with a shear modulus, Poisson's ratio and unit weight representative of the aluminium material used to construct the anchors in the centrifuge study. For both the soil and anchor, the unit weights input into the FE analysis were adjusted to account for the scale representation of the model. Each unit weight was therefore factored by n=50 to correspond with the centrifugal acceleration applied in the centrifuge model tests (as described in Chapter 5). In this way, the FE analyses modelled the centrifuge tests rather than their equivalent prototypes.

The analyses employed a coupled consolidation formulation that permitted pore water pressure dissipation during the course of uplift loading. The analyses did not however model changes in soil stiffness associated with the corresponding changes in effective stress due to the generation of suction in the soil below the anchor. A fully rough interface was assumed between the footing and soil and no limit was imposed on the magnitude of suction that could develop in the clay below the footing. Anchors were loaded, as in the centrifuge test series, by applying a constant upwards displacement rate to the head of the anchor stem.

The undrained shear strength profile of the clay used in the analyses was taken as the average of that measured in the centrifuge T-bar tests (at a penetration rate of 1mm/s and assuming $N_{T\text{-}bar}$=10.5) and shown in Figure 5.30 (for sand backfill tests) and Figure 5.31 (for clay backfill tests). This strength was represented indirectly in the analysis by specifying a friction angle (ϕ'=32°) for the clay beneath the footing base that would lead to an undrained strength in extension (see Chapter 4) similar to that measured in the T-bar test, as indicated in Figure 7.4. The actual stress path followed

by this clay (with an OCR of approximately 5) is expected to be similar to that shown in Figure 7.4. As a check on this approach, a total stress analysis was performed where the undrained shear strength was specified directly in the model. Results of this analysis were found to be in close agreement with the effective stress approach where a high anchor velocity was specified such that undrained behaviour would occur. The input parameters adopted for sand and clay soils are shown in Table 7.1.

Table 7.1 Initial input parameters for model anchor analysis

	Base Clay	**Backfill Sand**
γ_s **(kN/m^3)**	800	900
γ_w **(kN/m^3)**	500	500
E' (kPa)	$670s_{uT\text{-}bar}$	5000
ν	0.15	0.15
ϕ' (degrees)	32	32
$s_{uT\text{-}bar}$ at B/2 below footing base (kPa)	9.4	-

As mentioned previously, between the upper (fully bonded, undrained) and lower (breakaway, drained) limits of anchor behaviour partial dissipation of negative pore water pressures (suction) will encourage the development of a gap to initially form around the outside edge of the anchor. This gap will extend towards the centre of the anchor base during continued uplift as water is pulled in from the granular backfill to relieve the negative pore water pressures at the base. Accurate modelling of this gradual separation of the soil and anchor would require continual re-meshing during analysis and the use of an appropriate interface element such as that described by Ng and Small (1997). This procedure can place additional constraints upon the design process (and introduce further uncertainties such as cut off tension values) which are generally beyond the scope of the practitioner. In the finite element back-analysis a simplified approach is employed whereby the permeability of the clay at the anchor base is increased to simulate the formation of a gap at the clay-anchor interface. In this case the flow of water may still take place along the interface as would occur during gradual separation of the clay and anchor. Such an adjustment would have little effect on the suctions generated at the centre of the footing, where conditions are still essentially undrained, but would result in more rapid dissipation of suctions close to the outside edge of the anchor. It should be noted that, as separation of the anchor and

clay beneath it is not explicitly modelled, the post failure behaviour will not be well replicated in the analyses.

7.3 Results

Finite element analyses were undertaken to back-analyse the uplift behaviour of the centrifuge model tests presented in Chapter 6. The output of these analyses is compared with the centrifuge experimental results for the cases of drained, undrained and partially drained behaviour. The results of the FE back-analysis are also related to prototype analyses for use in the design of foundations for transmission tower and related applications.

7.3.1 Drained and undrained analyses

In the centrifuge experimental study the lower and upper limits of anchor capacity corresponded to the cases of (i) an anchor founded on sand (breakaway case) and (ii) an anchor founded on clay uplifted at a high displacement rate (fully bonded case) respectively. These limiting cases were modelled in the (effective stress) FE analyses assuming (i) fully drained conditions and (ii) fully undrained conditions. For condition (i) separation at the soil-anchor interface was represented, through the use of elements at the anchor base with reduced stiffness, in the same manner as described in Chapter 3 (Section 3.2.3) for the preliminary total stress analyses. For each analysis, displacements at the top of the anchor stem were increased incrementally until failure occurred and up to a specified maximum displacement thereafter.

In these initial limiting analyses the (equivalent linear) soil stiffness values used were adjusted in order to obtain the highest degree of agreement between the predicted and measured load-displacement response. In the drained analyses, where breakaway behaviour was replicated (with use of elements with reduced vertical stiffness), the initial load displacement response of the anchor will be controlled by the stiffness of the sand backfill. In this case, a constant backfill Young's modulus (E') of 5 MPa yielded reasonable agreement with the centrifuge test response. This value is indicative of loose sand and is in reasonable agreement with the CPT data for the sand

backfill discussed in Chapter 5 (Section 5.12.1). In reality the shear modulus of the sand backfill will not be constant and will more realistically increase with depth. In the undrained analysis, the same value of E' was specified for the sand backfill and a shear modulus to T-bar strength ratio ($G/s_{uT\text{-}bar}$) of approximately 225 was adopted for the clay so as to model a linear increase in stiffness with depth. These adopted parameters provided good agreement with the initial load displacement response in each limiting case and were used in all subsequent analyses. Although this technique is not representative of the design process, whereby the above parameters would be adopted based on the results of in-situ or laboratory testing the main focus of these analyses relates to ultimate capacity and not to serviceability limits which, in many cases, are pre-defined.

The load displacement plots obtained from the FE analyses of a 30 mm anchor for the limiting cases of drained and undrained behaviour are shown in Figure 7.5, where they are compared with those from the equivalent test case in the centrifuge. It is evident that the anchor capacity for the breakaway condition and the fully bonded condition are reasonably replicated both relatively and in absolute magnitudes.

Results from the FE analyses may be presented in terms of the uplift capacity factor N_{uc} which is defined in Chapter 6 (Equation 6.8) as relating to the contribution to resistance provided at the anchor base (i.e. from the failure mechanism developed in the clay beneath the anchor during undrained loading). For the FE analyses the maximum under-base suction is inferred from the difference between the fully drained and fully undrained capacity. A comparison of the N_{uc} value calculated for each embedment ratio used in the centrifuge tests (averaged from tests at which v_f >30mm/s) with those obtained from the FE analyses is presented in Figure 7.6. As expected given the agreement in peak capacities, it would appear that the results of the centrifuge experiments are generally well represented by those of the undrained FE analyses. At an H/B value of 0.75 however the centrifuge data appears to underestimate the value of N_{uc}. This discrepancy may be related to the problems experienced with the variation of uplift velocity seen in the centrifuge tests at this embedment ratio where the anchor capacity may be underestimated at higher velocities (Section 6.2.2).

7.3.2 Partial drainage analyses

Between the two limiting cases of drained and undrained behaviour the anchor uplift response will be affected by the drainage of pore water below the footing and hence the dissipation of suction generated during uplift. This dissipation is essentially controlled by the drainage path length and the consolidation characteristics of the underlying clay. For this case a coupled consolidation analysis was used to model the rate dependent uplift response of the anchor. The soil parameters for these analyses were as specified in Table 7.1 except, for the reasons related to the formation of a gap at the anchor edge as discussed previously, the coefficient of permeability (k) was varied to achieve the best fit with the centrifuge results; this adjusted permeability is referred to as k^*. The time to failure (t_f) was specified for the consolidation analysis and was calculated from an assigned maximum displacement (w_f) for each analysis and the velocity (v_f) employed in each centrifuge test from:

$$t_f = \frac{w_f}{v_f} \tag{7.1}$$

Each increment in a SAFE consolidation analysis represents an increment of time. A total time step was specified that corresponded to the time required to achieve the total imposed displacement at the top of the anchor stem. In this way the analyses were performed such that the anchors were effectively uplifted at constant uplift velocities, as was the case in the centrifuge tests. SAFE employs an additional iterative process to that used in drained and undrained analyses which runs concurrently for a consolidation analysis. The time increment adopted for each step of the analysis is selected by the program during the iterative process, making it possible to facilitate large time increments at stages of the computation where the pore water pressures are changing slowly. For a given state, as the time increment is increased, so volume changes will increase and consequently changes in the effective stress caused by volume change increase. The program iterates to find time increments which, for all elements, give maximum changes in effective stress as a specified percentage of current mean normal effective stress (p'). Consolidation analyses were performed for uplift rates varying from 0.03mm/s to 100 mm/s.

A comparison of the load displacement behaviour under partially drained conditions for a 30 mm wide anchor founded on clay is shown in Figure 7.7. This figure illustrates the load displacement response for anchors uplifted at v_f =3 mm/s and 0.3mm/s (i.e. the velocities at which anchor capacity is observed to be between the limits of drained and undrained behaviour in Figure 6.10) where a modified clay permeability (k^*) of 1×10^{-7} m/s was employed in the SAFE analyses. It is apparent that broad agreement between the results of the FE back-analyses and the centrifuge experimental data is obtained. The trend for higher capacity at higher uplift velocities observed in the centrifuge tests is also replicated in the FE analyses and is related to a lower degree of pore water pressure dissipation at higher anchor velocity. The uplift capacity measured in the centrifuge test for an anchor uplifted at 3 mm/s, shown in Figure 7.7(b), is evidently lower than that predicted by the FE back-analysis. This discrepancy may be related to the initial degree of contact at the clay-anchor interface. Whilst every effort was made to ensure a high degree of contact between the anchor base and the clay during the experimental setup, anomalies may have occurred in cases where full contact was not achieved. In this case a lesser degree of initial contact may have resulted in some loss of adhesion at the soil anchor interface during uplift and hence the reduced peak capacity observed in Figure 7.7(b). In the FE analyses perfect contact is modelled at the soil anchor interface.

It is evident from Figure 7.7 that, as expected, the post peak reduction in uplift capacity with increased displacement observed in the centrifuge test data is not replicated by the FE back-analyses, which models full contact at the soil anchor interface. The best-fit permeability value of 1×10^{-7}m/s used in the analyses is significantly higher (by a factor of between 10 and 100) than is representative of the permeability of the kaolin clay used in the centrifuge tests (as seen in Chapter 4). Given the reasonable agreement in the peak capacities obtained from the centrifuge tests and from the FE analyses this would appear to support the presence of the suction relief mechanism, discussed earlier, whereby the formation of a gap at the anchor periphery will promote dissipation of suction and separation of the anchor from the underlying soil. The effect on the peak capacity of this tendency for increased dissipation of suctions is reasonably well replicated by the single modification to the clay's permeability employed in the FE back-analyses.

It is clear from comparison of the centrifuge load displacement data that where a greater contribution to resistance is provided by the generation of suction at high uplift velocity, the peak anchor capacity occurs at a larger displacement. This trend is also observed in the load displacement response obtained from the FE back-analyses and is shown clearly in Figure 7.8. Evidently at high uplift velocity, suctions are sustained at significantly greater displacements than those at which peak resistance is mobilised in the backfill sand. At uplift rates leading to undrained behaviour the peak anchor capacity (related to the generation of suction) may not be generated until displacements close to 10% of the anchor width.

7.3.3 Modified uplift velocity analyses

The FE back-analyses employing the modified permeability (k^*) were performed for each of the uplift velocities used in the centrifuge test program. The predicted variation of the uplift capacity factor, N_{uc} (derived using Equation 6.8) with uplift velocity for 30 and 60 mm anchors is plotted in Figure 7.9, where it is compared with the rate dependence of N_{uc} as measured in the centrifuge model tests. These predictions were performed employing a k^* value of 1×10^{-7} m/s and are seen to provide a reasonable representation of the measured rate of gain in N_{uc} with uplift velocity and also its dependence on the anchor width (B). Anchor behaviour is evidently fully drained at an uplift velocity of around 0.001 mm/s and fully undrained at values of v_f greater than about 30 mm/s. The highest degree of variation between the measured and predicted values is observed within the region of partially drained behaviour. Within this region the generation and dissipation of suction at the anchor base is most likely to be affected by the initial degree of contact between the anchor base and the underlying clay and this is reflected in the scatter seen in the experimental data. At the highest anchor uplift velocities the values of N_{uc} measured in the centrifuge test program are approximately 10-15% below those predicted in the SAFE finite element analyses. This variation can be attributed to the differences in the contact at the anchor-clay interface between the two data sets. In the FE analyses full contact is maintained across the base of the anchor at all times during uplift displacement. This will generally not be the case for uplift tests conducted in the centrifuge where, as highlighted in Chapter 6, dissipation of suctions at the edge of the anchor will lead to the formation of a gap at the anchor-clay interface and thus reduce the degree of contact at the anchor base. While the use of an increased permeability in

the FE analyses will evidently replicate the effects of this interface behaviour in the partially drained region, for the undrained case the FE analyses will always replicate the perfect contact (i.e. fully bonded) behaviour case.

The suctions inferred from each centrifuge test and those predicted from the corresponding effective stress FE back-analysis are directly compared in Figure 7.10 where it is seen that the modified permeability (k*) employed is applicable for both B=30mm and B=60mm. It is further highlighted in this figure that the greatest degree of agreement between the centrifuge test results and the FE analyses is obtained where smaller suctions are developed at the anchor base.

The predicted pore pressure plots and corresponding velocity fields for the partially drained case (v_f =0.03 mm/s) and the fully undrained case (v_f >30 mm/s) are shown for 30 mm anchors in Figure 7.11. The suctions generated at the base of the anchor during uplift are clearly evident as is the relationship between the magnitude of generated suctions and the extent of the failure mechanism developed in the underlying clay. A much larger volume of soil is involved in the failure region developed below the anchor uplifted at the higher velocity of 30 mm/s. It is also clearly evident that much higher suctions are developed at the anchor periphery in the undrained case where no dissipation has occurred prior to the peak uplift capacity. At the lower uplift velocity of 0.03 mm/s the effect of partial drainage results in dissipation of the higher suctions developing at the edge of the anchor and the variation of negative pore water pressure is less pronounced.

7.3.4 Prototype analyses

It has already been stated that correct modelling of the breakaway mechanism occurring under partially drained conditions is complex (and uncertain) and the adoption of simplified approach has examined the potential benefits of conducting a more conventional FE analysis (i.e. assuming full contact) but with a modified permeability ($k=k^*$). Given the agreement observed between the FE analyses and the experimental data, such an approach could reasonably be used to infer the displacement rate dependence of full scale transmission tower foundations in the field.

SAFE finite element analyses of the equivalent prototype foundation to the 30mm square anchor tested at 50g in the centrifuge (i.e. a 1.5m wide footing founded at a depth of 2.25m) were performed and are compared in Figure 7.12 with the corresponding FE back-analyses of the centrifuge tests. The close agreement displayed by the two sets of data verifies that the FE procedures employed were appropriate in modelling both the model and prototype cases. It is observed that, as may be expected from consideration of the centrifuge scaling laws for a consolidation process, equivalence between the centrifuge model and prototype occurs when v_f in the prototype is n =50 times less than in the scale model (e.g. a v_f of 3 mm/s in the model related to a prototype velocity of 0.06 mm/s).

FE analyses undertaken for 60 mm wide anchor, shown in Figure 7.9, have highlighted the effect of anchor width and base permeability on the base suction generated with increasing uplift velocity. Further analyses of two prototype foundation widths have been performed to assess the effects of the permeability of the underlying clay using values for k equal to 2×10^{-9} and 2×10^{-11} m/s (i.e. input values of $k^*=1\times10^{-7}$ and 1×10^{-9} m/s respectively). These values are considered to encompass a sufficiently broad range of soil permeabilities to generally represent those typically associated with transmission tower foundations in the UK. The resulting variations of N_{uc} with v_f are shown in Figure 7.13 and may be of use to designers in order to assess the contribution to uplift capacity developed at the base of a foundation. The influence of foundation width and clay permeability is demonstrated. A 3m footing founded on a clay with an in-situ permeability of around 2×10^{-11} m/s will exhibit fully undrained behaviour at a velocity of approximately 200 times less than an equivalent 1.5m footing founded on clay with a permeability of 2×10^{-9} m/s. Figure 7.13 also shows that, in each case, the relationship between N_{uc} and v_f becomes constant after the development of fully undrained suction at an N_{uc} value of approximately 6. At these undrained velocities, the strain rate dependence of the undrained shear strength of the underlying clay will lead to an increase in capacity with v_f. These increases are not modelled directly in the FE analyses but may be approximated through use of an operational undrained shear strength which is adjusted for strain rate effects.

Clark et al. (2006) describe a series of field tests to determine the magnitude, pattern and the rate at which loads are applied to electricity transmission tower foundation

systems following a simulated broken wire event and which consequently imposed a rapid change in load to be applied to the tower footing system. An uplift rate of between 20mm/s and 200mm/s was inferred from the measured loading rate applied to a 3m wide footing (highlighted on Figure 7.13). This is significantly in excess of the calculated uplift rates required for a fully undrained response (calculated for a range for typical clay permeabilities). It appears therefore that, for the broken cable design case, fully undrained conditions and hence full base suctions may generally be assumed for typical clays. It should be noted that further improvement in the prediction of uplift capacity at these rates requires the assessment of the rate dependence of the foundation clay's undrained shear strength. This is likely to further increase the overall capacity of transmission tower foundations under rapidly applied loads.

7.4 Summary

A series of FE back-analyses of model anchors subjected to uplift has revealed a clear relationship between the uplift resistance of anchors on clay and the uplift velocity, soil permeability and anchor width. The FE analyses are in reasonable agreement with the results of the centrifuge experimental study described in Chapter 6. No numerical predictions have previously been reported for footings uplifted at partially drained rates. The FE analyses conducted in this Chapter indicate that:

(i) Where separation between the anchor base and underlying clay is not modelled, the breakaway mechanism that occurs at uplift velocities slower that that required for fully undrained conditions will not be replicated.

(ii) A reduction factor of between one and two orders of magnitude applied to the permeability of the soil below an anchor in a conventional FE analysis (which does not permit separation between elements) provides a simple means of allowing for the increased rate of drainage arising from the loss in contact that would be expected to take place between the anchor base and the underlying clay at partially drained uplift rates. Back analyses of centrifuge uplift tests with coarse grained backfill overlying kaolin clay indicate that this factor was independent of the anchor velocity and width.

The FE analyses and centrifuge model tests presented indicate that the sudden load changes induced by a transmission tower cable breakage event will, in the case where the foundation is directly founded on clay, lead to an undrained response during uplift. The resulting suctions generated will provide increased resistance to failure which may be estimated through use of a conventional effective stress finite element analysis employing a modification to the permeability of the underlying soil.

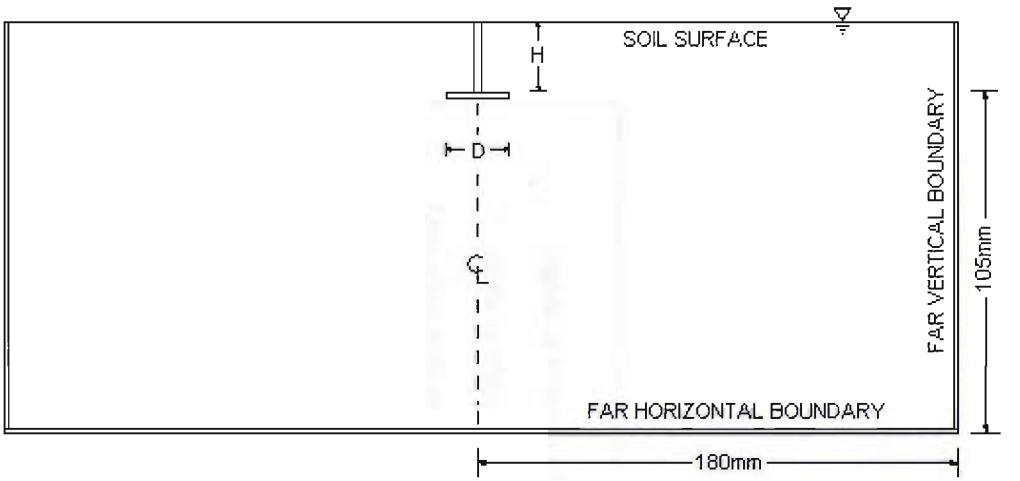

Figure 7.1 Problem boundaries for Finite Element back-analyses (not to scale)

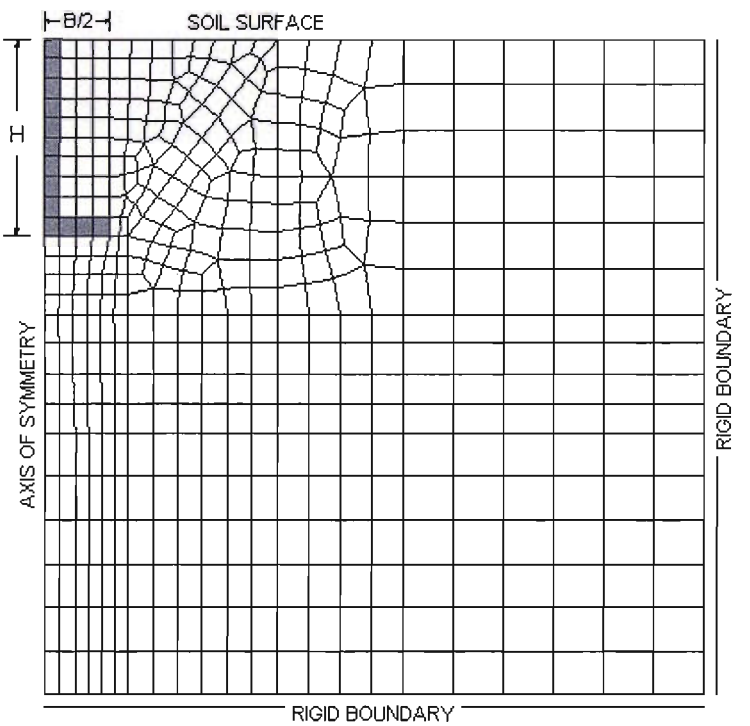

Figure 7.3 Finite Element mesh for effective stress back-analyses

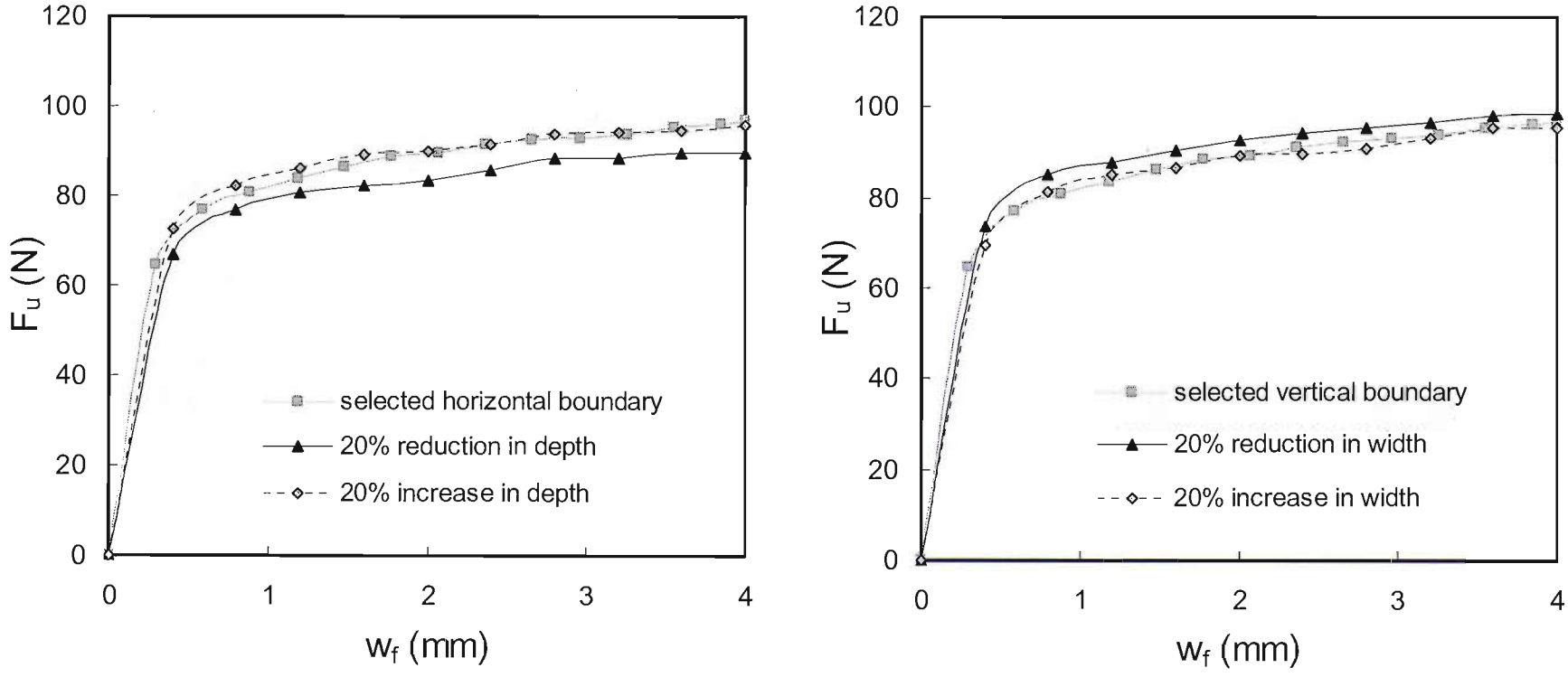

Figure 7.2 Verification of selected horizontal and vertical boundaries for the FE back-analyses

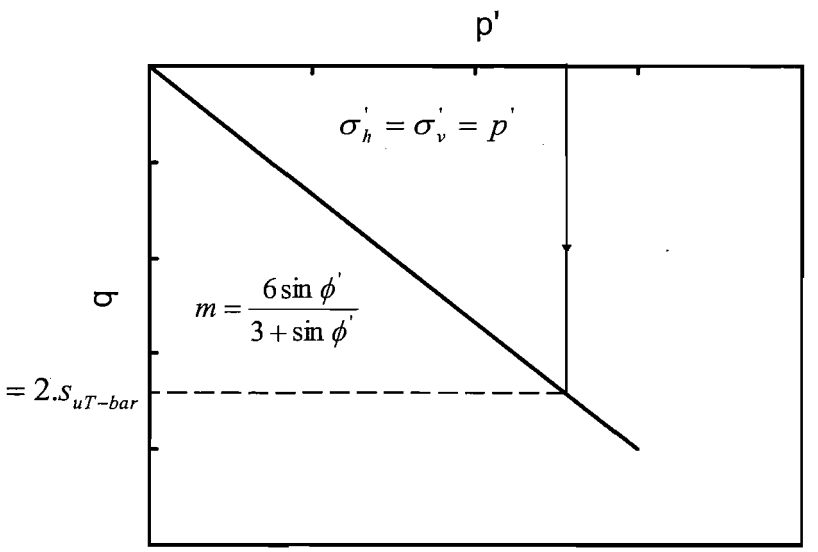

Figure 7.4 Modelled response (in q-p' space) of centrifuge clay (kaolin)

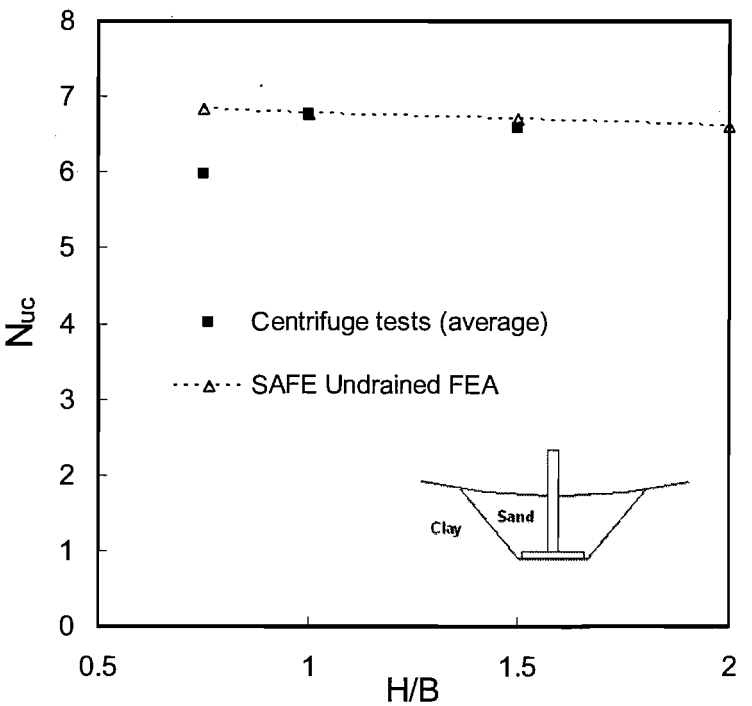

Figure 7.6 Comparison of uplift factors N_{uc} from centrifuge tests and undrained FE back-analyses

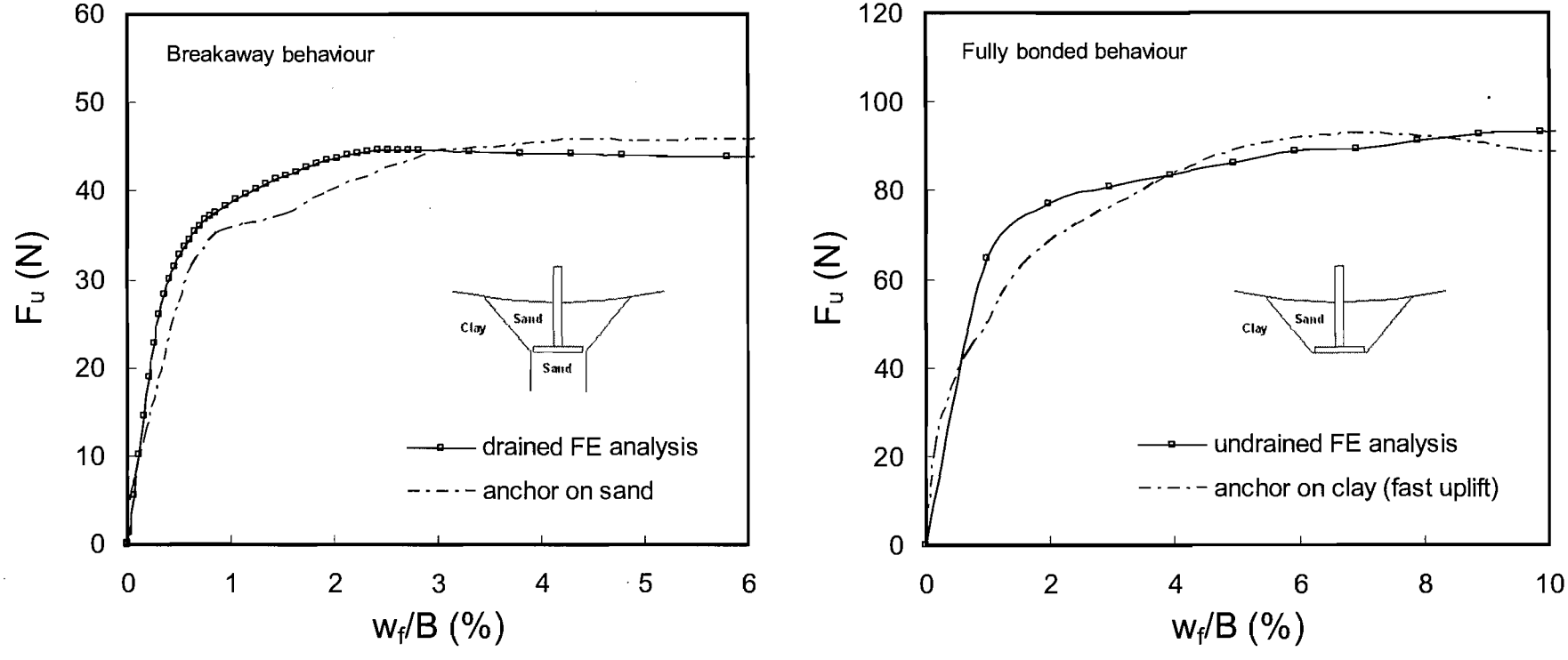

(a) Drained behaviour case

(b) Undrained behaviour case

Figure 7.5 Drained and undrained load displacement behaviour for 30 mm anchor

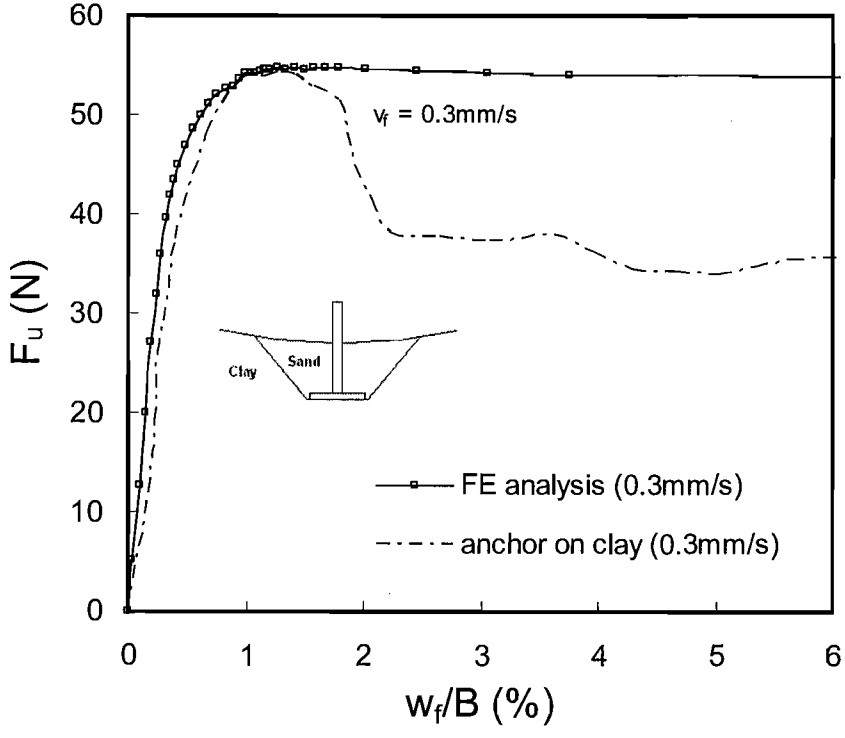

(a) Anchor on clay v_f=0.3 mm/s

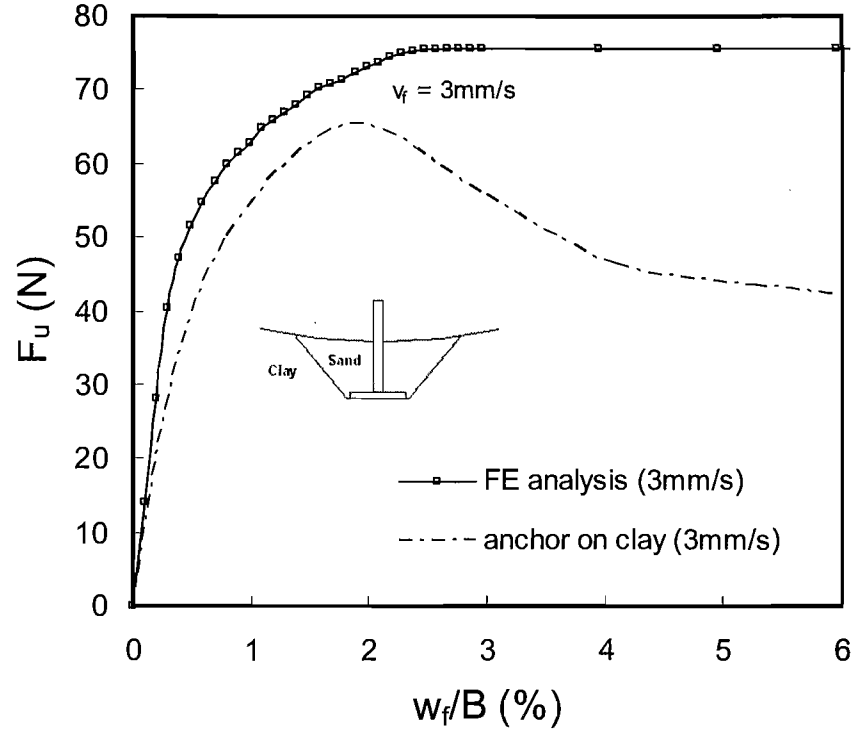

(b) Anchor on clay v_f=3 mm/s

Figure 7.7 Partially drained load displacement behaviour for 30 mm anchor

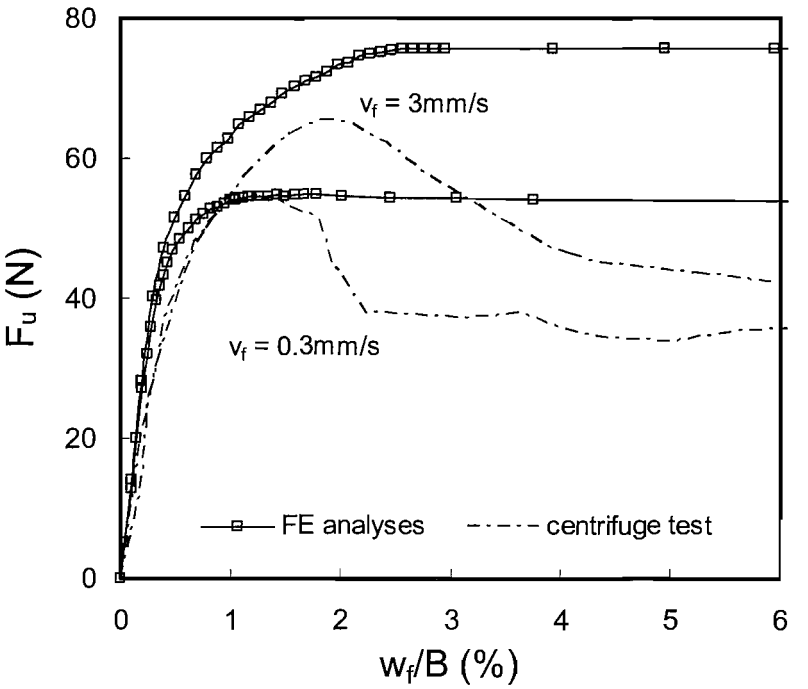

Figure 7.8 Comparison of partially drained load displacement behaviour

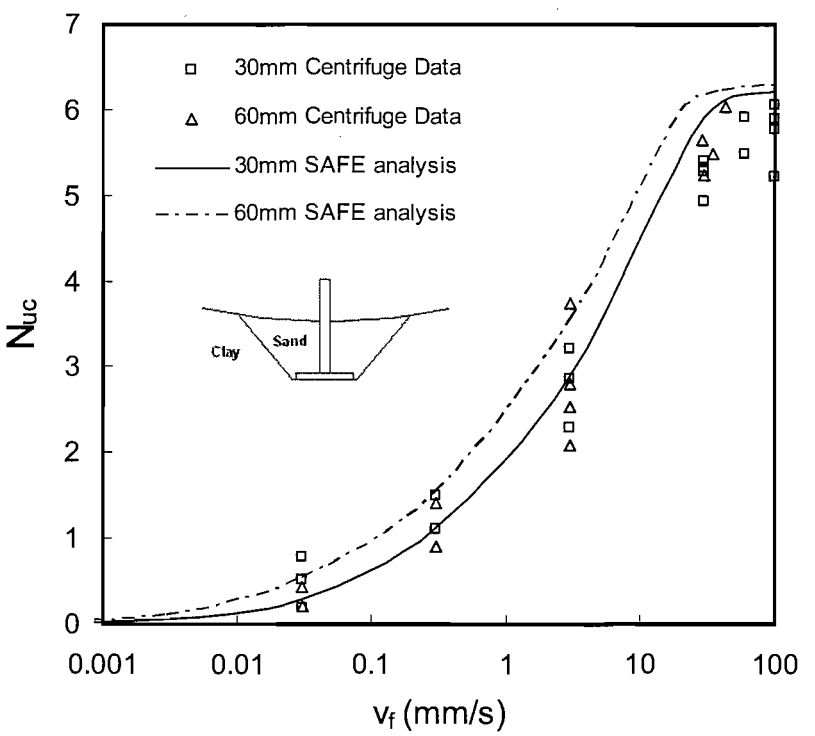

Figure 7.9 Variation of the uplift capacity factor N_{uc} predicted from SAFE analyses

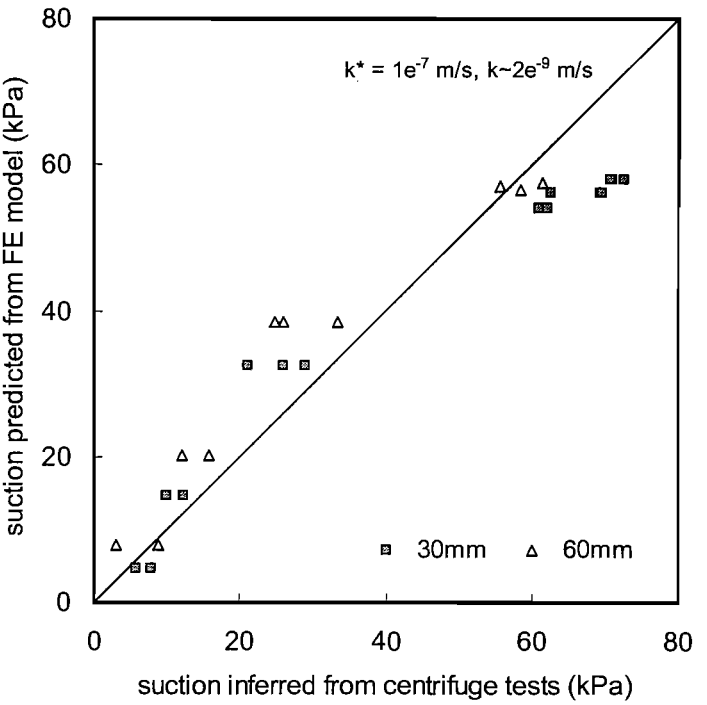

Figure 7.10 Comparison of predicted and inferred suction for B=30mm and B=60mm

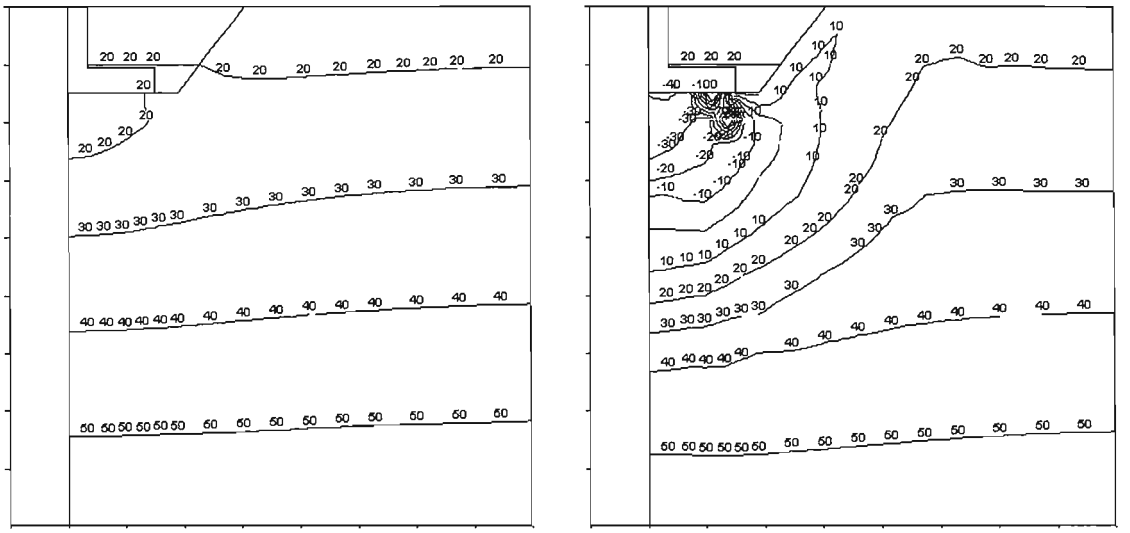

Pore pressure contours

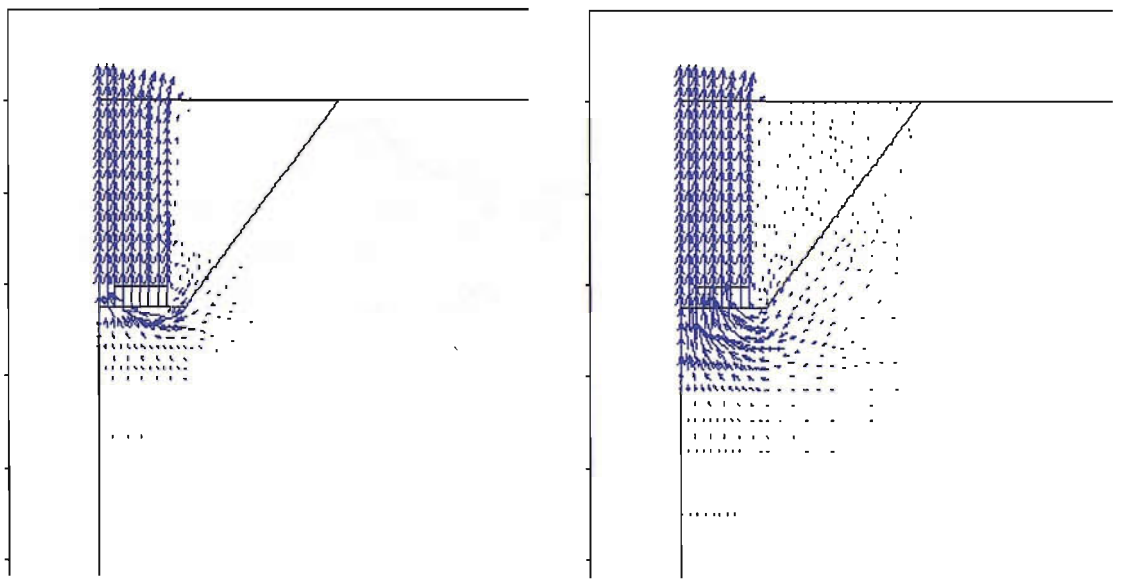

Velocity fields

(a) $v_f = 0.03$ mm/s (b) $v_f = 30$ mm/s

Figure 7.11 Predicted pore water pressure and velocity fields for sand backfilled anchors

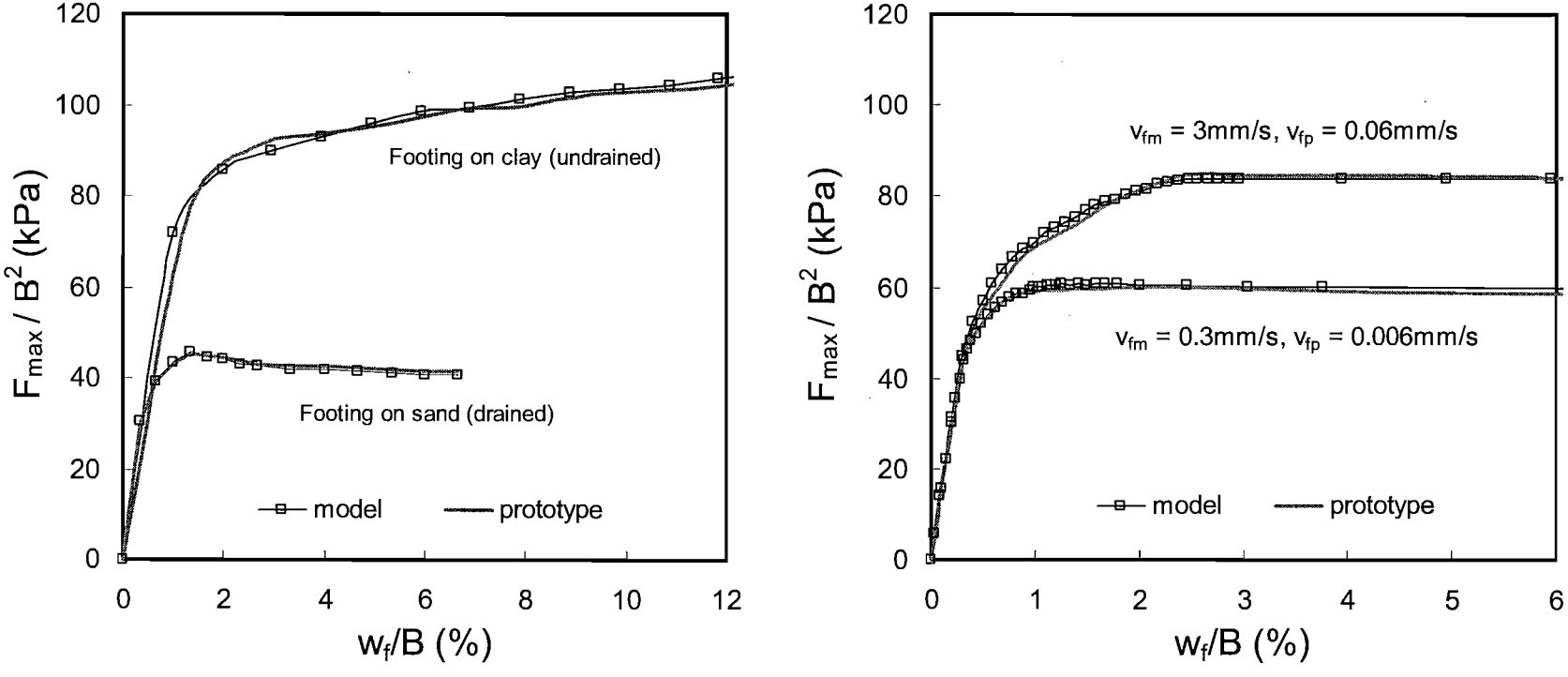

(a) drained/undrained cases

(b) partially drained cases

Figure 7.12 Comparison of predicted load displacement behaviour from model and prototype scale analyses

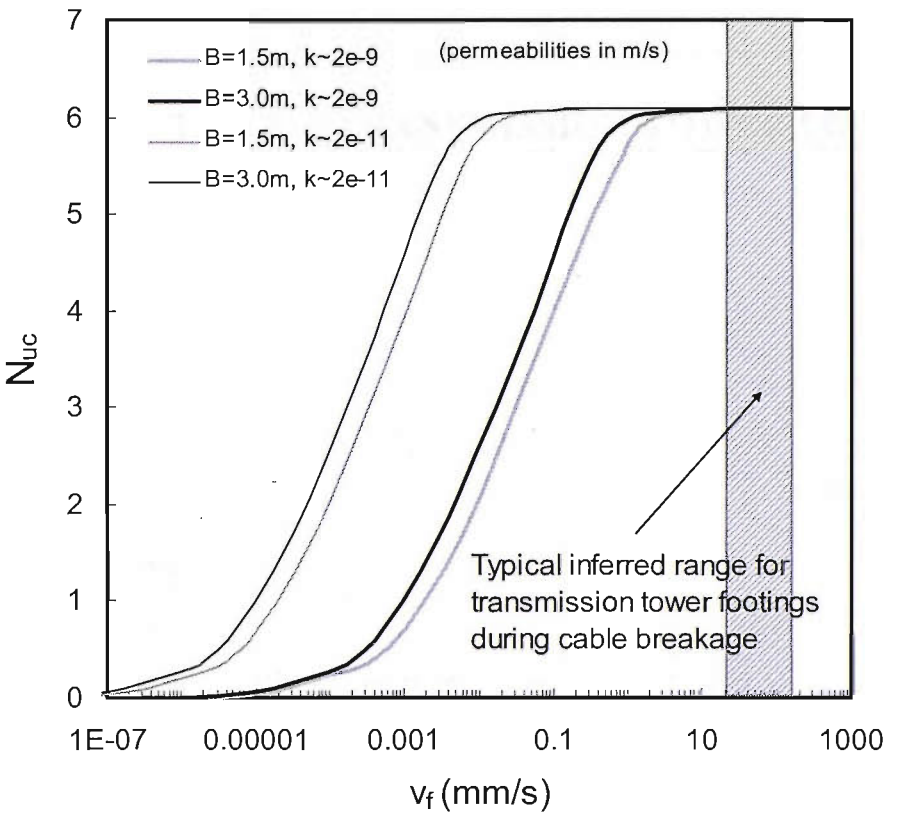

Figure 7.13 Effect of anchor width and base permeability on the variation of uplift capacity with increasing uplift velocity

Chapter 8

UPLIFT OF TRANSMISSION TOWER FOOTINGS

8.1 Introduction

It has been previously established from data presented by Clark et al. (2006) and the results of the effective stress finite element analyses presented in Chapter 7 that the loading rates transmitted to transmission tower footings are rapid and lead essentially to an undrained response for footings founded on a typical clay soil. Many transmission tower foundations are embedded in clay and therefore, given that the in-service uplift loads are usually applied rapidly, there is considerable interest in quantifying the contribution to uplift resistance of the suction that can develop at the under-side of the footing. Field tests reported by Yazdanbod et al. (1987) have had some success in measuring suctions at the base of footings subjected to uplift, while the investigations described in Chapter 6 have employed centrifuge modelling techniques to examine the influence of uplift rate on plate anchors founded on clay. These centrifuge experiments have inferred a rate dependence of under-base resistance by comparing the response of plate anchors founded on clay and those founded on sand. This chapter presents results from a series of centrifuge tests which provide direct measurements of the suction developed at the footing base and enables definitive conclusions to be drawn regarding the contribution to uplift performance provided at the base of a footing founded on clay at a variety of uplift rates. The benefits of using finite element analyses to model the variation of uplift capacity at increasing uplift velocities (as presented in Chapter 7) are also applied, where analyses are undertaken to incorporate the influence of strain rate on the undrained shear strength of the clay underlying the footing.

8.2 Overview of Uplift Test Results

The results of the transmission tower footing test series (TTFS) are presented. Tests have been conducted according to the programme outlined in Chapter 5 (Section 5.7.3).

Post processed load and displacement data for each footing uplift test conducted is collected in Appendix D, Figure D1(a-l) for the TTFS centrifuge test sample. These figures show the development of uplift force, vertical displacement and, where applicable, pore pressure measurement at the base of the footing with time for each test. The following points are noted:

- An increase in displacement rate is observed during the generation of peak load for uplift test 6. During testing the uplifted footing is monitored via a CCTV link inside the centrifuge through which no such change was witnessed. In this case the increase may be attributed to a 'spike' in the logged data signal.
- In all tests using the modified footing, the response of the pore pressure transducer (PPTT) located in the footing base was rapid and maximum suctions generally correspond with the generation of peak load. Pore pressures below -100 kPa were recorded as expected for Tests 2 and 8 (v_f =100 mm/s), indicating that cavitation did not occur before this point and that the device remained fully saturated throughout each test.

In order to facilitate interpretation the results of the experimental study will be separated into two categories (i) footings on sand, presented in Table 8.1 and (ii) footings on clay, presented in Table 8.2. In case (i) some results are taken from plate anchor series 1 (PASB) for comparison and these results are reproduced in Table 8.1 for ease of reference. The test geometries relating to each case (i) and (ii) are shown in Figure 5.13.

Table 8.1 Summary of results for footings on sand (TTFS & PASB)

Footings on sand							
Test	B	θ	H/B	v_f	F_{up}	w_p	w_p/B
(-)	mm	°		(mm/s)	(N)	(mm)	(%)
PASB-S1-3	30	0	1.5	3	43.8	0.9	3.2
PASB-S3-10	30	0	1.5	3	45.1	1.1	3.3
PASB-S2-7	45	0	1	3	89	1.8	4
PASB-S3-17	60	0	0.75	3	113.7	2.5	4.2
TTFS-S1-1	40	9.3	1.6	3	139.9	2.4	6
TTFS-S1-4	40	0	1.6	3	148.2	2.8	7

Table 8.2 Summary of results for footings on clay (TTFS)

Footings on clay (B=40mm for all footings)							
Test	θ	v_f	F_{up}	w_p	u_i	u_{min}	s (measured)
(-)	°	(mm/s)	(N)	(mm)	(kPa)	(kPa)	(kPa)
TTFS-S1-2	0	30	405.12	3.8	29.8	-96.81	126.61
TTFS-S1-3	9.3	30	314.4	3	-	-	-
TTFS-S1-5	0	3	258.38	1.3	29.4	-37.15	66.55
TTFS-S1-6	0	0.1	171.2	2.72	28.1	16.0	12.1
TTFS-S1-7	9.3	3	198.56	1.8	-	-	-
TTFS-S1-8	0	100	430.54	3.2	29.3	-108.37	137.47

A preliminary overview of Tables 8.1 and 8.2 reveals that:

i. The uplift resistance of footings founded on clay may be up to approximately 3 times greater than for the equivalent footing founded on sand. This increase in capacity is of a similar magnitude to that observed in Chapter 6 for plate anchors on clay.

ii. The uplift capacity for straight and inclined footings founded on sand is in reasonably close agreement indicating that there is no significant effect on the failure mechanism above the footing that can be attributed to a footing inclination of 9.3°.

iii. The uplift capacity for inclined footings on clay is significantly less than that for straight footings at corresponding uplift rates. This difference becomes more pronounced with increasing uplift rate and is presumably related to the stability of the footing as discussed for plate anchors in Chapter 6.

iv. The overall measured change in pore pressure increases significantly with increasing uplift rate

v. At the slowest uplift rate of 0.1 mm/s the generation of negative pore pressure at the base indicates that footing behaviour is partially undrained at this uplift rate

8.3 Uplift of Footings on Sand

Although the primary focus of the transmission tower footing test series is to examine the response to uplift of footings on clay, two uplift tests were performed on footings founded on sand to assist interpretation of the contribution of the clay to the uplift resistance. The peak uplift resistance (F_{up}) and the displacement corresponding to this resistance (w_p) for these two tests are compared with the results of uplift tests on plate anchors founded on sand from PASB in Table 8.1. The uplift capacity factor, N_{us}, may be derived for each footing according to Equation 6.1, which is modified to negate the contribution to resistance of the footing weight and allow comparison of results from the two test series:

$$N_{us} = \frac{F_{up} - W_f}{B^2 \gamma' H} \tag{8.1}$$

where W_f is the weight of the footing (at an acceleration of 50*g*) and assuming a submerged unit weight of 8 kN/m^3 for the backfill sand. Equation 8.1 is of the same form to that proposed by Kulhawy et al. (1987) to assess the uplift capacity of field scale foundations in loose, medium dense and dense sand. Values of N_{us} for the plate anchors (PASB) and model tower footings (TTFS) are plotted in Figure 8.1 against embedment ratio (H/B) where they are compared with the results of Kulhawy et al. (1987) for loose and medium dense backfill. It is evident that the variation with H/B in the measured values of N_{us} is similar to that shown by Kulhawy et al. for loose sand. This trend is in keeping with the expectation that the backfilling procedure, which involved simple placement of the sand by hand (with care taken to avoid any disturbance to the footing stem) led to the formation of a loose deposit. It is also observed that values of N_{us} calculated for the transmission tower footings are comparable with those of the plate anchors, which have been shown in Chapter 6 to be

well represented by the limit equilibrium solutions of Murray and Geddes (1987). It is therefore suggested that the additional effort required to construct a pyramidal footing may be un-necessary where the footing weight is not a significant portion of the uplift resistance.

8.4 Uplift of Footings on Clay

The uplift response of transmission tower footings founded on clay is examined in the following sections. The peak uplift resistance (F_{up}), measured peak suction pressure (s) and the displacement at peak load (w_p) for these tests are detailed in Table 8.2.

8.4.1 Load displacement response

The variations of normalised uplift resistance (q_{fu}) and pore pressure (u_b, measured at the footing base) are plotted with normalised displacement (w_f/B) for each uplift velocity (0.1, 3, 30 and 100 mm/s) in Figure 8.2(a-d). Also plotted in each figure is the variation of q_{fu} with w/B indicated by the same (straight) pyramidal footing on sand.

The load displacement response for a footing on clay uplifted at 0.1mm/s, shown in Figure 8.2(a), is comparable to that for the same footing founded on sand indicating that little resistance to uplift is provided at the clay base. It may therefore be inferred that at a velocity of 0.1mm/s the majority of the negative pore pressures that may be generated below the footing during uplift are dissipated and separation of the base from the underlying clay occurs at failure. The pore pressures measured by the PPTT are in keeping with this trend and indicate a maximum reduction in pressure of approximately 10 kPa at w_f/B of around 2%.

The contribution to uplift resistance of the clay at the base of the footing can be seen in Figure 8.2(b) which shows the uplift behaviour at v_f =3 mm/s. A clear difference is seen in the load displacement behaviour of the footing on clay to that of the same footing on sand. A higher peak resistance for the footing on clay is seen to coincide with an overall reduction in pressure at the base of the footing of around 60 kPa at a w_f/B of approximately 3.5%. After this initial peak the footing resistance reduces with

increasing displacement as the maximum sustainable suction is dissipated and at a w_f/B value of around 5% the uplift resistance is comparable to that for the same footing on sand. No clay was seen to have adhered to the base of this footing or to the footing tested at 0.1mm/s when examined on completion of loading, suggesting that separation at the clay-footing interface occurred at peak resistance.

The effect of the clay at the footing base is further highlighted at velocities of 30 and 100 mm/s, shown in Figure 8.2(c) and (d) respectively. The capacity of these footings is approximately 2.5 times greater than that of the footing on sand but is only reached at a relatively large normalised footing displacement (w_f/B) of between 8 and 10%. Despite this the initial uplift stiffness of these footings is significantly higher than those of the equivalent footing founded on sand. The variation with w/B of measured pore pressure beneath the centre of the footings is similar to the uplift resistance, verifying the significant contribution of under-base suction. Evidently at high velocities separation of the footing base and underlying clay does not take place and failure is controlled by the undrained strength of the clay underneath the footing. A conical wedge of clay with a depth of approximately B/2 was seen attached to the base of these footings after their removal from the centrifuge suggesting that failure arose due to an inverted bearing capacity mechanism within the clay.

8.4.2 Peak uplift capacity and measured suction

The variation with footing velocity (v_f) of the uplift capacity (q_{fu}) and the maximum under-base suction (s_{max}) is presented in Figure 8.3. A significant increase in q_{fu} with v_f is evident across the range of uplift rates considered, with the largest gain in capacity occurring for v_f between 3 and 30 mm/s. It is seen that suctions begin to contribute to the uplift resistance at velocities of around 0.1mm/s and a steady increase in s_{max} is observed with v_f in the range 0.1-30 mm/s. As highlighted previously in Chapter 6 for plate anchors founded on clay, partial consolidation is likely to be the dominant mechanism controlling the magnitude of the suction that can be generated in this velocity range. The rate of gain in capacity decreases above a velocity of 30 mm/s to a level which is approximately consistent with increases due to viscous effects in the clay below the anchor. It may be inferred therefore that at $v_f \geq 30$ mm/s conditions become essentially fully undrained and partial drainage does not

occur below the footing. Maximum suctions measured at these high velocities are large, approximately 130kPa for v_f=100 mm/s, with absolute pore pressures measured directly below the footing of around -100kPa. These maximum recorded suctions are in the region of 6-6.5$s_{uT\text{-}bar}$ measured at the footing base, which is similar to that seen in Chapter 6 for approximated maximum suction below plate anchors founded on clay. A v_f value of 30mm/s, which is equivalent to a normalised velocity of approximately 10000, is much higher than required for undrained conditions to be established when footings are loaded in compression (Booker & Small 1986). This observation has previously been noted in Chapter 6 with relation to plate anchors founded on clay, where it was suggested that the difference arises because the uplift mode provides easier access for relief of excess pore pressures generated at the base of the footing.

In Chapter 6 suctions developed at the base of the anchors were estimated by comparison of the uplift capacity of footings founded on clay and those founded on sand. Figure 8.4 presents a comparison of maximum suction approximated using Equations 6.6 and 6.7 and those measured directly at the centre of the footing base. Good agreement is seen between the measured and approximated suctions for $v_f \leq 3$ mm/s however at velocities greater than 3 mm/s the approximated suctions are higher than those measured directly. This discrepancy can be related to the non-uniform distribution of contact pressure across the base of a rigid foundation under undrained loading as described by Tomlinson (2001). The suction developed at the centre of the footing, where the PPTT is located, is at the low point of a parabolic pore pressure distribution and hence the measured value will be lower than the average pressure across the entire footing width. If, at any given velocity, the difference between the uplift resistance and the measured suction of a footing on clay is assumed to be approximately equal to the uplift resistance of a footing on sand then, as shown on Figure 8.3, this difference may be predicted with reasonable accuracy if the measured base suction was factored by 4/3.

It should be noted that minimum absolute pore pressures of -97 kPa and -108 kPa were recorded in the footing tests performed at 30mm/s and 100mm/s respectively. As seen in Figures 8.2(c) and 8.2(d), the measured pore pressures increased again as the overall footing resistance reduced after reaching peak capacity. It can therefore be

inferred that cavitation of these sensors did not occur and that these measured pore pressures are reliable.

8.4.3 Generalisation of uplift test data

The reverse bearing capacity factors (N_{uc}) are calculated according to Equation 6.8 for each uplift test and plotted with anchor velocity in Figure 8.5 where they are compared with N_{uc} values from the PASB test series. In each case the uplift capacity factors are calculated using the strain rate corrected T-bar undrained shear strength assessed from Equation 6.9 and thus the variation of N_{uc} is thought to be independent of the effects of clay viscosity. It is evident that the values of N_{uc} evaluated from each of the studies display a high degree of conformity across both footing width and type, illustrating the legitimacy of the reverse bearing capacity factor in assessing the increased contribution of base resistance with increasing uplift rate of shallow footings. As would be expected, given that that factor N_{uc} represents the contribution to uplift resistance mobilised at the base of the foundation only, a similar variation of N_{uc} is observed for the pyramidal footings as has been seen previously for plate anchors in Chapter 6. For this reason the trends associated with development of the uplift capacity factor N_{uc} discussed in Chapter 6 are also thought to be applicable to other foundation geometries.

8.4.4 Influence of anchor inclination

The maximum uplift capacity is plotted against footing inclination in Figure 8.6 for uplift tests undertaken at 3 and 30 mm/s on footings founded on clay and on sand. For footings founded on clay a decrease in q_{fu} is observed with increasing footing inclination at both uplift rates. The footing connection used in the TTFS test series was similar to that described in Chapter 6 (Section 6.2.7) for the plate anchor test series. As such, in the case of the inclined footing, this non-rigid connection may result in simultaneous rotation of the footing at the head and at the leading edge of the base of the footing during uplift which may impede the development of suction. The observed decrease in uplift capacity is greater at v_f =30 mm/s, where the suction generated would be higher, indicates that this assumption is valid. There appears to be no significant difference in uplift capacity with increasing inclination for footings founded directly on sand, where no suctions would be expected to develop.

8.5 Finite Element Back-Analysis

The finite element analyses described in Chapter 7 show that the uplift loading rate applied to transmission tower footings following a broken-wire event will lead to an undrained response in the clay at the base of the footing. In order to demonstrate the assessment of the operational undrained strength appropriate for such an event, a further series of FE back-analyses of the centrifuge footing uplift tests were performed using SAFE and assuming an undrained response in the underlying clay. The FE approach is a convenient method of assessing the uplift capacity of foundations where no analytical solutions are available for the particular geometries investigated, in this case in the centrifuge model tests (i.e. for a footing founded on clay and backfilled with loose sand).

8.5.1 The FE model

The mesh developed for the axisymmetrical back-analysis of the pyramidal footing is shown in Figure 8.7 and comprised of 660 8-noded quadrilateral elements each with 4 Gauss points. The elements were biased to provide a significantly higher mesh density in the regions around the anchor where the greatest changes in stress, and therefore strain, would occur during the imposed displacement. Model scale dimensions were used with all unit weights factored by n = 50 (the acceleration level used in the centrifuge tests). As described in Chapters 3 and 7, the square base of the footing was modelled as an equivalent circular area and the footing was loaded to failure incrementally by applying a vertical displacement to the nodes at the top of the footing stem.

The centrifuge sand and clay were both assumed to behave as isotropic elastic-perfectly plastic materials. The sand was free draining with a friction angle (ϕ) of 32° and the clay strength was defined in terms of its total shear strength (s_u). A constant E_u/s_u ratio equal to 67 was assumed for the clay in all the analyses.

Given that the stress path experienced in the clay underlying the footing base during uplift is expected to be broadly similar to that imposed during triaxial extension, the undrained shear strength ratio (s_u/σ'_v) was taken as being equal to that derived for the

triaxial extension tests undertaken on samples of kaolin clay and described in Chapter 4, for which:

$$\frac{s_{ute}}{\sigma_v'} = 0.13.OCR^{0.8} \qquad (8.2)$$

This assumption implied that for the OCR profile in the clay beneath the footings, shown in Figure 5.35(a), the undrained shear strength increased approximately linearly with depth below the footing. It should also be noted that for the reasons stated in Chapter 5 (Section 5.11.5) the use of an undrained shear strength derived from triaxial extension tests may not be representative of the soil behaviour across the entire developed failure mechanism (if similarity is assumed between uplift and bearing capacity behaviour for a fully bonded anchor). In this case, given the conclusions drawn in Chapter 6 (Section 6.2.5) with regard to the developed undrained failure mechanism, it is thought that the use of an undrained shear strength in triaxial extension will be representative for soil deformation directly below the footing base.

For the back analyses of footings uplifted at 30 and 100 mm/s it has been shown in Chapter 6 that corrections should be made to account for the strain rate dependency of the undrained shear strength of the clay. Atkinson (2000) has shown that the average operational vertical strain beneath a footing loaded in compression is approximately $w_f/3B$. It follows that the average strain rate would be approximately equal to $v_f/3B$ for a footing undergoing uplift with no loss of suction at the underside of the footing base (i.e. the fully bonded behaviour case). The rate dependence of the undrained shear strength of kaolin clay was assessed in Chapter 4 using Equation 4.5, which is applied for the centrifuge uplift tests as being equal to:

$$s_{ute} = s_{uref}\left(\frac{v_f/3B}{\dot{\varepsilon}_{ref}}\right)^{0.05} \quad with\ \dot{\varepsilon}_{ref} = 0.0001\ \%/s \qquad (8.3)$$

where s_{uref} is the undrained shear strength implied from Equation 8.2. The strength enhancement assessed from Equation 8.3 implies undrained shear strengths in triaxial

extension, at a depth of B/2 below the footing base, of equal to 31 kPa at v_f = 30 mm/s and 33 kPa at v_f = 100 mm/s. These values were used in the respective FE back analyses for footings uplifted at these velocities.

8.5.2 Undrained capacity

The load displacement response recorded for pyramidal footings founded on sand and on clay at (undrained) uplift velocities of 30mm/s and 100mm/s are compared on Figure 8.8 with predictions obtained from the FE back analyses using the soil parameters outlined previously. Back-analyses of the footing on sand indicated acceptable agreement with the observed response for a Young's modulus (E) value of 4 MPa. This value was then used for the sand backfill in the FE analyses for footings founded on clay.

Adequate agreement is seen between the measured and predicted load displacement response shown in Figure 8.8 for footings founded on clay at uplift velocities of 30 and 100 mm/s. As described previously in Chapter 7, due to the mechanism developed at the footing-clay interface in the centrifuge model tests the post peak load displacement behaviour measured in the centrifuge is not replicated in the FE analyses. The ultimate uplift capacity measured in the centrifuge uplift tests is however seen to be reasonably well represented by the FE predictions at each uplift velocity. This indicates that the operational strength, at least for the cases examined, is close to the undrained strength measured in triaxial extension but with (a significant) correction made for the viscous rate effects. The best-fit E_u/s_u ratio of 67 is considerably lower than a typical ratio of 200 to 500 generally employed in the settlement estimates of foundations in compression (Poulos et al. 2001). This lower ratio is however representative of the large displacements required to attain peak capacity observed in the measured footing response and is consistent with that measured in triaxial extension tests (shown in Figure 4.11b) for axial strains greater than approximately 1%.

8.6 Summary

Centrifuge tests have shown that the uplift stiffness and capacity of a footing founded on clay is strongly rate dependent and is related to the degree of dissipation of suctions at the footing-clay interface. Specifically it has been observed that:

i. The uplift capacity of a footing founded on clay may be up to 3 times the capacity of an equivalent footing on sand. Suctions greater than 130 kPa were recorded at undrained uplift velocities and are likely related to the undrained shear strength of the underlying clay.
ii. The initial uplift stiffness of a footing founded on clay is significantly higher than that of the equivalent footing founded on sand
iii. For footing inclinations related to those used in transmission tower applications, there appears to be no influence of the footing inclination on the uplift capacity of a footing founded on sand.

Finite element back-analyses of centrifuge model tests at higher (undrained) rates of displacement indicated that incorporation of the assumed rate dependence of stiffness and undrained strength occurring at high uplift velocities, as inferred from the triaxial extension tests presented in Chapter 4, is necessary if realistic predictions of uplift performance are to be achieved using a conventional finite element analysis.

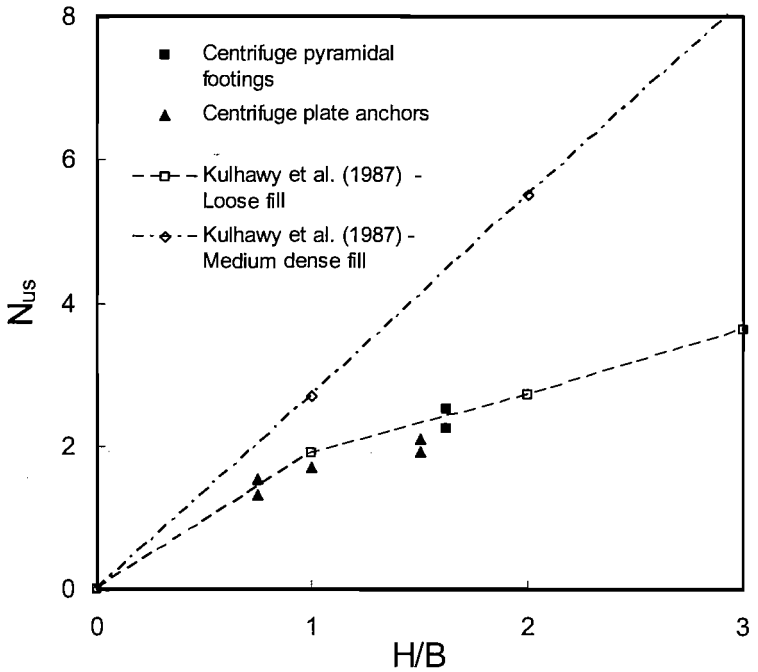

Figure 8.1 Comparison of N_{us} factor from centrifuge tests on pyramidal footings and plate anchors

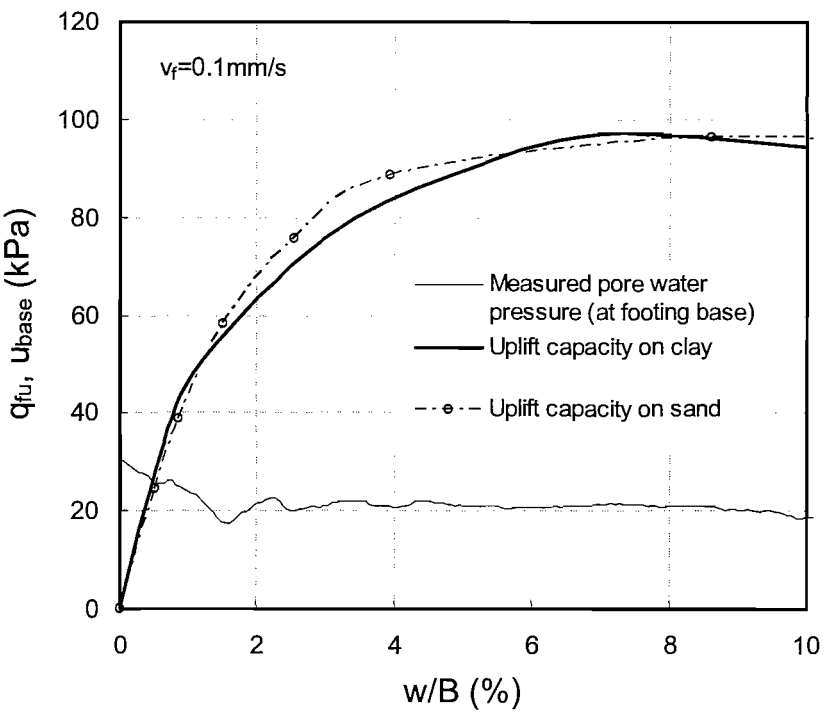

Figure 8.2(a) Variation of uplift resistance and measured pore water pressure with displacement for v_f =0.1 mm/s

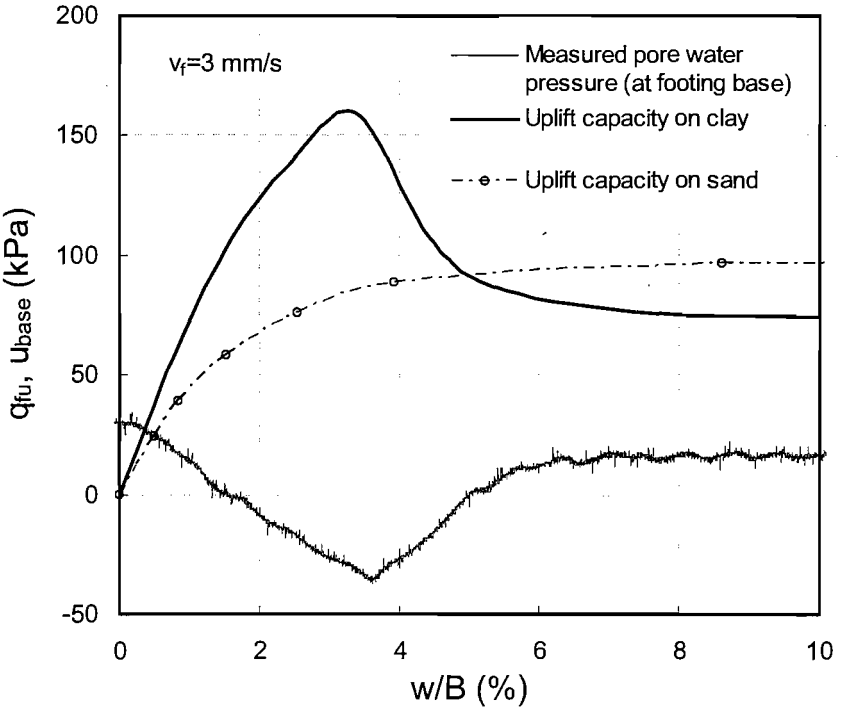

Figure 8.2(b) Variation of uplift resistance and measured pore water pressure with displacement for v_f =3 mm/s

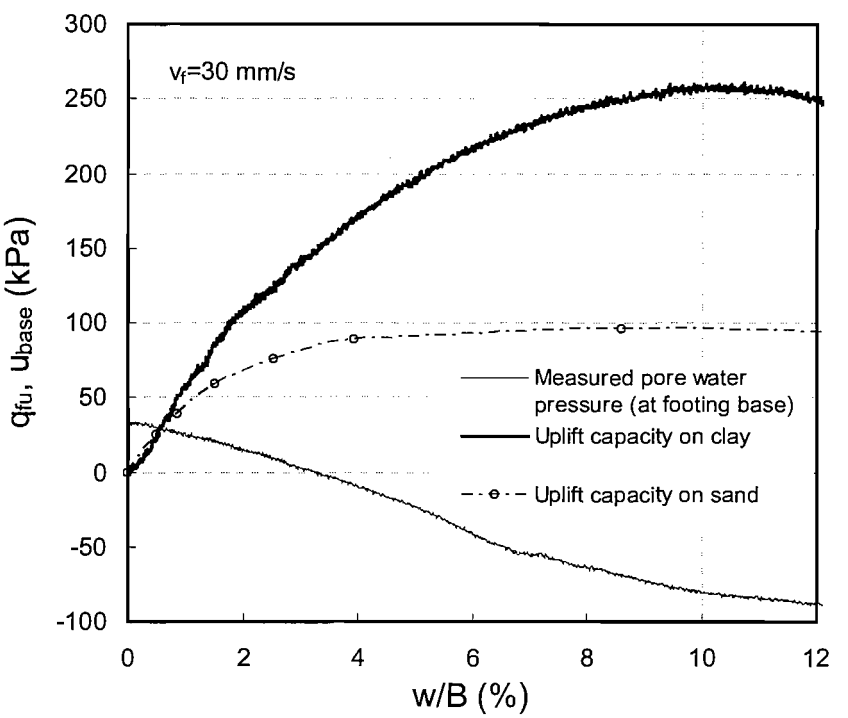

Figure 8.2(c) Variation of uplift resistance and measured pore water pressure with displacement for v_f =30 mm/s

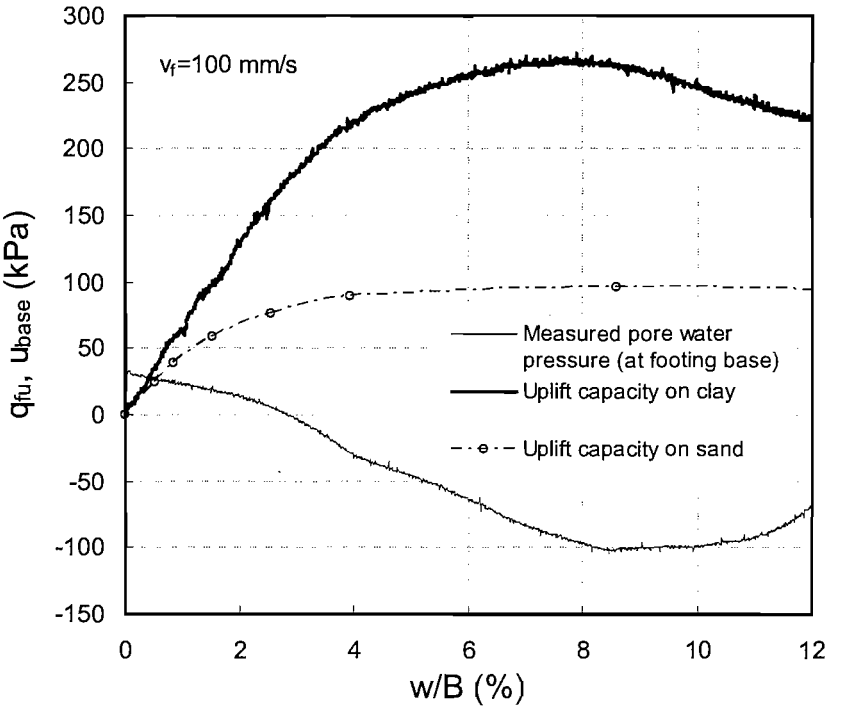

Figure 8.2(d) Variation of uplift resistance and measured pore water pressure with displacement for v_f =100 mm/s

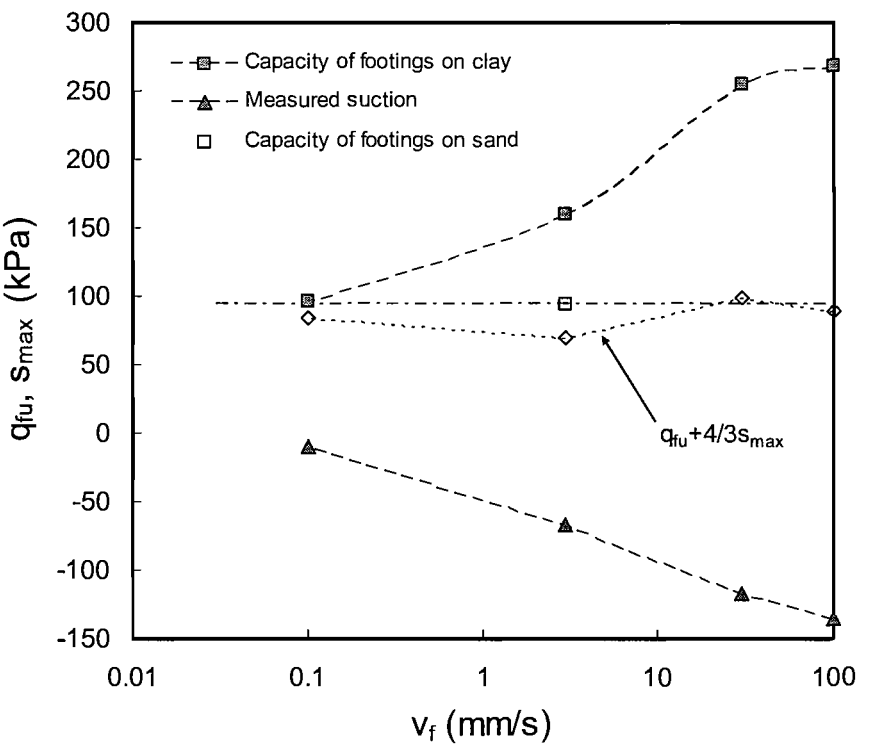

Figure 8.3 Footing capacity and measured suction with uplift velocity for footings founded on clay and sand

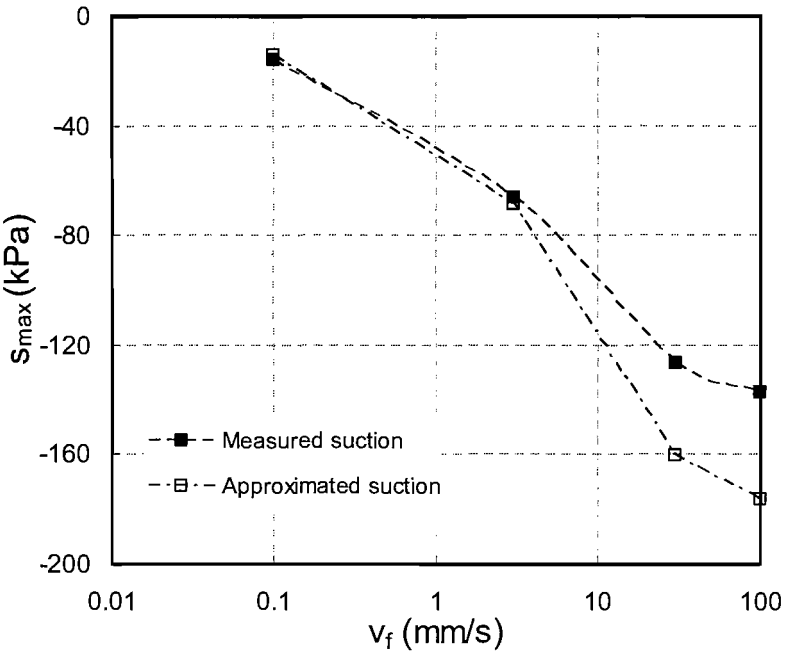

Figure 8.4 Comparison of measured and approximated suction for footings founded on clay

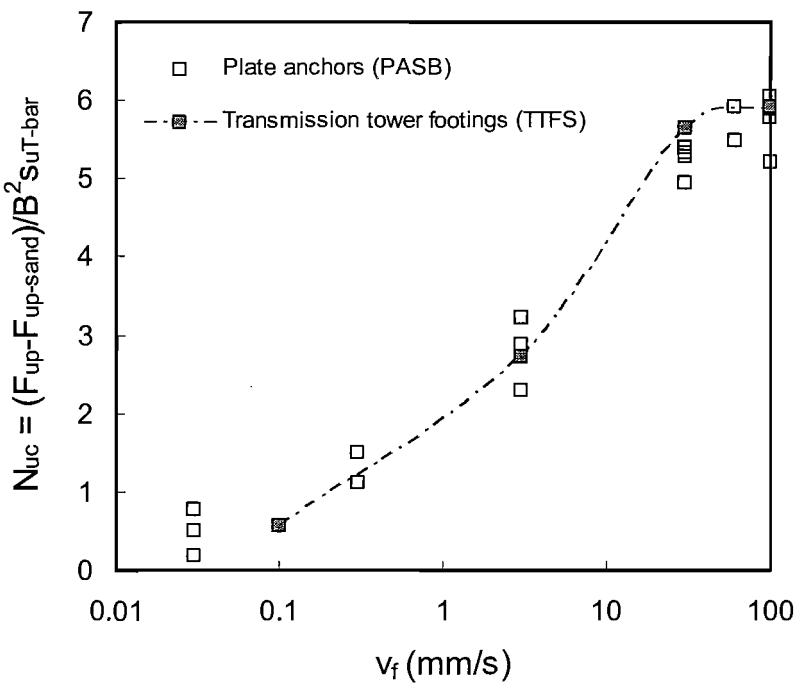

Figure 8.5 Comparison of uplift capacity factor (N_{uc}) for transmission tower footing and plate anchor tests

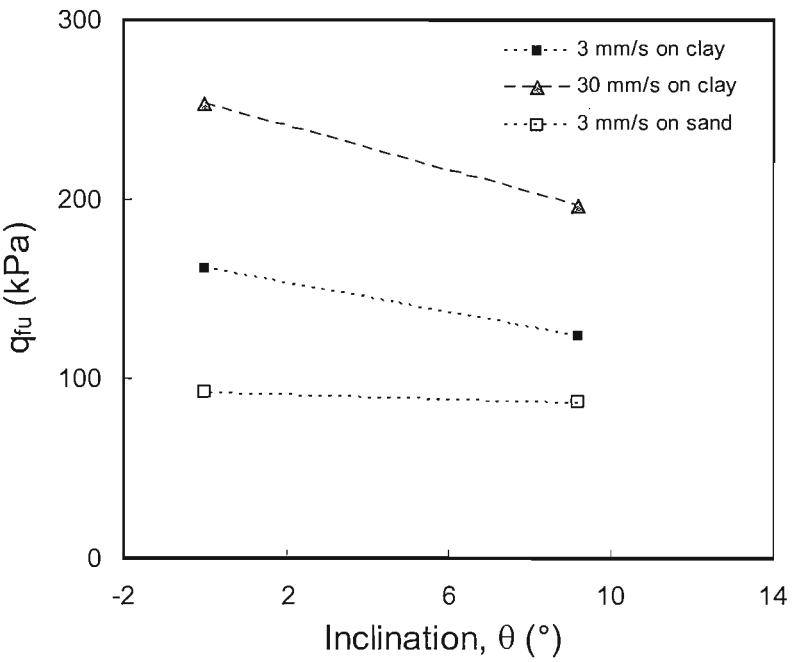

Figure 8.6 Footing capacity with stem inclination for footings founded on clay and sand

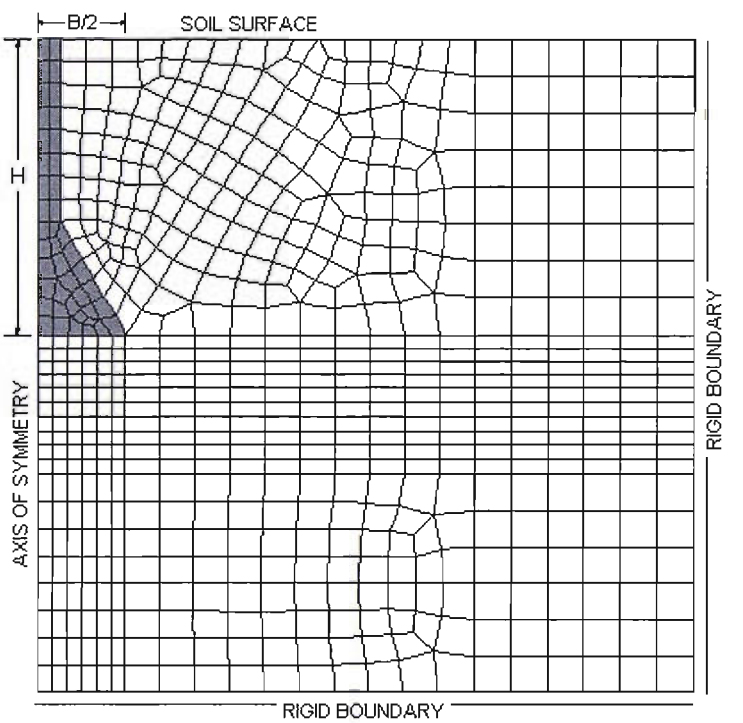

Figure 8.7 Finite element mesh for pyramidal footing back analyses

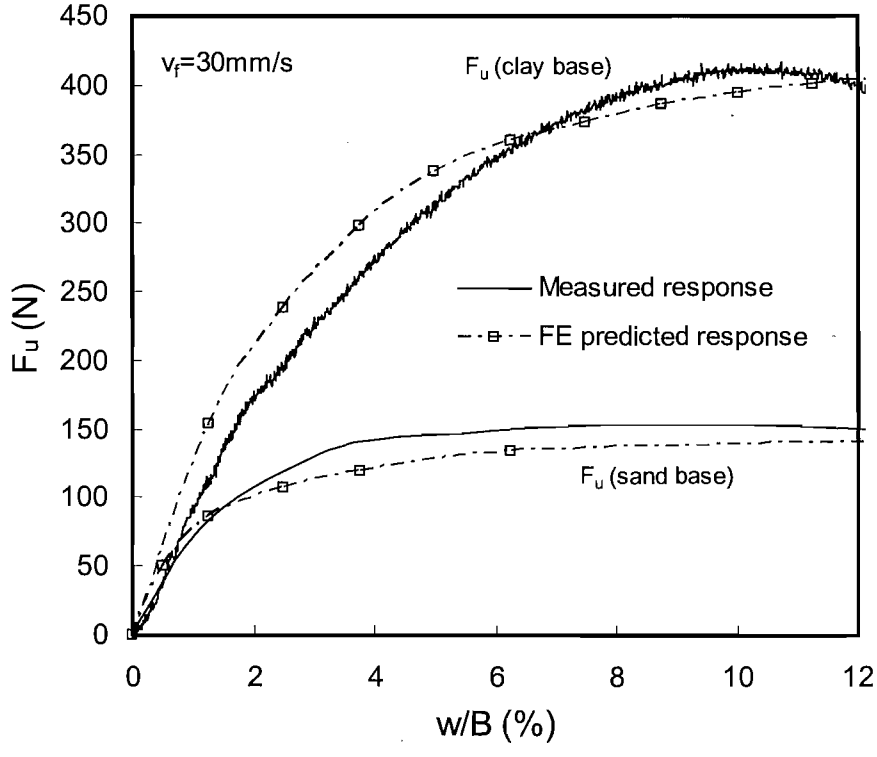

(a) v_f = 30 mm/s

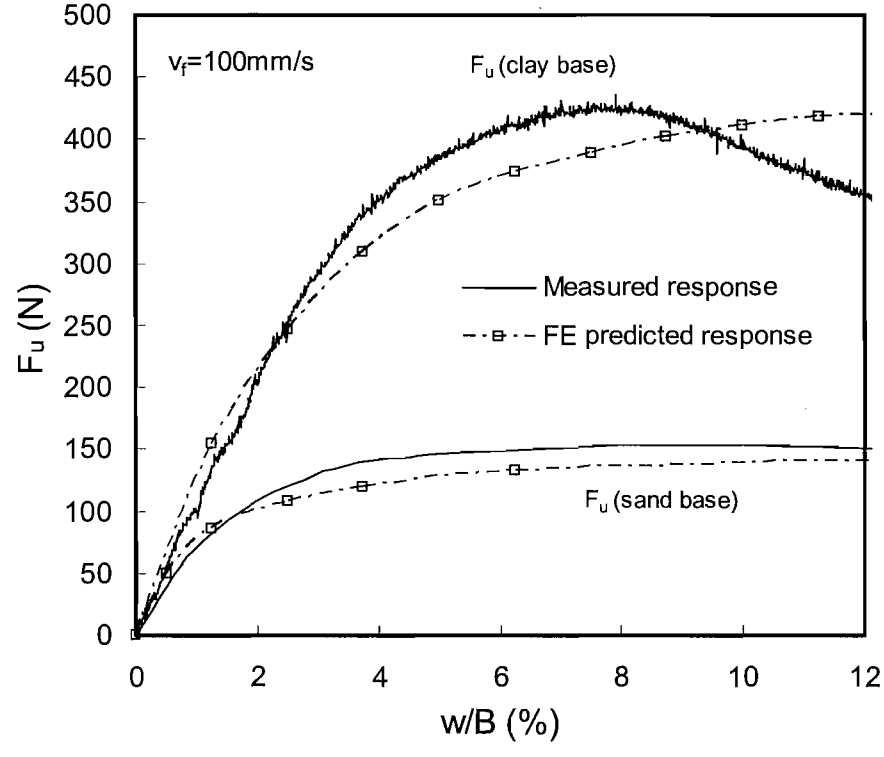

(b) v_f = 100 mm/s

Figure 8.8 Comparison of measured and predicted load displacement response for footings on sand and footings on clay at v_f = 30 and 100 mm/s

Chapter 9

ANCHORS WITH CEMENT STABILISED BACKFILL

9.1 Introduction

This chapter presents the results of a series of centrifuge model tests undertaken to investigate the effect of cement stabilisation on the uplift performance of shallow anchors in loose sand backfill. Uplift tests on anchors with cement stabilised backfill at varying ratios are compared with the results of Finite Element analyses using soil properties determined from the results of laboratory testing presented in Chapter 4.

9.2 Soil Stabilisation in Practice

As discussed in Chapter 2 transmission tower foundations are required to resist both uplift and compressive loading and generally comprise shallow spread footings constructed using reinforced concrete, steel grillages or pressed plates. Where loose or unstable soils exist near the surface inclined piles or pile-rafts may be used as an alternative design solution, often at increased cost. A more cost effective alternative to pile installation involves the use of existing footings and in-situ stabilisation of the backfill material.

Soil stabilisation is an established practice for road construction where the control of settlement is required. Similarly, soil stabilisation techniques have also been developed to improve both the stability of marginal slopes and to limit deformations associated with tunnelling operations. These techniques typically involve the mixing

of a hardening agent such as cement or lime with the soil to create a bond between the soil and stabiliser thus enhancing its mechanical properties. The hardening agent can be applied either in-situ or ex-situ depending upon the application. The use of Portland cement as a soil stabilising agent was trialled in Japan (Terashi and Tanaka, 1981) and applied in-situ using a slurry to distribute the cement within the soil matrix. Subsequent investigations indicated that significantly greater increases in soil strength following curing may be obtained by distributing the cement using a dry-mixing process rather than through a similar volume contained within a slurry. Field studies of spread footings have been carried out evaluating the use of compacted layers made up of soil mixed with cementing agents (e.g. Stefanoff et al. 1983, Consoli et al. 2003, Thomé et al. 2005). These studies were restricted to layered systems under compressive forces and have shown a noteworthy increase in the bearing capacity of foundations placed on improved layers built over a weak soil stratum.

9.3 Plate Anchor Series 3 – Cemented Backfill

The results of plate anchor series 3 (PAIB) are presented and anchor response in cemented sand backfill is examined. The test series was undertaken according to the experimental programme outlined in Chapter 5 (Section 5.7.3).

9.3.1 Uplift test results

An overview of the measurements made at the peak uplift resistance (F_{up}) and the anchor displacement at peak resistance (w_p) for the 4 anchor uplift tests conducted is presented in Table 9.1. Also included in Table 9.1 are the values of the uplift capacity factor N_{us} derived using Equation 6.1 (Section 6.2.1), assuming a buoyant sand unit weight (γ') of 8 kN/m^3. The following points are noted:

i. Regarding the anchor capacity. The value of F_{up} increases strongly with the proportion of cement in the backfill. For a cement content of 5% the value of F_{up} is about 5 times greater than for the un-cemented case. Even with the relatively modest addition of 1% cement to the backfill, the capacity is twice that of the un-cemented case.

ii. Regarding the anchor displacement. Overall, the value of w_p is generally observed to decrease with increasing cement content indicating a stiffer response of the backfill material. At 5% cement the value of w_p is just over half of that for the un-cemented test.

iii. The N_{us} value of 3.1 calculated for the anchor test employing the un-cemented backfill is a little lower than the value of around 4, approximated for an H/B value of 1.5, from the previously published studies reviewed in Chapter 3. The value is however reasonably well represented by the results of previous centrifuge tests discussed in Chapter 6 (Section 6.2.4).

Table 9.1 Summary of results for PAIB – 1st Sample

Sample 1						
Test	**B**	**Backfill cement ratio**	**F_{up}**	**q_{fu}**	**w_p**	**N_{us}**
(-)	**(mm)**	**(%)**	**(N)**	**(kPa)**	**(mm)**	
S1-1	30	0	50.0	55.5	0.53	3.1
S1-2	30	1	89.8	99.7	0.39	5.5
S1-3	30	3	148.0	164.4	0.42	9.1
S1-4	30	5	226.4	251.5	0.29	14.0

9.3.2 Load displacement response

The variation of uplift resistance (q_{fu}) with normalised displacement (w_p/B) for each of the 4 uplift tests undertaken is compared in Figure 9.1. It is evident that along with the overall uplift resistance, the initial pre-peak anchor stiffness also benefits strongly from the addition of cement to the sand backfill. The addition of cement does, however, lead to a brittle response and uplift resistance reduces sharply after the peak resistance is mobilised at a displacement of 1.2 ±0.2% of the footing width, this behaviour becoming more prevalent with increasing ratio of cement. The increased peak resistance is considered to be a result of the bonding between the soil and cement which allows a greater development of load in the soil skeleton, as observed in unconfined compression tests described previously in Chapter 4. After peak resistance the soil cement bindings are presumably broken (i.e. the c' component of strength is reduced) and fissures are formed within the backfill material resulting in a substantial loss of strength with only relatively small displacements. The cementation of the soil is gradually broken down further as the backfill shears under increased anchor displacement and the overall resistance drops toward that observed for the un-

cemented case. The variations shown in Figure 9.1 are analogous to the shear stress-displacement responses observed from direct shear tests and presented in Figure 4.12 for the cemented sand.

9.3.3 Peak uplift capacity

In order for a reasonable assessment of the effect of cement stabilisation on the peak anchor uplift resistance correlation may be obtained between the measured anchor capacities and the percentage of cement incorporated within the backfill sand. The properties of the cemented and un-cemented sand were obtained from laboratory tests as described in Chapter 4. The relationships between these backfill properties and the peak uplift capacities measured in the centrifuge tests are explored in Figure 9.2, which plots measured q_{fu} values against (a) the shear box c' values, (b) the G_o values at mean effective stress of 20 kPa, (c) the CPT q_c recorded at a depth of 22.5mm in the centrifuge (i.e. half the depth of anchor embedment) and (d) the unconfined compressive strengths q_{uc}. It is apparent that:

- The uplift resistance varies approximately linearly with values of c' obtained from direct shear tests. This result is indicative of the increased proportion of bonding present within the soil matrix at higher cement ratios. A similar trend is also observed in the variation of q_{fu} with G_0 values obtained from bender element test suggesting that the relative change in any value of these parameters (including cement content) provides a direct indication of the corresponding change in q_{fu}.
- There appears to be no linear relationship between q_{fu} and either q_c or q_{uc}. From the data observed in Figure 9.2(d) however, q_{fu} may be shown to vary approximately with $(q_{uc})^{0.5}$. This observed trend is similar to that inferred by Rowe & Armitage (1987) from a large number of field tests on rock sockets where the side shear resistance of a cemented material was better correlated with $(q_{uc})^{0.5}$.
- Despite the somewhat limited evidence, it may also be suggested that q_{fu} varies approximately with $q_c^{0.5}$ rather than directly with q_c although this trend requires further investigation.

Finally, it should be noted that q_{fu} cannot be expected to increase indefinitely as c' increases. Ultimately, as discussed later, the uplift capacity will be limited by the

weight of the cemented block in the excavation, when the c' value is sufficient to allow the material to behave as a unit.

9.4 Comparison with Numerical Analyses

The centrifuge test results presented in Section 9.3 have shown that considerable benefit to the uplift behaviour may be obtained from the addition of cement to sand backfill for the anchor type under consideration. To facilitate generalisation of these results, finite element (FE) analyses of the centrifuge tests were undertaken to investigate if the observed response could be replicated for use in design.

9.4.1 The Finite Element model

As described previously in Chapter 3, and for simplicity, all soils in the analyses were assumed to behave as isotropic linear elastic-perfectly plastic materials with the Mohr-Coulomb strength parameters inferred from direct shear box tests (see Table 4.5). For each anchor test two distinct analyses were undertaken (i) to predict the peak capacity using the peak strength parameters c' and ϕ'_p and (ii) to model the ultimate uplift condition, when the cement bonds had completely broken, using the same value of ϕ'_p but with c' set to zero.

The FE analyses were performed using the SAFE Finite Element program (SAFE, OASYS 2002). The analyses adopted an axisymmetric mode of deformation thereby modelling the square footing and stem used in each centrifuge test as circular sections of equivalent volume. As noted previously and in line with the analyses undertaken by Merifield et al (2006) this modelling convenience may overestimate the uplift capacity by up to approximately 10% at shallow embedment. Fully rough interfaces were assumed between the anchor and surrounding soil and tension was not permitted at the anchor base interface. The Young's modulus, E', for each type of backfill was varied as a set multiple of the very small strain shear modulus (G_0) listed for each cement ratio in Table 4.5. The best-fit to the predictions discussed below was obtained by assuming $E' = G_0/30$ in each analysis. For the clay outside the excavated area, a nominal E' value of 20 MPa was assigned however this value had no effect on the

predicted anchor response. E' values for the aluminium stem and steel base of 70 GPa and 200 GPa respectively were employed.

The Finite Element (FE) mesh is shown in Figure 9.3 and consisted of 530, 8-noded quadrilateral elements each with 4 Gauss points. The unit weights of soil and pore water input into the numerical model were factored by n=50 consistent with the centrifugal acceleration applied in the centrifuge tests. The numerical analyses therefore directly modelled the centrifuge tests rather than their equivalent prototypes. The location of the lower horizontal boundary of the mesh was specified at the same depth as the base of the centrifuge channel and the far vertical boundary was located at ten times the equivalent footing radius from the axis of symmetry. A series of analyses employing meshes with increased and reduced far vertical boundary locations confirmed that the selected boundary position was suitable. Each (effective stress) analysis assumed fully drained conditions and displacements at the top of the anchor stem were increased incrementally until failure occurred.

9.4.2 Comparison of uplift behaviour

The predicted variation of q_{fu} with w/B from the Finite Element analyses are compared with the measured footing response from the centrifuge pullout tests in Figure 9.4. It is evident that the predicted peak capacities are within 15% of the observed peak values for all cases and are well representative of the capacities measured with backfill cement contents of 3% and 5%. The ultimate capacities at w/B=10% are also well predicted by assuming c'=0. Evidently the true ultimate capacity of the anchor with a backfill cement content of 5% is not reached at w/B=10%.

The predictions on Figure 9.4 indicate that use of a constant backfill stiffness of E' $=G_0/30$ allows the pre-peak stiffness and the displacement to peak capacity to be estimated with a reasonable level of accuracy. It is therefore clear that the stiffness of the anchor increases in the same manner with the backfill c' value (and cement ratio) as does the anchor capacity shown in Figure 9.2(a).

The computed displacement vectors at peak uplift load for the un-cemented and cemented backfill are presented in Figure 9.5 and illustrate the failure mechanisms

developed during uplift. It is evident that the addition of cement to the backfill sand has a large effect on the horizontal extent of the failure plane, both at the surface of the backfill and the soil surrounding the anchor. It is this progressive outward shift that provides the additional anchor stiffness and strength and results in the increased uplift resistance measured for cemented sand. For the case when the backfill cement content is 5%, it is apparent that the failure zone encompasses the entire backfill region and simply involves lifting of the entire block within the excavation. It follows that any further increase in the level of cementation will not lead to an increase in anchor capacity. This was verified in additional FE analyses which predicted a similar q_{fu} value for any value of c' above about 60 kPa (≡cement content just above 5%).

9.5 Summary

Centrifuge tests and parallel finite element analyses have shown that very significant gains in stiffness and capacity may be obtained for shallow anchors subjected to uplift when relatively small amounts of cement are added to the sand backfill. These trends are important where soil stabilisation may be applied to existing transmission tower footings to increase uplift capacity and allow for foundation re-use under the increased loading of new conductor sets. It is observed that:

i. The peak and ultimate capacities of anchors in cemented soil predicted using finite element analysis with strength parameters obtained from direct shear tests were in good agreement with results from a series of physical modelling tests.

ii. The rate of gain in anchor stiffness and capacity varies directly with the backfill c', which, in the experiments reported here varies approximately with the backfill cement content. No increase in capacity is possible above a cement content at which the backfill acts as an integral block.

iii. Anchors with cemented backfill exhibit a brittle response and a large reduction in available capacity after normalised displacements (w_f/B) in the region of 1.2 ±0.2%.

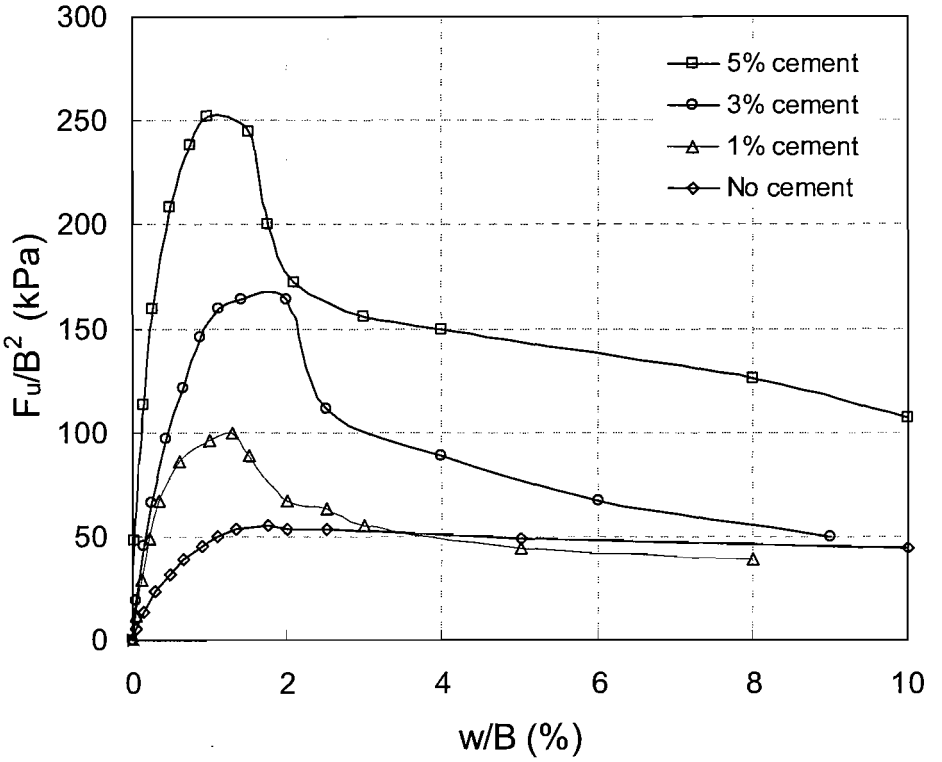

Figure 9.1 PAIB - Variation of uplift resistance with displacement for increasing cement content

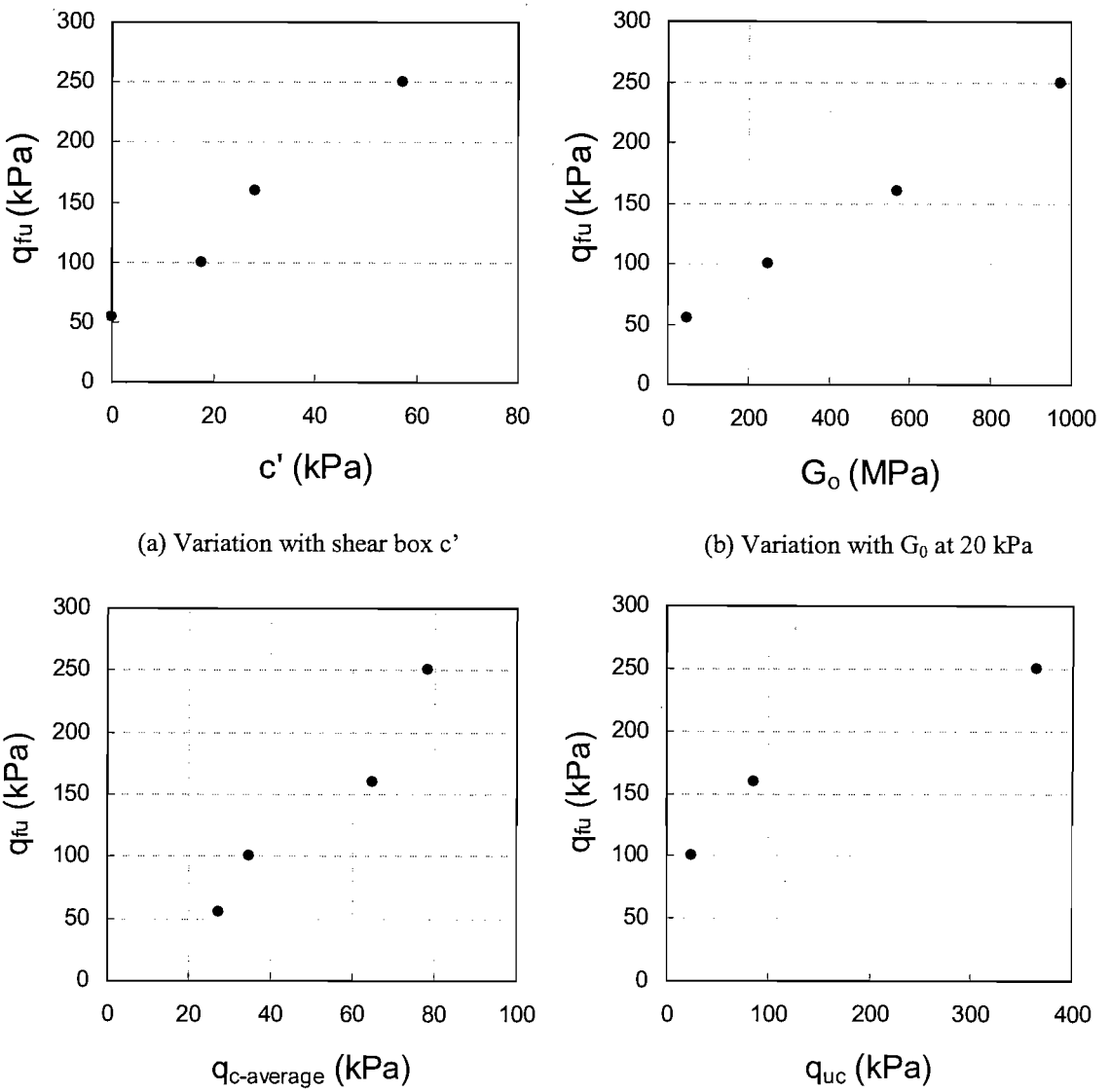

(a) Variation with shear box c'

(b) Variation with G_0 at 20 kPa

(c) Variation with q_c at half backfill depth

(d) Variation with q_{uc} from UC test

Figure 9.2 PAIB – Variation of uplift resistance with backfill properties determined in Chapter 4

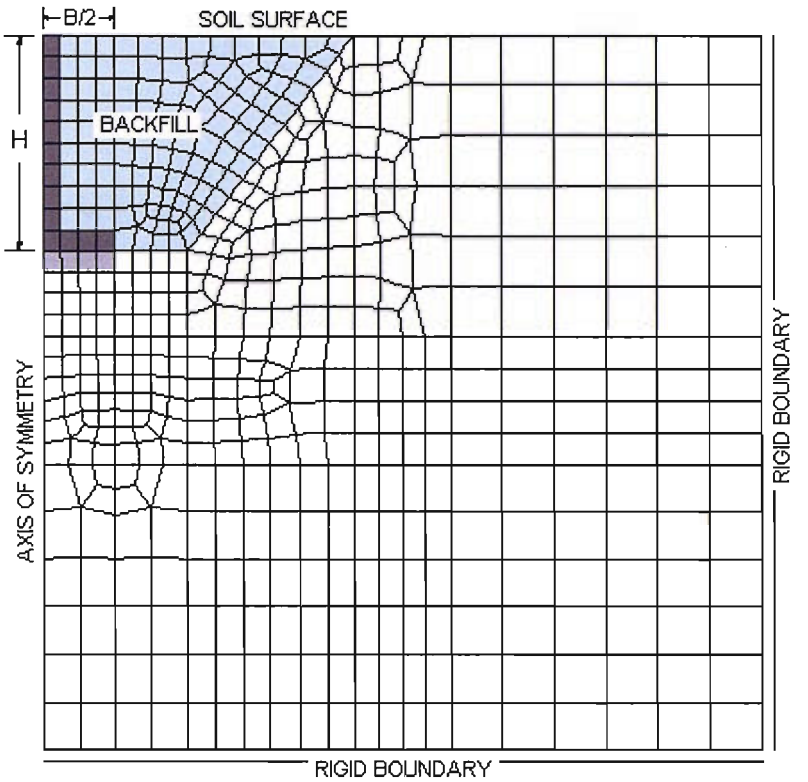

Figure 9.3 PAIB – Finite Element mesh

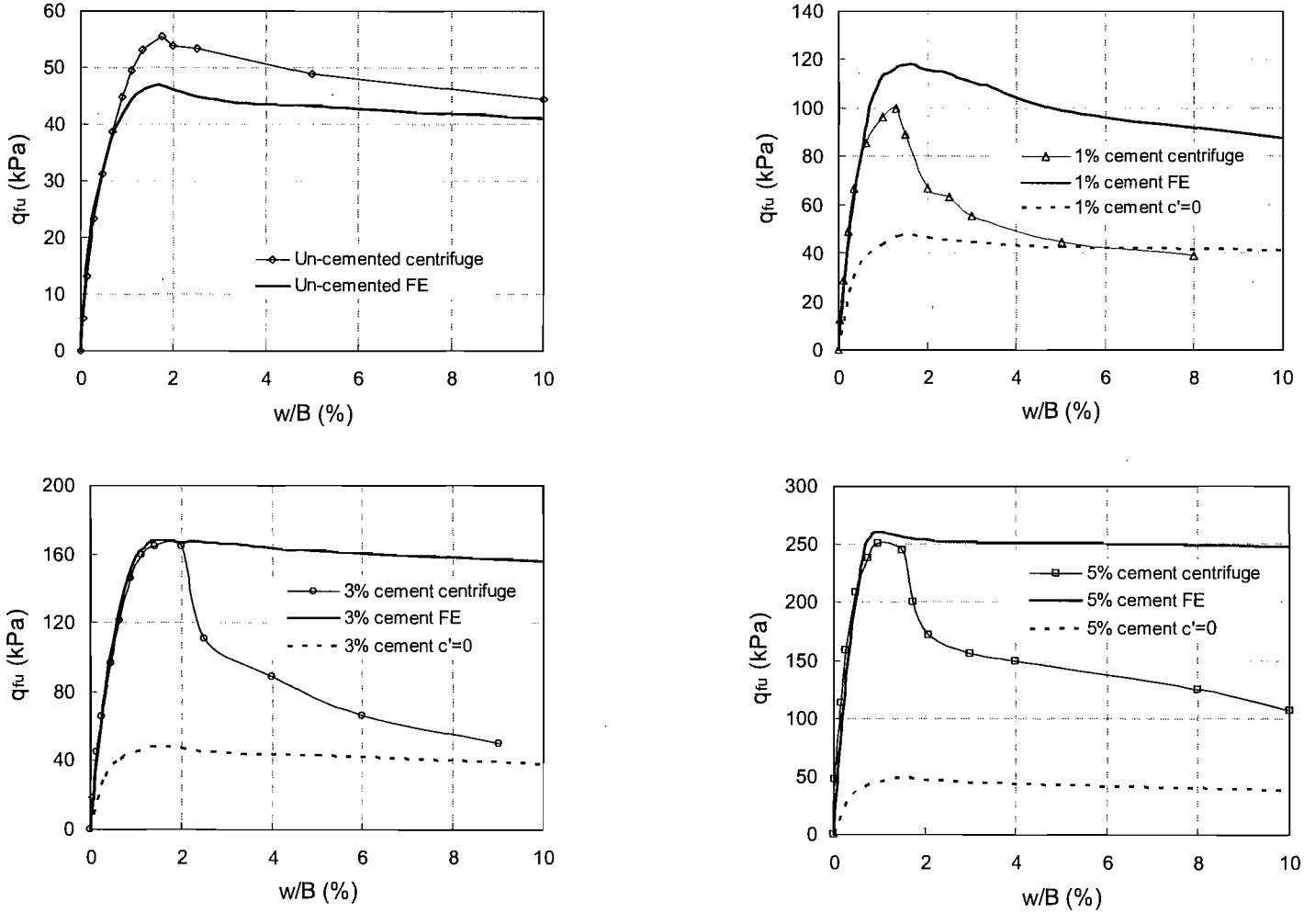

Figure 9.4 PAIB – Comparison of predicted and measured uplift behaviour

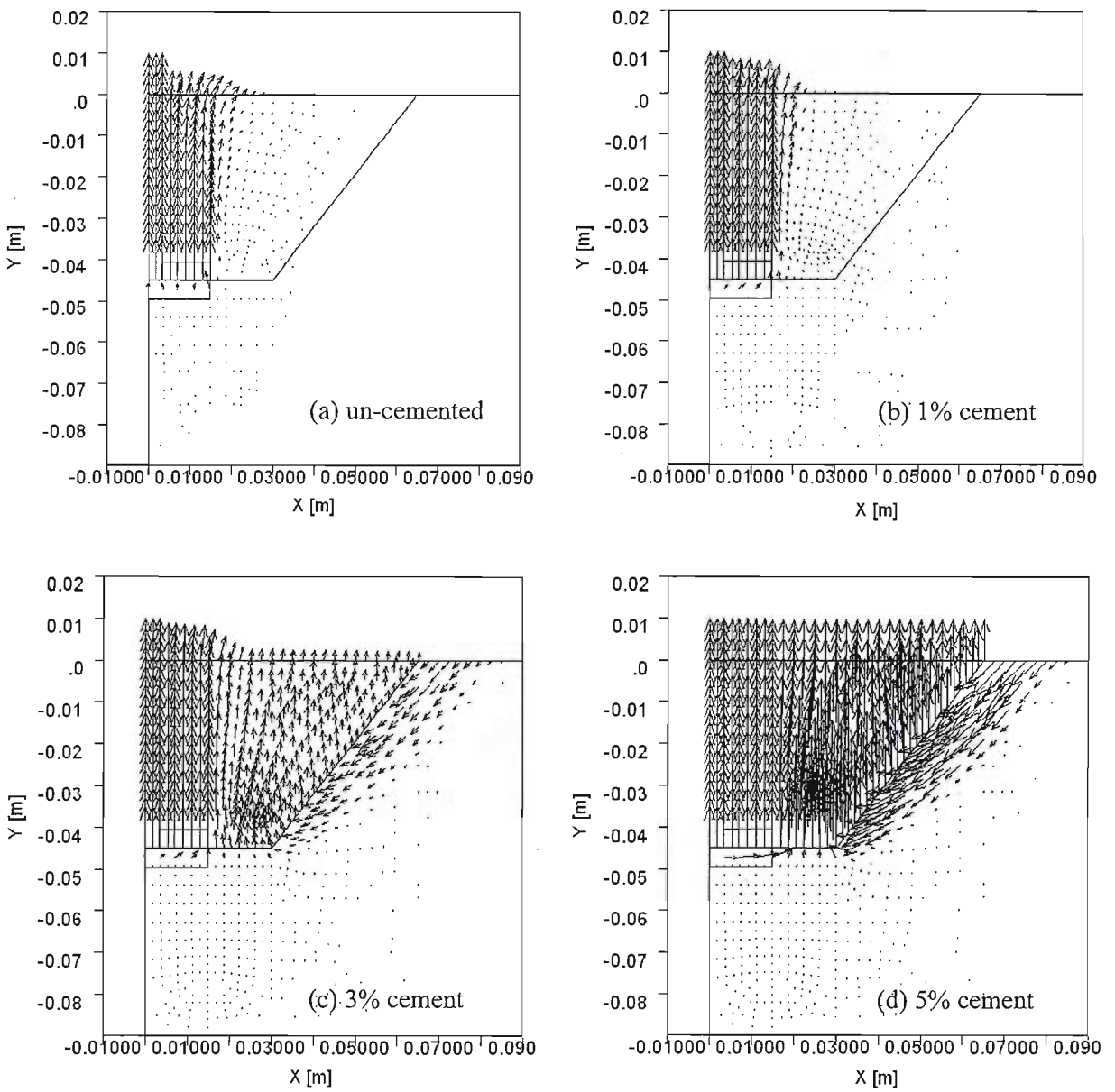

Figure 9.5 PAIB – Displacement vectors from FE analysis for each backfill cement content

Chapter 10

CONCLUSIONS

10.1 Introduction

This thesis has been concerned with the uplift performance of shallow foundations for transmission tower structures subject to rapid loading conditions. The research has been conducted using centrifuge modelling techniques and the results of these tests have been analysed using laboratory test data and compared with the output from a complimentary finite element investigation. This final chapter outlines the main conclusions arising from the research and provides recommendations for future work.

10.2 The Uplift Behaviour of Plate Anchors

A new actuator system was constructed for use in a geotechnical centrifuge to allow the application of high displacement rates to model anchors whilst providing fast, high quality data acquisition. A series of 65 uplift tests were conducted on model plate anchors founded on clay and sand in six centrifuge test samples. The influence of uplift velocity, anchor width and load inclination was investigated.

These tests have confirmed the generation of negative pore pressures (suctions), developed in the clay underlying the anchor base during uplift loading through comparison of the behaviour of anchors founded on clay and those founded on sand. It is shown that the magnitude of these developed suctions is related to the tendency for pore water drainage at the anchor base and as such will increase with increasing

anchor uplift velocity where less opportunity is available for drainage to occur. It has been observed from inspection of test anchors that a wedge of clay had adhered to the base of anchors uplifted at high velocities. From this observation it is concluded that where high soil suctions are sustained, at uplift velocities leading to undrained anchor response, a fully bonded condition will arise at the anchor base-clay interface and the uplift capacity will be dependent upon the undrained shear strength of the clay below the anchor. In such cases the contribution to anchor uplift capacity mobilised at the anchor base may then be estimated from a reverse bearing capacity type failure mechanism using an uplift capacity factor (N_{uc}) of 6.

At lower uplift velocities partial drainage in the underlying clay will result in the more rapid dissipation of developed suctions and the fully bonded failure condition will not occur. Suctions generated are relieved by the heave necessary to achieve the undrained uplift resistance and the flow of water along the underside of the anchor. Essentially a drainage path is developed which is propagated by the separation of the clay at the edge of the anchor base where the initial dissipation of suction occurs. During uplift loading full separation of the anchor base and underlying clay will occur at some displacement, depending on how much time is available for drainage, which is related to the uplift velocity of the anchor. As drainage occurs by water being pulled through the overlying backfill soil the permeability of the backfill material has also been shown to influence the uplift velocities at which partially drained and fully undrained anchor behaviour is developed. Anchors founded on clay with sand backfill require normalised velocities approximately an order of magnitude higher than those for an equivalent anchor with clay backfill in order to develop full undrained response. Due to the mechanism of breakaway described above this same normalised displacement is approximately two orders of magnitude higher than that required to develop full undrained response for a foundation loaded in compression, where full contact at the foundation base is implicit during loading.

10.2.1 Implications for design methods

In order for this research to be of use in field applications for shallow foundations subject to uplift loading, a means of incorporating a method of predicting the rate dependent uplift capacity in routine design should be sought. Precise finite element modelling of the breakaway mechanism, described above, which occurs at the anchor

base during uplift at partially drained velocities is complex and generally beyond the scope of the practitioner. The use of a conventional FE analysis (which does not permit separation between elements) employing a reduction factor applied to the permeability of the soil below the anchor has been shown to provide a simple means of modelling the increased drainage arising from the loss in contact that would be expected to take place between the anchor base and the underlying clay at partially drained uplift rates. Back analyses of the centrifuge uplift tests with sand backfill overlying kaolin clay have indicated that this procedure will provide a very reasonable estimate of the anchor uplift capacity across a range of uplift velocities.

10.3 The Uplift Performance of Transmission Tower Footings

A review of the available literature has highlighted the development of suction at the anchor base and the positive strain rate dependence of the undrained shear strength of the underlying clay as areas of uncertainty concerning the uplift behaviour of shallow foundations. Both of these factors are of significant importance in the design of foundations for transmission tower applications where high load rates have been observed to be transferred to the foundations from rapid tower load events. A series of 8 uplift tests were conducted on model transmission tower footings founded on clay and sand. The direct measurements of suctions developing at the footing base were undertaken using a miniature pore pressure transducer installed in the model footing. The influence of uplift velocity and load inclination was investigated.

The results of these tests have shown that the uplift stiffness and capacity of a transmission tower footing founded on clay varies significantly with uplift rate and is related to the magnitude of suctions developed at the footing-clay interface. Suctions measured at the base of the footing during uplift have been seen to be slightly underestimated at high uplift velocities due to the pore water pressure distribution across the footing base. The suctions measured are however seen to be compatible with those assessed during centrifuge investigation into the uplift behaviour of plate anchors.

It is shown that where high footing uplift capacities are observed to develop at high uplift velocities, displacements of up to 10% of the footing width may be required in order to generate the full capacity. For a typical transmission tower foundation this relates to displacements in excess of around 200 mm required for generation of the maximum available uplift resistance, a value which is well in excess of the serviceability constraints placed on such foundations. This conclusion has obvious implications where foundation capacity should be assessed in relation to the deflection criteria imposed by the structure above.

It has been observed that there appears to be no influence of the footing inclination on the uplift capacity of a footing founded on sand where footing inclinations are within the limits of those conventionally used for transmission tower foundations in the UK.

It is also concluded that there is no significant difference in the overall performance of the pyramidal footing, conventionally used for transmission tower foundation in the UK, compared with that of the plate anchors, discussed in Chapter 6. From this it is suggested that there may be no obvious benefit of constructing these more complex footing geometries other than to increase the overall weight of the footing.

10.3.1 Rate dependence in design

For footings founded on clay, consideration of the rate dependence of the stiffness and undrained shear strength of the clay has been shown to be essential in order to provide a realistic prediction of the uplift performance under rapid loading. As noted with regard to the uplift behaviour of shallow plate anchors, precise numerical modelling of all the factors relating to uplift behaviour with increasing displacement rate is subject to some uncertainty and may beyond the scope of conventional design. For a footing founded on clay and uplifted at high velocities the stress path experienced by the underlying clay will be similar to that imposed during rapid undrained shear in a triaxial extension test. It has been shown that, for such a footing, use of a conventional finite element analysis incorporating rate dependent soil parameters derived from the results of triaxial extension tests at high axial strain rates, will yield a reasonable estimation of the increase in ultimate uplift capacity and the pre-peak load displacement response. Results from such FE analyses have shown good agreement

with the measured response from the uplift tests conducted on model transmission tower footings in the centrifuge.

10.4 Cement Stabilisation of Shallow Anchors

The results of field uplift tests undertaken on redundant transmission tower foundations since 1967 have displayed a trend for foundations failing at loads well below those predicted in design. In a large majority of these test cases it has been shown that variations in the quality of the backfill soil, compared to that of the virgin soil, are likely to have contributed to such reduced capacities. A series of 4 centrifuge uplift tests were conducted on model anchors backfilled with varying degrees of cemented sand. Laboratory studies and cone penetrometer tests were also undertaken to characterise the cemented backfill material. Where soil stabilisation may be applied to existing transmission tower footings to increase uplift capacity and allow for foundation re-use under the increased loading of new conductor sets it is important that the trends associated with backfill cementation are well understood.

The results of these tests have shown that very significant gains in stiffness and capacity may be obtained for shallow anchors subjected to uplift when relatively small amounts of cement are added to the sand backfill. The rate of gain in anchor stiffness and capacity are seen to vary directly with the backfill c', which has been shown to vary approximately linearly with the backfill cement content. Anchors with cemented backfill are observed to display a brittle load displacement response similar to that seen for sample of cemented sand tested in direct simple shear. A large reduction in the available capacity is shown to occur at displacements in the region of 1.2 ±0.2% of the anchor width after which the uplift resistance reduces to approximately the same value as that for an anchor in un-cemented sand backfill.

10.3.1 Soil stabilisation in design

Where soil stabilisation is sought as a viable means of increasing the capacity of existing foundations it is important to be able to predict the foundation behaviour and related increases in uplift capacity with backfill cement content. The peak uplift

capacities of anchors in cemented soil have been predicted using finite element analysis with strength parameters obtained from direct shear tests and were seen to be in good agreement with results from the centrifuge model tests. The trend for increasing uplift capacity with cement content observed in the centrifuge model investigation was well represented by the results of the FE analyses. The FE analyses have shown that while significant increases in uplift capacity are obtained with increasing cement content, that after a certain percentage of cement is added to the backfill the material will begin to act as an integral block and no further increase in capacity will be achieved with increasing percentage of cement after this point.

10.5 Recommendations for Further Research

10.5.1 Regarding the uplift failure surface

The nature of the failure surface developed, during uplift, above an anchor embedded in either sand or clay is still a source of contention between studies. While some investigations have reported failure planes defined through monitoring of soil deformation during uplift of half-cut anchors in laboratory studies (Ilamparuthi et al. 2002), it is recommended that Particle Image Velocimetry (PIV) techniques be used to define soil deformations in centrifuge model tests where the stress distribution and overburden pressures are representative of field applications. A further understanding of the failure surfaces developed during uplift of anchors in both sand and clay would provide a higher degree of accuracy to existing design methods where assumptions regarding the shape of such surfaces can be rather arbitrary.

10.5.2 Regarding the reverse bearing capacity failure mechanism

Prediction of the contribution to uplift capacity mobilised at the base of a footing founded on clay is highly dependent upon the mechanism of failure assumed to develop in the clay. The development of this mechanism is related to the generation of suctions in the underlying clay which has been shown to be affected by the permeability of the backfill soil and the uplift displacement rate applied to the foundation. This research has revealed that the resistance generated at the base of the footing may be assessed, in terms of peak capacity, through the assumption of a

reverse bearing capacity type mechanism and the application of an appropriate uplift capacity factor. It is recommended that further testing be undertaken to clarify the mechanism of failure developing at the base of a footing during uplift a high displacement rates. The velocities required for the development of full base resistance will generally negate the use of conventional soil deformation monitoring techniques however the use of the PIV method with high-speed photography may provide a most useful investigation in this area.

This research would provide an improved understanding of the mechanism of failure related to the uplift resistance mobilised at the base of a footing during uplift over a range of velocities Such understanding could then be applied to the development of a precise numerical model to account for the breakaway mechanism concluded in this research to occur at velocities leading to partially drained uplift response. A better appreciation of the gradual separation, due to the drainage of pore water, thought to propagate from the edge of a footing during uplift could lead to a more defined method of predicting foundation uplift capacity for partially drained response.

10.5.3 Regarding foundation system performance

The focus of this research has been towards foundation performance for individual footings. In reality, for a conventional transmission tower foundation arrangement, the footings will interact as a group rather than as four isolated foundations. Footings will be subject to compression, tension and moment loading as loads are transferred from the tower structure and distributed between the footings. The problem of analysing the transmission tower structure and foundations as a complete system is further complicated by the behaviour of the soil below the foundations. For a systematic approach, elastic analysis may be undertaken where rigidity is assumed in the tower supports however such calculations will differ from the real behaviour where the soil below the foundation exhibits a plastic response.

It is recommended that research be undertaken into the performance of transmission tower foundations as part of a complete structural system where the distribution of loading may be adequately modelled. Such investigation may realistically be undertaken in the centrifuge where a scaled model incorporating a complete transmission tower (or a portion of) and foundations could be subjected to lateral

loading representative of the wind loading experienced in service. Such research would provide valuable information relating to both the geotechnical and structural design criteria for transmission towers.

REFERENCES

Adachi, T. and Oka, F. (1982). Constitutive equations for normally consolidated clay based on elasto-viscoplasticity. *Soils and Foundations*, **22**(4), 57-70

Akai, K., Adachi, T. and Ando, N. (1975). Existence of a unique stress-strain-time relation of clays. *Soils and Foundations*, **15**(1), 1-16

Ali, M.S. (1968). Pullout resistance of anchor plates and anchor piles in soft bentonite clay. MS Thesis, Duke University, Durham, USA

Al-Tabbaa, A. and Wood, D.M. (1987). Some measurements of the permeability of kaolin. *Geotechnique*, **37**(4), 499-503

Atkinson, J.H. (2000). Non-linear soil stiffness in routine design. *Geotechnique*, **50**(5), 487-507

Baba, H.U., Gulhati, S.K. and Datta, M. (1989). Suction effect in plate anchors in soft clays. *Proc 12th Int. Conf. Soil Mechanics & Foundation Eng.* Rio de Janeiro, Brazil, ISSMFE, **1**(1), 409-412

Balla, A. (1961). The resistance to breaking out of mushroom foundations for pylons. *Proc. 5th Int. Conf. Soil Mechanics & Foundation Engineering*, **1**(1), 389-576

Beckwith, G.H., and Hansen, L.A. (1982). Calcareous soils of the southwestern United States. *Proc. Geotechnical Properties, Behaviour and Performance of Calcareous Soils*, Philadelphia, ASTM, **1**(1), 16-35

Bemben, S.M. and Kupferman, M. (1975). The vertical holding capacity of marine anchor flukes subjected to static and cyclic loading. *Proc. of the Offshore Tech. Conf.* OTC 2185, 363-374

Bhatterai, B. (2002). Soils laboratory data. School of Civil & Resource Engineering, The University of Western Australia. *Presented in Lehane et al. 2007

Bjerumm, L., Simons, N. and Torblaa, I. (1958). The effect of time on the shear strength of a soft marine clay. *Proc. of the Conf. on Earth Pressure Problems*

Borja, R.I. and Kavazanjian, E. (1985). A constitutive model for the stress-strain-time behaviour of 'wet' clays. *Geotechnique*, **35**(3), 283-298

Booker, J.R. and Small, J.C. (1986). The behaviour of an impermeable flexible raft on a deep layer of consolidating soil. *International Journal for Numerical and Analytical Methods in Geomechanics*, **10**(1), 311-327

Casagrande, A., Shannon, W.L. 1949. Strength of soils under dynamic loads. *Transactions of ASCE*, **114**(1), 755-772

Casagrande, A., Wilson, S.D. 1951. Effect of rate of loading on the strength of clays and shales at constant water content. *Geotechnique*, **2**(3), 251-263

Clark, M., Richards, D. J. and Clutterbuck, D. (2006). Measured dynamic performance of electricity transmission towers following controlled broken-wire events. *CIGRE 41, International Council on large Electrical Systems*, August 2006, Paris, France. Paper B2-313, ISBN 2-85873-020-2

Clayton, C. R. I., Parke, G. A., Woods, R. I. and Ali, A. (1994). The design of transmission tower foundations to resist uplift. Report No. CBGE9403/1, Department of Civil Engineering, University of Surrey

Clemence, S.P. and Veesaert, C.J. 1977. Dynamic pullout resistance of anchors in sand. *Proc. of the Int. Sym. on Soil Structure Interaction*, India, **1**(1), 389-397

Consoli, N.C., Vendruscolo, M.A., and Prietto, P.D.M. (2003). Behavior of plate load tests on soil layers improved with cement and fiber. *Journal of Geotechnical Engineering*, ASCE, **129**(1), 96-101

Das, B. M. (1978). Model tests for uplift capacity of foundations in clay. *Soils and Foundations*, **18**(2), 17-24

Das, B.M. and Singh, G. (1994). Uplift capacity of plate anchors in clay. *Proc. 4th Int. Offshore and Polar Eng. Conf. 1994*, **1**(1), 436-442

Das, B.M., Shin, E.C., Dass, R.N. and Omar, M.T. (1994). Suction force below plate anchors in soft clay. *Marine Georesources and Geotechnology*, **12**(1), 71-81

Das, B.M. and Singh, G. (1995). Holding capacity of plate anchors in sand: a review. *Proc. 5th Int. Offshore and Polar Eng. Conf. 1995*. **1**(1), 414-419

Davie, J. R. and Sutherland, H. B. (1977). Uplift resistance of cohesive soils. *Journal of Soil Mechanics, Foundations Division*, ASCE, **103**(9), 935-952

Davis, E.H. and Booker, J.R. (1973). The effect of increasing strength with depth on the bearing capacity of clays. *Geotechnique*, **23**(4), 551-563

Dembicki E. (2005). The effect of inclined loads on overhead line tower foundation uplift resistance. *Electra*, **219**(1)

Dickin, E. A. (1988). Uplift behaviour of horizontal anchor plates in sand. *Journal of the Geotechnical Engineering Division*, ASCE, **114**(11), 1300-1317

Dickin, E.A., Leung, C.F. (1983). Centrifugal model tests on vertical anchor plates. *Journal of Geotechnical Engineering*, ASCE, **109**(1), 1503-1525

Dickin, E.A., Leung, C.F. 1990. Performance of Piles with enlarged bases subjected to uplift forces. *Canadian Geotechnical Journal*, **27**(1), 546-556

Downs, D.I., Chieurzzi, R. 1966. Transmission tower foundations. *Journal of the Power Division*, ASCE, **92**(2), 91-114

Finn, W.D.L., Byrne, P.M. 1972. The evaluation of the breakout force for a submerged ocean platform. *Offshore Technology Conf.*, 1972, OTC1604

Finnie, I.M.S. and Randolph, M.F. (1994). Punch-through and liquefaction induced failure of shallow foundations on calcareous sediments. *Proc. Int. Conf. on Behaviour of Offshore Structures*, Boston, USA, 217-230

Frydman, S. and Shaham, I. 1989. Pullout Capacity of Slab Anchors in Sand. *Canadian Geotechnical Journal*, **26**(1), 385-400

Goodwin, N. and Lehane, B.M. (2003). Base resistance of deep plate anchors founded at the surface of a clay layer. *Proc. 2003 Final Year Sym.*, School of Civil & Resource Engineering, University of Western Australia.

Graham, J., Crooks, J.H.A. and Bell, A.L. (1983). Time effects on the stress-strain behaviour of natural soft clays. *Geotechnique,* **33**(3), 327-340

Hardingham, A.D. (1994). Development of an engineering description of cemented soils and calcrete duricrust. *Proc. 1st Int. Sym. on Eng. Characteristics of Arid Soils*, Rotterdam, **1**(1), 87-90

Head, K.H. (1982). Manual of Soil Laboratory Testing, Volume 1, Pentech Press, London

Houlsby, G.T., Kelly, R.B., Huxtable, J. and Byrne, B.W. (2006). Field trials for suction caissons on sand for offshore wind turbine foundations. *Geotechnique,* **56**(1), 3-10

Ilamparuthi, K. and Muthukrisnaiah, K. (1999). Anchors in sand: delineation of rupture surface. *Ocean Engineering Journal*, **26**(1), 1249-1273

Ilamparuthi, K., Dickin, E.A. and Muthukrisnaiah, K. (2002). Experimental investigation of the uplift behaviour or circular plate anchors embedded in sand. *Canadian Geotechnical Journal*, **39**(3), 648-664

Jovicic, V., Coop, M.R., and Simic, M. (1996). Objective criteria for determining G_{max} from bender element tests. *Géotechnique*, **46**(2), 357-362

Katti, D.R., Tang, J. and Yazdani, S. (2003). Undrained response of clays to varying strain rate. *Journal of Geotechnical and Engineering*, ASCE, **129**(3), 278- 282

Khadilkar, B.S. (1971). Study of rupture surface and ultimate resistance of anchor foundations. *Proc. 4th Asian Regional Conf. on Soil Mechanics and Foundation Eng.* **1**(1), 121-127

Koutsabeloulis, N.C. and Griffiths, D.V. (1989). Numerical modelling of the trapdoor problem. *Geotechnique*, **39**(1), 77-89

Kulhawy, F. H., Trautmann, C. H., Beech, J. F., O'Rourke, T. D., McGuire, W., Wood, W. A. and Capono, C. (1983). Transmission line structure foundations for uplift-compression loading. Report EL-2870, Electric Power Research Institute (EPRI), Palo Alto, USA

Kulhawy, F. H., Trautmann, C. H. and Nicolaides, C. N. (1987). Spread foundations in uplift: experimental study. *Foundations for Transmission Line Towers*, ASCE Geotechnical Special Publication 8, 96-109

Kulhawy, F.H. and Mayne, P.W. (1990). Manual on estimating soil properties for foundation design. Report EL-6800, Electric Power Research Institute (EPRI), Palo Alto, USA

Kumar, P (1993). Development of suction during uplift and compression of plates in soft clays. M. Tech Thesis, Indian Institute of Technology, New Delhi

Kupferman, M. (1971). The vertical holding capacity of marine anchors in clay subjected to static and cyclic loading. MS Thesis, University of Massachusetts, USA

Kutter, B.L. and Sathialingam, N. (1992). Elastic-viscoplastic modelling of the rate-dependent behaviour of clays. *Geotechnique*, **42**(3), 427-441

Ladd, C.C. and Foot, R. (1974). New design procedure for stability of soft clays. *Journal of the Geotechnical Engineering Division*, ASCE, **100**(7), 763-786

Ladd, C.C., Foot, R., Ishihara, K., Schlosser, F. and Poulos, H.G. (1977) Stress-deformation and strength characteristics. *Proc 9th Int. Conf. Soil Mechanics and Foundation Eng.* Tokyo, **1**(2) 421-494

Ladd, R.S. (1978). Preparing test specimens using undercompaction. *Geotechnical Testing Journal*, ASTM, **1**(1), 16-23

Ladd, C.C., Young, G.A., Kraemer, S.R., Burke, D.M. (1999). Engineering properties of Boston Blue Clay from special testing program. *Special*

Geotechnical Testing. Central Artery/Tunnel Project in Boston, Massachusetts. ASCE Geotechnical Special Publication 91, 1-24

Lade, P.V. (1994). Creep effects on static and cyclic instability of granular soils. *Journal of Geotechnical Engineering*, ASCE, **120**(2), 404-419

Lade, P.V. and Liu, C.T. (1998). Experimental study of drained creep behaviour of sand. *Journal of Geotechnical Engineering*, ASCE, **124**(8), 912-920

Lee, K.L., Bolton, H. and Dunlop, P. (1969). Effects of transient loading on the strength of sand. *Proc. 7th Int. Conf. on Soil Mechanics and Foundation Engineering*, **1**(1), 239-247

Lefebvre, G. and LeBoeuf, D. (1987). Rate effects and cyclic loading of sensitive clays. *Journal of Geotechnical Engineering*, ASCE, **113**(5), 476-489.

Lefebvre, G. and Pfendler, P. 1996. Strain rate and preshear effects in cyclic resistance of soft clay. *Journal of Geotechnical Engineering*, ASCE, **122**(2), 21-26

Lehane B.M., O' Loughlin C., Gaudin C. and Randolph M.F. (2007). Rate effects on penetrometer resistance in kaolin. University of Western Australia, Research Report: C06-111

Leroueil S. and Hight D.W. (2003). Behaviour and properties of natural soils and soft rocks. *Proc. Characterisation and Engineering Properties of Natural Soils*, Singapore, **1**(1), 29-254

Lin H. and Penumadu D. (2005). Experimental investigation on principal stress rotation in kaolin clay. *Journal of Geotechnical Engineering,* ASCE., **131**(5), 633-642

Lunne, T., Robertson, P.K. and Powell, J.J.M. (1997). Cone Penetration Testing in geotechnical practice, Blackie Academic and Professional, London

Martin C.M. (2001). Vertical bearing capacity of skirted circular foundations on Tresca soil. *Proc. 15th Int. Conf. Soil Mechanics and Geotechnical Engineering*, Istanbul, **1**(1), 743-746

Majer, J. 1955. Zur berechnung von zugfundamenten (in German). Osterreichische Bauzeitschrift, **10**(5), 85-90

Mariupol'skii, L.G. 1965. The bearing capacity of anchor foundations. *Osnovaniya Fundamenty I Mekhanika Gruntov,* **3**(1), 14-18

Matsuo, M. 1968. Study of uplift resistance of footings. *Soils and Foundations*, **8**(1), 18-48

Merifield, R. S., Sloane, S. W. and Yu, H. S. (2001). Stability of plate anchors in undrained clay. *Geotechnique*, **51**(2), 141-153

Merifield, R.S., Lyamin, A.V., Sloan, S.W. and Yu, H.S. (2003). Three-dimensional lower bound solutions for stability of plate anchors in clay. *Journal of Geotechnical Engineering*, ASCE, **129**(3), 243-53

Merifield, R. S., Lyamin, A. V. and Sloan, S. W. (2006). Three-dimensional lower-bound solutions for the stability of plate anchors in sand. *Geotechnique*, **56**(2), 123-132

Mesri, G. (2001). Undrained shear strength of soft clays from push cone penetration test. *Geotechnique*, **51**(2), 167-168

Meyerhof, G. G. and Adams, J. L. (1968). The ultimate uplift capacity of foundations. *Canadian Geotechnical Journal*, **5**(4), 225-244

Mors, H. (1959). The behaviour of mast foundations subject to tensile forces. *Bautechnik*, **10**(1), 367-378

Murray, E.J. and Geddes, J.D. (1987). Uplift of anchor plates in sand. *Journal of the Geotechnical Engineering Division*, ASCE, **113**(3), 202-215

Nhiem, T.V. (1975). Uplift resistance of anchor slabs in soft clay. *Proc. 4th Int. Conf. on Soil Mechanics and Foundation Eng.*, Istanbul., **1**(2), 14-123

Oasys (2002). SAFE Users manual, Ove Arup & Partners, London W1P, UK.

Ovesen, N.K. (1979). The use of physical models in design: the scaling law relationship. *Proc. 7th Euro. Conf. on Soil Mechanics and Foundation Engineering*, England, **1**(4), 318-323

Ovesen, N.K. (1981). Centrifuge tests to determine the uplift capacity of anchor slabs in sand. *Proc. 10th Int. Conf. on Soil Mechanics and Foundation Eng.*, Stockholm. **1**(1), 717-722

Perzyna, P. (1963). The constitutive equations for rate sensitive plastic materials. *Quarterly of Applied Mathematics*, **20**(1), 321-332

Perzyna, P. (1966). Fundamental problems in viscoplasticity. *Advances in Applied Mathematics*, **9**(1), 343-377

Prashant, A. and Penumadu, D. (2005). A laboratory study of normally consolidated kaolin clay. *Canadian Geotechnical Journal*, **42**(1), 27-37

Rad, N.S., and Clough, G.W. (1985). Static behavior of variably cemented beach sands. *Proc. of the Symp. on Strength Testing of Marine Soils: Laboratory and In-situ Measurement,* Philadelphia, ASTM, **1**(1), 306-317

Randolph, M.F. and Houlsby, G.T. (1984). The limiting pressure on a circular pile loaded laterally in cohesive soil. *Geotechnique*, **34**(4), 613-623

Randolph M.F. and Hope S. (2004). Effect of cone velocity on cone resistance and excess pore pressures. *Proc. of the Int. Symp. on Eng. Practice and Performance of Soft Deposits*, Japan, 147-152

Rao, N. S. and Datta, M. (2001). A comparison of uplift and bearing behaviour of plate anchors in soft clay. *Proc. Int. Offshore and Polar Engineering Conf. 2001*, Norway, **1**(2), 560-565

Richards, D.J. (2002). The determination of dynamic resistance of transmission tower footings to uplift using centrifuge modelling techniques. Report No. NGDR/C/RD003/Report/F1. Dept of Civ. Eng., University of Southampton, UK

Richardson, A. and Whitman, R.V. (1963). Effect of strain rate upon undrained shear resistance. *Geotechnique*, **13**(3), 310-324

Rowe, R.K. and Armitage, H.H. (1987). A design method for drilled piers in soft rock. *Canadian Geotechnical Journal*, Vol. **24**(1), 126-142

Rowe, R. K. and Davis, E. H. (1982). The behaviour of anchor plates in clay. *Geotechnique*, **32**(1), 9-23

Rowe, R. K. and Davis, E. H. (1982). The behaviour of anchor plates in sand. *Geotechnique*, **32**(1), 25-41

Sarac, D.Z. (1989). Uplift capacity of shallow buried anchor slabs. *Proc. 12th Int. Conf. on Soil Mechanics and Foundation Eng.*, **1**(2), 1213-1218

Schneider, J.A. and Lehane, B.M. (2006). Effects of width for square centrifuge displacement piles in sand. *Proceedings 6th Int. Conf. Physical Modelling in Geotechnics*, Hong Kong, China, **1**(1), 867-873

Seed, H.B. and Lundgren, R. (1954). Investigation of the effect of transient loading on the strength and deformation characteristics of saturated sand. *Proceedings,* ASTM, **54**(1), 1288-1306

Sheahan, T.C., Ladd, C.C. and Germaine, J.T. (1996). Rate dependant undrained shear behaviour of saturated clay. *Journal of Geotechnical Engineering*, ASCE, **122**(2), 99-108

Shin, E. C., Dass, R. N., Omar, M. T., Das B. M. and Cook, E. E. (1994). Mud suction force in the uplift of plate anchors in clay. *Proc. Int. Offshore and Polar Engineering Conf. 1994*, Japan, **1**(1), 462-466

Shirley, D.J. and Hampton, L.D. (1977). Shear-wave measurements in laboratory sediments. *Journal of Acoustics Society of America*, **63**(2), 607-613

Skempton, A.W. (1951). The bearing capacity of clays. *Proc. Building Research Congress*, **1**(1), 180-189

Stefanoff, G, Jellev, J., Tsankova, N., Karachorov, P., and Slavov, P. (1983). Stress and strain state of a cement-loess cushion. *Proc. 8th Euro. Conf. on Soil Mechanics and Foundation Engineering*, Helsinki, Rotterdam, **1**(1), 811-816.

Stewart, D.P. (1990). Lateral loading of piles in soft clay due to nearby embankment construction. Research Report GEO:90086, Department of Civil and Resource Engineering, The University of Western Australia.

Stewart, D.P. and Randolph, M.F. (1991). A new site investigation tool for the centrifuge. *Proc. Int. Conf. Centrifuge 1991*, Rotterdam, **1**(1), 531-538

Stewart, D.P. and Randolph, M.F. (1994). T-bar penetration testing in soft clay. *Journal of Geotechnical Engineering Division*, ASCE, **120**(2), 2230-2235

Stewart, D. P., Boyle, R. S. and Randolph, M. F. (1998). Experience with a new drum centrifuge. *Proc. Int. Conf. Centrifuge 1998*, Tokyo, **1**(1), 35-40

Sutherland, H.B. (1988). Uplift resistance of soils. *Geotechnique*, **38**(4), 493-516

Sutherland, H.B., Finlay, T.W., Fadl, M.O. 1982. Uplift capacity of embedded anchors in sand. *Proc. of the 3rd Int. Conf. on the Behaviour of Offshore Structures*, Cambridge 1982, **1**(1), 451-463

Tagaya, K., Tanaka, A. and Aboshi, H. (1983). Application of finite element method to pullout resistance of buried anchor. *Soil and Foundations*, **23**(3), 91-104

Tagaya, K., Scott, R.F. and Aboshi, H. (1988). Pullout resistance of buried anchor in sand. *Soils and Foundations*, **28**(3), 114-130

Take, W.A. and Bolton, M.D. (2003). Tensiometer saturation and the reliable measurement of soil suction. *Geotechnique*, **53**(2), 159-172

Taylor, D.W. (1943). Cylindrical compression research program on stress-deformation and strength characteristics of soils. Ninth Progress Report on Shear Research to U.S. Engineers. Cambridge. M.I.T. Publication

Terashi, M. and Tanaka, H. (1981). Ground improvement by deep mixing method. *Proc. 10th Int. Conf. on Soil Mechanics and Foundation Eng.*, Stockholm, **1**(3), 777-780

Thomé, A., Donato, M., Consoli, N.C., and Graham J. (2005). Circular footings on a cemented layer above weak foundation soil. *Canadian Geotechnical Journal*, **42**(4), 1569-1584

Thorne, C. P., Wang, C. X. and Carter, J. P. (2004). Uplift capacity of rapidly loaded strip anchors in uniform strength clay. *Geotechnique*, **54**(8), 507-517

Trautmann, C.H. and Kulhawy, F.H. 1988. Uplift load-displacement behaviour of spread foundations. *Journal of the Geotechnical Engineering Division*, ASCE, **114**(2), 168-184

Vaid, Y.P. and Campanella, R.G. (1977). Time dependent behaviour of undisturbed clays. *Journal of the Geotechnical Engineering Division*, ASCE, **103**(7), 693-709

Vanner, M.J. (1964). A survey of the relation between the strengths of backfill and of undisturbed soil along overhead line routes. Report No. 5085. The Electrical Research Association. October 1964

Vanner, M.J. (1982). Foundation uplift resistance: the effects of foundation type and of seasonal changes in ground conditions. *Proc. of the IEE*, **129**(4), 295-305.

VDE 0210 (1985). Planning and design of overhead power lines with rated voltages above 1kV. VDE Verlag GmbH, Berlin (*trans*, BSI), 145

Vermeer, P.A. and Sutjiadi, W. (1985). The uplift resistance of shallow embedded anchors. *Proc. 11th Int. Conf. on Soil Mechanics and Foundation Eng.*, San Francisco, **1**(4), 1635-1638

Vesic, A. S. (1971). Breakout resistance of objects embedded in the ocean bottom. *Journal of Soil Mechanics, Foundations Division, ASCE*, 97(9), 1185-1205

Vesic, A.S. (1972). Expansion of cavities in infinite soil mass. *Journal of the Soil Mechanics and Foundations Division*, ASCE, **98**(3), 265-290

Watson, P.G. (1999). PhD thesis, The University of Western Australia

Whitman, R.V. and Healy, K.A. (1962). Shear strength of sands during rapid loadings. *Journal of the Soil Mechanics and Foundations Division*, ASCE, **88**(2), 99-132

Whitman, R.V. and Healy, K.A. (1963). The shearing resistance of sands during rapid loading. *Transactions*, ASCE, **128**(1), 1553-1594

Yamamuro, J.A. and Lade, P.V. (1993). Effects of strain rate on instability of granular soils. *Geotechnical Testing Journal*, **16**(3), 304-313

Yamamuro, J.A., Bopp, P.A., Lade, P.V. (1996). One dimensional compression of sands at high pressures. *Journal of Geotechnical Engineering*, ASCE, **122**(2), 147-154

Yazdanbod, A., Sheikh, S.A. and O'Neill, M.W. (1987). Uplift of shallow under-reams in jointed clay. *Foundations for Transmission Line Towers*, ASCE Geotechnical Special Publication 8, 110-127

Yin, J.H. and Graham, J. (1989) Viscous-elastic-plastic modelling of one-dimensional time-dependent behaviour of clays. *Canadian Geotechnical Journal*, **26**(1), 199-209

Yin, J.H. and Graham, J. (1994). Equivalent times and one-dimensional elastic viscoplastic modelling of time-dependent stress-strain behaviour of clays. *Canadian Geotechnical Journal*, **31**(1), 42-52

Yin, J.H. and Graham, J. (1999). Elastic viscoplastic modelling of the time-dependent stress-strain behaviour of soils. *Canadian Geotechnical Journal*, **36**(3), 736-745

Yong, R.N. and Japp, R.D. (1969). Stress-strain behaviour of clays in dynamic compression. *Vibrational Effects of Earthquakes on Soils and Foundations*, ASTM, Special Technical Publication 450, 233-262

Yu, H.S. (2000). Cavity expansion methods in Geomechanics. Kluwer Academic Pub.

APPENDIX A

NATIONAL GRID DESIGN METHOD

CONCRETE SPREAD FOUNDATIONS

This foundation takes the form of a truncated pyramid surmounted by a chimney. Alternatively the truncated pyramid may be replaced and/or used in conjunction with a reinforced concrete pad. The included angle between the horizontal and the sides of the pyramid shall not exceed 70°.

Uplift resistance is assumed to be provided by the weight of the foundation, the weight of soil contained within the assumed failure surface and the shear strength mobilised along the failure or slip surface. Due consideration shall be taken of buoyancy effects and reduced backfill densities.

For design under compression loading the area of the base is determined by the design ground bearing pressure under ultimate limit state loading. In assessing the bearing pressure beneath the foundation, the additional weight of the foundation over the displaced soil shall be multiplied by the appropriate partial factor for permanent actions.

Reinforced concrete chimneys for use with spread foundations shall be designed to withstand the maximum horizontal resultant residual shear component, with due allowance given, where appropriate, to the lateral (passive) earth resistance of the backfill or surrounding soil. A parabolic distribution of pressure may be assumed. A minimum allowance of 750 mm shall be considered for seasonal effects and/or depth of material not suitable for providing lateral support. The residual shears are considered to act at the lowest bracing point of the tower.

No allowance shall be made for the nominal strength of concrete in tension and the stub shall not be considered as providing any part of the tensile area of reinforcement.

In weak homogeneous rock, where the long term stability of the rock can be assured, an alternative type of foundation may be used where a nominally reinforced concrete block is cast in-situ against the undisturbed rock. A nominal (150 mm) undercut should be provided at the lower edge if possible. Uplift resistance is assumed to be provided by the skin friction developed at the concrete-rock interface and any soil-rock overburden.

DESIGN PARAMETERS SPREAD FOUNDATIONS

Unless the Contractor can provide evidence that higher values can be assumed, the soil parameters indicated in table A1 or A2 are to be considered as maxima in the design of pyramid type foundations. In selecting the values for the ultimate bearing pressure under ultimate loads, the Contractor is to take due consideration of strata beneath the foundation level which may adversely affect settlement or cause shear failure. The settlement of the foundation under ultimate loading shall not exceed 40 mm.

OTHER DESIGN PARAMETERS

i. Concrete is to be grade C35 in accordance with the specification

ii. The density of the concrete in pyramid foundations is to be taken as $2.25 Mg/m^3$

iii. The angle between the horizontal and sides of pyramid foundations is not to exceed 70°Ultimate load stress between the galvanised steel stub and concrete in the design for compression loading is to be 1.1 N/mm^2.

FOUNDATION GEOTECHNICAL DESIGN PARAMETERS

Parameter		Value of Standard Penetration Test for Non-cohesive materials (N)			
		10 < N < 20		N > 20	
		Above water table	Submerged	Above water table	Submerged
Bulk density (Mg/m^3)	Soil	1.8	1.0	1.9	1.0
	Backfill	1.6	0.9	1.6	0.9
Maximum design ground bearing pressure under ultimate applied loading (kN/m^2)		150	150	345	345
Frustum Angle (Degrees)		15	15	25	25
Design passive pressure on the chimney under ultimate applied loading (kN/m^2)		240	120	240	120

Table A1 – Design Parameters for Non-cohesive Soils

Parameter		Value of undrained shear strength for cohesive materials (kN/m^2)	
		35 < C < 49	C > 50
Bulk density (Mg/m^3)	Soil	1.7	1.9
	Backfill	1.6	1.6
Maximum Design ground bearing pressure under ultimate applied loading (kN/m^2)		200	345
Frustum Angle (Degrees)		15	25
Design passive pressure on the chimney under ultimate applied loading (kN/m^2)		120	240

Table A2 – Design Parameters for Cohesive Soils

APPENDIX B

PASB UPLIFT TEST DATA

B Anchor width

v_f Uplift displacement rate

H Embedment depth

Dyn Position of centrifuge actuator

θ Anchor inclination

Soil Soil at anchor base

Anchor		Test S1-1	
B=	30 mm	v=	3 mm/s
H=	45 mm	Dyn=	23.5°
θ=	0°	Soil	Clay
Pore Pressure			
PP50		51 kPa	
PP75		34.4 kPa	
PP100		23.3 kPa	

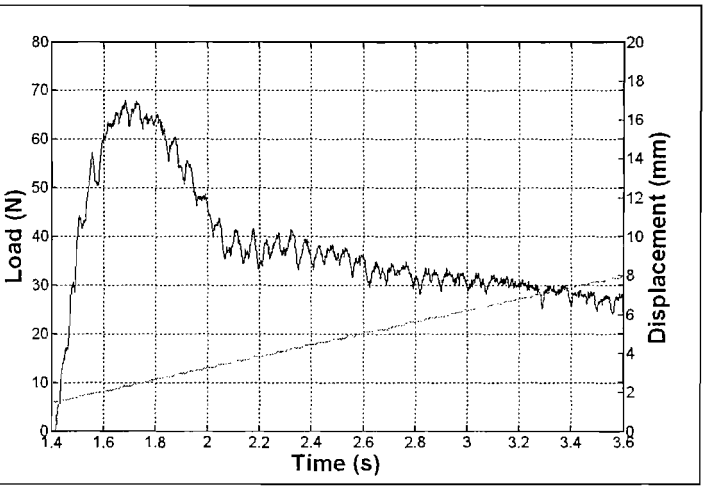

Figure B1(a) Load and displacement curves for test No 1. Sample 1

Anchor		Test S1-2	
B=	30 mm	v=	3 mm/s
H=	45 mm	Dyn=	90°
θ=	0°	Soil	Clay
Pore Pressure			
PP50		51.7 kPa	
PP75		35 kPa	
PP100		24.2 kPa	

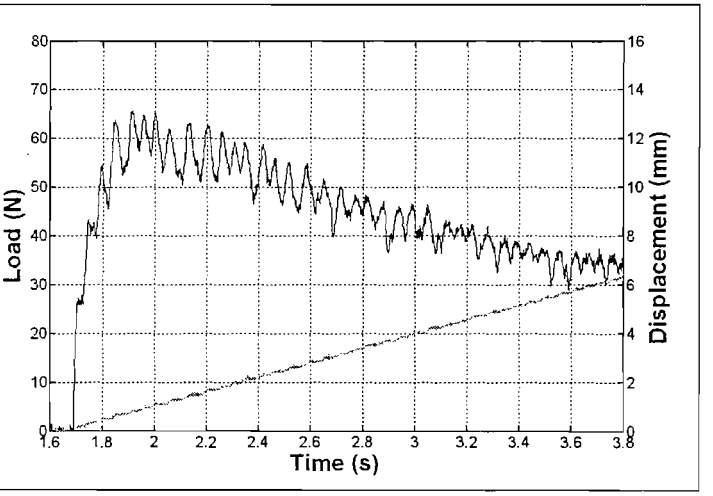

Figure B1(b) Load and displacement curves for test No 2. Sample 1

Anchor		Test S1-3	
B=	30 mm	v=	3 mm/s
H=	45 mm	Dyn=	158°
θ=	0°	Soil	Sand
Pore Pressure			
PP50		51.7 kPa	
PP75		35 kPa	
PP100		24.2 kPa	

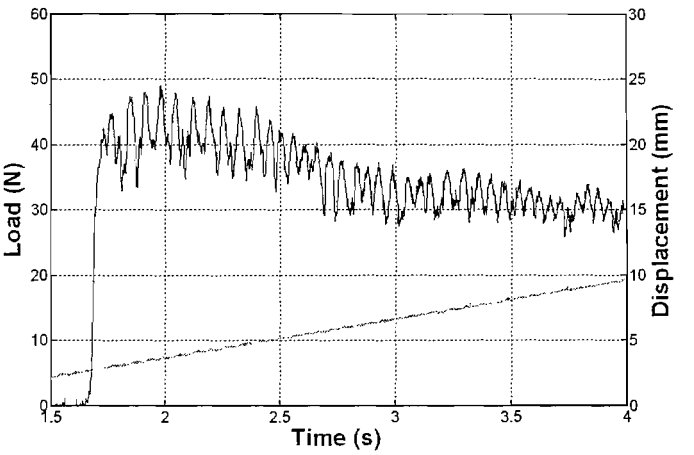

Figure B1(c) Load and displacement curves for test No 3. Sample 1

Anchor		Test S1-4	
B=	30 mm	v=	3 mm/s
H=	45 mm	Dyn=	180°
θ=	5°	Soil	Clay
Pore Pressure			
PP50		51.7 kPa	
PP75		35 kPa	
PP100		24.2 kPa	

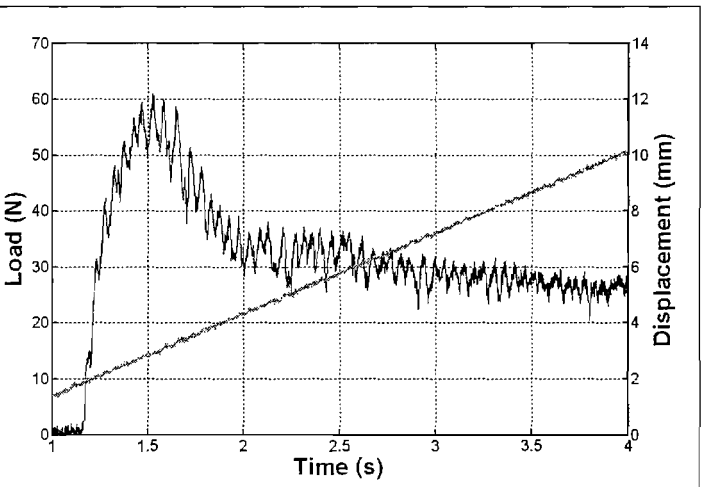

Figure B1(d) Load and displacement curves for test No 4. Sample 1

Anchor		Test S1-5	
B=	30 mm	v=	3 mm/s
H=	45 mm	Dyn=	203°
θ=	10°	Soil	Clay
Pore Pressure			
PP50		51.7 kPa	
PP75		35 kPa	
PP100		24.2 kPa	

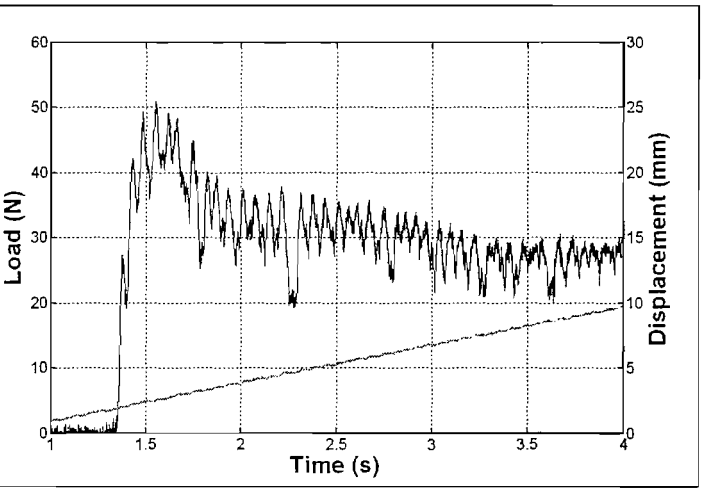

Figure B1(e) Load and displacement curves for test No 5. Sample 1

Anchor		Test S1-6	
B=	30 mm	v=	3 mm/s
H=	45 mm	Dyn=	225°
θ=	15°	Soil	Clay
Pore Pressure			
PP50		51.7 kPa	
PP75		35 kPa	
PP100		24.2 kPa	

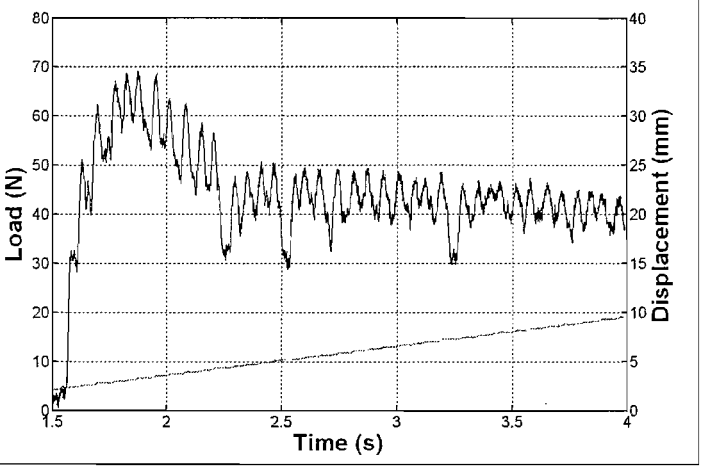

Figure B1(f) Load and displacement curves for test No 6. Sample 1

Anchor		Test S1-7	
B=	30 mm	v=	3 mm/s
H=	45 mm	Dyn=	248°
θ=	15°	Soil	Sand
Pore Pressure			
PP50		51.7 kPa	
PP75		35 kPa	
PP100		24.2 kPa	

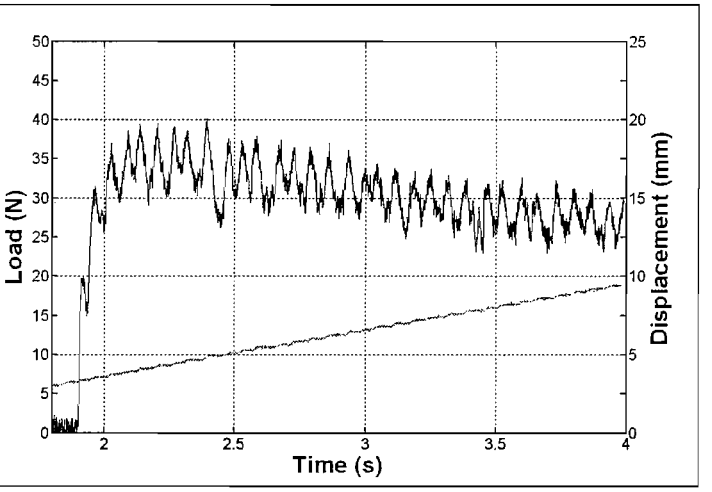

Figure B1(g) Load and displacement curves for test No 7. Sample 1

Anchor		Test S2-1	
B=	30 mm	v=	0.03 mm/s
H=	45 mm	Dyn=	0°
θ=	0°	Soil	Clay
Pore Pressure			
PP50		52.1 kPa	
PP75		36.3 kPa	
PP100		25.4 kPa	

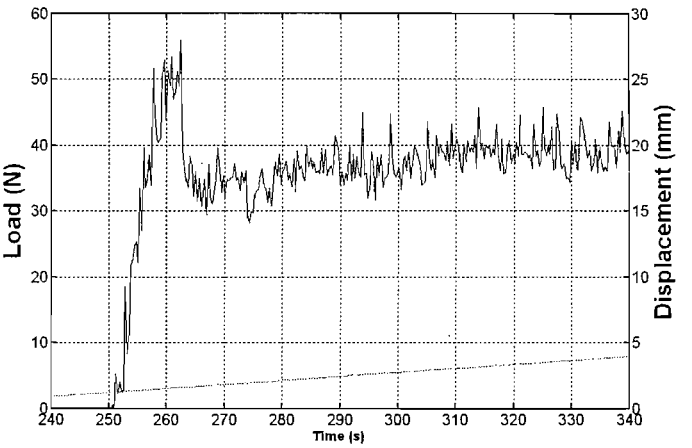

Figure B2(a) Load and displacement curves for test No 1. Sample 2

Anchor		Test S2-2	
B=	30 mm	v=	0.3 mm/s
H=	45 mm	Dyn=	22.5°
θ=	0°	Soil	Clay
Pore Pressure			
PP50		52.1 kPa	
PP75		36.3 kPa	
PP100		25.4 kPa	

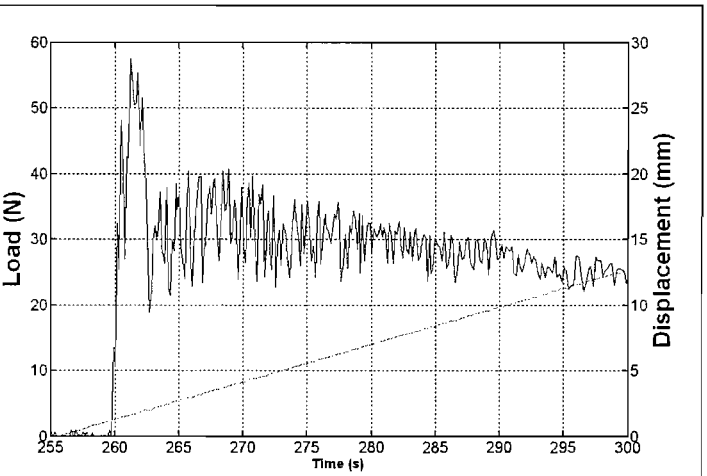

Figure B2(b) Load and displacement curves for test No 2. Sample 2

Anchor		Test S2-3	
B=	30 mm	v=	60 mm/s
H=	45 mm	Dyn=	67.5°
θ=	0°	Soil	Clay
Pore Pressure			
PP50		52.1 kPa	
PP75		36.3 kPa	
PP100		25.4 kPa	

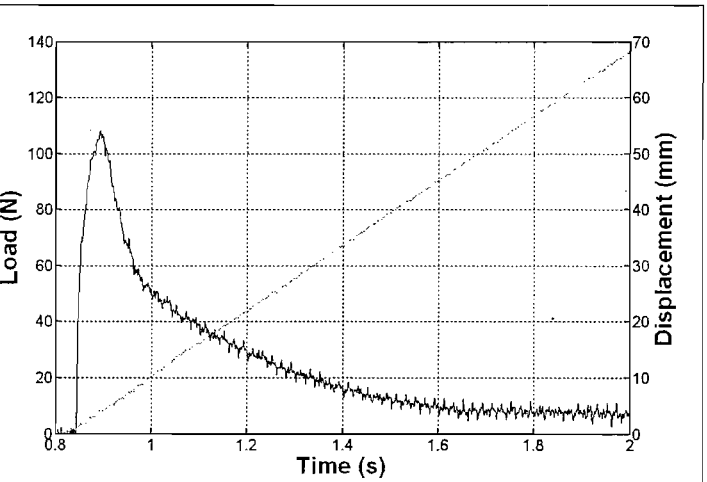

Figure B2(c) Load and displacement curves for test No 3. Sample 2

Anchor		Test S2-4	
B=	30 mm	v=	100 mm/s
H=	45 mm	Dyn=	45°
θ=	0°	Soil	Clay
Pore Pressure			
PP50		52.1 kPa	
PP75		36.3 kPa	
PP100		25.4 kPa	

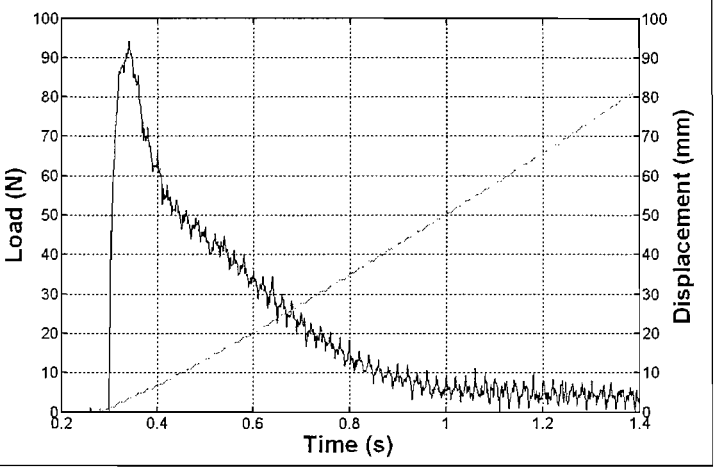

Figure B2(d) Load and displacement curves for test No 4. Sample 2

Anchor		Test S2-6	
B=	45 mm	v=	30 mm/s
H=	45 mm	Dyn=	112.5°
θ=	0°	Soil	Clay
Pore Pressure			
PP50		51.9 kPa	
PP75		36.2 kPa	
PP100		25.2 kPa	

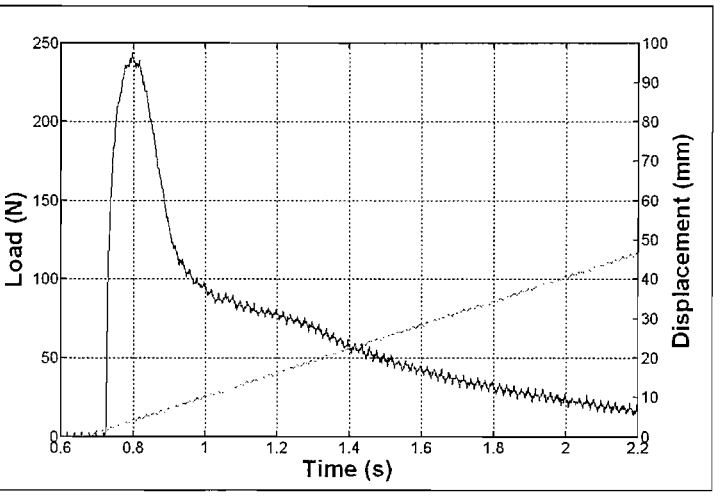

Figure B2(e) Load and displacement curves for test No 6. Sample 2

Anchor		Test S2-7	
B=	45 mm	v=	3 mm/s
H=	45 mm	Dyn=	135°
θ=	0°	Soil	Sand
Pore Pressure			
PP50		51.9 kPa	
PP75		36.2 kPa	
PP100		25.2 kPa	

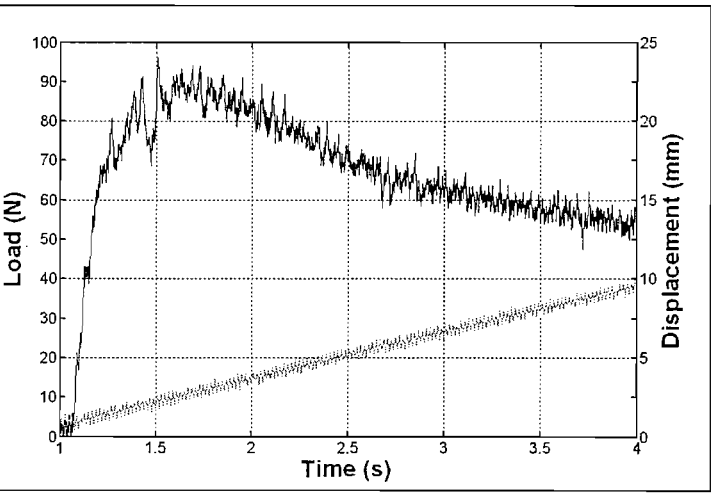

Figure B2(f) Load and displacement curves for test No 7. Sample 2

Anchor		Test S2-8	
B=	30 mm	v=	3 mm/s
H=	45 mm	Dyn=	138°
θ=	15°	Soil	Clay
Pore Pressure			
PP50		51.4 kPa	
PP75		35.6 kPa	
PP100		25.6 kPa	

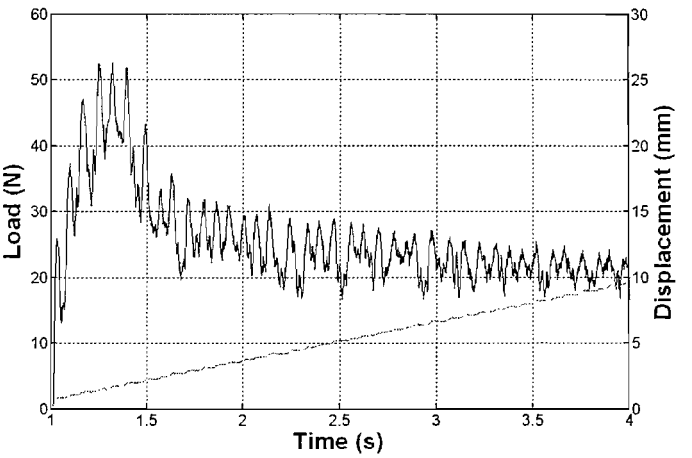

Figure B2(g) Load and displacement curves for test No 8. Sample 2

Anchor		Test S2-9	
B=	30 mm	v=	30 mm/s
H=	45 mm	Dyn=	160°
θ=	15°	Soil	Clay
Pore Pressure			
PP50		51.4 kPa	
PP75		35.6 kPa	
PP100		25.6 kPa	

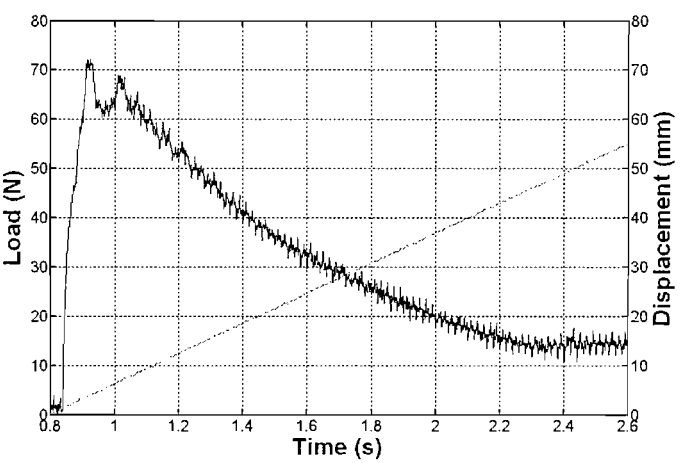

Figure B2(h) Load and displacement curves for test No 9. Sample 2

Anchor		Test S2-10	
B=	30 mm	v=	3 mm/s
H=	45 mm	Dyn=	185°
θ=	10°	Soil	Sand
Pore Pressure			
PP50		51.4 kPa	
PP75		35.6 kPa	
PP100		25.6 kPa	

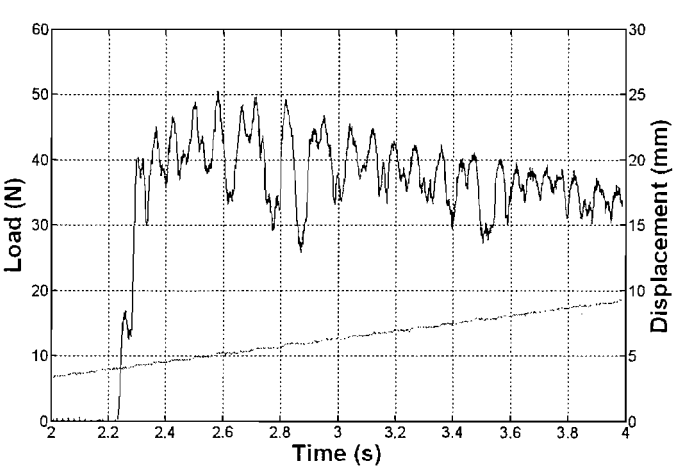

Figure B2(i) Load and displacement curves for test No 10. Sample 2

Anchor		Test S2-11	
B=	30 mm	v=	3 mm/s
H=	45 mm	Dyn=	0°
θ=	5°	Soil	Sand
Pore Pressure			
PP50		51.4 kPa	
PP75		35.6 kPa	
PP100		25.6 kPa	

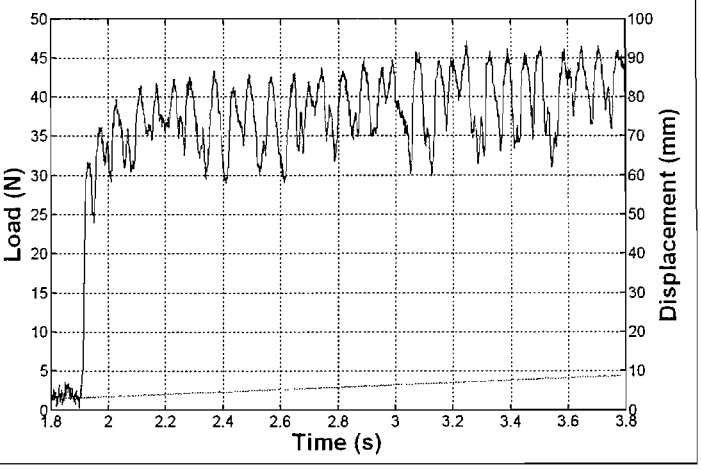

Figure B2(j) Load and displacement curves for test No 11. Sample 2

Anchor		Test S3-1	
B=	30 mm	V=	100 mm/s
H=	45 mm	Dyn=	0°
θ=	0°	Soil	Clay
Pore Pressure			
PP50		34.4	
PP75		23.7	
PP100		12.0	

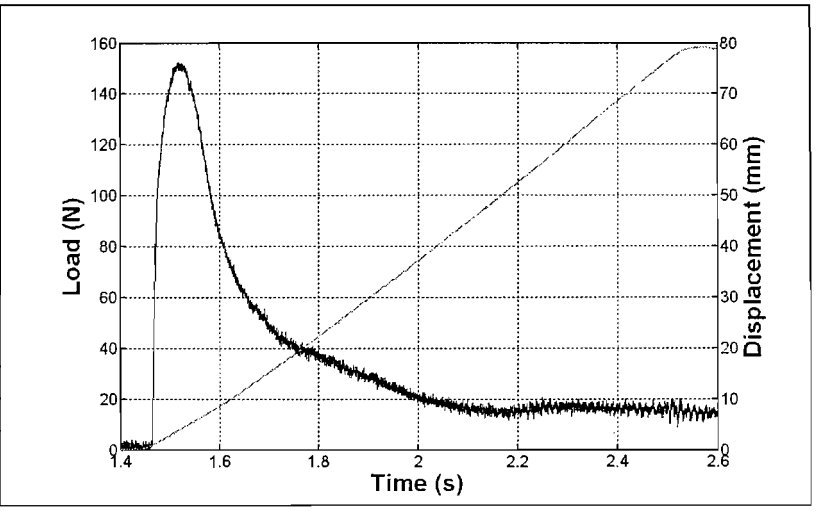

Figure B3(a) Load and displacement curves for test No 1. Sample 3

Anchor		Test S3-2	
B=	30 mm	V=	60 mm/s
H=	45 mm	Dyn=	22.5°
θ=	0°	Soil	Clay
Pore Pressure			
PP50		34.4	
PP75		23.7	
PP100		12.0	

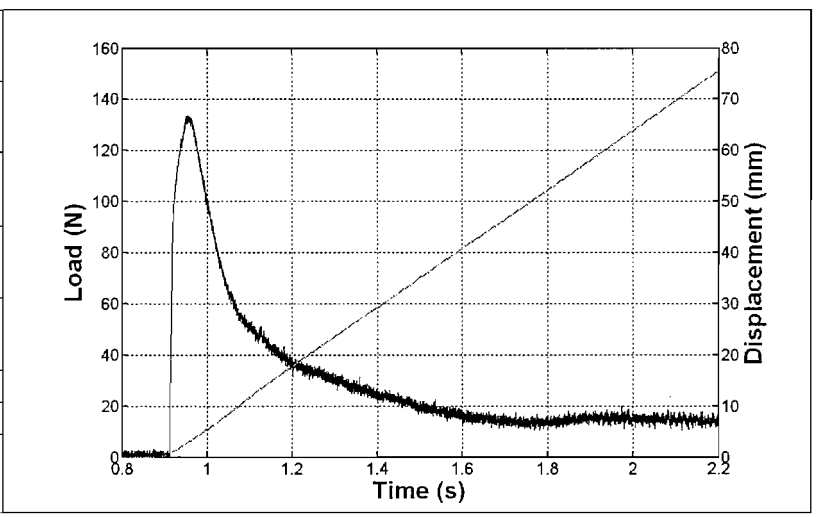

Figure B3(b) Load and displacement curves for test No 2. Sample 3

Anchor		Test S3-3	
B=	30 mm	V=	30 mm/s
H=	45 mm	Dyn=	45°
θ=	0°	Soil	Clay
Pore Pressure			
PP50		34.4	
PP75		23.7	
PP100		12.0	

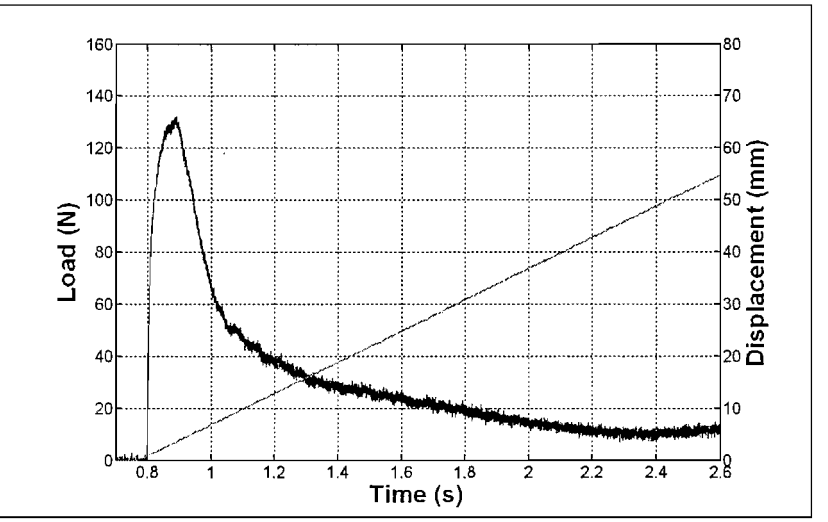

Figure B3(c) Load and displacement curves for test No 3. Sample 3

Anchor		Test S3-4	
B=	30 mm	V=	3 mm/s
H=	45 mm	Dyn=	67.5°
θ=	0°	Soil	Clay
Pore Pressure			
PP50		34.4	
PP75		23.7	
PP100		12.0	

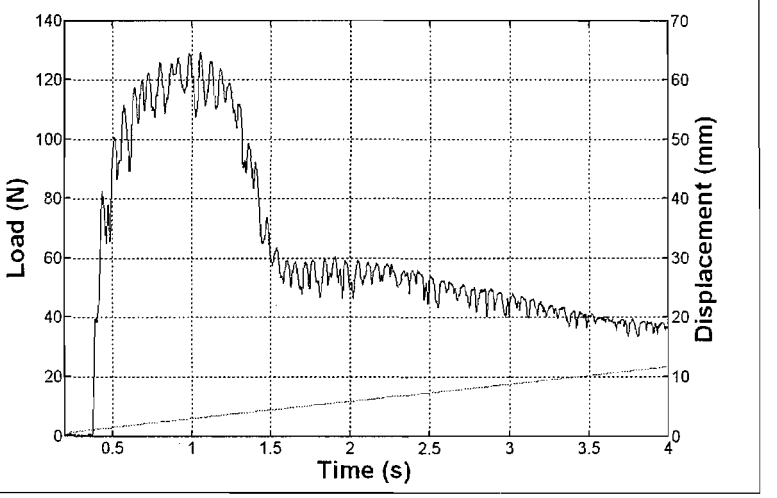

Figure B3(d) Load and displacement curves for test No 4. Sample 3

Anchor		Test S3-5	
B=	30 mm	V=	0.3 mm/s
H=	45 mm	Dyn=	90°
θ=	0°	Soil	Clay
Pore Pressure			
PP50		34.4	
PP75		23.7	
PP100		12.0	

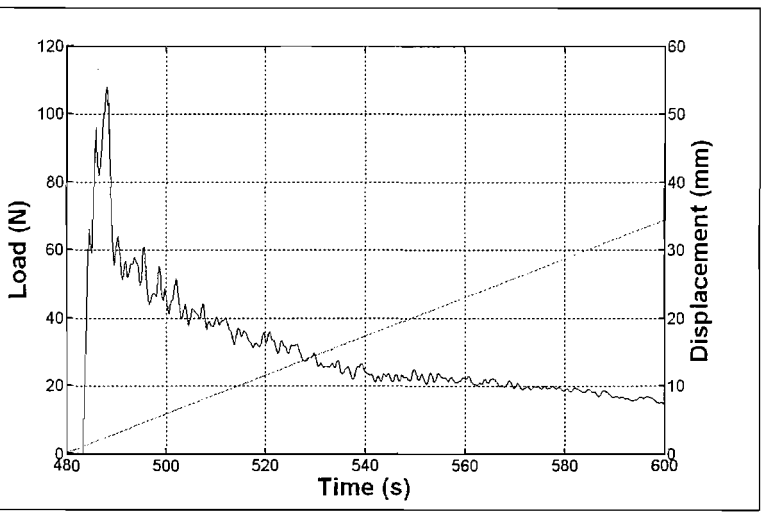

Figure B3(e) Load and displacement curves for test No 5. Sample 3

Anchor		Test S3-6	
B=	30 mm	V=	0.03 mm/s
H=	45 mm	Dyn=	112.5°
θ=	0°	Soil	Clay
Pore Pressure			
PP50		34.4	
PP75		23.7	
PP100		12.0	

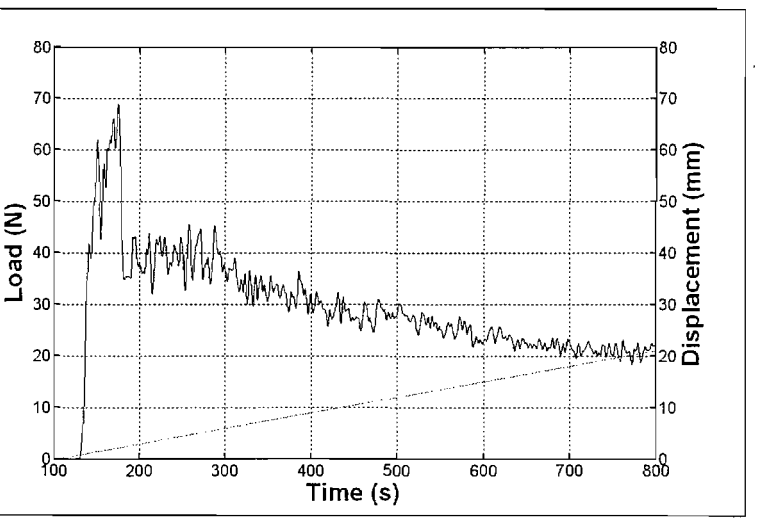

Figure B3(f) Load and displacement curves for test No 6. Sample 3

Anchor		Test S3-7	
B=	60 mm	V=	100 mm/s
H=	45 mm	Dyn=	157.5°
θ=	0°	Soil	Clay
Pore Pressure			
PP50	34.4		
PP75	23.7		
PP100	12.0		

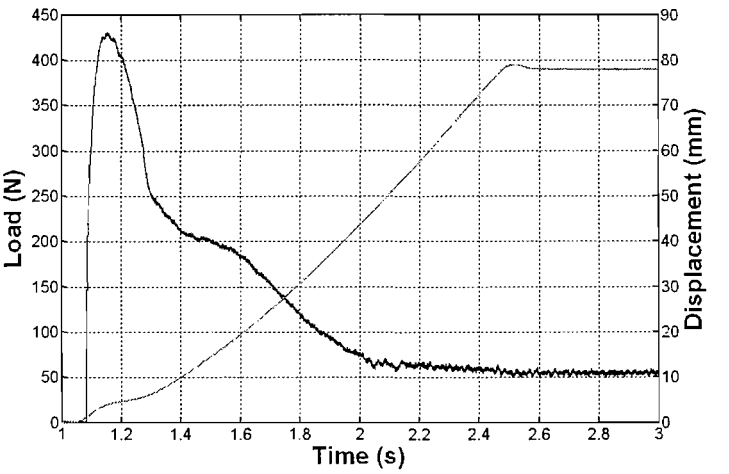

Figure B3(g) Load and displacement curves for test No 7. Sample 3

Anchor		Test S3-8	
B=	60 mm	V=	60 mm/s
H=	45 mm	Dyn=	180°
θ=	0°	Soil	Clay
Pore Pressure			
PP50	34.4		
PP75	23.7		
PP100	12.0		

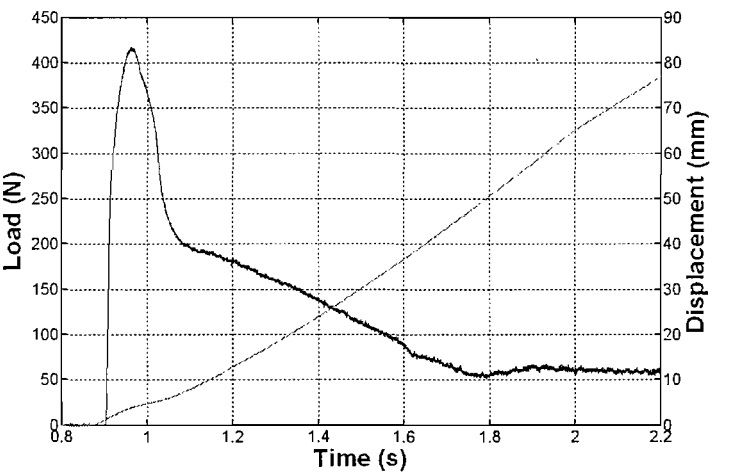

Figure B3(h) Load and displacement curves for test No 8. Sample 3

Anchor		Test S3-9	
B=	60 mm	V=	30 mm/s
H=	45 mm	Dyn=	202.5°
θ=	0°	Soil	Clay
Pore Pressure			
PP50	34.4		
PP75	23.7		
PP100	12.0		

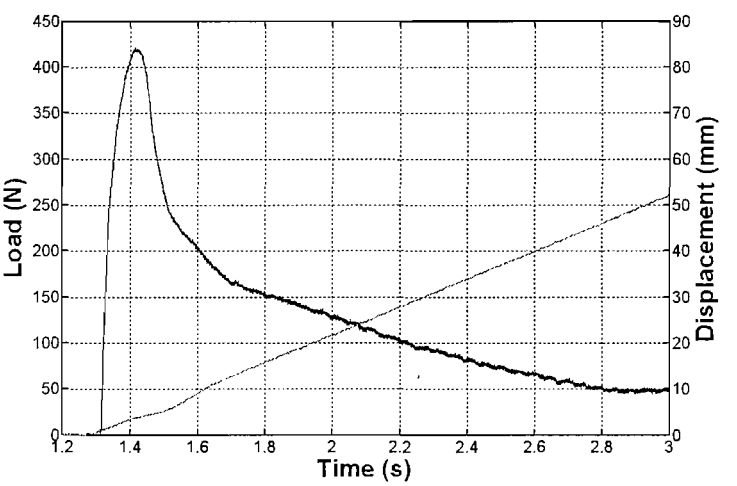

Figure B3(i) Load and displacement curves for test No 9. Sample 3

Anchor		Test S3-10	
B=	30 mm	V=	3 mm/s
H=	45 mm	Dyn=	135°
θ=	0°	Soil	Sand
Pore Pressure			
PP50		34.4	
PP75		23.7	
PP100		12.0	

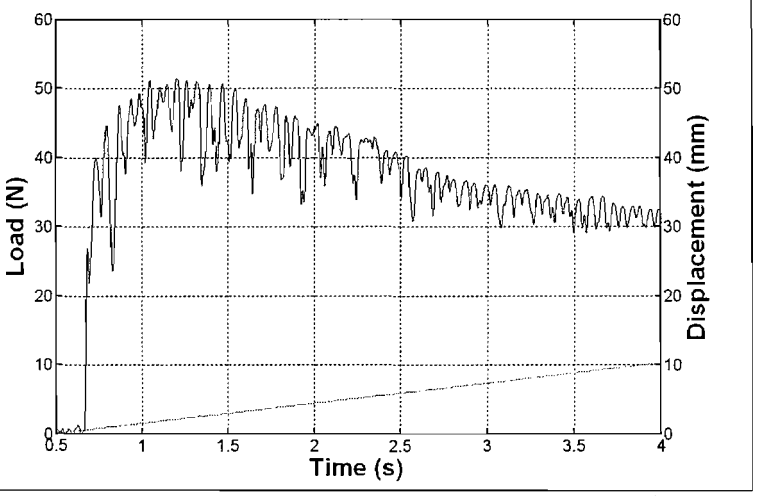

Figure B3(j) Load and displacement curves for test No 10. Sample 3

Anchor		Test S3-11	
B=	60 mm	V=	3 mm/s
H=	45 mm	Dyn=	225°
θ=	0°	Soil	Clay
Pore Pressure			
PP50		34.4	
PP75		23.7	
PP100		12.0	

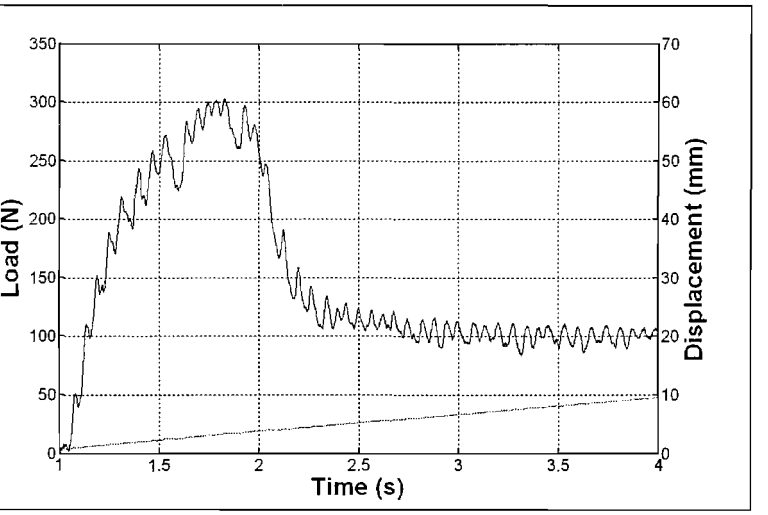

Figure B3(k) Load and displacement curves for test No 11. Sample 3

Anchor		Test S3-12	
B=	60 mm	V=	0.3 mm/s
H=	45 mm	Dyn=	247.5°
θ=	0°	Soil	Clay
Pore Pressure			
PP50		34.4	
PP75		23.7	
PP100		12.0	

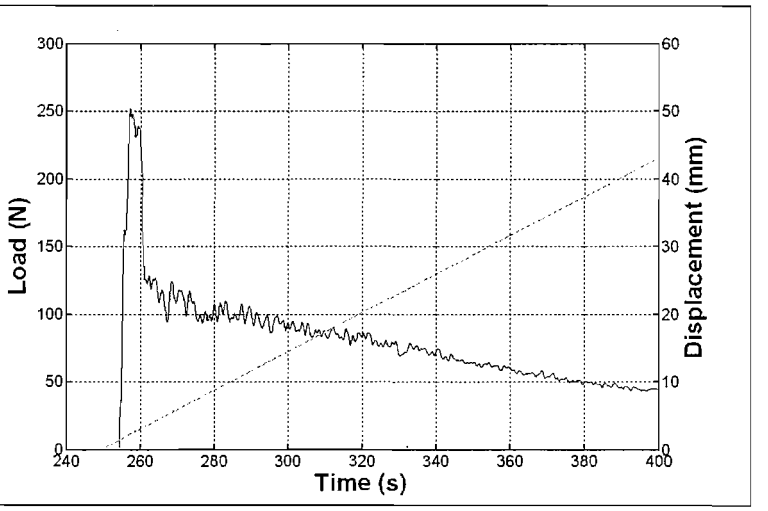

Figure B3(l) Load and displacement curves for test No 12. Sample 3

Anchor		Test S3-13	
B=	60 mm	V=	0.03 mm/s
H=	45 mm	Dyn=	270°
θ=	0°	Soil	Clay
Pore Pressure			
PP50	34.4		
PP75	23.7		
PP100	12.0		

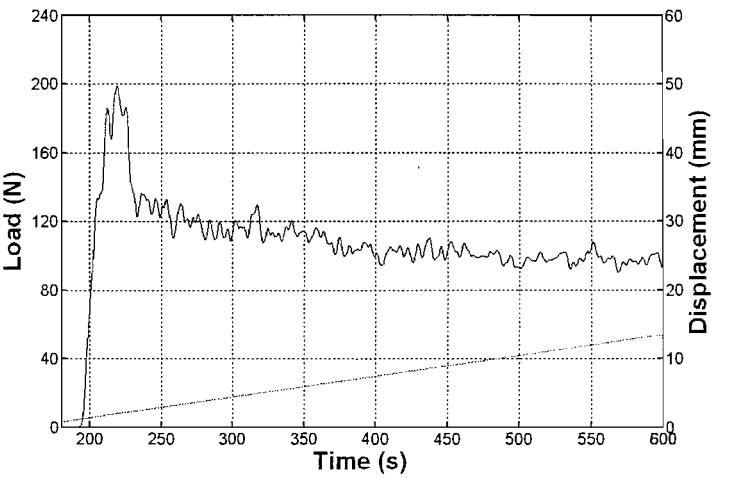

Figure B3(m) Load and displacement curves for test No 13. Sample 3

Anchor		Test S3-16	
B=	60 mm	V=	30 mm/s
H=	45 mm	Dyn=	292.5°
θ=	0°	Soil	Clay
Pore Pressure			
PP50	34.4		
PP75	23.7		
PP100	12.0		

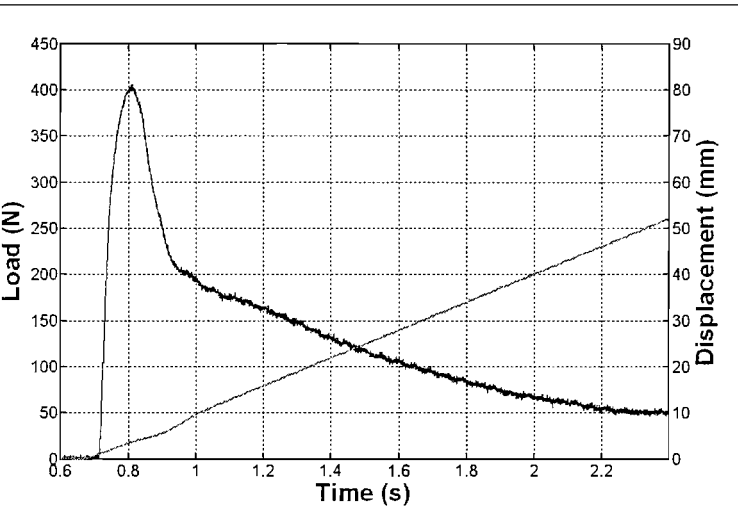

Figure B3(n) Load and displacement curves for test No 16. Sample 3

Anchor		Test S3-17	
B=	60 mm	V=	3 mm/s
H=	45 mm	Dyn=	292.5°
θ=	0°	Soil	Sand
Pore Pressure			
PP50	34.4		
PP75	23.7		
PP100	12.0		

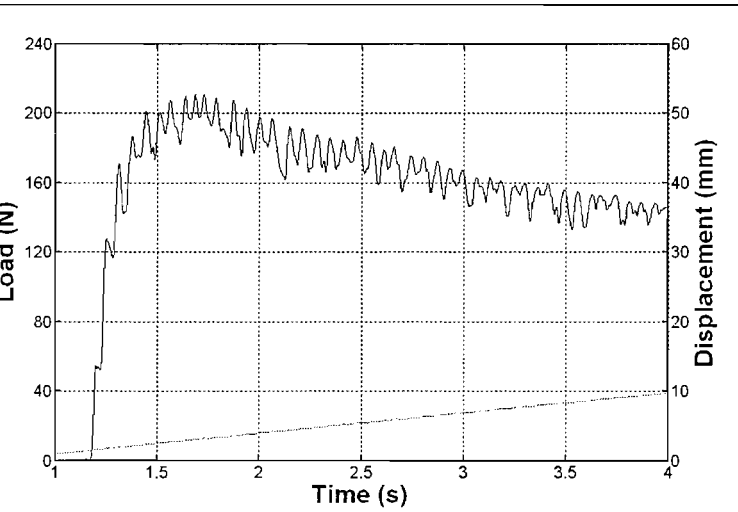

Figure B3(o) Load and displacement curves for test No 17. Sample 3

Anchor		Test S4-1	
B=	30 mm	V=	0.3 mm/s
H=	45 mm	Dyn=	112.5°
θ=	0°	Soil	Clay
Pore Pressure			
PP50			
PP75			
PP100		29.1	

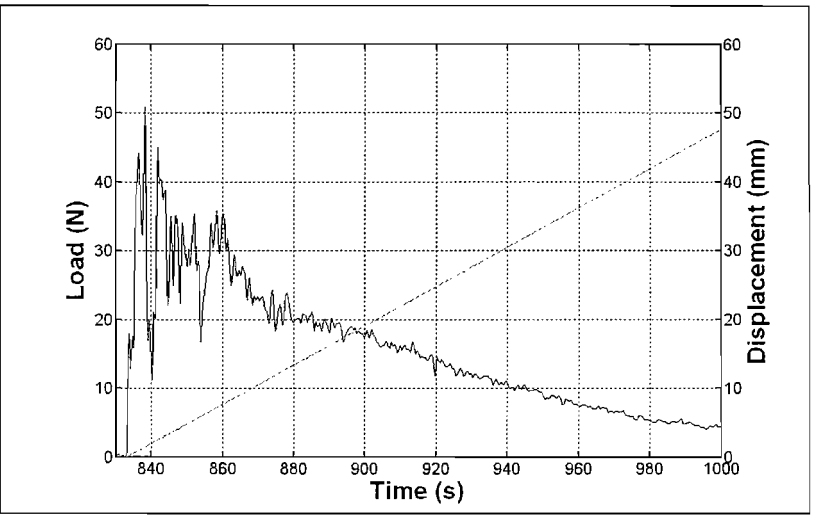

Figure B4(a) Load and displacement curves for test No 1. Sample 4

Anchor		Test S4-2	
B=	45 mm	V=	3 mm/s
H=	45 mm	Dyn=	202.5°
θ=	0°	Soil	Clay
Pore Pressure			
PP50			
PP75			
PP100		29.1	

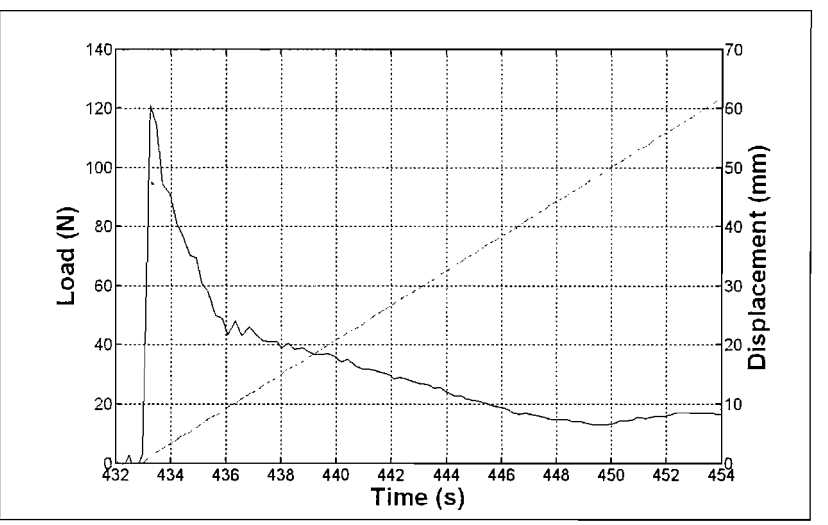

Figure B4(b) Load and displacement curves for test No 2. Sample 4

Anchor		Test S4-3	
B=	30 mm	V=	100 mm/s
H=	45 mm	Dyn=	180°
θ=	0°	Soil	Clay
Pore Pressure			
PP50			
PP75			
PP100		29.1	

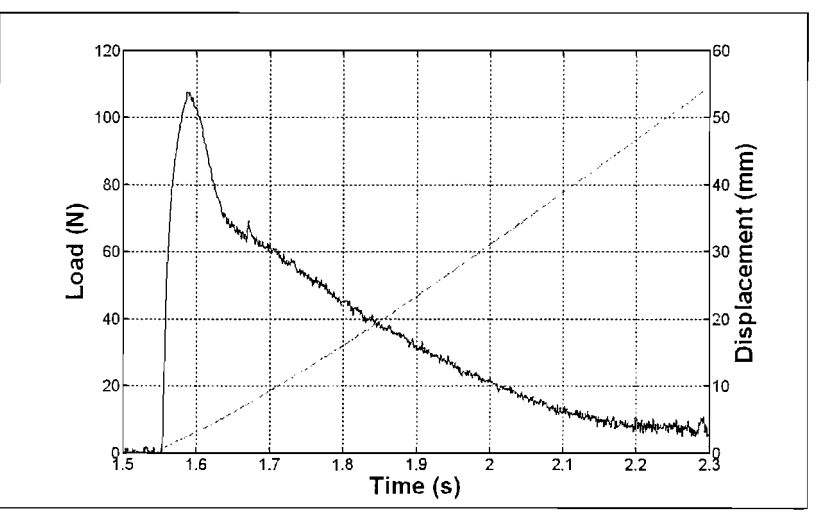

Figure B4(c) Load and displacement curves for test No 3. Sample 4

Anchor		Test S4-4	
B=	30 mm	V=	30 mm/s
H=	45 mm	Dyn=	157.5°
θ=	0°	Soil	Clay
Pore Pressure			
PP50			
PP75			
PP100		29.1	

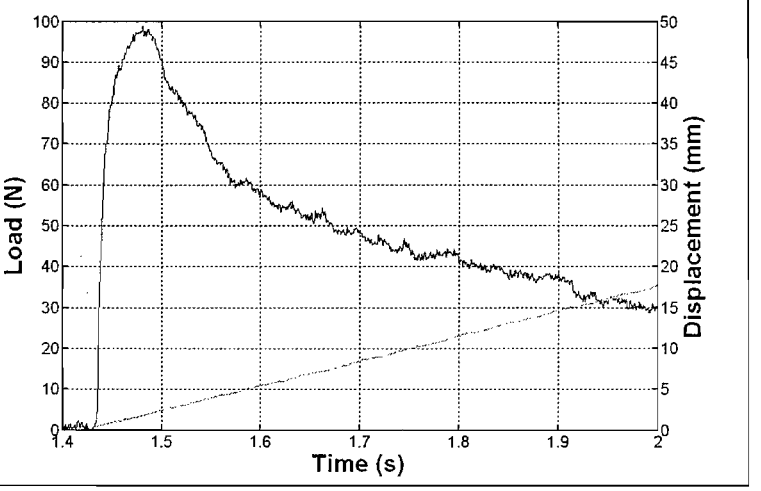

Figure B4(d) Load and displacement curves for test No 4. Sample 4

Anchor		Test S4-5	
B=	30 mm	V=	0.03 mm/s
H=	45 mm	Dyn=	112.5°
θ=	0°	Soil	Clay
Pore Pressure			
PP50			
PP75			
PP100		29.1	

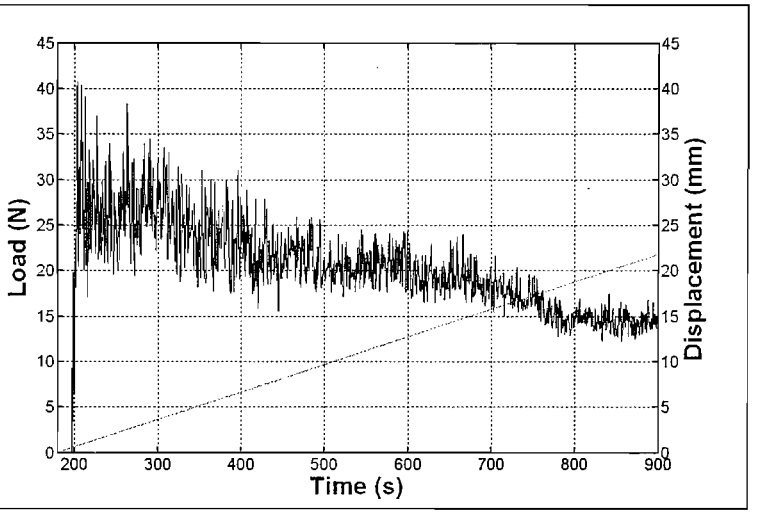

Figure B4(e) Load and displacement curves for test No 5. Sample 4

Anchor		Test S4-6	
B=	30 mm	V=	3 mm/s
H=	45 mm	Dyn=	90°
θ=	0°	Soil	Clay
Pore Pressure			
PP50			
PP75			
PP100		29.1	

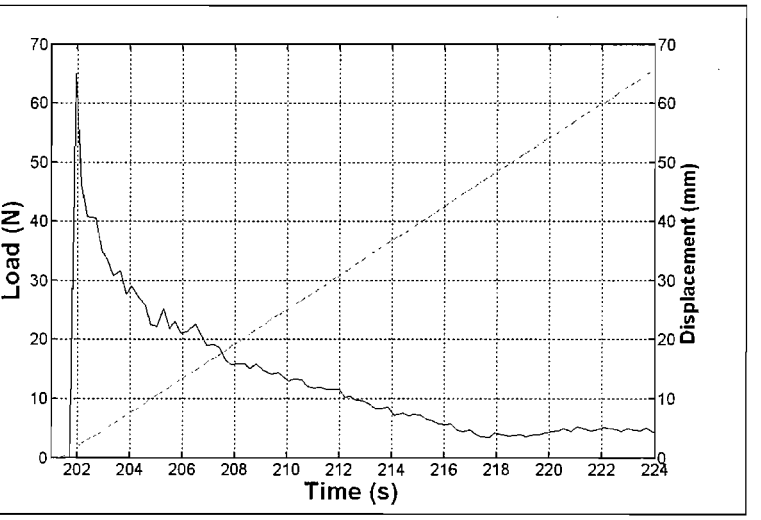

Figure B4(f) Load and displacement curves for test No 6. Sample 4

Anchor		Test S4-7	
B=	30 mm	V=	30 mm/s
H=	45 mm	Dyn=	308.6°
θ=	0°	Soil	Clay
Pore Pressure			
PP50			
PP75			
PP100		29.1	

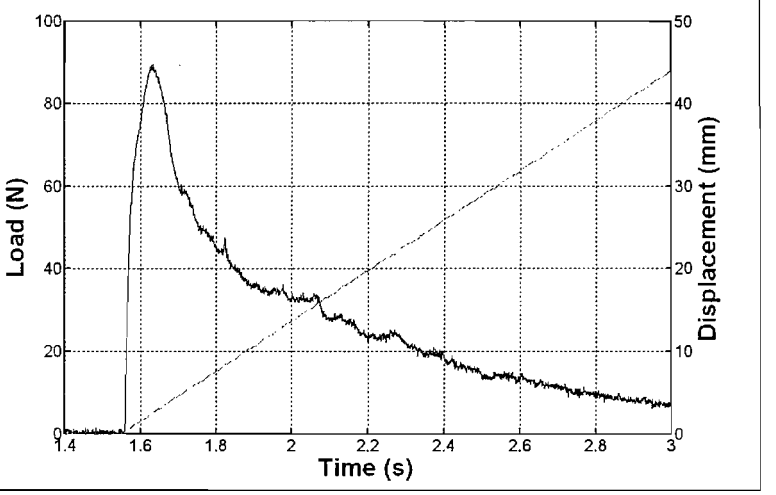

Figure B4(g) Load and displacement curves for test No 7. Sample 4

Anchor		Test S4-8	
B=	30 mm	V=	60 mm/s
H=	45 mm	Dyn=	33.75°
θ=	0°	Soil	Clay
Pore Pressure			
PP50			
PP75			
PP100		29.1	

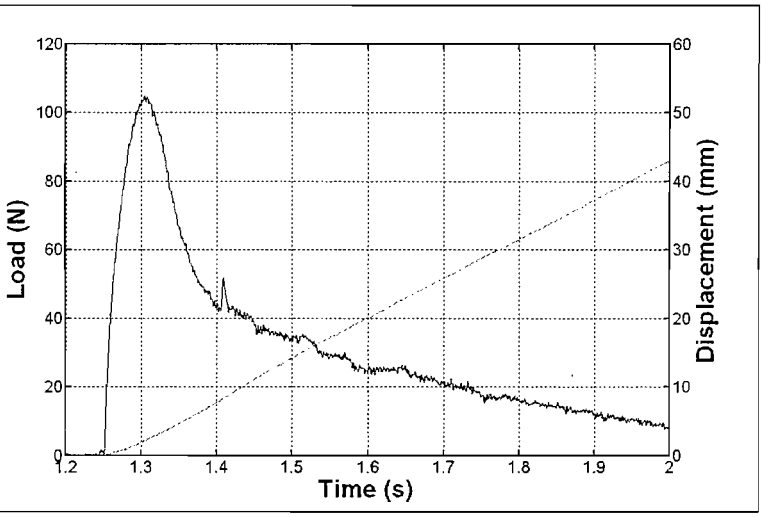

Figure B4(h) Load and displacement curves for test No 8. Sample 4

Anchor		Test S4-9	
B=	60 mm	V=	3 mm/s
H=	45 mm	Dyn=	257°
θ=	0°	Soil	Clay
Pore Pressure			
PP50			
PP75			
PP100		29.1	

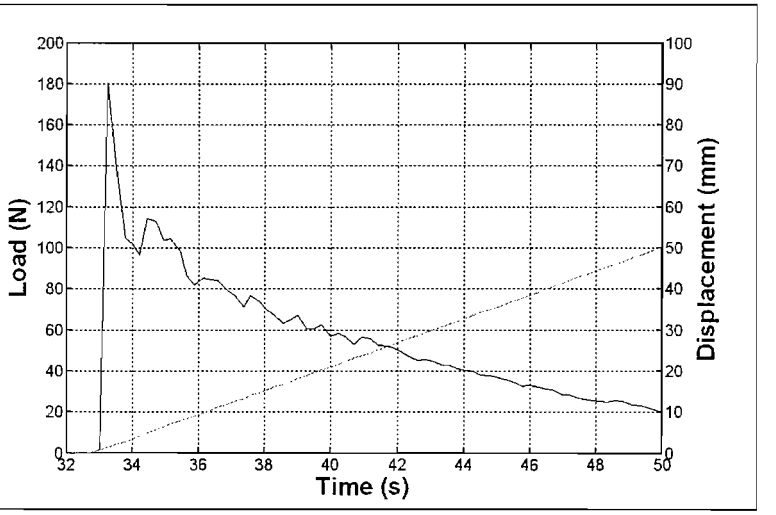

Figure B4(i) Load and displacement curves for test No 9. Sample 4

Anchor		Test S4-10	
B=	30 mm	V=	3 mm/s
H=	45 mm	Dyn=	337.5°
θ=	15°	Soil	Clay
Pore Pressure			
PP50			
PP75			
PP100	29.1		

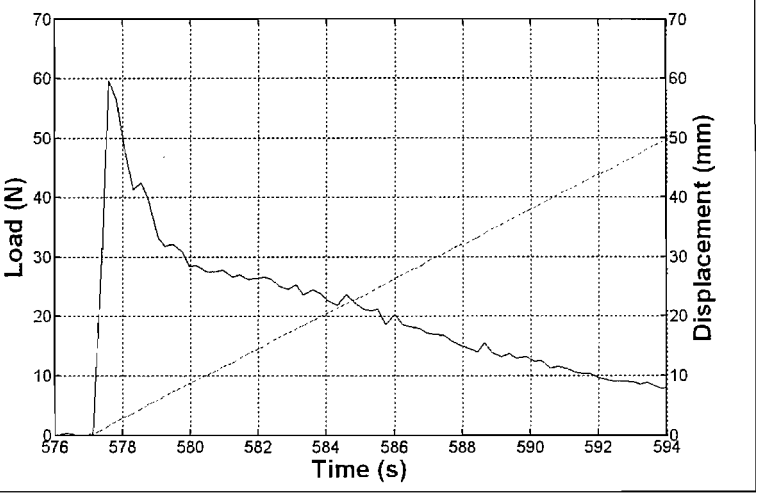

Figure B4(j) Load and displacement curves for test No 10. Sample 4

Anchor		Test S4-11	
B=	30 mm	V=	30 mm/s
H=	45 mm	Dyn=	247.5°
θ=	0°	Soil	Clay
Pore Pressure			
PP50			
PP75			
PP100	29.1		

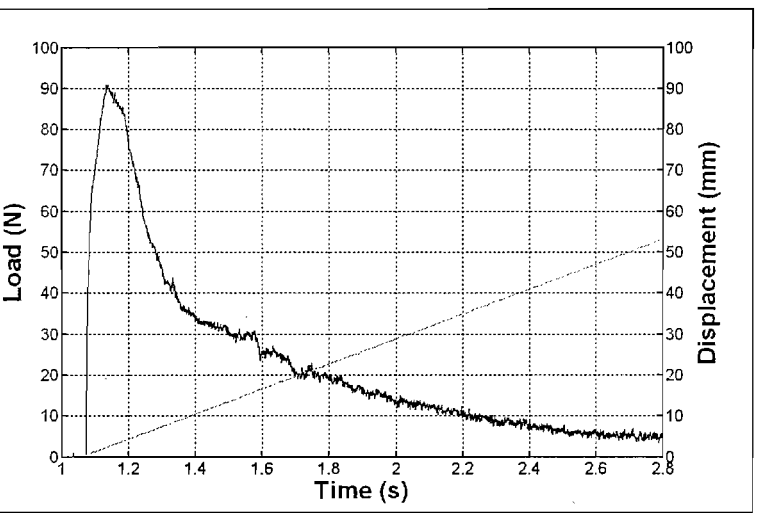

Figure B4(k) Load and displacement curves for test No 11. Sample 4

Anchor		Test S4-12	
B=	60 mm	V=	3 mm/s
H=	45 mm	Dyn=	227°
θ=	0°	Soil	Clay
Pore Pressure			
PP50			
PP75			
PP100	29.1		

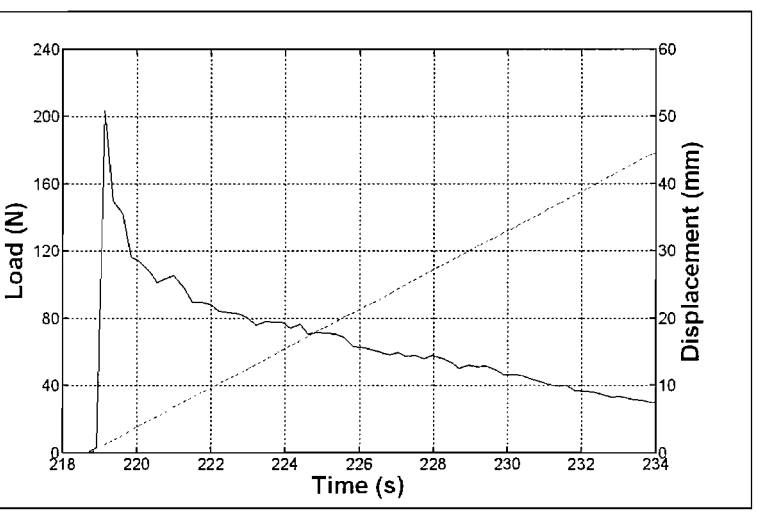

Figure B4(l) Load and displacement curves for test No 12. Sample 4

Anchor		Test S4-13	
B=	30 mm	V=	100 mm/s
H=	45 mm	Dyn=	69°
θ=	0°	Soil	Clay
Pore Pressure			
PP50			
PP75			
PP100	29.1		

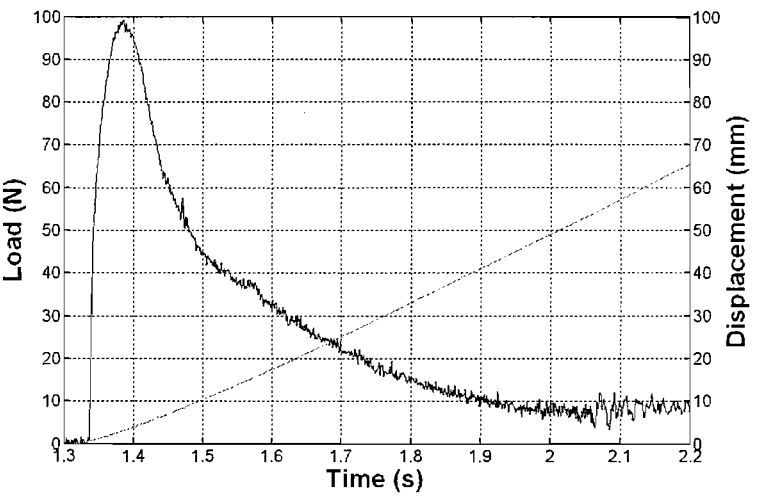

Figure B4(m) Load and displacement curves for test No 13. Sample 4

Anchor		Test S5-1	
B=	45 mm	V=	3 mm/s
H=	45 mm	Dyn=	112.5°
θ=	0°	Soil	Clay
Pore Pressure			
PP50			
PP75			
PP100	29.1		

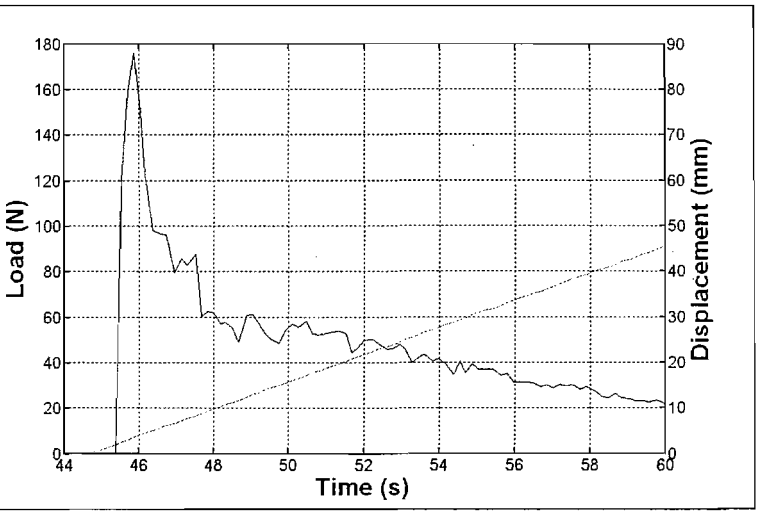

Figure B5(a) Load and displacement curves for test No 1. Sample 5

Anchor		Test S5-2	
B=	60 mm	V=	0.03 mm/s
H=	45 mm	Dyn=	202.5°
θ=	0°	Soil	Clay
Pore Pressure			
PP50			
PP75			
PP100	29.1		

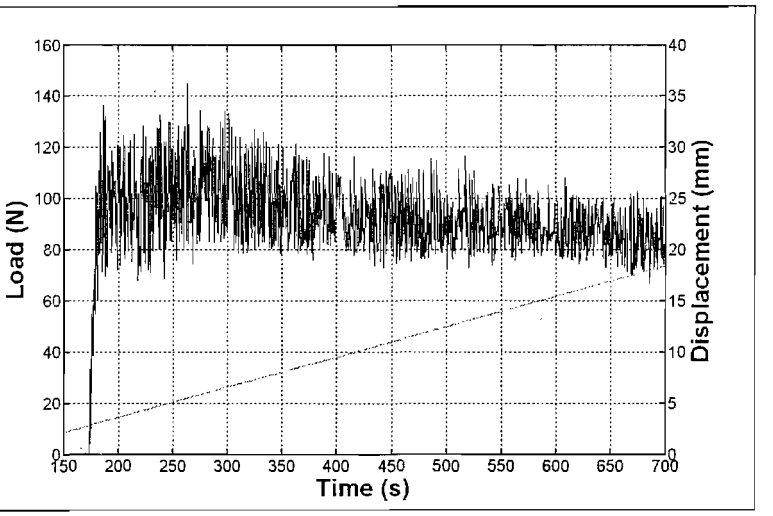

Figure B5(b) Load and displacement curves for test No 2. Sample 5

Anchor		Test S5-3	
B=	60 mm	V=	0.3 mm/s
H=	45 mm	Dyn=	180°
θ=	0°	Soil	Clay
Pore Pressure			
PP50			
PP75			
PP100	29.1		

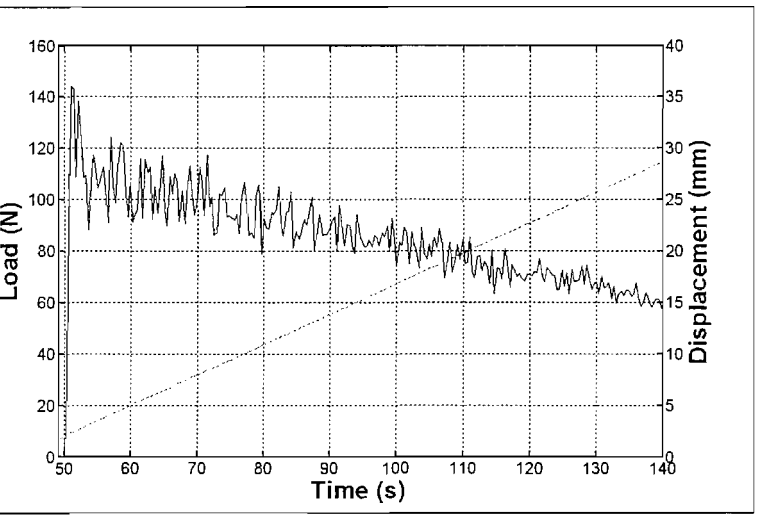

Figure B5(c) Load and displacement curves for test No 3. Sample 5

Anchor		Test S5-4	
B=	60 mm	V=	3 mm/s
H=	45 mm	Dyn=	157.5°
θ=	0°	Soil	Clay
Pore Pressure			
PP50			
PP75			
PP100		29.1	

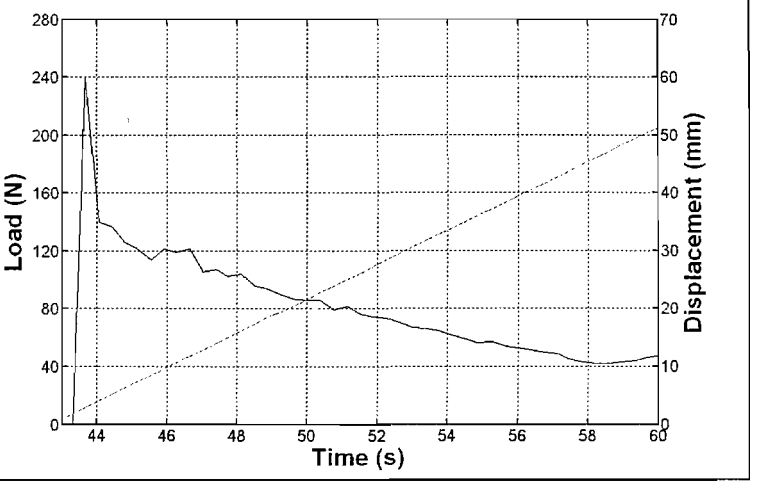

Figure B5(d) Load and displacement curves for test No 4. Sample 5

Anchor		Test S5-5	
B=	30 mm	V=	3 mm/s
H=	45 mm	Dyn=	112.5°
θ=	5°	Soil	Clay
Pore Pressure			
PP50			
PP75			
PP100		29.1	

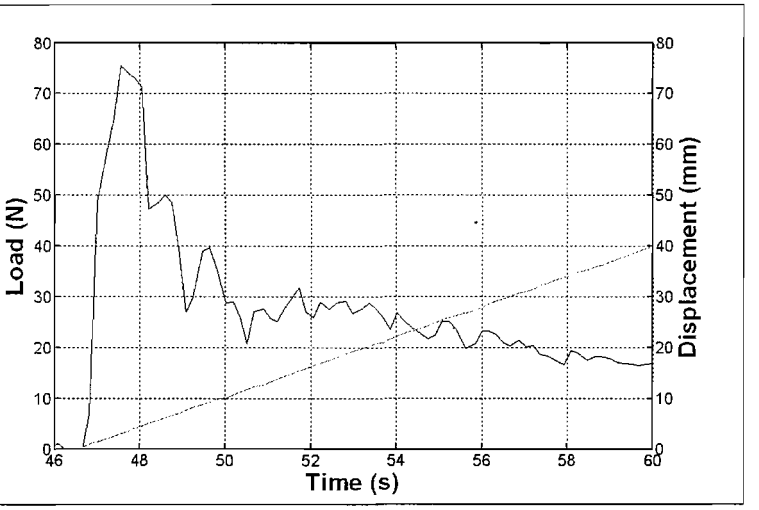

Figure B5(e) Load and displacement curves for test No 5. Sample 5

Anchor		Test S5-6	
B=	30 mm	V=	3 mm/s
H=	45 mm	Dyn=	90°
θ=	10°	Soil	Clay
Pore Pressure			
PP50			
PP75			
PP100		29.1	

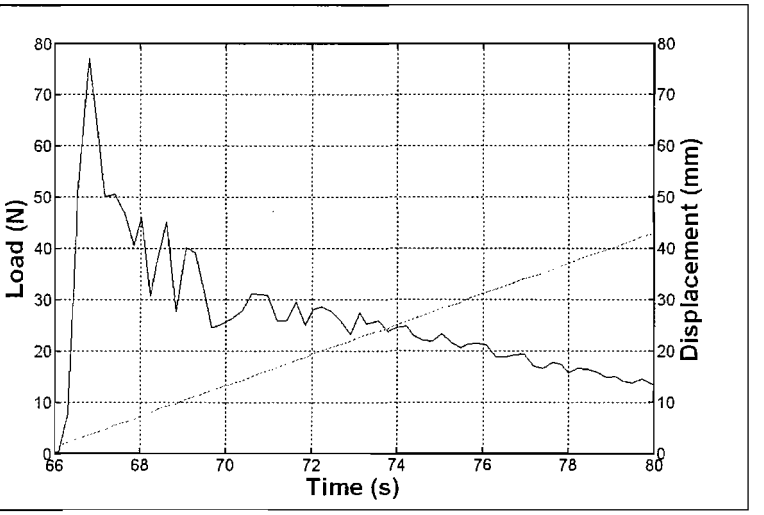

Figure B5(f) Load and displacement curves for test No 6. Sample 5

Anchor		Test S5-7	
B=	30 mm	V=	3 mm/s
H=	45 mm	Dyn=	308.6°
θ=	15°	Soil	Clay
Pore Pressure			
PP50			
PP75			
PP100		29.1	

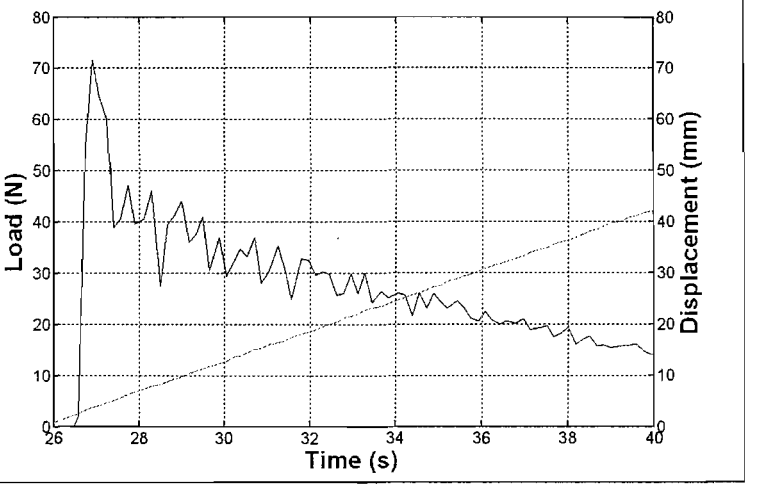

Figure B5(g) Load and displacement curves for test No 7. Sample 5

Anchor		Test S5-8	
B=	30 mm	V=	3 mm/s
H=	45 mm	Dyn=	33.75°
θ=	20°	Soil	Clay
Pore Pressure			
PP50			
PP75			
PP100		29.1	

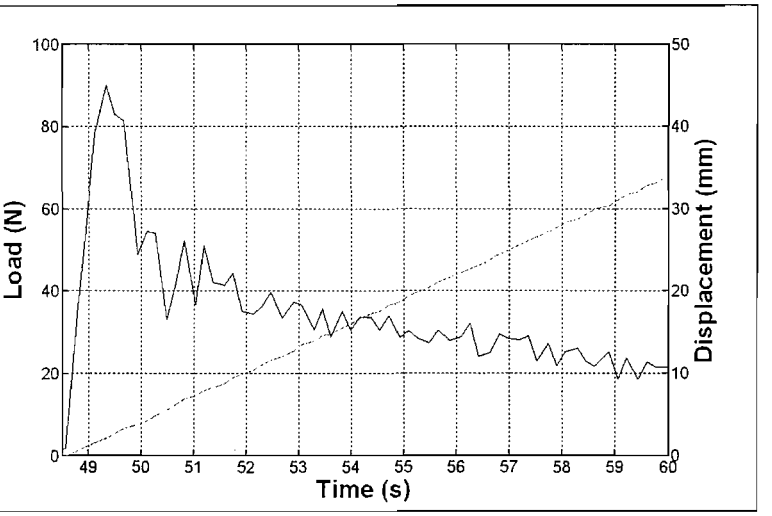

Figure B5(h) Load and displacement curves for test No 8. Sample 5

Anchor		Test S5-9	
B=	30 mm	V=	3 mm/s
H=	45 mm	Dyn=	257°
θ=	15°	Soil	Sand
Pore Pressure			
PP50			
PP75			
PP100		29.1	

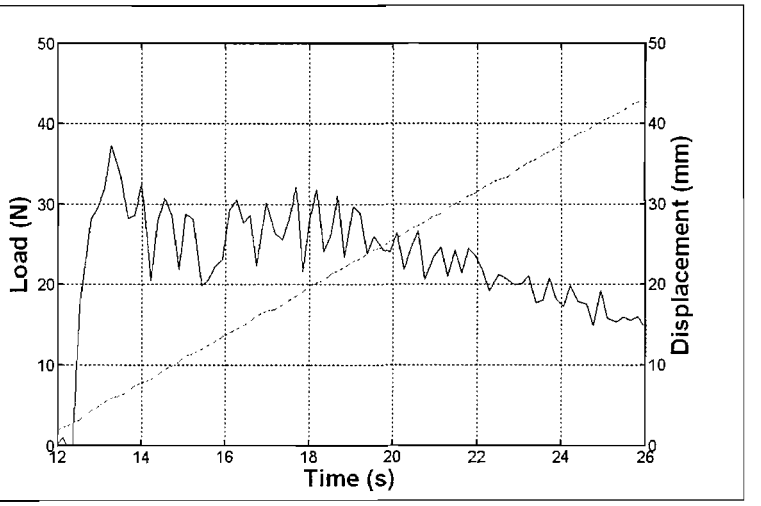

Figure B5(i) Load and displacement curves for test No 9. Sample 5

Anchor		Test S5-10	
B=	60 mm	V=	3 mm/s
H=	45 mm	Dyn=	225°
θ=	0°	Soil	Sand
Pore Pressure			
PP50			
PP75			
PP100		29.1	

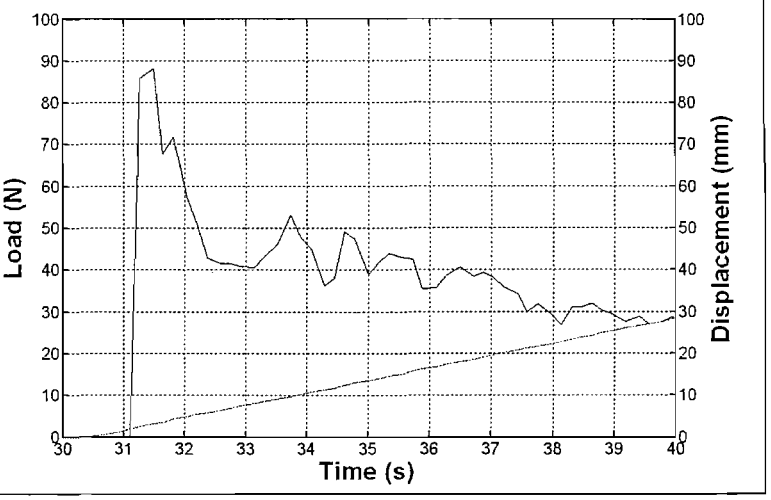

Figure B5(j) Load and displacement curves for test No 10. Sample 5

APPENDIX C

PACB UPLIFT TEST DATA

B Anchor width

v_f Uplift displacement rate

H Embedment depth

Dyn Position of centrifuge actuator

θ Anchor inclination

Soil Soil at anchor base

Anchor		Test S1-1	
B=	30 mm	v=	3 mm/s
H=	45 mm	Dyn=	337°
θ=	0°	Soil	Clay
Pore Pressure			
PP50		50.8 kPa	
PP75		34.6 kPa	
PP100		24.6 kPa	

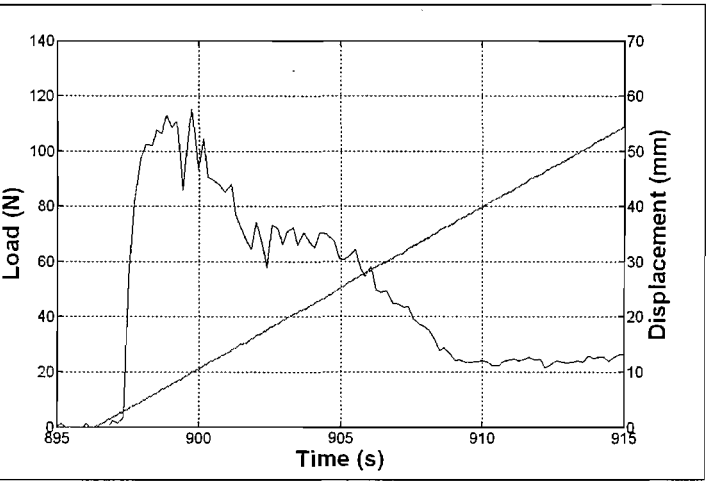

Figure C1(a) Load and displacement curves for test No 1.

Anchor		Test S1-2	
B=	30 mm	v=	30 mm/s
H=	45 mm	Dyn=	225°
θ=	0°	Soil	Clay
Pore Pressure			
PP50		50.8 kPa	
PP75		34.6 kPa	
PP100		24.6 kPa	

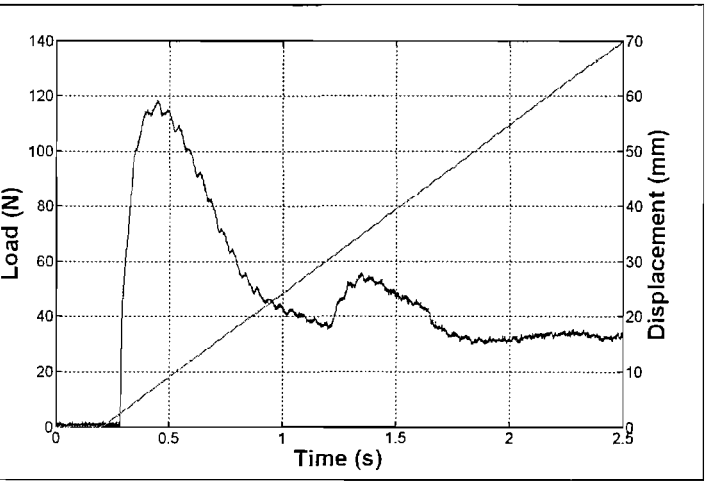

Figure C1(b) Load and displacement curves for test No 2.

Anchor		Test S1-3	
B=	30 mm	v=	100 mm/s
H=	45 mm	Dyn=	113°
θ=	0°	Soil	Clay
Pore Pressure			
PP50		50.8 kPa	
PP75		34.6 kPa	
PP100		24.6 kPa	

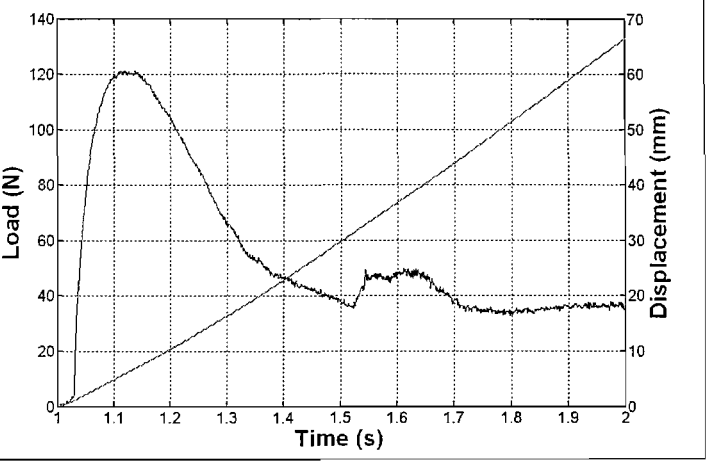

Figure C1(c) Load and displacement curves for test No 3.

Anchor		Test S1-4	
B=	30 mm	v=	0.03 mm/s
H=	45 mm	Dyn=	45°
θ=	0°	Soil	Clay
Pore Pressure			
PP50		50.8 kPa	
PP75		34.6 kPa	
PP100		24.6 kPa	

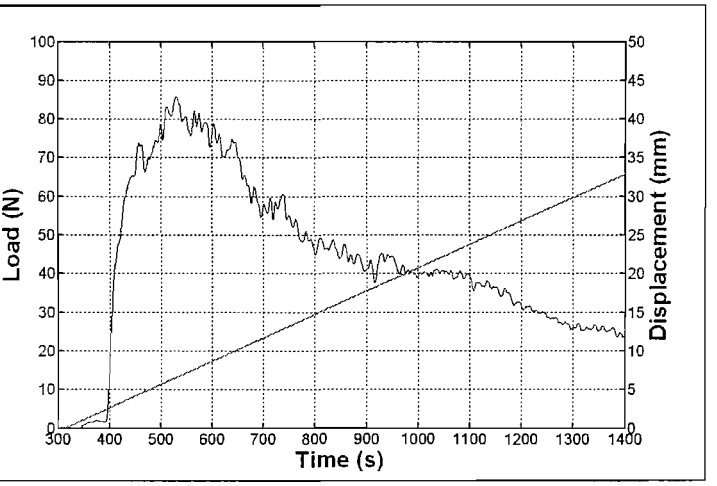

Figure C1(d) Load and displacement curves for test No 4.

Anchor		Test S1-5	
B=	30 mm	v=	3 mm/s
H=	45 mm	Dyn=	135°
θ=	0°	Soil	Sand
Pore Pressure			
PP50		50.8 kPa	
PP75		34.6 kPa	
PP100		24.6 kPa	

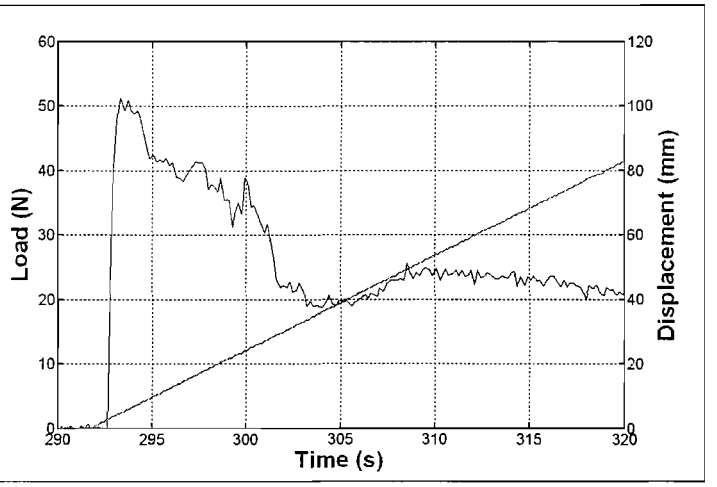

Figure C1(e) Load and displacement curves for test No 5.

Anchor		Test S1-7	
B=	45 mm	v=	3 mm/s
H=	45 mm	Dyn=	270°
θ=	0°	Soil	Sand
Pore Pressure			
PP50		50.8 kPa	
PP75		34.6 kPa	
PP100		24.6 kPa	

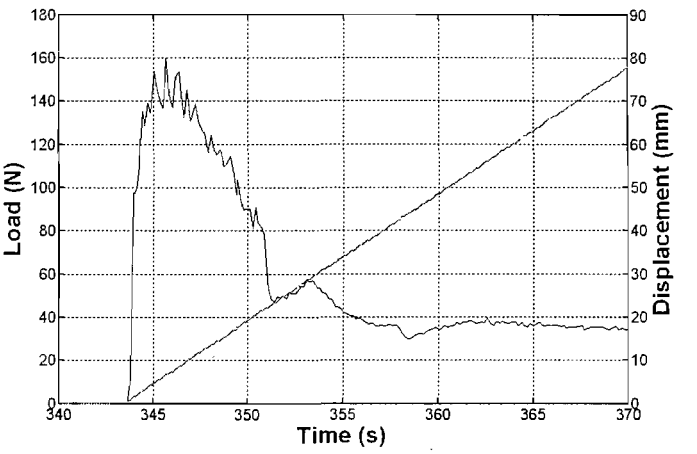

Figure C1(f) Load and displacement curves for test No 7.

Anchor		Test S1-8	
B=	45 mm	v=	3 mm/s
H=	45 mm	Dyn=	293°
θ=	0°	Soil	Clay
Pore Pressure			
PP50		50.8 kPa	
PP75		34.6 kPa	
PP100		24.6 kPa	

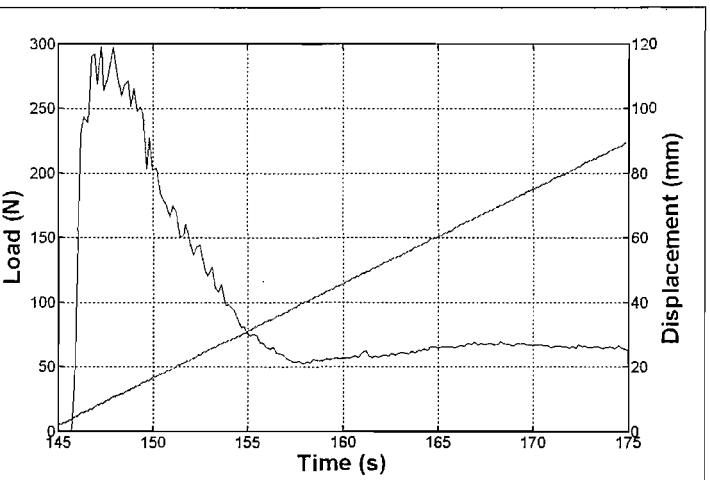

Figure C1(g) Load and displacement curves for test No 8.

APPENDIX D

TTFS UPLIFT TEST DATA

B Anchor width

v_f Uplift displacement rate

H Embedment depth

Dyn Position of centrifuge actuator

θ Anchor inclination

Soil Soil at anchor base

Footing		Test S1-1	
B=	40 mm	v=	3 mm/s
H=	65 mm	Dyn=	23.5°
θ=	9.2°	Soil	Sand
Pore Pressure			
PP50		52.2 kPa	
PP75		36.9 kPa	
PP100		24.3 kPa	

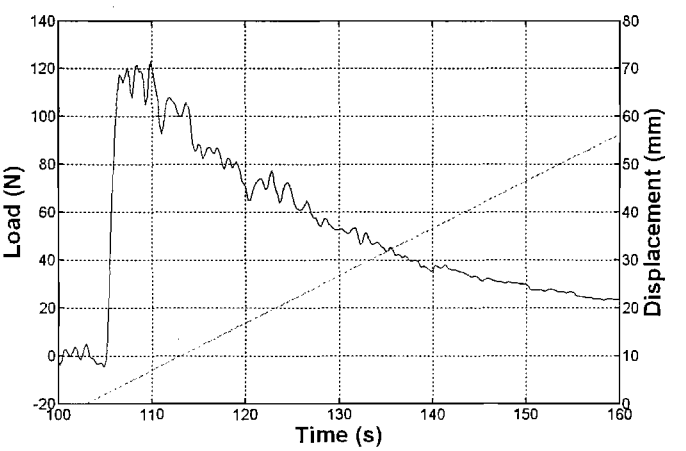

Figure D1(a) Load and displacement curves for test No 1.

Footing		Test S1-2	
B=	40 mm	v=	30 mm/s
H=	65 mm	Dyn=	23.5°
θ=	0°	Soil	Clay
Pore Pressure			
PP50		52.2 kPa	
PP75		36.9 kPa	
PP100		24.3 kPa	

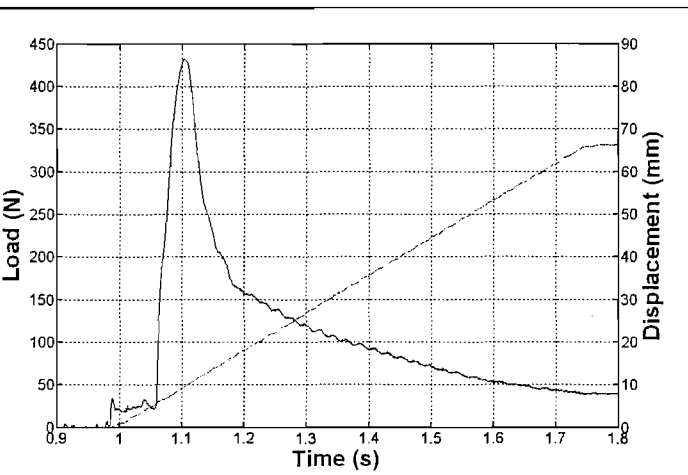

Figure D1(b) Load and displacement curves for test No 2.

Footing		Test S1-2	
B=	40 mm	v=	30 mm/s
H=	65 mm	Dyn=	23.5°
θ=	0°	Soil	Clay
Pore Pressure			
PPTT initial reading		29.8	

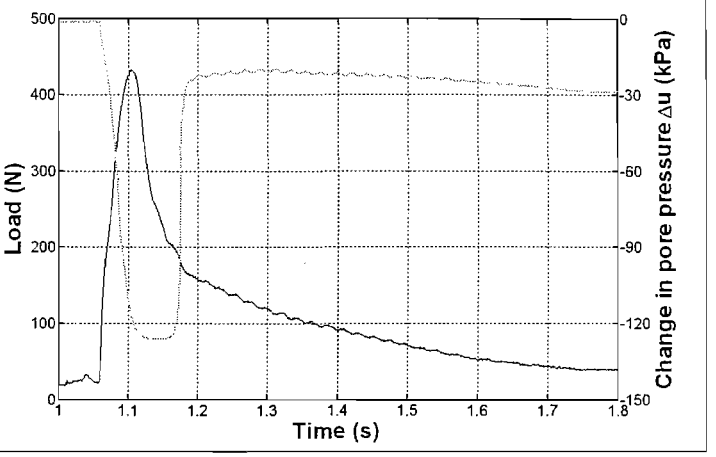

Figure D1(c) Load and pore pressure curves for test No 2.

Footing		Test S1-3	
B=	40 mm	v=	30 mm/s
H=	65 mm	Dyn=	23.5°
θ=	9.3°	Soil	Clay
Pore Pressure			
PP50		52.2 kPa	
PP75		36.9 kPa	
PP100		24.3 kPa	

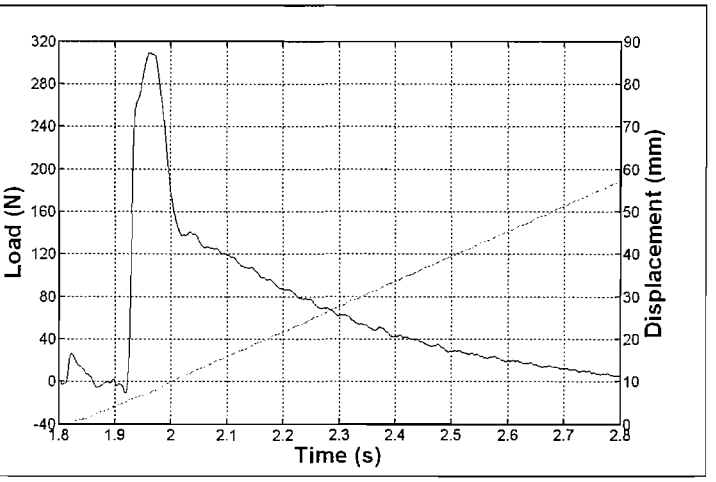

Figure D1(d) Load and displacement curves for test No 3.

Footing		Test S1-4	
B=	40 mm	v=	3 mm/s
H=	65 mm	Dyn=	23.5°
θ=	0°	Soil	Sand
Pore Pressure			
PP50		52.2 kPa	
PP75		36.9 kPa	
PP100		24.3 kPa	

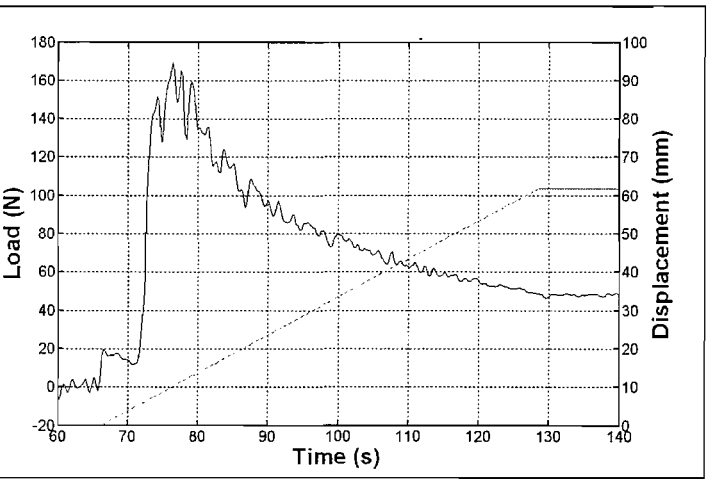

Figure D1(e) Load and displacement curves for test No 4.

Footing		Test S1-5	
B=	40 mm	v=	3 mm/s
H=	65 mm	Dyn=	23.5°
θ=	0°	Soil	Clay
Pore Pressure			
PP50		52.2 kPa	
PP75		36.9 kPa	
PP100		24.3 kPa	

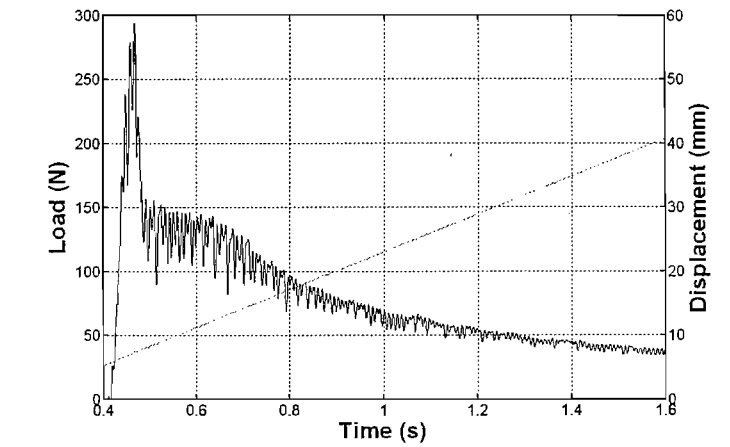

Figure D1(f) Load and displacement curves for test No 5.

Footing		Test S1-5	
B=	40 mm	v=	3 mm/s
H=	65 mm	Dyn=	23.5°
θ=	0°	Soil	Clay
Pore Pressure			
PPTT initial reading		29.4	

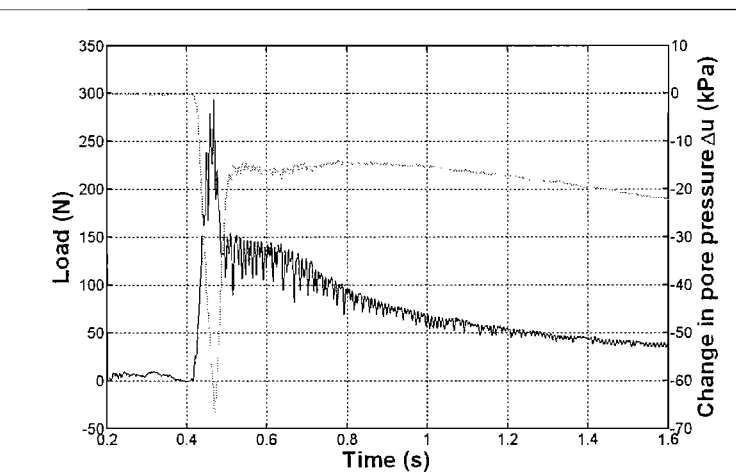

Figure D1(g) Load and pore pressure curves for test No 5.

Footing		Test S1-6	
B=	40 mm	v=	0.1 mm/s
H=	65 mm	Dyn=	23.5°
θ=	0°	Soil	Clay
Pore Pressure			
PP50		52.2 kPa	
PP75		36.9 kPa	
PP100		24.3 kPa	

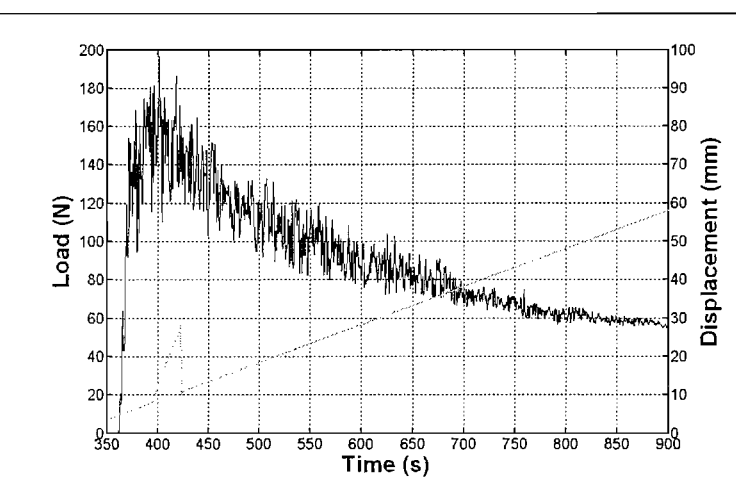

Figure D1(h) Load and displacement curves for test No 6.

Footing		Test S1-6	
B=	40 mm	v=	0.1 mm/s
H=	65 mm	Dyn=	23.5°
θ=	0°	Soil	Clay
Pore Pressure			
PPTT initial reading		30.2	

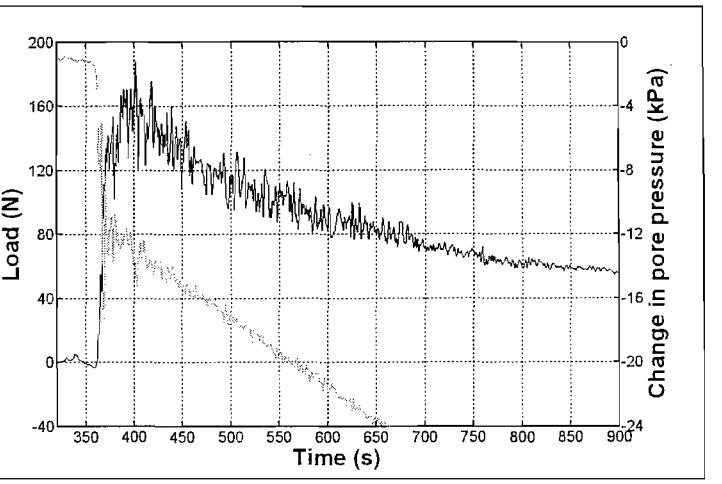

Figure D1(i) Load and pore pressure curves for test No 6.

Footing		Test S1-7	
B=	40 mm	v=	3 mm/s
H=	65 mm	Dyn=	23.5°
θ=	9.2°	Soil	Clay
Pore Pressure			
PP50		52.2 kPa	
PP75		36.9 kPa	
PP100		24.3 kPa	

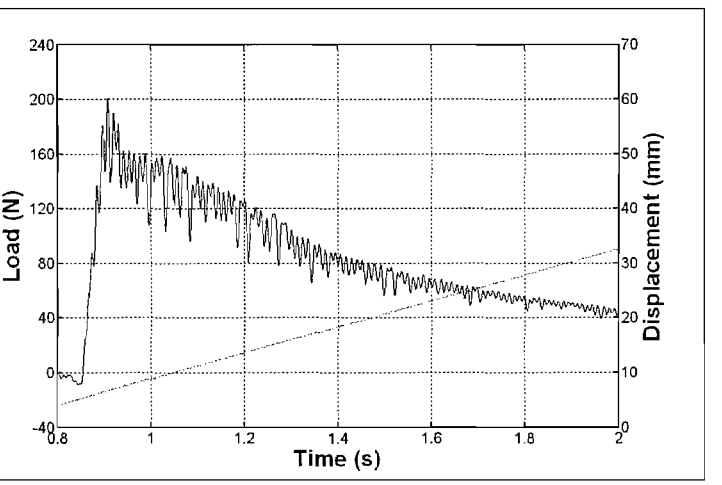

Figure D1(j) Load and displacement curves for test No 7.

Footing		Test S1-8	
B=	40 mm	v=	100 mm/s
H=	65 mm	Dyn=	23.5°
θ=	0°	Soil	Clay
Pore Pressure			
PP50		52.2 kPa	
PP75		36.9 kPa	
PP100		24.3 kPa	

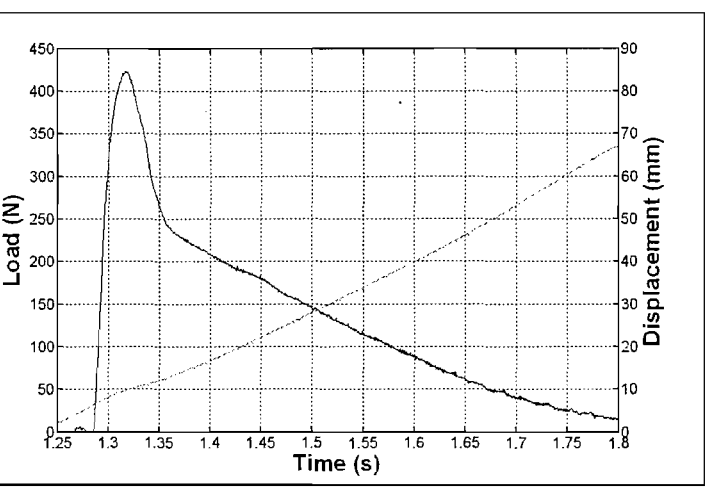

Figure D1(k) Load and displacement curves for test No 8.

Footing		Test S1-8	
B=	40 mm	v=	100 mm/s
H=	65 mm	Dyn=	23.5°
θ=	0°	Soil	Clay
Pore Pressure			
PPTT initial reading		29.1	

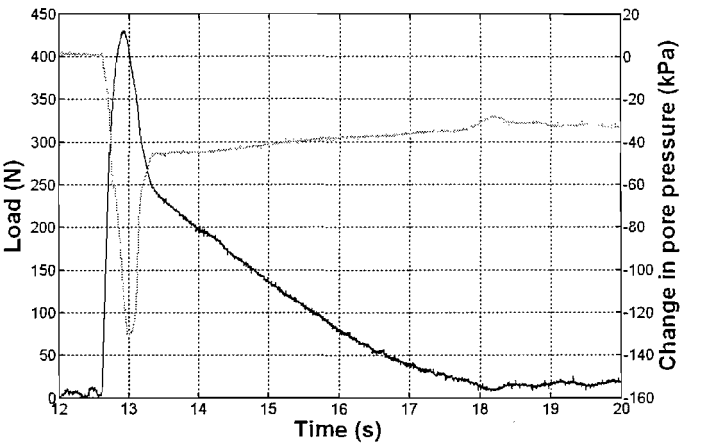

Figure D1(l) Load and pore pressure curves for test No 8.